Secondary metabolism of the forest pathogen *Dothistroma septosporum*

A thesis presented in the partial fulfilment of the requirements for the degree of

Doctor of Philosophy (PhD)

in

Genetics

at Massey University, Manawatu, New Zealand

Ibrahim Kutay Ozturk

2016

ABSTRACT

Dothistroma septosporum is a fungus causing the disease Dothistroma needle blight (DNB) on more than 80 pine species in 76 countries, and causes serious economic losses. A secondary metabolite (SM) dothistromin, produced by *D. septosporum*, is a virulence factor required for full disease expression but is not needed for the initial formation of disease lesions. Unlike the majority of fungal SMs whose biosynthetic enzyme genes are arranged in a gene cluster, dothistromin genes are dispersed in a fragmented arrangement. Therefore, it was of interest whether *D. septosporum* has other SMs that are required in the disease process, as well as having SM genes that are clustered as in other fungi.

Genome sequencing of *D. septosporum* revealed that *D. septosporum* has 11 SM core genes, which is fewer than in closely related species. In this project, gene cluster analyses around the SM core genes were done to assess if there are intact or other fragmented gene clusters. In addition, one of the core SM genes, *DsNps3,* that was highly expressed at an early stage of plant infection, was knocked out and the phenotype of this mutant was analysed. Then, evolutionary selection pressures on the SM core genes were analysed using the SM core gene sequences across 19 *D. septosporum* strains from around the world. Finally, phylogenetic analyses on some of the SM core genes were done to find out if these genes have functionally characterised orthologs.

Analysis of the ten *D. septosporum* SM core genes studied in this project showed that two of them were pseudogenes, and five others had very low expression levels *in planta*. Three of the SM core genes showed high expression levels *in planta*. These three genes, *DsPks1*, *DsPks2* and *DsNps3,* were key genes of interest in this project. But despite the different expression levels, evolutionary selection pressure analyses showed that all of the SM core genes apart from the pseudogenes are under negative selection, suggesting that *D. septosporum* might actively use most of its SMs under certain conditions.

In silico predictions based on the amino acid sequences of the proteins encoded by SM core genes and gene cluster analyses showed that four of the SM core genes are predicted to produce known metabolites. These are melanin (*DsPks1*), cyclosporin (*DsNps1*), ferricrocin (*DsNps2*) and cyclopiazonic acid (*DsHps1*). Gene cluster analyses revealed that at least three of the *D. septosporum* SMs might be produced by fragmented gene clusters (*DsPks1*, *DsNps1*, *DsNps2*). This suggested that dothistromin might not be the only fragmented SM gene cluster in *D. septosporum*.

According to phylogenetic analyses, some of the *D. septosporum* SM core genes have no orthologs among its class (Dothideomycetes), suggesting some of the *D. septosporum* SMs may be unique. One such example is the metabolite produced by DsNps3. Comparison of wild type and *ΔDsNps3 D. septosporum* strains showed that the *ΔDsNps3* strain produces fewer spores, less hyphal surface network at an early stage of plant infection, and lower levels of fungal biomass in disease lesions compared to wild type, suggesting that the *DsNps3* SM may be a virulence factor. Attempts to identify a metabolite associated with DsNps3, and to knockout another gene of key interest, *DsPks2*, for functional characterization were unsuccessful.

Further work is required to confirm the gene clusters, characterise the SMs and their roles. However, the findings so far suggest that dothistromin is unlikely to be the only *D. septosporum* SM that is a virulence factor in since the DsNps3 SM also appears to be involved in virulence. Likewise the fragmented dothistromin cluster may not be the only one in the genome and there may be at least three more fragmented SM gene clusters.

Acknowledgements

First of all, I am immensely grateful to my supervisor Dr. Rosie Bradshaw for her support and encouragement throughout my PhD. Even when none of my experiments were working and I wasn't believing in myself, she kept believing in me and supported me in every way possible. I don't believe there is a word in any language to express my level of gratitude. I could not be where I am now without her support.

I also want to thank my co-supervisors Dr. Rebecca McDougal and Dr. Carla Eaton for their valuable suggestions and constructive criticism whenever I asked for assistance.

I also acknowledge Andre Sim, Dr. Sinan Ugur Umu, and especially Dr. Pierre Yves-Dupont for their assistance with bioinformatics tools. Special thanks to Pierre for teaching me some bioinformatics and providing critical readings.

I also want to thank all former and current members of the "Fungal Jungle" lab group. I specially want to thank our lab manager Mrs Carole Flyger for her assistance and rapid help in finding everything I needed. I can't thank Pranav Chettri enough for helping me solve many problems regarding experiments, advising with the experimental setups, and our valuable discussions about my results. He was always willing to help even when he was too busy. I also want to specially thank Melissa Guo for her valuable advice and support. I also want to thank Lukas Hunziker for having patience to set up experiments with me until midnight. I also specially thank Md. Kabir for his valuable suggestions and help even after he graduated. I want to extend my thanks also to Yanfei, Andre and Simren. I feel very lucky to be part of this group.

I sincerely thank Dr. Mark Patchett for his valuable suggestions on the optimization of solvent systems.

I thank my family members at home, Galip, Nimet, Buket, and Elifnur Ozturk as well as Mustafa, Sema, and Halil Yalinkilic for their endless support and faith in me. I always felt their good wishes supporting me, even from thousands of kilometers away. I want to extend my gratitude to Tarcin Yalinkilic for making my family smile even when we were very depressed.

Most importantly, I want to thank my beloved wife Aslinur. I can't thank her enough for her love, support, and sacrifice in this long journey. She always did her best to help me with anything I asked, sacrificed from her precious sleep, always picked me up or brought me outstanding meals anytime I wanted. I have to give my special thanks for her incredible baking skills, which gave me energy and motivation to study long hours. I feel I am the most lucky man in the world for having such a great, understanding, and supportive wife.

I am very grateful to BioProtection Research Centre for funding me for the three years of my project. I would also like to thank the Institute of Fundamental Sciences, IFS, for providing financial assistance after the third year of my PhD.

Finally, I want to thank all good, smiling people of New Zealand. It feels great to be part of such a warm, welcoming community.

Table of Contents

List of Tables

List of Figures

List of Abbreviations

A (domain)	Adenylation
ABC (transporter)	ATP-binding cassette
ACP	Acyl carrier protein
AF	Aflatoxin
aLRT	Approximate likelihood ratio test
AT	Acyltransferase
ATMT	*Agrobacterium tumefaciens* mediated transformation
Avr (gene/protein)	Avirulence
BA	Benzoic acid
bp	Base pairs
C (domain)	Condensation
CM	C-methyltransferase
Ct	Cycle threshold
Cyc (domain)	Heterocyclization
ddH_2O	Double distilled water
DH	Dehydratase
DM	Dothistroma medium
Dma	Dimethylallyl tryptophan synthase
DMF	Dimethyl formamide
DMSO	Dimethyl sulfoxide
dN	Non-synonymous mutation number
DNA	Deoxyribonucleic acid
DNB	Dothistroma needle blight

dpi	Days post-inoculation
dS	Synonymous mutation number
DSM	Dothistroma sporulation medium
ER	Enoylreductase
EtAc	Ethyl acetate
EtBr	Ethidium bromide
EtOH	Ethanol
ETS	Effector-triggered susceptibility
F (domain)	Formylation
FAD	Flavin adenine dinucleotide
FAS	Fatty acid synthase
FDR	False discovery rate
GFP	Green fluorescent protein
HPLC	High performance liquid chromatography
Hph	Hygromycin B phosphotransferase
HPS	Hybrid polyketide - nonribosomal peptide synthetase
HR	Hypersensitive response
HR-PKS	Highly-reducing PKS
HST	Host-specific toxin
kb	Kilo base pairs
KO	Knockout mutant
KR	Ketoreductase
KS	Keto-synthase
LAS	Leica application suite

LB	Luria broth
MAFFT	Multiple alignment fast Fourier transform
MCO	Multicopper oxidase
MeOH	Methanol
MFS (transporter)	Major facilitator superfamily
ML	Maximum likelihood
MMIC	The Manawatu Microscopy & Imaging Centre
MS	Mass spectrometry
NaPDoS	Natural product domain seeker
NCBI	National center for biotechnology information
NHST	Non-host-specific toxin
NM	N-methyltransferase
NMR	Nuclear magnetic resonance
Non-norm	Non-normalized
Norm.	Normalized
NR-PKS	Non-reducing PKS
NRP	Nonribosomal peptide
NRPS/NPS	Nonribosomal peptide synthetase
Ox (domain)	Oxidation
PAMP/MAMP	Pathogen/microbe-associated molecular pattern
PKS	Polyketide synthase
PMMG	Pine needle minimal medium + glucose
PR-PKS	Partially reducing PKS
PT	Product template

PTI	PAMP-triggered immunity
R (domain)	Reduction
R (gene/protein)	Resistance
Rf	Retention factor
RPMK	Fungal reads per million per kilobase
SAM	S-adenosyl-L-methionine
SAT	Starter unit acyl-carrier protein transacylase
SBSPKS	Structure based sequence analysis of polyketide synthases
SCD	Scytalone dehydratase
SLR	Sitewise likelihood-ratio
SM	Secondary metabolite
ST	Sterigmatocystin
T	Thiolation
T3HN	1,3,8- trihydroxynaphthalene
T4HN	1,3,6,8-tetrahydroxynaphthalene
TE	Thioesterase
TLC	Thin layer chromatography
wpi	Weeks post-inoculation
WT	Wild type
µg	Microgram
µL	Microliter
µM	Micromolar

1. Introduction

1.1. Dothistroma needle blight

Dothistroma needle blight (DNB) is one of the most harmful pine diseases in both natural forests and plantations spread throughout the world (Drenkhan et al., 2016). Outbreaks of DNB have been observed since the 1950s in *Pinus radiata* plantations of the Southern Hemisphere, as well as in several regions of North America (Gibson 1972, Gibson 1974). The disease significantly affected large-scale *Pinus radiata* planting projects in India (Bakshi and Singh, 1968), East Africa (Gibson, 1974), and Oregon (Peterson and Harvey, 1976). Within the last 50 years, DNB outbreaks have caused serious damage in East African countries, Chile, New Zealand, Canada, and parts of Europe (Gibson, 1974; Woods et al., 2005; Brown, 2005; Woods et al., 2016). The disease has increased its prevalence in the Northern Hemisphere since the 1990s, especially in Canada and a number of European countries (Drenkhan et al., 2016). A recent study showed that DNB has now been observed in 76 countries (Drenkhan et al., 2016) (Figure 1.1). DNB is still a major problem for pine plantations in the Southern Hemisphere, especially New Zealand (Bulman et al., 2013, Rodas et al., 2016).

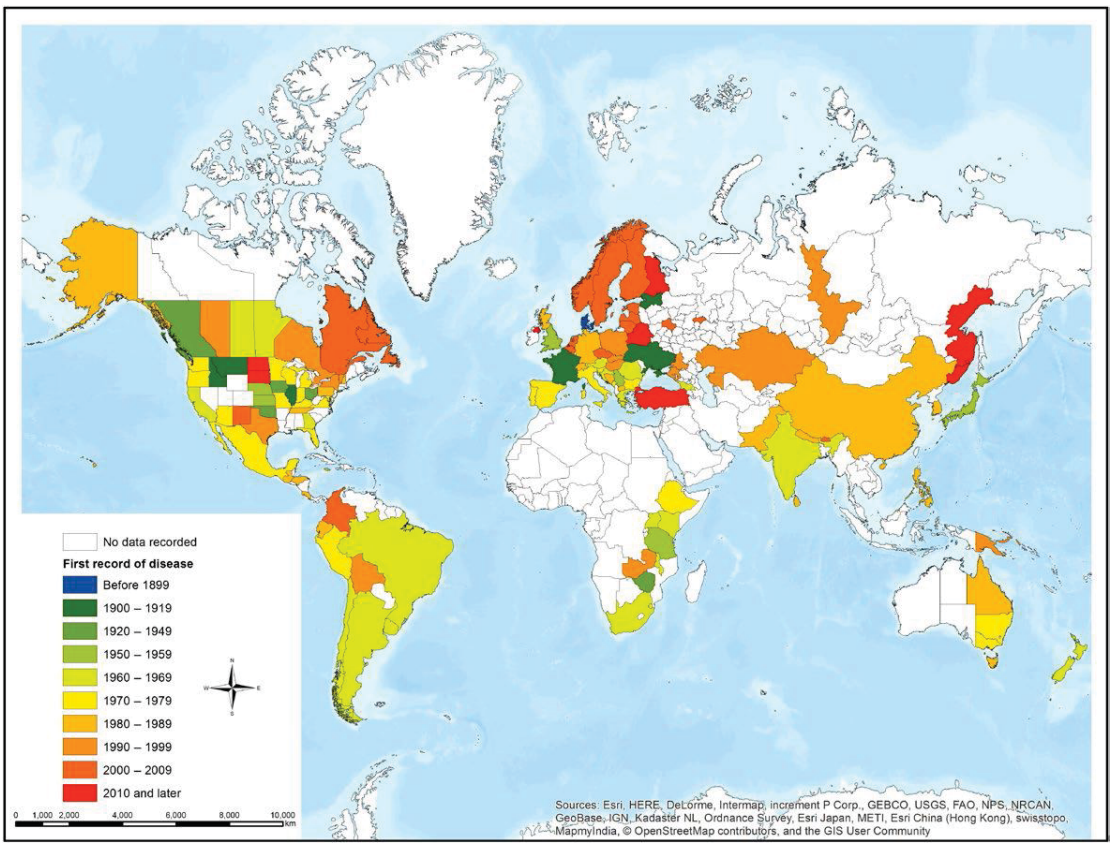

Figure 1.1. *Dothistroma spp.* global distribution. Shading indicates the date in which DNB was first recorded in each region. Image reproduced from Drenkhan *et al*. (2016).

The infection rate and distribution pattern of DNB is strongly dependent on host density and climate (Guernier et al., 2004). Climatic conditions have a strong influence on DNB infections because temperature affects pathogen growth and survival in winter, while rainfall provides a good opportunity for dispersal of the pathogen (Watt et al., 2009; Woods et al., 2016). Although the main method for dispersal of the pathogen is considered rain splash, recent studies have shown that the pathogen can spread over five times further than previously anticipated, probably because of transport of the spores via mist or wind (Mullett et al., 2016). Because of its suitable climatic conditions, New Zealand was found to be one of the countries most susceptible to DNB since 1961 (Figure 1.2) (Watt et al., 2009, Bulman et al., 2013).

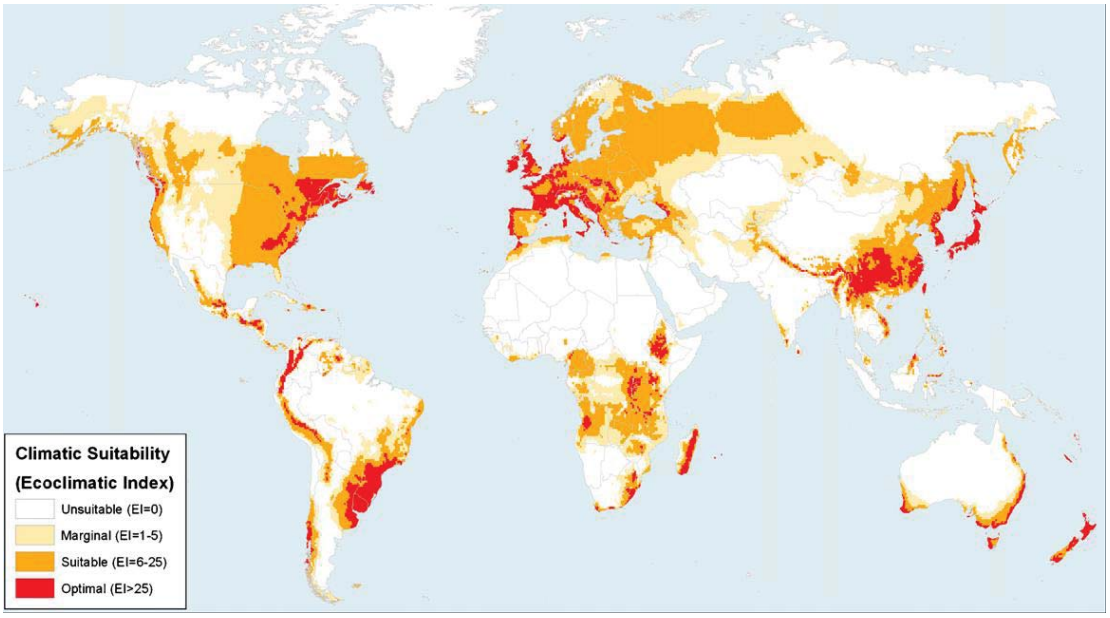

Figure 1.2. Global climatic suitability of DNB based on 1961-1990 climate normals. Image reproduced from Watt et al. (2009).

Initial symptoms of DNB are yellow spots on needles, which then turn into red necrotic bands. Red bands appear because of the accumulation of dothistromin (Bassett et al., 1970), and black fruiting bodies emerge during the late stages of infection (Figure 1.3a). The symptoms of the disease usually involve dead tips but a green base of the needle (Figure 1.3b) (Gadgil, 1967; Shain and Franich, 1981; Bradshaw, 2004).

The mortality rate of DNB was orginally thought to be very low when it was the sole type of disease in a tree (Woods et al., 2005). Plants weakened by heavy DNB become susceptible to mortality caused by other agents such as *Armillaria* spp. (Shaw and Toes, 1977; Woollons and Hayward, 1984). In the last two decades, however, serious DNB outbreaks with high mortality rates have been observed with the epidemics in British Columbia that even killed mature native pine trees in an extraordinary occurrence and there are currently also epidemics in the UK and Columbia (Woods, 2003; Woods et al., 2005; Brown and Webber, 2008; Rodas et al., 2016; Woods et al., 2016).

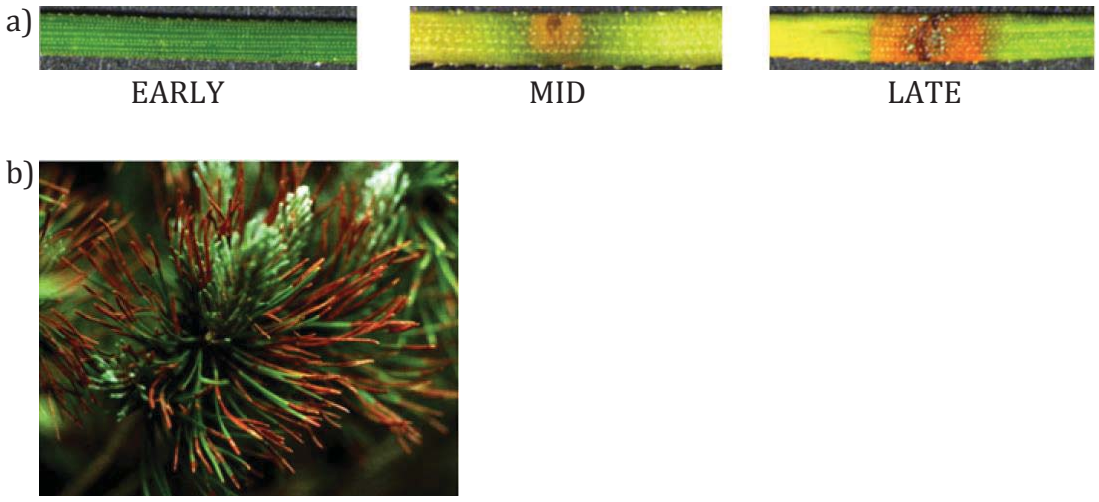

Figure 1.3. Pine needles during DNB disease progression. a) Stages of DNB in a controlled laboratory infection. During the early stage of disease (3-4 weeks post inoculation/wpi), epiphytic growth and penetration of host tissue take place. At 6-8 wpi (middle stage), early lesions appear indicating the start of host necrosis. During the late stage of infection (10-12 wpi), extended lesions and fruiting bodies erupting from the epidermis are clearly visible. Image reproduced from Kabir et al. (2015). b) *D. septosporum* infected branch of *Pinus mugo*. Image reproduced from (OEPP/EPPO, 2008)

DNB has significant effects on the economy of some affected countries. For the New Zealand economy, forestry is one of the key components with $5 billion annual revenue and employing 20,000 people (http://www.ffr.co.nz/new-wood-products-partnership-launched; accessed on 14 April, 2016). The estimated cost of DNB for the New Zealand forest industry is $19.8 m per annum, which increased from $6.1 million in two decades (Watt et al., 2011; New, 1989).

1.2. *Dothistroma septosporum*

Dothistroma septosporum, an ascomycete belonging to the class Dothideomycetes, is one of two fungal species that cause the disease DNB. The other species, *D. pini*, has a narrower distribution and is less well studied than *D. septosporum* (Drenkhan et al., 2016). *D. septosporum* infects more than 107 Pinaceae host species, of which 93 are *Pinus* species (Drenkhan et al., 2016) and the others are non-pine hosts such as *Cedrus* and *Abies* species (Mullett and Fraser, 2015; Drenkhan et al. 2016). *D. septosporum* is a hemibiotrophic species closely related to the tomato pathogen *Cladosporium fulvum* (de Wit et al., 2012).

1.3. Plant-pathogen interactions

Plant disease resistance mechanisms are crucial for the host plant protection from insects, pests, infectious bacteria, viruses, and fungi (Brunner et al., 2012). Plant-pathogen interactions involve two-way communication. On one hand, plants must be able to detect and respond to the pathogen. Since plants lack mobile immune cells and no circulatory system to detect the pathogens, they rely on innate immunity of individual cells and the systemic signals originating from the infection site (Spoel and Dong, 2012, Ausubel, 2005). On the other hand, the pathogen needs to manipulate the host plant biology in order to provide itself a suitable environment for growth and reproduction.

Plant defense responses operate at two levels, which can be represented by a zigzag model (Jones and Dangl, 2006) (Figure 1.4). First, the plant detects pathogen (or microbe)-associated molecular patterns (PAMPs/MAMPs) by plant pattern recognition receptors (PRRs) and activates general defense responses named PAMP-triggered immunity (PTI), which is sufficient to repel most pathogens (Boyd et al., 2013). PTI responses include reactive H_2O_2 accumulation, callose deposition and production of salicylic acid and ethylene (Lamb and Dixon, 1997; Zipfel and Robatzek, 2010). PAMPs are essential molecules highly conserved around a broad spectrum of pathogen species. The best-studied fungal PAMP is chitin, an essential constituent of fungal and insect cell walls (Monaghan and Zipfel, 2012). It was also discovered that PRRs could sense cell wall fragments or peptides released during wounding or infection, which are named damage-associated molecular patterns (DAMPs) (De Lorenzo et al., 2011).

In order to overcome PTI, a pathogen manipulates the host cellular environment. Both suppression of plant defense responses and changing the host cellular environment are required in order to make it suitable for growth and reproduction of the pathogen. This is achieved by the use of proteins collectively named as effectors (virulence factors) that target host defense pathways and metabolism (Koeck et al., 2011). Whole genome sequencing has enabled bioinformatics approaches to identify candidate effectors. Candidate effector proteins can be

selected from small proteins with signal peptides and, in some cases, short conserved sequences (Haas et al., 2009; Dean et al., 2005; Oberhaensli, et al., 2011). For example, the conserved sequences RXLR and LFLAK define some cytoplasmic effectors in *Phytophthora* spp. (Schornack et al., 2009). As a result of co-evolution with pathogens, plants evolved intracellular or membrane-bound receptors called Resistance (R) proteins that recognize specific effectors (called avirulence proteins (Avr) to achieve effector triggered immunity (ETI) that often leads to a hypersensitive response (HR) (Spoel and Dong, 2012). To overcome ETI, pathogens either mutate the effector that can still perform the same activity but is not recognized by host R proteins, or gain new effectors, and plants evolve new R proteins to detect these new virulence factors (Thomma et al., 2011). This R/Avr gene interaction is named as gene-for-gene resistance (Flor, 1942).

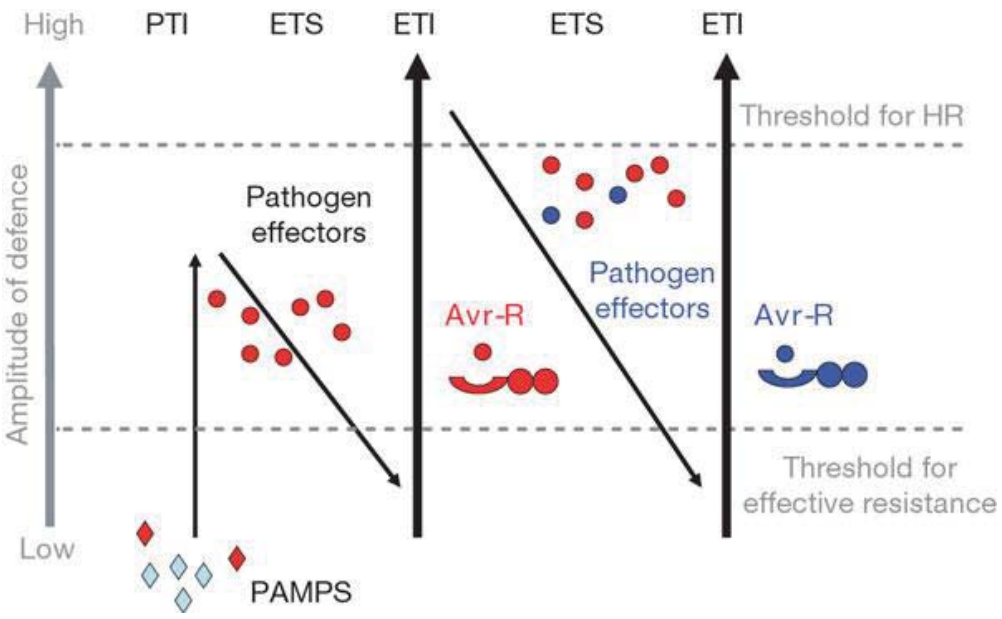

Figure 1.4. The Zigzag model of plant pathogen interactions. In phase 1, pathogen recognition occurs through detection of PAMPS such as chitin, leading PAMP-triggered immunity (PTI). In phase 2, pathogen effectors interfere with PTI, causing effector-triggered susceptibility (ETS). In phase 3, R proteins recognize effectors (now called Avr), leading effector-triggered immunity (ETI). In phase 4, effectors either mutate or new effectors are gained to avoid detection by R proteins. This applies selective pressure on plant R genes in order to detect the newly evolved virulence factors. Image reproduced from Jones and Dangl (2006).

Fungal secondary metabolites also play a role in plant pathogenicity as effectors. One group of fungal secondary metabolites are known as host-specific toxins (HSTs) (Collemare and Lebrun, 2011) (Figure 1.5a). HSTs are effectors that induce

toxicity only in the host species in the presence of susceptibility target proteins to this specific HST (Friesen et al., 2008). Resistance to HSTs on host plants is only possible in the absence of the dominant susceptibility target gene. Therefore, HST-host gene interactions are usually termed as "inverse gene-for-gene" systems (Friesen et al., 2007; Fenton et al., 2009)

Some examples of HSTs include the nonribosomal peptide victorin from *Cochliobolus victoriae* (Tada et al., 2005), HC-toxin from *Cochliobolus carbonum* (Walton, 2006), polyketide depudecin from *Alternaria brassicicola* (Wight et al, 2009), and T-toxin from *Cochliobolus heterostrophus* (Inderbitzin et al., 2010).

Another group of fungal secondary metabolites are non-host-specific toxins (NHSTs) (Figure 1.5b). These mycotoxins promote necrosis or chlorosis in a spectrum of plant species, causing part or all of the disease symptoms of the pathogen (Collemare and Lebrun, 2011). Fumonisin, an example of a mycotoxin produced by some *Fusarium* spp., enhances both disease severity and host range of the species that produce it (Williams et al., 2007; Glenn et al, 2008). Other examples of NHSTs include cercosporin from *Cercospora* spp. (Choquer et al., 2005), elsinochrome from *Elsinoe fawcettii* (Liao and Chung, 2008), and sirodesmin from *Leptosphaeria maculans* (Elliott et al., 2007). The studies on fungal SMs have shown that the common plant targets for these effectors include mitochondria, chloroplast, ribosome-mediated protein synthesis, and plasma membrane (Mahoney et al., 2003; Kim et al., 2004; Meiss et al., 2008; Collemare and Lebrun, 2011; Dayan et al., 2008).

a)

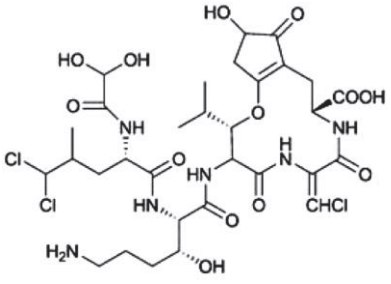

Victorin

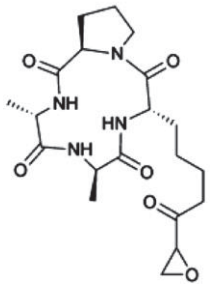

HC-toxin

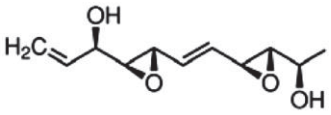

Depudecin

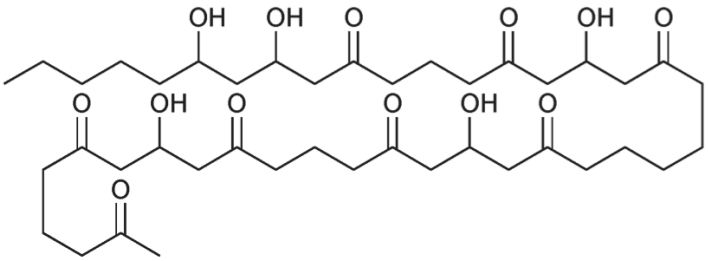

T-toxin

b)

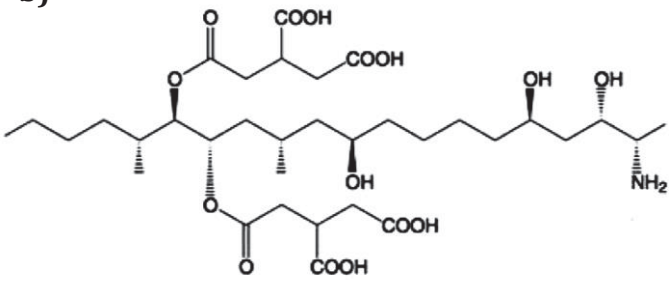

Fumonisin

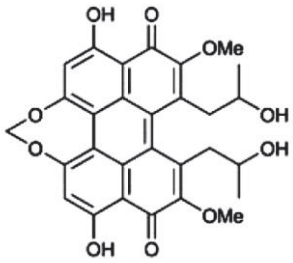

Cercosporin

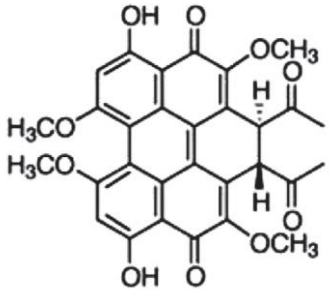

Elsinochrome

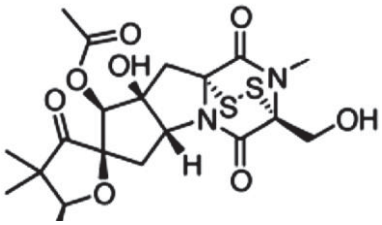

Sirodesmin

Figure 1.5. Secondary metabolites involved in plant pathogenicity. a) Victorin, HC-toxin, depudecin, and T-toxin are HSTs. b) Fumonisin, cercosporin, elsinochrome and sirodesmin are NHSTs. Images adapted from Collemare and Lebrun (2011).

1.4. Fungal secondary metabolism

Fungi contain many unique and diverse secondary metabolism biosynthetic pathways. Products of some of these pathways include important antibiotics such as penicillin, toxins such as aflatoxin, or sometimes compounds with both beneficial and detrimental characteristics such as ergot alkaloids. Secondary metabolites can be classified according to their effect on human interests such as plant toxins, pharmaceuticals or growth hormones. However, a chemical classification system classifies these compounds according to their general type based on key enzyme classes involved in their biosynthesis: polyketides, nonribosomal peptides, hybrid polyketide-nonribosomal peptides, terpenes (Collado et al., 2007) and indole alkaloids (Xu et al., 2014). Unlike primary metabolites, secondary metabolites (SMs) are not directly required for the growth of the organism at least under laboratory conditions (Keller et al., 2015). However, in some cases the absence of secondary metabolites can result in long-term impairment of survivability/fecundity of the fungi (Turgeon and Bushley, 2010). Secondary metabolite production usually occurs at the end of exponential phase (Calvo et al., 2002).

Initial systematic studies of fungal secondary metabolites began in 1922 by Harold Raistrick, but identification and practical use of the secondary metabolites only started after the discovery of penicillin by Alexander Fleming in 1929 (Raistrick, 1950). Additional roles of SMs such as immunosuppressants and inhibitors were found later on (Omura, 1992; Umezawa, 1972). Increasing interest in secondary metabolites resulted in identification of thousands of these compounds. A study of 1500 compounds that were isolated and characterised between 1993 and 2001 showed that more than half of them have antitumor, antifungal, or antibacterial activity (Pelaez, 2004).

Even though secondary metabolites have many properties of commercial or medical interest, their biological functions from the fungal perspective have gained less attention. From the fungal perspective, SMs can provide competitive advantages against other organisms (Ramaswamy, 2002; Sim, 2001), work as

metal transporting agents (Haas, 2014), enable symbiosis with other organisms (Rohlfs and Churchill, 2011; Boustie and Grube, 2005), act as sex hormones (Guzmán-de-Peña et al., 1998; Champe et al., 1987) and affect differentiation of the fungi such as sporulation and germination (Schroeder and Johnson, 1995; Kawamura et al., 1999). Some SMs activate sporulation (Calvo et al., 2001; Champe and el-Zayat, 1989; Mazur et al., 1991) and some are pigments that provide resistance against UV light (Kawamura et al., 1999). Germination can either be stimulated or inhibited through use of secondary metabolites (Eaton and Ensign, 1980; Lazaridis, 1980, Charlang et al., 1982, Horowitz et al., 1976). Loss of some secondary metabolites causes reduced growth rate and conidiation (Calvo et al., 2002).

1.4.1. Polyketide synthases (PKSs)

Polyketides are a large diverse group of natural products produced by plants, bacteria, marine organisms, and fungi (Cox, 2007). Polyketides are not only sources of many medicines such as lovastatin, but also virulence factors and toxins of pathogens including aflatoxin and fumonisin (reviewed by Hertweck, 2009). Although studies on polyketides were reported as early as 1893 recent advances in genetic tools enabled rapid accumulation of new information regarding these compounds over the last few decades (Cox, 2007). Thanks to the availability of genome sequences, many novel polyketide compounds such as asperthecin of *A. nidulans* have also been discovered (Chiang et al., 2013).

Polyketide synthesis is very similar to fatty acid synthesis, as first noted by Birch and Donovan (1953), and their reaction mechanisms have been studied in detail (reviewed by Staunton and Weissmann, 2001; Cox, 2007). Polyketide synthesis involves a conserved general mechanism using iterative elongation of carboxylic acid units such as propionate and acetate (Chooi and Tang, 2012). Both PKS and fatty acid synthases (FAS) condense these carboxylic acid units with malonyl thioesters to form carbon-carbon bond in a Claisen-condensation reaction catalysed by keto-synthase (also called β-ketoacyl-synthase; KS or KAS). The malonyl thioester unit used in this reaction is carried by an acyl carrier protein

(ACP), and acyl groups are transferred from CoA onto KS and ACP components by an acyl transferase (also called malonyl-acetyl transferase; AT or MAT) domain. These three domains are essential for almost all PKS and FAS proteins (Chooi and Tang, 2012). Some PKSs and FASs use additional domains to further modify the product by reduction with a ketoacyl reductase (KR), dehydratase (DH) or enoyl reductase (ER). Figure 1.6 illustrates reactions catalysed by PKS domains. Even though PKS and FAS have many similarities, the PKS have a few capabilities that FAS lacks (reviewed by Cox, 2007). For example, PKS can control the reduction level during each condensation cycle. In addition, PKS can control starter and extender unit selection as well as the level of chain methylation in each cycle.

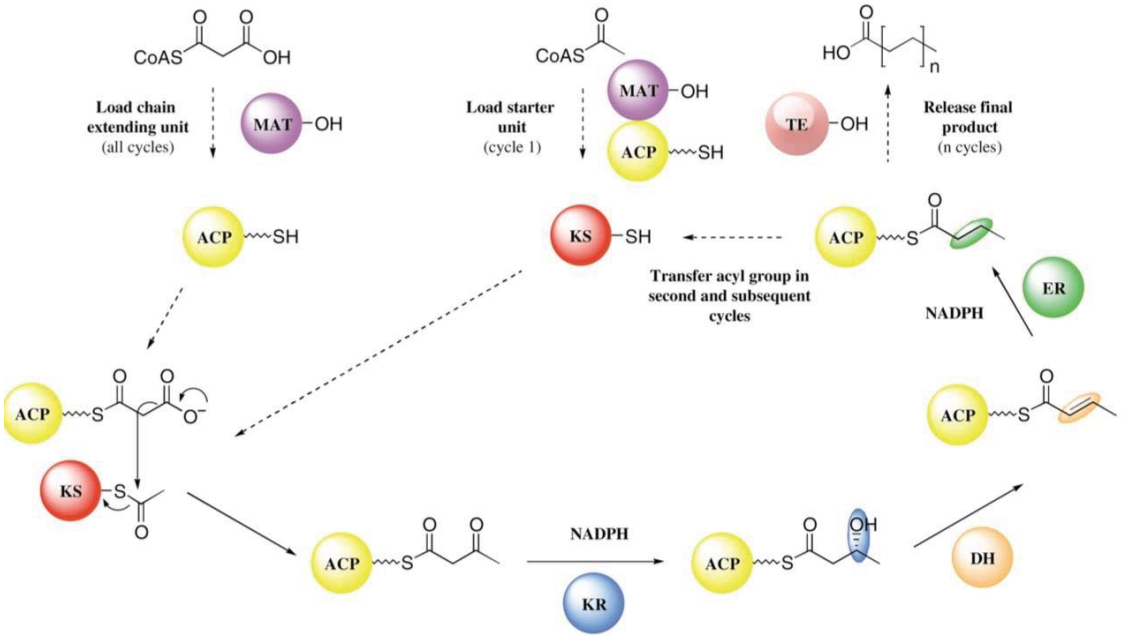

Figure 1.6. Reactions catalysed by PKS catalytic domains. MAT: acyl-transferase, ACP: acyl carrier protein; KS: keto-synthase; KR: ketoreductase; DH: dehydratase; ER: enoylreductase. Image reproduced from Staunton and Weissman (2001).

Organization and usage of these domains indicates the level of reduction of a PKS product and therefore the type of PKS. A non-reducing PKS (NR-PKS) does not contain any of the additional KR, DH, or ER domains, however, it may contain other functional domains including starter unit ACP transacylase (SAT), product template (PT) or thioesterase (TE) domains (Chooi and Tang, 2012). A highly-reducing PKS (HR-PKS) contains all three KR, DH, and ER reduction domains. A partially reducing PKS (PR-PKS), such as 6-methylsalicylic acid synthase of

Penicillium patulum, has only a single reduction domain (Beck et al., 1990; Fujii et al., 1996).

Based on their protein architecture, PKSs are divided into three groups. Most fungal PKSs are type I, very large, multidomain proteins that usually use each domain iteratively (Castoe et al., 2007). Type II PKSs are present in bacteria, and each domain is found in an individual protein instead of multiple domains being grouped in a single large protein as in type I PKSs. Type III PKSs are composed of only KS domains, and are present in plant, fungi and bacteria (Cox, 2007).

Fungal PKSs can catalyse the synthesis of a broad range of polyketides. This can be a simple compound such as orsellinic acid or a complex metabolite like T-toxin. Biosynthesis of polyketides usually requires other enzymes modifying the basic PKS product. Most of the polyketides require activity of multiple proteins encoded by genes usually localized in close proximity to each other, forming a gene cluster. A well-characterised polyketide gene cluster is aflatoxin from *A. parasiticus* (Yu et al., 2004). Some of the genes in aflatoxin gene cluster are predicted to encode reductase, dehydrogenase, P450 monooxygenase and alcohol dehydrogenase enzymes. *D. septosporum* produces a similar compound to aflatoxin, named dothistromin. The dothistromin gene cluster and it's biosynthetic pathway is explained in detail at Section 1.4.5.1. Figure 1.7 and Table 1.1 show some of the well-known fungal polyketides.

Table 1.1. Functionally characterised fungal polyketides.

Organism	PKS name	Polyketide product	Reference
Aspergillus parasiticus	PksA	Aflatoxin*	Minto and Townsend (1997)
Aspergillus nidulans	PksA	Sterigmatocystin*	Minto and Townsend (1997)
Dothistroma septosporum	PksA	Dothistromin*	Bradshaw et. al. (2006)
Cochliobolus heterostrophus	PKS18	Melanin*	Eliahu et al. (2007)
Wangiella dermatitidis	WdPKS1	Tetrahydroxynaphthalene	Feng et al. (2001)
Gibberella zeae	PKS13	Zearalenone	Gaffoor and Trail (2006)
Monascus purpureus	pksCT	Citrinin	Shimizu et al. (2005)
Penicillium expansum	PePks	Patulin*	Sanzani et al. (2012)
Aspergillus terreus	atX	6-MSA	Fujii et al. (1996)
Glarea lozoyensis	pks2	6-MSA	Lu et al. (2005)
Aspergillus terreus	lovB	Lovastatin	Kennedy et al. (1999)
Penicillium citrinum	mlcA	Compactin	Abe et al. (2002)
Phoma spp.	PhPKS1	Squalestatin tetraketide	Cox et al. (2004)
Cochliobolus heterostrophus	Pks1	T-toxin*	Baker et al. (2006)
Fusarium moniliforme	ORF3	Fumonisin B1*	Proctor et al. (1999)
Cercospora spp.	CTB1	Cercosporin*	Newman et al. (2012)

Table adapted from Cox (2007).
An asterisk indicates polyketides with known importance to plants.

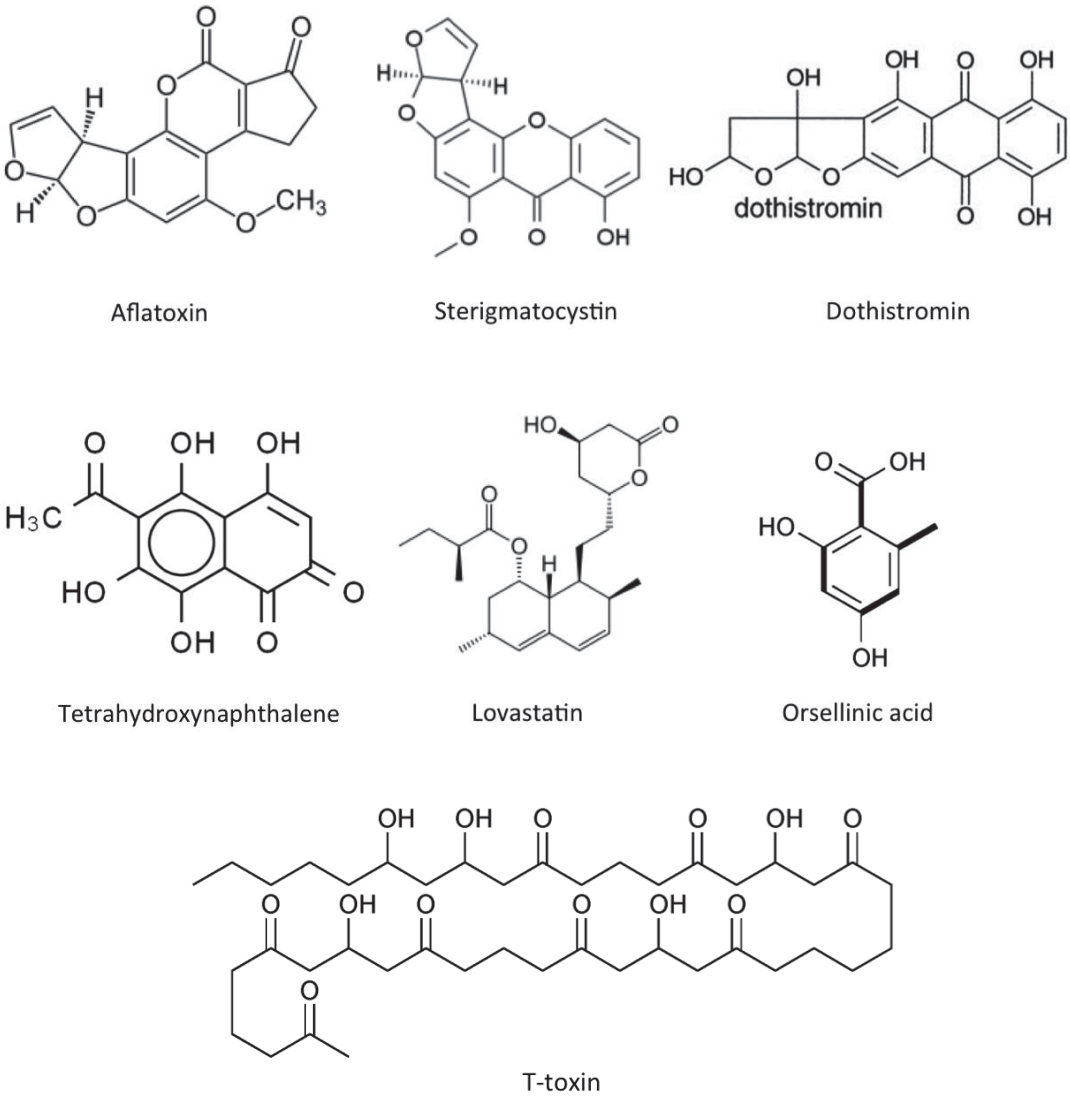

Figure 1.7. Chemical structures of some fungal polyketides.

1.4.2. Nonribosomal peptide synthetases (NRPSs)

Nonribosomal peptide synthethases (NRPSs), present in fungi and bacteria, are the core proteins catalyzing biosynthesis of peptides without the use of ribosomes (Turgeon and Bushley, 2010; Strieker, 2010). Many nonribosomal peptides have pharmacological importance and are used for a variety of purposes such as antibiotics, immunosuppressive and cytostatic agents (Schwarzer et al., 2003). Nonribosomal peptide studies are important not only because of the peptides' current roles in modern medicine, but also because of the possibilities to develop new drugs by using different strategies such as site-directed mutagenesis of substrate binding pockets (Finking and Marahiel, 2004; Williams, 2013).

Nonribosomal peptide synthesis is a well-studied process and its shows some similarities with ribosomal machinery. NRP synthesis requires a minimum of three domains: adenylation (A), peptidyl carrier protein (PCP) (also called thiolation (T)), and condensation (C) (Figure 1.8B). The A domain first activates one amino acid (or hydroxy acid) as amino acyl adenylate, and then enables covalent bonding to the cofactor of the PCP domain called the phosphopantetheine attachment site. Afterwards, the C domain catalyzes the peptide bond formation between two amino acids (Lautru and Challis, 2004). This is why first modules of most NRPSs don't contain a C domain. Exceptions are named as starter C domains, which acylate the first amino acid with a fatty acid (Rausch et al., 2005). The NRPS modules with domains ordered as C-A-PCP are named Type A, linear NRPS. Type B NRPSs use all their modules more than once, and are named iterative NRPSs. Type C NRPSs, also known as nonlinear NRPSs, don't follow the usual C-A-PCP domain organization pattern, but instead use some domains more than once (Felnagle et al., 2008). Monomodular NRPSs have one of each A, PCP, and C domains, and multimodular NRPSs have repetitive A, PCP, and C domains (Glinski et al., 2002; Mootz et al., 2002; Bushley and Turgeon, 2010).

The similarities between nonribosomal and ribosomal peptide synthesis can be observed for each step. The function of the NRPS A domain is similar to aa-tRNA synthetase activity, but the NRPS A domain and aa-tRNA synthetase are

structurally unrelated (Conti et al., 1997; May et al., 2002; Stachelhaus et al., 1999). The function of PCP in NRP synthesis is similar to the function of tRNA in ribosomal synthesis. Finally, peptide bond formation done by the ribosome is catalysed by the C-domain of an NRPS. A key difference between nonribosomal and ribosomal peptide synthesis is the lack of proofreading in NRP synthesis (Weber et al., 2000).

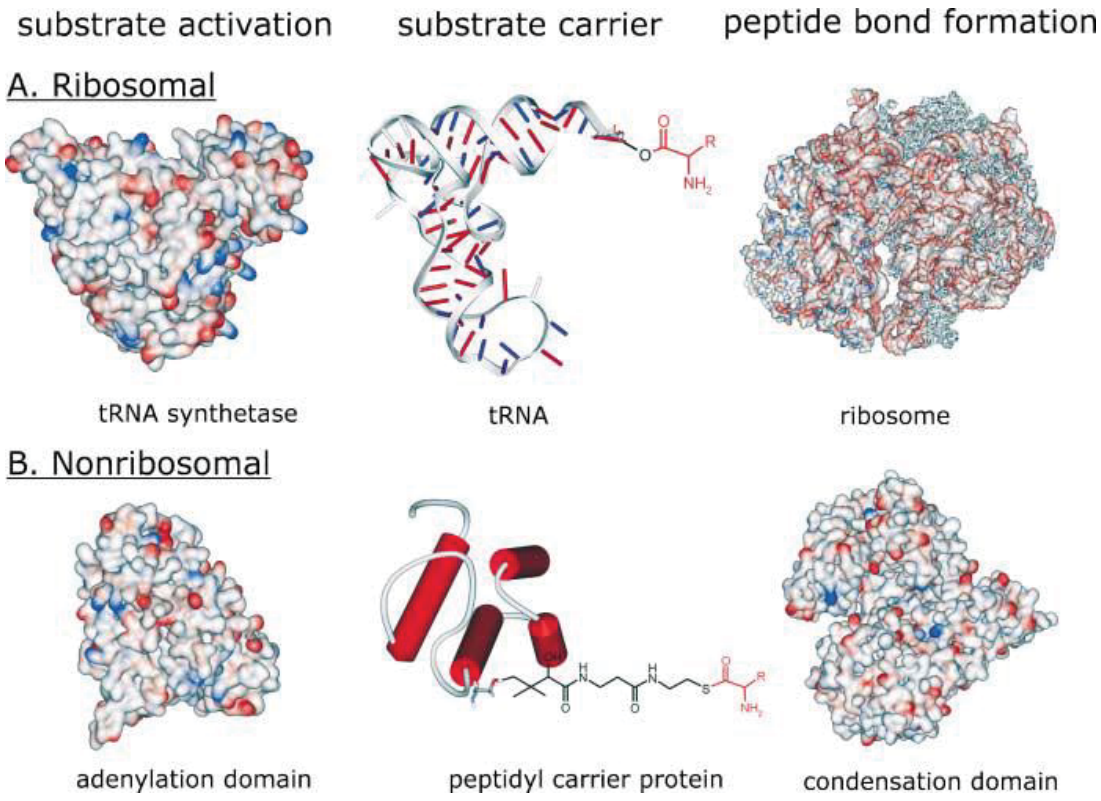

Figure 1.8 A comparison of ribosomal and nonribosomal protein synthesis A. Ribosomal machinery for peptide and protein biosynthesis. B. Nonribosomal machinery. The molecules with similar functions are aligned with each other. Image obtained from Finking and Marahiel (2004).

In addition to the three key domains, there are several other domains that can be present in different NRPSs, making the nonribosomal peptides highly variable (Schwarzer et al., 2003). Heterocyclization (Cyc) domains catalyze peptide bond formation as well heterocyclization of cysteine, serine, and threonine residues in a three-step mechanism, therefore increase rigidity of the NRP and protect it against proteolytic degradation (Rausch et al., 2007; Miller and Walsh, 2001; Patel et al., 2003). In some cases, Cyc-domain activity is followed by oxidation or reduction catalyzed by oxidation (Ox) or reduction (R) domains, respectively. These domains

catalyze two-electron transfers on the heterocycles, therefore further modifying the final products (Reimmann et al., 2001; Du et al., 2000). A thioesterase (TE) domain is present in most of the NRPSs, catalyzing the liberation of the product and thereby terminating the synthesis (Schneider and Marahiel, 1998; Sieber and Marahiel, 2003). Protection of the peptide against proteolytic breakdown is provided by methylation of the ends of the peptide by N- or C-methyltransferases (N-Mt, C-Mt) (Gehring et al., 1998; Reimmann et al., 2001; Walsh et al., 2001). Finally, formylation (F) domains modify by adding a formyl group to the N-termini of the nonribosomal peptides (Schoenafinger et al., 2006). Examples of the reactions catalyzed by these domains are shown in Figure 1.9.

Biosynthetic genes encoding for nonribosomal peptide assembly and the biosynthesis of the amino acids are generally physically close to each other, forming a gene cluster. An example is the gliotoxin gene cluster from *Aspergillus fumigatus*, in which 8 of 12 genes encode enzymes required for biosynthesis and tailoring of monomers required for glitoxin biosynthesis (Cramer et al., 2006).

Both ribosomal and nonribosomal systems have advantages over each other, making them ideal for their specific functions. With the proofreading mechanism that nonribosomal peptide synthesis lacks, ribosomal peptide synthesis has high precision for the biosynthesis of primary metabolism proteins. On the other hand, nonribosomal peptides are very variable in structure and, as of 8 November 2016, the database of nonribosomal peptides (Norine) contains 1184 peptides (http://bioinfo.lifl.fr/norine/) and genomic databases have thousands more NRPS gene clusters that haven't been biochemically characterised yet (Walsh and Fischbach, 2010; Caboche et al., 2008). While ribosomal systems are restricted to 20 amino acids as building blocks, there are currently >530 monomers that can be used as substrates for the NRPS assemblies. In addition to diversification in the selection of the monomers, further diversifications are present during the chain assembly and chain termination by the domains mentioned above, thus producing NRPs with different compositions and structures (Du and Lou, 2010). Finally, there are further post-assembly-line tailoring reactions (Walsh et al., 2001) that can be compared with post-translational modifications (PTM) that are done following

ribosomal biosynthesis. However, while PTM is the only diversifying tool for ribosomal machinery, postassembly-line tailoring is one of the many steps for the NRP synthesis mechanism. Therefore, structural variety is higher for the nonribosomal peptides. Figure 1.10 and Table 1.2 show some well-known NRPSs.

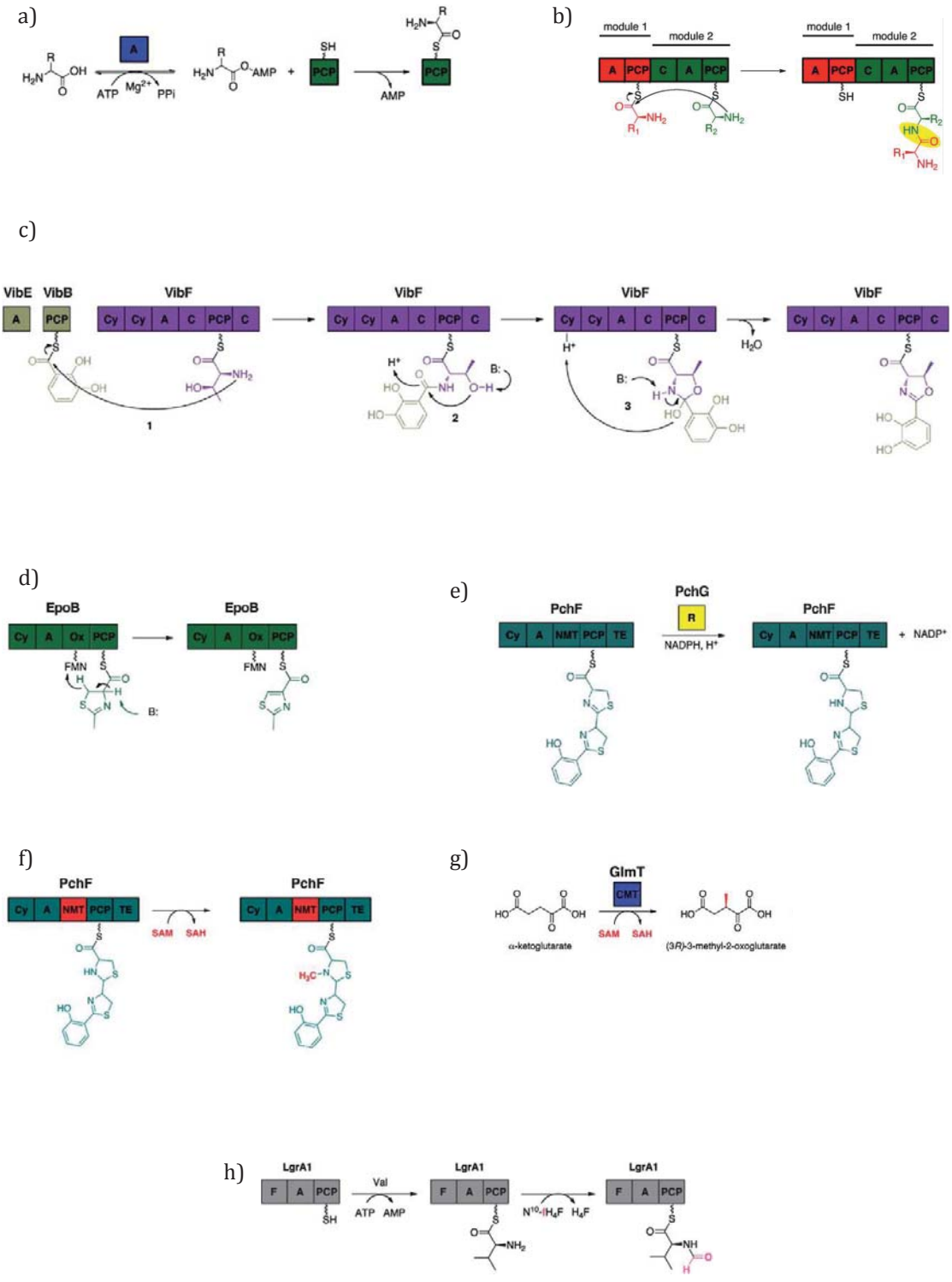

Figure 1.9 Examples of reactions catalyzed by NRPS domains. a) Adenylation, b) Condensation, c) Heterocyclization, d) Oxidation, e) Reduction, f) N-methylation, g) C-methylation, h) Formylation. Domains are abbreviated as A: adenylation, PCP: peptidyl carrier protein, C: condensation, Cy: heterocyclization, Ox: oxidation, R: reduction, NMT: N-methylation, CMT: C-methylation, and F: formylation. Images were obtained from Hur et al. (2012).

Table 1.2. Functionally annotated NRPSs and their products.

Organism	PKS name	NRP product	Reference
Bacillus brevis	tyrocidin A	Tyrocidine	Mootz and Marahiel (1997)
Bacillus brevis	GS 1	Gramicidin S	Hori et al. (1989)
Bacillus licheniformis	Bacitracin synthetase	Bacitracin	Konz et al. (1997)
Amycolatopsis orientalis	CepA, CepB, CepC	Chloroeremomycin	van Wageningen et al. (1998)
Stigmatella aurantiaca	MxcG	Myxochelin A	Silakowski et al. (2000)
Bacillus subtilis	DhbF	Bacillibactin	May et al. (2001)
Streptomyces acidiscabies	TxtA	Thaxtomin A*	Healy et al. (2000)
Penicillium chrysogenum	ACVS	ACV	Smith et al. (1990)
Trichoderma virens	Peptaibol synthetase	Peptaibol	Wiest et al. (2002)
Cochliobolus victoriae	Unknown	Victorin*	Sweat et al. (2008)
Aspergillus nidulans	SidC	Ferricrocin*	Eisendle et al. (2003)
Dickeya didantii	IndC	Indigodin	Reverchon et al. (2002)

An asterisk indicates NRPs with known importance to plants.

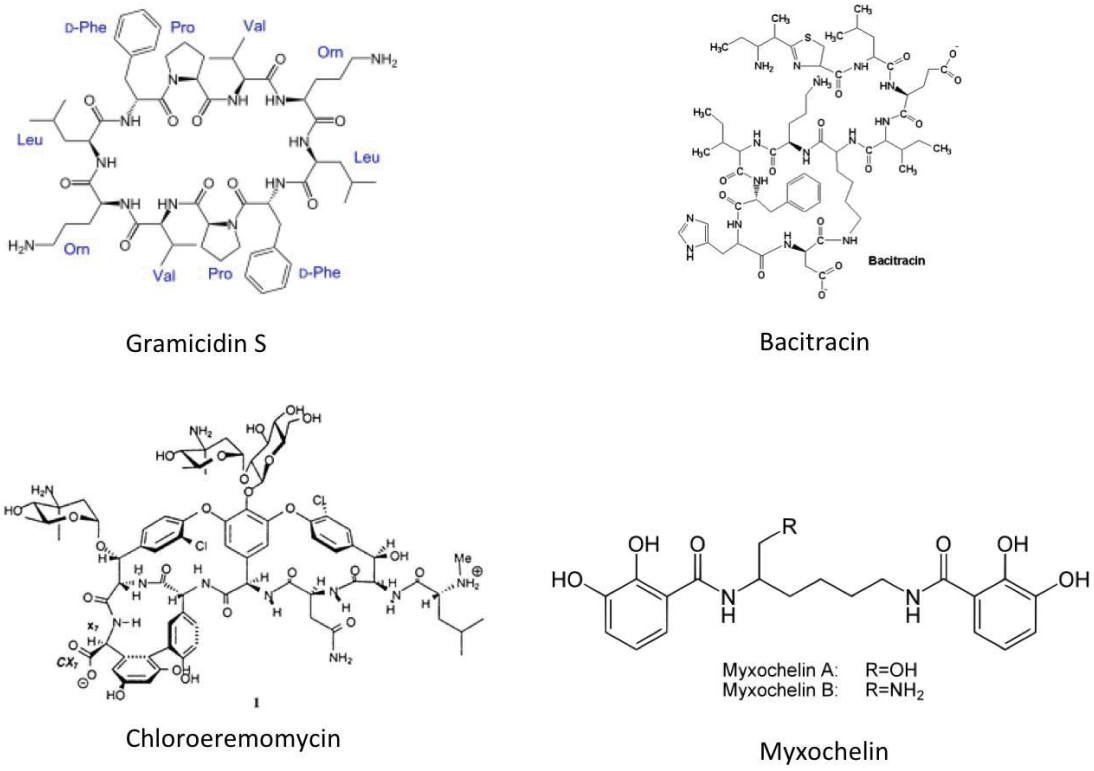

Figure 1.10. Chemical structures of some nonribosomal peptides.

1.4.3. Hybrid peptide-polyketide synthases (HPSs)

In addition to polyketides and nonribosomal peptides, some SMs, named PKS-NRPS hybrids, are produced by combined action of both PKS and NRPS biosynthetic pathways (Du et al., 2003). PKS-NRPS hybrids are usually found in fungi and involve a PKS followed by a single NRPS, thereby connecting a polyketide with an amino acid chain (reviewed by Fisch, 2013). PKS-NRPS hybrids are a large and highly variable group of complex structures and include many mycotoxins and

virulence factors (Wiemann et al., 2010; Collemare et al., 2008). Aside from their roles in the producing organism, PKS-NRPS hybrids have important pharmaceutical potential due to their ability to synthesize compounds which are hard to produce by chemical synthesis (Boettger and Hertweck, 2013). Figure 1.11 illustrates the typical domain structure of a PKS-NRPS hybrid.

Figure 1.11. Domain organization of a typical HPS. PKS (red) and NRPS (blue) domains are indicated as KS: keto-synthase, AT: acyltransferase, DH: dehydratase, CM: C-methyltransferase, KR: ketoreductase, ACP: acyl carrier protein, C: condensation, A: adenylation, T: thiolation domains.

Some well-known products of fungal hybrid PKS-NRPSs are shown in Table 1.3 and Figure 1.12.

Table 1.3 Some of the well-known products of PKS-NRPS hybrids.

Organism	HPS name	Hybrid PKS-NRPS product	Reference
Aspergillus nidulans	ApdA	Aspyridone	Xu et al. (2010)
Penicillium expansum	CheA	Chaetoglobosin A*	Schümann and Hertweck (2007)
Aspergillus spp.	CpaS	Cyclopiazonic acid*	Tokuoka et al. (2008)
Aspergillus clavatus	CcsA	Cytochalasin E	Scherlach et al. (2010)
Fusarium heterosporum	EqiS	Equisetin	Sims et al. (2005)
Aspergillus terreus	ATEG_00325	Isoflavipucine	Gressler et al. (2011)
Metarhizium robertsii	NGS1	NG-391	Hayashi et al. (2002)
Aspergillus fumigatus	PsoA	Pseurotin A	Komagata et al. (1996)
Beauveria bassiana	TenS,	Tenellin	Eley et al. (2007)
Beauveria bassiana	DmbS	Desmethyl-bassianin	Eley et al. (2007)
Xylaria spp.	PKS3	Xyrrolin	Phonghanpot et al. (2012)
Fusarium spp.	*fusA*	Fusarin C	Song et al. (2004)

An asterisk indicates hybrids with known importance to plants.

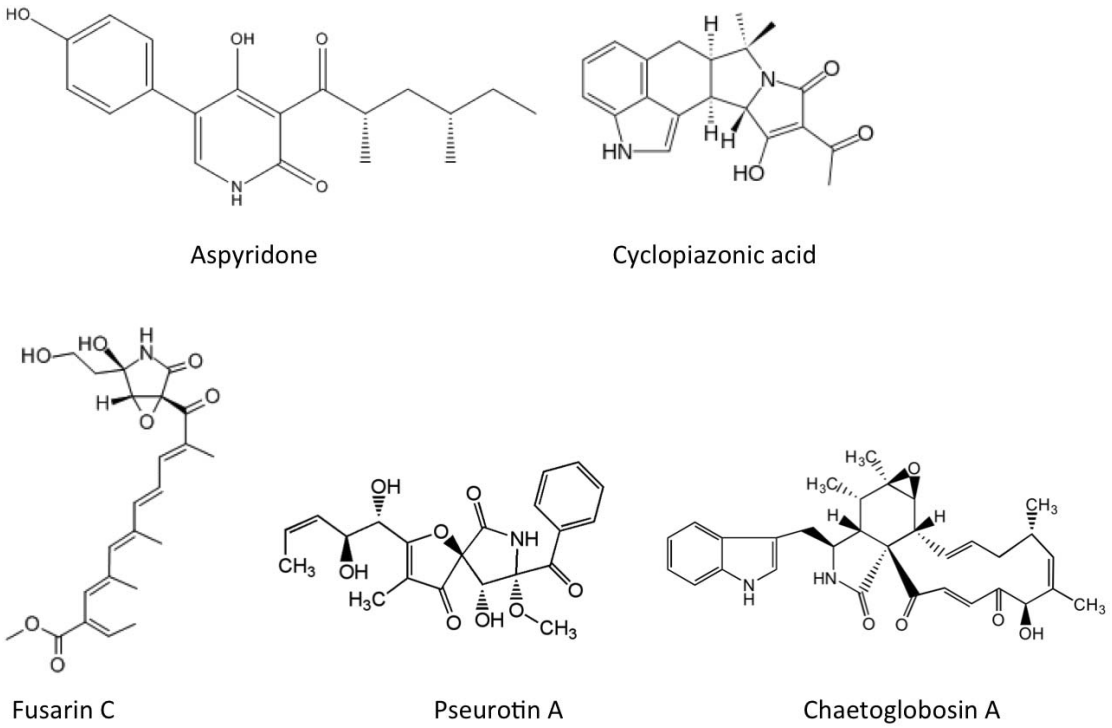

Figure 1.12. Chemical structures of some hybrid PKS-NRPS products.

1.4.4. *Dothistroma septosporum* secondary metabolism

It is proposed that biotrophy in fungi is associated with fewer numbers of SM biosynthetic pathways compared to those associated with necrotrophic or saprophytic lifestyles (Spanu et al., 2010). However, a study by de Wit et al. (2012) has shown the hemibiotroph *D. septosporum* has 11 core secondary metabolite (SM) genes, which is less than that of the closely related biotroph *Cladosporium fulvum*, which has 23 SM genes (Table 1.4). In addition, only three of the key SM core genes are predicted to be homologous, which shows there is a much lower level of similarity between the SM repertoires of the two species compared to genome-level similarities between the two species. The three common genes are predicted to encode enzymes involved in production of melanin, siderophore, and dothistromin (de Wit et al., 2012).

Table 1.4 Number of key secondary metabolite genes in select Ascomycetes.

Fungal species	Lifestyle	SM number
Dothistroma septosporum	Hemibiotroph	11
Cladosporium fulvum	Biotroph	23
Zymoseptoria tritici	Hemibiotroph	20
Parastagonospora nodorum	Necrotroph	38
Magnaporthe oryzae	Hemibiotroph	46
Fusarium graminearum	Necrotroph	30
Aspergillus nidulans	Saprophyte	45
Neurospora crassa	Saprophyte	12

Table adapted from de Wit et al. (2012).

1.4.4.1. Dothistromin

Among *Dothistroma septosporum* secondary metabolites, the polyketide dothistromin is the only one studied in detail (Bassett et al., 1970; Shain and Franich, 1981; Bradshaw, 2004; Schwelm et al., 2009; Schwelm and Bradshaw, 2010; Chettri et al., 2013; Bradshaw et al., 2013; Kabir et al., 2015). When dothistromin was injected into pine needles, appearance of DNB symptoms such as red bands and necrotic regions on the needles was reported (Shain and Franich, 1981). The molecular structure of dothistromin is very similar to an intermediate substrate in synthesis of sterigmatocystin and aflatoxins produced by some species of *Aspergillus* (Shaw et al., 1978). Using a ^{13}C labelling method, it was shown that the bistetrahydrofurano side-chain labelling during the dothistromin biosynthesis was identical to that of aflatoxin B_1 and sterigmatocystin biosynthesis pathways in *Aspergillus* spp. (Shaw et al., 1978), suggesting common steps in the biosynthesis of these compounds.

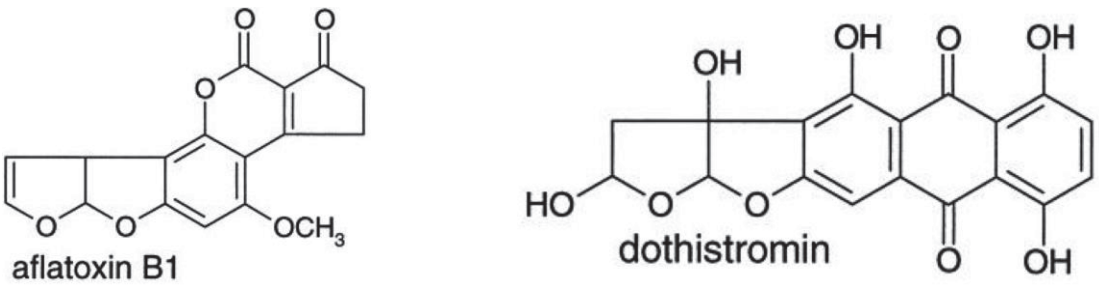

Figure 1.13. Chemical structures of aflatoxin B_1 and dothistromin. Image reproduced from Bradshaw (2002).

For a long time, it was questioned whether dothistromin is a pathogenicity factor (obligatory for disease occurrence) or virulence factor (increasing disease severity) (Shaner et al., 1992). Injection of dothistromin into pine needles evoked a strong host defence response and accumulation of benzoic acid (BA), an antimicrobial agent synthesized by plants that is known to inhibit *D. septosporum*, in the plant cells surrounding the lesions (Franich, 1986). Most of the dothistromin was degraded to oxalic acid and CO_2 in the plant tissues after 24 hours, possibly due to the presence of the light, since it has been shown that light affects the breakdown of dothistromin outside of plant tissue (Harvey et al., 1976). The continuous expansion of the necrotic lesions on the pine needles after the majority of injected dothistromin was presumably degraded could have been because of the BA accumulation, since BA is also toxic to plant cells in high concentrations (Franich et al., 1986; Bradshaw, 2004). Exposure of cell suspension cultures of *P. radiata* to *D. septosporum* cell wall fragments caused host defense reactions such as phenolic compound biosynthesis, showing host defense responses could also be activated in the absence of dothistromin (Hotter, 1997).

Generation of dothistromin-deficient *D. septosporum* mutants (Bradshaw et al., 2006) finally enabled the determination of whether dothistromin is a pathogenicity or virulence factor. Schwelm et al. (2009) showed that dothistromin-deficient *D. septosporum* strains were able to complete the disease cycle on the pine needles, confirming that dothistromin is not a pathogenicity factor and led to the idea that that dothistromin may be produced for providing competitive benefits over other microorganisms. However, it was later shown that *P. radiata* needles infected with dothistromin-deficient *D. septosporum* strains had smaller lesions, less sporulation of the pathogen and lower levels of mesophyll colonization than those infected with wild type *D. septosporum*, suggesting that dothistromin production is correlated with increased host colonization and necrosis inducing ability of *D. septosporum*, and showing that dothistromin is a virulence factor (Kabir et. al., 2015). Nevertheless, the presence of small lesions on plants infected with dothistromin-deficient *D. septosporum* led to the question of whether another compound such as another SM or proteinaceous effector is required to initiate lesion formation in DNB (Kabir et al., 2015).

Early lesions of needles infected with *D. septosporum* have dark green regions outside of the lesion, termed "green islands" (Kabir et al., 2015). Green islands are regions where the pathogen slows down senescence and maintains photosynthetic activity of the host. This term was first associated with biotrophic organisms, but they were later seen in plants infected with hemibiotrophic or necrotrophic pathogens (Walters et al., 2008). Even though green islands were observed on *D. septosporum* infected pine needles; they were lost or reduced as DNB progressed, which led to the hypothesis that dothistromin may be targeting chloroplasts or chlorophyll (Kabir et al., 2015). The necrotic areas caused by dothistromin deficient mutants had more chlorophyll compared to necrotic areas caused by wild type, suggesting that dothistromin potentially targets chloroplast or chlorophyll (Kabir et. al., 2015). Further work needs to be conducted to identify the specific interaction of dothistromin with plant organelles.

Dothistromin is toxic towards plants other than pine, as well as to microorganisms and animal cells (reviewed by Bradshaw, 2004). Dothistromin is known to be mutagenic, clastogenic, and cytotoxic to animal cells, therefore concerns for human health, especially for workers in the forest industry, was brought to discussion (Elliott et al., 1989; Stoessl et al., 1990). Moreover, it has structural similarity to one of the strongest natural carcinogenic molecules, aflatoxin B_1 (reviewed by Eaton and Gallagher, 1994). Comprehensive research on the toxicity of dothistromin showed that dothistromin can cause growth inhibition, mutagenicity, chromosomal abnormalities and cell lysis on different types of cells on variety of organisms and mammalian cells (Elliot et. al., 1989). Although dothistromin demonstrated carcinogenic properties, its severity level was found to be less than that of aflatoxin B_1 (Elliot et. al., 1989). Currently measures are taken to prevent exposure to forest workers (Bulman et al., 2004).

1.4.5. Fungal SM gene clusters

As mentioned in Section 1.4, there are many types of fungal secondary metabolites with very diverse functions. PKS, NRPS, or HPS are named as core enzymes and required for many of the secondary metabolism pathways apart from terpenes and

indole alkaloids (Brakhage et al., 2009; Hertweck, 2009; Strieker et al., 2010; Crawford and Townsend, 2010). However, most fungal secondary metabolite pathways require use of multiple enzymes together, generally located in close proximity with each other. Products of the genes neighboring the core genes can have varying roles such as enzymes required for a multi-step biosynthetic pathway, transporters, or regulatory elements (reviewed by Keller et al., 2005). Studies on secondary metabolite gene clusters have shown that the genes within each cluster are generally co-expressed (Keller and Hohn, 1997). One well-studied example is the sterigmatocystin biosynthesis gene cluster that contains 25 genes spanning a 60-kb region in *A. nidulans*, all of which are co-expressed under inducing conditions (Brown et al., 1996). However, even though some automated methods to predict gene clusters rely on the co-expression of these genes (Umemura et al., 2015; Andersen et al., 2013), it has been questioned whether or not this is always the case (Turgeon and Bushley, 2010). Indeed, genes for the well-studied SM dothistromin shows that there may be exceptions.

1.4.5.1. Dothistromin gene cluster

Because dothistromin is structurally similar to versicolorin B, an intermediate in sterigmatocystin and aflatoxin biosynthesis, the first candidate genes for dothistromin biosynthesis were determined based on the aflatoxin genes using degenerate PCR primers and hybridization probes (Bradshaw et al., 2006; Zhang et al., 2007). The complete set of dothistromin genes was not found until the *D. septosporum* genome sequence was available several years later, and this revealed that the dothistromin putative gene cluster was fragmented into 6 separate regions in chromosome 12, unlike the tight gene clusters of sterigmatocystin and aflatoxin (Chettri et al., 2013). Similar fragmented dothistromin gene clusters were also found in *D. septosporum* close relatives *Passalora arachidicola* (Zhang et al., 2010) and *C. fulvum* (de Wit et al., 2012). It is not yet known why dothistromin gene clusters are fragmented in these species. One possibility is that fragmentation may allow genes to avoid localized chromatin-level or telomere-associated regulation by positioning away from the telomeres (Palmer and Keller, 2010; Shaaban et al., 2010; Bradshaw et al., 2013). Alternatively, a fragmented gene

cluster may enable pathway diversification by recruitment of genes in different fragments. For example, *DotB* and *DotC* of the *D. septosporum* dothistromin fragmented gene cluster have no orthologs in sterigmatocystin and aflatoxin gene clusters but are clustered together with *Ver1*, the ortholog of a key aflatoxin biosynthetic gene (Bradshaw et al., 2013). Dothistromin is not the only SM with a fragmented gene cluster, as aflatrem gene clusters of *Aspergillus flavus* and *A. oryzae* (Nicholson et al., 2009) and the meroterpenoid gene cluster of *A. nidulans* (Lo et al., 2012) are each distributed in two chromosomes.

The dothistromin biosynthesis pathway is quite well-characterised. Figure 1.14 shows the chromosomal organization of the dothistromin fragmented gene cluster and its proposed biosynthesis pathway (Chettri et al., 2013). Many of the genes in the dothistromin fragmented gene cluster have been functionally characterised by loss of function gene knockout mutants. The first dothistromin gene to be characterised was *DsVer1* (formerly known as *DsDotA*), encoding a ketoreductase (Bradshaw et al., 2002). The core polyketide synthase gene of dothistromin biosynthesis, *DsPksA,* was subsequently shown to be required for dothistromin biosynthesis (Bradshaw et al., 2006). When *ΔDsPksA* mutants were supplied with norsolorinic acid or versicolorin A, they were able to produce dothistromin, supporting the hypothesis that the dothistromin biosynthesis pathway has similarities to those of sterigmatocystin and aflatoxin (Bradshaw et al., 2006). Shortly after the functional characterization of *DsPksA*, a gene predicted to encode versicolorin B synthase, *DsVbsA* was functionally characterised by gene knock out and complementation assays (Zhang et al., 2007). Continued analyses on dothistromin cluster genes enabled functional characterization of genes predicted to encode alcohol dehydrogenase (*DsAdhA*), fatty acid synthase (*DsHexA*), peroxidase (*DsDotB*), NAD(P) reductase (*DsOrdB*) and regulators of the dothistromin gene cluster (*DsAflR* and *DsAflJ*) (Chettri et al., 2013; Chettri et al., 2014; Chettri et al., 2015). Table 1.5 lists genes involved in dothistromin biosynthesis.

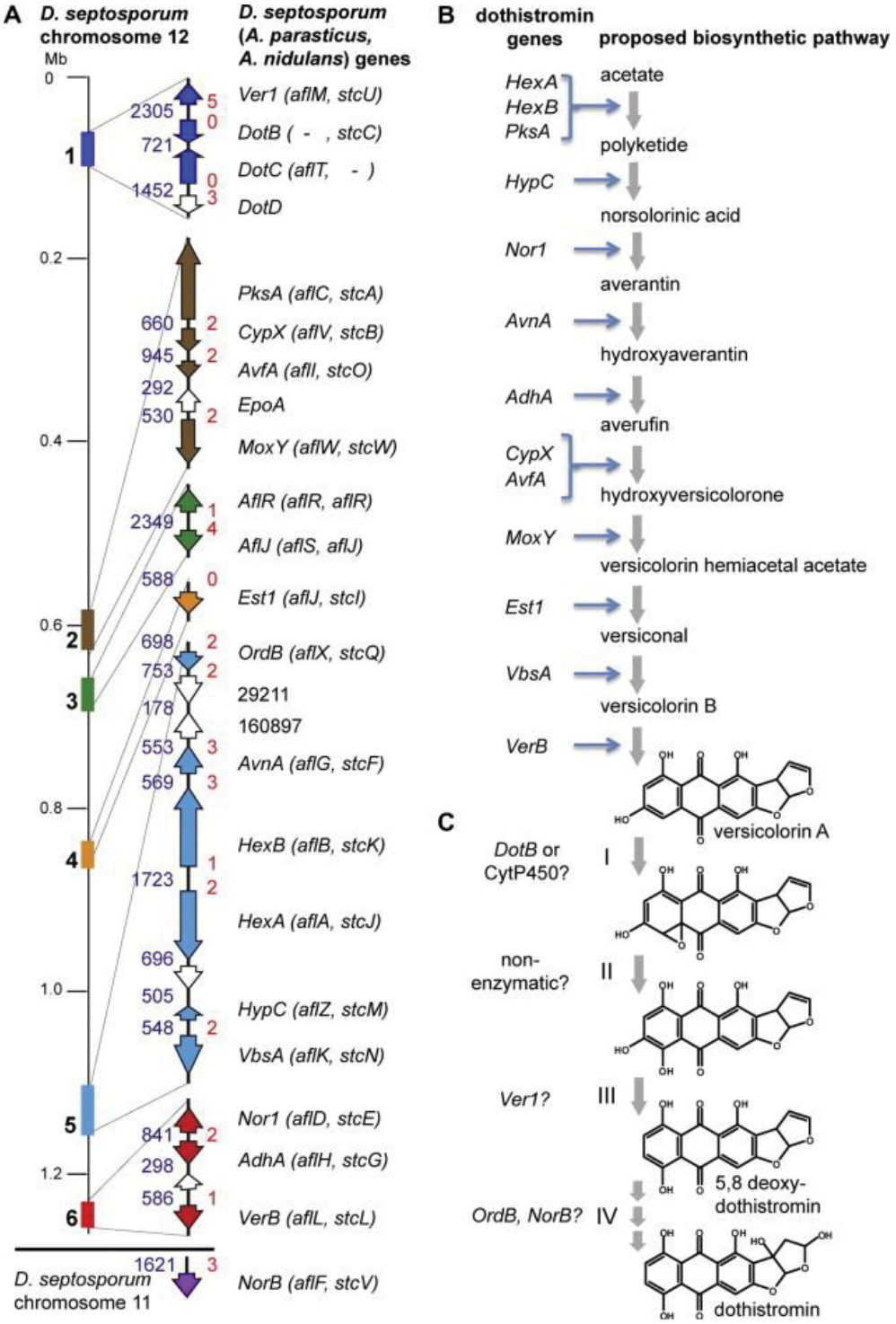

Figure 1.14. Organization and predicted pathway of dothistromin gene cluster in *D. septosporum*. A) Six loci (indicated 1 to 6) showing the fragmented gene cluster of dothistromin. Colorless arrows show genes with no predicted function related to dothistromin biosynthesis. Distances between each gene within a locus are shown as bp. Red numbers to the right of the genes indicate the numbers of putative aflR binding sites. *DsNorB* gene was initially thought to be part of the cluster but functional characterization showed no NorB involvement in dothistromin biosynthesis (Chettri et al., 2014). B) Proposed dothistromin biosynthesis pathway up to versicolorin A based on the orthology to aflatoxin biosynthesis genes. C) Putative biosynthetic pathway from versicolorin A to dothistromin. Image reproduced from Chettri et al. (2013).

Table 1.5. Genes in dothistromin fragmented gene cluster.

Name	JGI Protein ID[a]	Predicted function
DsVer1	192193	NAD(P) reductase
DsDotB	75412	Peroxidase
DsDotC	75413	MFS transporter
DsPksA	192192	Polyketide synthase
DsCypX	139960	P450 monooxygenase
DsAvfA	75546	NAD(P) reductase
DsMoxY	75547	Flavin-binding monooxygenase
DsAflR	75566	Regulatory protein
DsAflJ	57214	Methyltransferase
DsEst1	75609	Esterase (alpha/beta hydrolase)
DsOrdB	75648	NAD(P) reductase
DsAvnA	57312	P450 monooxygenase
DsHexB	181128	Fatty acid synthase
DsHexA	66976	Fatty acid synthase
DsHypC	75655	Anthrone oxidase
DsVbsA	75656	VerB synthase (cyclase)
DsNor1	75691	NAD(P) reductase
DsAdhA	48495	Alcohol dehydrogenase
DsVerB	75692	Desaturase (P450 monooxygenase)

[a] http://genome.jgi.doe.gov/Dotse1/Dotse1.home.html
Table adapted from Chettri et al. (2013).

Transcriptomics analysis of *D. septosporum* throughout its infection cycle (Bradshaw et al., 2016) enabled analysis of dothistromin gene expression (Figure 1.15). Even though most of the genes within the fragmented gene cluster share a similar expression pattern, it is seen that some genes such as and *DotB* have different expression patterns. Therefore, even though co-expression of the genes within the putative gene cluster may support the hypothesis that it is part of the gene cluster, the genes with different expression levels should not be ruled out only because they share different expression patterns.

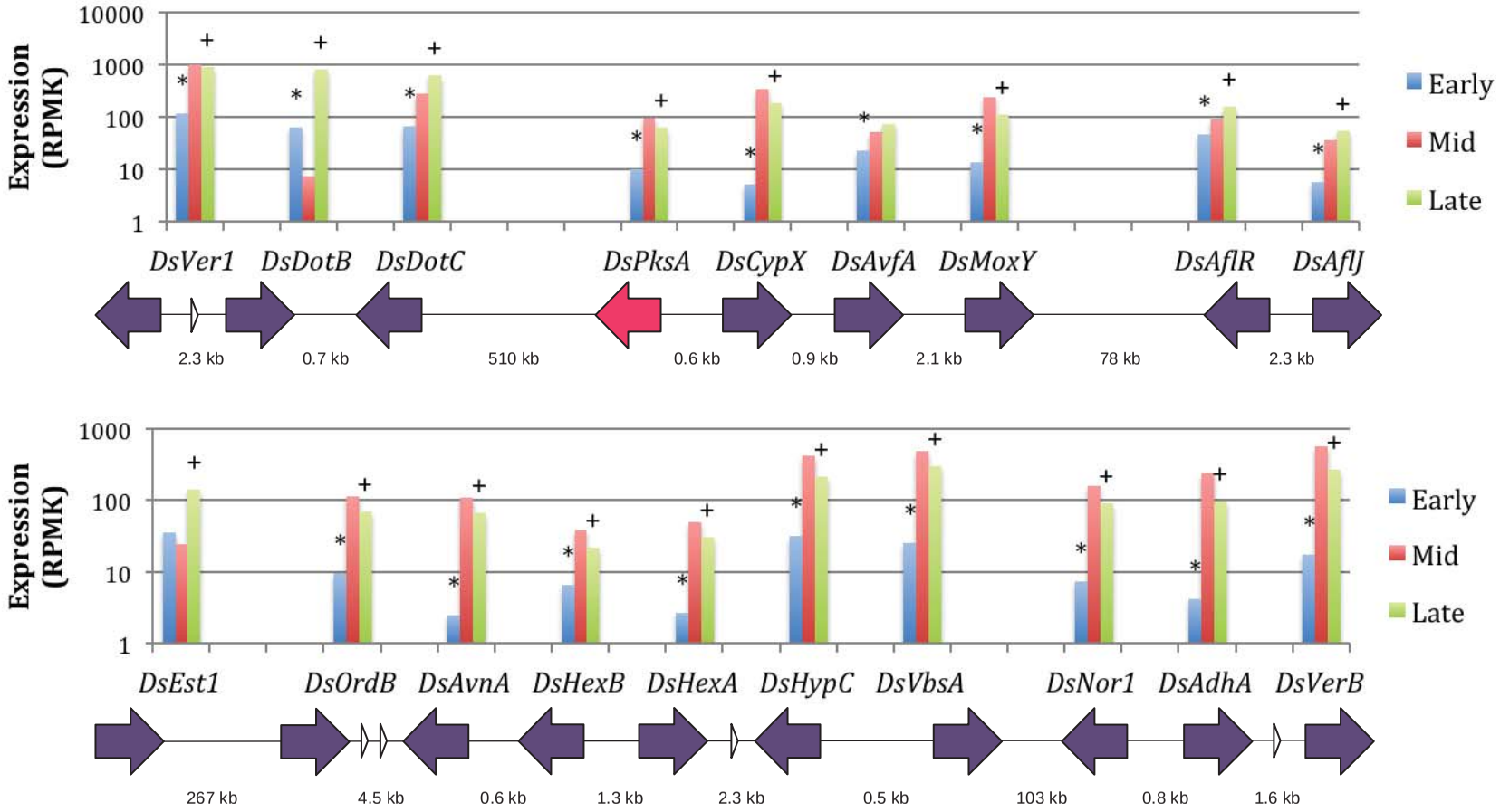

Figure 1.15. Organization and expression of dothistromin genes. Pink: Secondary metabolite core gene (*DsPksA*). Purple: Fragmented dothistromin cluster genes. Small white arrows: genes without predicted SM functions. Significant differences between early-mid and mid-late stages were marked with "*" and "+", respectively ($p<0.05$). The differences between early and late stages were also significant for all cluster genes. Figure adapted from Bradshaw et al. (2016).

1.5. Regulation of secondary metabolism

Secondary metabolism is generally a complex and resource-consuming process (Calvo et al., 2002). Therefore, SM production is under regulation to avoid unnecessary expenditure of energy and resources. SM regulation in filamentous fungi occurs in many different ways.

As explained in Section 1.4.5, fungal SM biosynthesis usually occurs through gene clusters. Many fungal SM gene clusters are regulated by transcription factors encoded by genes that are generally located near the genes involved in the SM biosynthesis. One well-known example of such regulatory transcription factors are the aflR proteins in sterigmatocystin, aflatoxin, and dothistromin biosynthesis (Section 1.4.5.1). AflR proteins are $Zn(II)_2Cys_6$ transcription factors that bind to palindromic DNA sequences within promoter regions of the biosynthetic cluster genes (Ehrlich et al., 1999; Fernandes et al., 1998). Elimination of *aflR* genes caused loss or decrease of sterigmatocystin, aflatoxin, and dothistromin production in the producing organisms (Yu et al., 1996; Chettri et al., 2013).

In addition to regulators within the gene clusters, SM production is also controlled in fungi using global regulators. One of the most commonly known global regulators of fungal secondary metabolism is a gene predicted to encode a methyltransferase named LaeA (loss of *aflR* expression) (Bok and Keller, 2004). After its first identification in *A. nidulans*, LaeA was studied extensively and its orthologs were found in many fungal species (reviewed by Jain and Keller, 2013). *LaeA* deletion mutants had decreased ability to produce many well-known fungal SMs such as sterigmatocystin, aflatoxin and gliotoxin (Bok and Keller, 2004; Amaike and Keller, 2009; Bok et al., 2005). LaeA is thought to regulate SM biosynthesis using chromatin-level modification (Strauss and Reyes-Dominguez, 2011). Another global regulator of fungal SMs is VeA (velvet). In *A. nidulans* VeA regulates SM gene clusters in response to light (Purschwitz et al., 2008) and interacts with other regulatory proteins such as LaeA (Sarikaya Bayram et al., 2010). Studies on *D. septosporum* showed that both DsLaeA and DsVeA are regulators of *D. septosporum* SMs (Chettri and Bradshaw, 2016; Chettri et al.,

2012). However, in contrast to their functionally characterised orthologs in *Aspergillus* spp., *DsLaeA* negatively regulates dothistromin biosynthesis (Chettri and Bradshaw, 2016) and DsVeA regulates SMs in a light-independent manner (Chettri et al., 2012).

Apart from the use of cluster-specific and global regulatory proteins, SM gene clusters are also regulated by environmental factors. These factors are carbon source, nitrogen source, temperature, pH, light, and salinity, as well as biotic challenges such as competing microorganisms (reviewed by Takahashi et al., 2013). Some environmental changes modify SM production by use of Cys_2His_2 zinc-finger proteins such as CreA for carbon signalling (Dowzer and Kelly, 1991) or AreA for nitrogen signalling (Hynes, 1975). Modification of environmental conditions is a common method to activate SM gene clusters that are otherwise silent in laboratory conditions, and such a modification was also attempted in this project which will be explained in Section 3.1.3.

The developmental stage of the fungus is also influential in SM production. This way, fungi can produce specific SMs in certain stages of their life cycle when they are most needed. The most common developmental process associated with fungal SM is sporulation (reviewed by Calvo et al., 2002). This is usually achieved using G–protein signalling pathways that regulate both developmental pathways and SM gene clusters (reviewed by Brodhagen and Keller, 2006).

1.6. Aims and Objectives

D. septosporum has 11 SM core genes and only one of them, *DsPksA* used in dothistromin biosynthesis, has been studied previously. Dothistromin is a virulence factor in DNB disease and its production involves an unusual fragmented gene cluster. This research focused on the other 10 SM core genes to define the whole set of *D. septosporum* SMs, and to determine if there are other DNB virulence factors or fragmented gene clusters jn addition to dothistromin.

Aim 1:

Define the complete set of SMs.

Objectives:

a) Determine the *D. septosporum* SM profiles by analysing the effects of different media conditions on *D. septosporum* metabolite production.
b) Confirm the SM core gene models that were predicted by the Joint Genome Institute (JGI) by aligning the protein sequences with close homologs and analysing RNA-seq data that were mapped to the gene models.
c) Assess evolutionary selection pressure on the SM core genes based on gene sequences from 19 *D. septosporum* strains.
d) Determine if there are functional orthologs of the SM core genes in other species by phylogenetic analysis.

Aim 2:

Make predictions about gene clusters associated with the SM core genes.

Objectives:

a) Identify the genes that might be involved in SM biosynthesis and in close proximity to the SM core genes, by searching for genes with similar predicted functions in known fungal SM gene clusters.
b) Determine if there are other genes required for biosynthesis of known SMs similar to the *D. septosporum* predicted SMs by comparing putative SM gene

clusters of *D. septosporum* with characterised gene clusters for the known SMs in other species.

Aim 3:

Identify potential virulence factors involved in Dothistroma needle blight.

Objectives:

a) Determine *in planta* expression levels of SM core genes by analysis of existing RNA seq data.
b) Mutate at least one SM core gene by targeted gene knock out.
c) Characterise the phenotype of the SM mutant(s) by comparing wild type and SM mutant(s) radial growth rate, sporulation rate, and virulence on pines.
d) Attempt to chemically characterise candidate virulence factor SMs.

2. Materials and Methods

2.1. Biological Materials

2.1.1. *Dothistroma septosporum* strains

Dothistroma septosporum wild type strain NZE10 (CBS128990) was isolated from an infected *Pinus radiata* needle in New Zealand, and is the strain that was sequenced by the Joint Genome Institute (http://genome.jgi.doe.gov/Dotse1/Dotse1.home.html). Other *D. septosporum* strains used and developed in this project are shown in Table 2.1.

Table 2.1 Strains of *D. septosporum* used in this project.

Fungal strain	Plasmid	Genotype	Reference
NZE10	-	Wild type	Barron (2006)
FJT96 (*ΔDsVeA* KO1)	pR297	NZE10/ *ΔDsVeA::hph*	Chettri et al. (2012)
FJT130 (*ΔDsLaeA* KO2)	pR324	NZE10/ *ΔDsLaeA:: hph*	Chettri et al. (2016)
FJT157 (*ΔDsNps3* KO1*)*	pR411	NZE10/ *ΔDsNps3:: hph*	This study
FJT158 (*ΔDsNps3* KO2*)*	pR411	NZE10/ *ΔDsNps3:: hph*	This study

hph: Hygromycin resistance gene (hygromycin B phosphotransferase)

2.1.2. *Escherichia coli* strains

E. coli Top10 (F– *mcr*A Δ(*mrr-hsd*RMS-*mcr*BC) Φ80*lac*ZΔM15 Δ*lac*X74 *rec*A1 *ara*D139 Δ(*ara leu*) 7697 *gal*U *gal*K *rps*L (Str^R) *end*A1 *nup*G) (Life Technologies, Carlsbad, CA, USA) was used for plasmid production and maintenance.

E. coli One Shot® *ccd*B Survival™ 2 T1^R cells (F$^-$*mcr*A Δ(*mrr-hsd*RMS-*mcr*BC) Φ80*lac*ZΔM15 Δ*lac*X74 *rec*A1 *ara*Δ139 Δ(*ara-leu*) 7697 *gal*U *gal*K *rps*L (Str^R) *end*A1 *nup*G *fhu*A::*IS2*) were used for production of Gateway® vectors (Life Technologies, Carlsbad, CA, USA) which contain a *ccdB* gene as a selection marker (Bernard & Couturier, 1992; Loris et al., 1999).

2.1.3. Plant material

Less than 1 year old *Pinus radiata* seedlings from families with different *D. septosporum* resistance levels were used for inoculation. Four different clones, named P1 to P4, were supplied from Scion, Rotorua, New Zealand and kept in the Massey University greenhouse.

2.2. Growth and maintenance of the biological cultures

2.2.1. Growth and maintenance of *E. coli*

Cells were grown in Luria Broth (LB) with shaking at 180 rpm or on LB agar (Appendix 1) plates at 37°C overnight.

LB agar plates were sealed with parafilm and stored at 4°C for short-term storage. *E. coli* cultures were mixed with 50% (v/v) sterile glycerol to a final concentration of 15% (v/v) and stored at -80°C for long term storage.

2.2.2. Growth, maintenance, and sporulation of *D. septosporum*

Inoculum for growth and sporulation of *D. septosporum* NZE10 was obtained by cutting the edge of an actively growing colony of *D. septosporum* in a rich medium named Dothistroma medium (DM) (Appendix 1), then grinding the mycelium using a sterile micro pestle in a microcentrifuge tube with 600 µL sterile MilliQ water. Then 200 µL of that suspension was spread onto DM, Dothistroma sporulation medium (DSM) (Appendix 1) or Pine needle minimal medium + Glucose (PMMG) (Appendix 1) plates or inoculated into 25 mL of DM or PMMG broth in 125 mL flasks, followed by incubation at 22°C for 7-15 days. Subculturing onto fresh DM plates was performed every 3 months for maintenance of the *D. septosporum* strains. For longer-term storage, sections of mycelia obtained by cutting the edge of actively growing colonies were ground up using sterile micropestles, and stored in 50% (v/v) glycerol at -80°C.

D. septosporum spores were obtained by preparing inoculum as above, then 200 µL of that suspension was spread onto DSM or PMMG plates and incubated at 22°C for 7 days. Approximately 2 mL sterile, double distilled water (ddH_2O) was added to the plates, spread with a sterile glass spreader and incubated for 10 minutes to facilitate spore release into the water. The spore suspension was then transferred to a sterile microcentrifuge tube.

For determination of the effects of different media conditions on *D. septosporum* metabolite profiles, variations of PMMG were produced with 3% glucose, 10 µM $FeSO_47H_2O$, and NH_4NO_3, as in Appendix 1 except: (a) 1% glucose, (b) no $FeSO_47H_2O$ (c) $(NH_4)_2SO_4$ as sole nitrogen source (d) KNO_3 as sole nitrogen source.

2.3. DNA extraction, purification, and quantification

2.3.1. Maxiprep fungal gDNA extraction

Genomic DNA from *D. septosporum* cultures grown in 5 mL DM in 25 mL flasks for 15 days was extracted using a protocol adapted from a Genomic DNA Mini Kit (Plant) (Geneaid, New Taipei City, Taiwan). First, the mycelia were harvested using a sterile funnel and nappy liners. Harvested mycelia were freeze-dried overnight and powdered in liquid nitrogen using a mortar and pestle, then transferred to microcentrifuge tubes. Afterwards, 400 µL of GP1 (Geneaid) buffer and 5 µL RNase A were added to the samples and vortexed. The samples were then incubated at 65°C for 10 minutes with vortexing every 3 minutes, followed by addition of 100 µL GP2 (Geneaid) buffer, vortexing and incubating in ice for 3 minutes. The samples were then transferred to filter columns in 2 mL collection tubes. The filter columns were centrifuged for 1 minute at 1000× g, and each eluate was mixed with 1.5 volumes of GP3 buffer containing isopropanol in a microcentrifuge tube. The samples were then vortexed immediately for 5 seconds and placed in GD columns in 2 mL collection tubes, centrifuged and the eluates were discarded. GD columns were washed first with 400 µL W1 buffer and then with 600 µL wash buffer containing ethanol, by centrifuging at 16,000 g for 30 seconds after adding each buffer and discarding the eluates. After washing, the columns were centrifuged for

3 minutes to dry the column matrix. The dry columns were transferred into clean microcentrifuge tubes, 100 µL elution buffer pre-heated to 65°C was added and the tubes were incubated for 5 minutes at room temperature. Finally, purified DNA was obtained by centrifuging the columns at 16,000 g for 30 seconds.

2.3.2. Miniprep fungal gDNA extraction

Miniprep gDNA extraction was performed for rapid collection of gDNA from numerous colonies to screen for mutant candidates. Genomic DNA from *D. septosporum* was extracted using a CTAB protocol adapted from Zhang et al. (2010). Small sections taken from the edges of growing *D. septosporum* colonies were transferred into microcentrifuge tubes. The sections were then crushed in 600 µL 2% CTAB buffer (Appendix 2) using a sterile micropestle, followed by incubation at 65°C for 10 minutes. After cooling to room temperature, 500 µL chloroform was added, vortexed and centrifuged at 16,200 g for 3 minutes. Then 400 µL of the supernatant was taken and mixed with 600 µL of chilled 96% ethanol (EtOH), inverted several times, and kept at –20°C for 20 minutes. The samples were then centrifuged at 16,200 g for 5 minutes; the pellets were air dried and resuspended in 35 µL TE buffer (Appendix 2).

2.3.3. Plasmid DNA extraction

Plasmid from overnight grown (16 hours) *E. coli* cultures (Section 2.2.1) were extracted using a High Pure Plasmid Isolation Kit (Roche) according to the manufacturer's protocol.

2.3.4. Agarose gel electrophoresis

Analysis of PCR products and gDNA was carried out by melting 0.7%-1.5% (w/v) agarose (Gold Bio, St Louis, USA) in 1x TBE buffer (Appendix 2) based on the molecular weight of the DNA sample. Gels were poured and run with 1x TBE buffer in a gel box (Bio-Rad, Hercules, CA, USA).

DNA samples were mixed with 6× loading dye (Appendix 2) and loaded onto the gel along with 1 Kb Plus DNA molecular size marker (Invitrogen, CA, USA). The electrophoresis was carried out at 80 volts for small (50 mL) gels and 40 volts for big (200 mL) gels, until the dye was approximately 2 cm away from the end of the gel. Afterwards, the gel was stained in ethidium bromide (EtBr) solution (1 µg/mL – Appendix 2) for 20 min, rinsed in ddH_2O, visualised with Gel-Doc™XR documentation system (Bio-Rad) and photographed with Image Lab™ software.

2.3.5. Agarose gel extraction of DNA

After agarose gel electrophoresis, specific PCR fragments or restriction digestion products were cut out from the gel using a sterile scalpel while visualizing on 365 nm UV transilluminator (Alpha Innotech, Johannesburg, S.A) and transferred to sterile pre-weighed microcentrifuge tubes. The DNA was then recovered from the agarose block using a PureLinkTM Quick Gel Extraction Kit (Invitrogen) according to the manufacturer's instructions.

2.3.6. Nucleic acid quantification

Quantification of PCR products and plasmid DNA was performed using a Nanodrop® ND-1000 UV-Vis spectrophotometer with software version 3.1.0 (Nanodrop Technologies Inc, Wilmington) according to the manufacturer's instructions. Quantification of gDNA samples was performed by using a Hoefer DyNA Quant 200 fluorometer (Amersham Biosciences, UK) according to the manufacturer's instructions.

2.4. Restriction endonuclease digestion

Restriction endonuclease (RE) digestion of DNA was done by mixing 20 units of a selected RE per 1 μg of DNA in a total volume of 50 μL according to the manufacturer's instructions. The reaction mixtures were incubated in an appropriate temperature overnight to digest the DNA samples. Since the restriction enzymes used in this project (EcoRV and SacI) could be heat-inactivated, the reactions were stopped by incubating the reaction mixtures at 65°C for 15 minutes.

2.5. *E. coli* transformation

2.5.1. Competent cell preparation

The protocol for competent cell preparation was adapted from Chung and Miller (1993). An isolated *E. coli* Top 10 colony (Section 2.2.1) was inoculated into 5 mL LB and incubated at 180 rpm, 37°C overnight. From this culture, 0.5 mL was inoculated into 50 mL LB in a 250 mL flask and shaken at 37°C until the OD_{600} was 0.45-0.6. The culture was chilled on ice for 10 minutes, and equally distributed between two sterile centrifuge tubes. These cells were then centrifuged at 5,320 g for 5 minutes at 4°C in an Eppendorf 5415R microcentrifuge (Eppendorf, Hamburg, Germany). After the supernatant was discarded, the cells were resuspended in 12.5 mL of chilled 0.1 M $CaCl_2$ and left on ice for 10 minutes. The cells were then centrifuged again using the same conditions, but this time resuspended in 1.25 mL of chilled 0.1 M $CaCl_2$. Finally, the cells were left on ice for a minimum of 30 minutes and either used for immediate transformation, or 133 μL of cells were mixed with 67 μL of 50 % glycerol/0.1 M $CaCl_2$ and kept at –80°C for long-term storage.

2.5.2. Transformation *E. coli* Top 10

Up to 5 µL of BP or LR reaction products (Sections 2.7.1 and 2.7.2), or approximately 10 ng (<1 µL) of target plasmid suspension was added to 200 µL of competent cells, and the mixture was chilled on ice for 30 minutes. Heat shock was applied by transferring the chilled mixture to 42°C for 2 minutes, followed by immediate chilling in ice for 2 minutes. To the mixture, 1 mL of LB was added and incubated at 37°C for 1 hour for the recovery of bacteria and expression of selection marker encoded by plasmid. From this cell suspension, 50, 100 and 200 µL volumes were spread onto plates of LB-agar containing 50µg/mL of the appropriate antibiotic such as spectinomycin for BP reaction products of OSCAR cloning, and incubated overnight at 37°C. For transformations with low expectancy of positive colonies such as BP or LR reaction products, the cells were pelleted at 10,000 g for 30 seconds. Then half of the supernatant was discarded, the cells resuspended in the remaining supernatant, and equally distributed over 3 plates then incubated at 37°C overnight.

2.6. Polymerase chain reaction (PCR)

2.6.1. Primer design

All primers were designed using Primer3 v2.3.4 (http://primer3.sourceforge.net /releases.php/) and synthesized by Integrated DNA technologies (Coralville, IA, USA). Primers were stored at 200 µM stock concentrations at -20°C and diluted to 5 µM before use. A list of all primers used in this study is in Appendix 3.

2.6.2. Standard PCR conditions

All PCR reactions were carried out in PCR tubes (Axygen, CA, USA) using an Eppendorf Gradient Mastercycler® (Eppendorf). PCR conditions were adjusted for the amplification of single specific amplicons by changing the annealing temperature according to the primer specificities and following the manufacturer's

specifications for the other parameters. Each PCR reaction was carried out in a 25 µL volume containing: 2.5 µL of 10× PCR buffer without Mg (200 mM Tris-HCl (pH8.4), 500 mM KCl), 1.5 mM $MgCl_2$, 200 µM dNTP, 0.2 µM of each primer, 1-20 ng of template, and 1 U of Platinum™ Taq DNA Polymerase (Invitrogen). Cycling conditions were 94°C initial denaturation for 5 minutes, then 30 cycles of reactions including 94°C denaturation for 30 seconds, annealing for decided annealing temperature for 30 seconds, and extension at 72°C set according to the amplicon size (1 minute/kb), with a final extension at 72°C for 10 minutes. For PCR reactions required in the construction of vectors, 1 U of Platinum® Taq DNA Polymerase High Fidelity was used (Invitrogen). PCR reactions using high fidelity enzyme were carried out in 50 µL volumes and the same constituents as above except the use of 5 µL 10× High fidelity PCR buffer (600 mM Tris-SO_4 (pH8.9), 180 mM $(NH_4)_2SO_4$) and 1.5 mM MgSO4.

2.6.3. Colony PCR for clone screening

For the confirmation of transformed *E. coli* clones, cells were collected from colonies using sterile tips and resuspended in 10 µL sterile water for single colony PCR. In case of large-scale screening, cells from up to 10 colonies were pooled in 50 µL sterile water. The cells were then boiled for 10 minutes and kept on ice for 2 minutes. Afterwards, the cells were centrifuged at 21,100 g for 1 minute and 1 µL of supernatant was used as template for PCR reaction.

2.7. Vector construction

One of the most common methods used in functional characterization of genes is the use of gene knockout (KO) mutants. In fungi, targeted gene replacement is achieved by homologous recombination (Weld et al., 2006). This requires transformation of fungi with a vector containing the same DNA sequences as the flanking regions of the gene of interest for recombination and a selectable marker to select the transformants (Figure 2.1). Two different methods for vector

preparation were used, Multisite GATEWAY® and One Step Construction of Agrobacterium Recombination-ready plasmids (OSCAR).

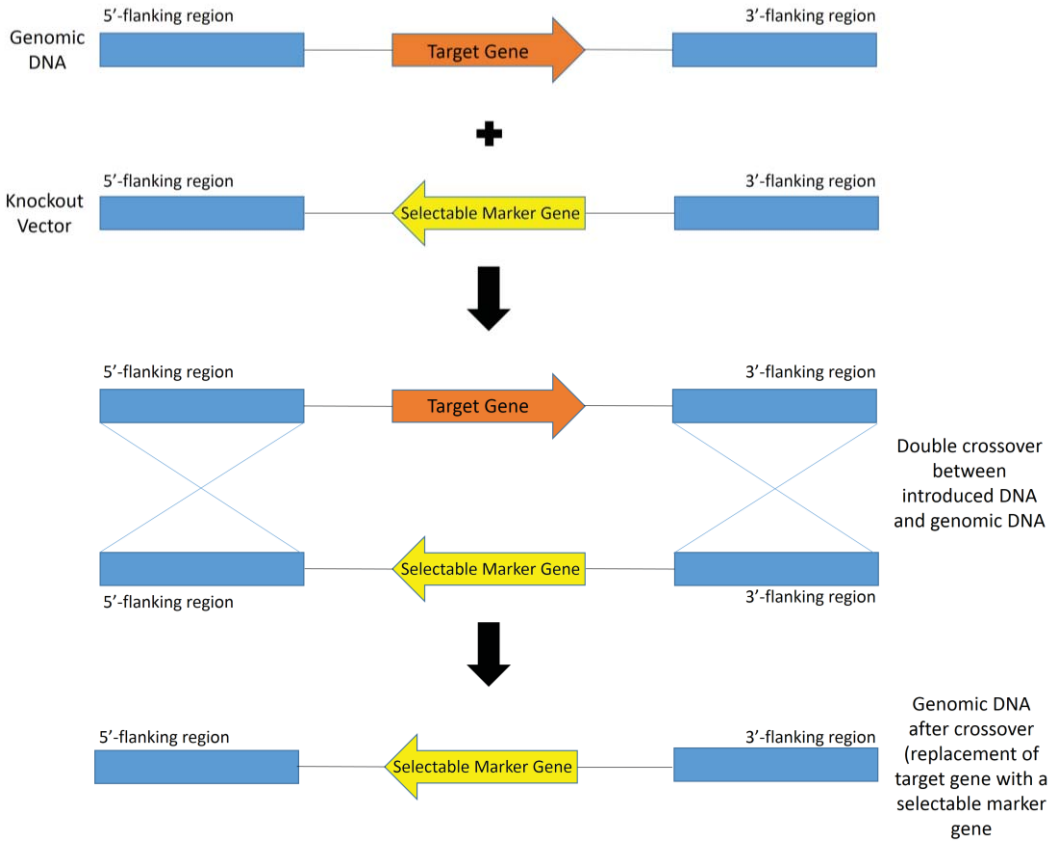

Figure 2.1. Schematic representation of homologous recombination for gene knockout preparation in fungi. Image adapted from http://www.rasmusfrandsen.dk/technologies.htm

2.7.1. Vector construction using GATEWAY

MultiSite Gateway® Technology is a cloning method based on the bacteriophage lambda site-specific recombination system (Bushman et al., 1985; Landy, 1989; Ptashne, 1992). Site-specific recombination between phage and *E. coli* occurs at specific sequences named *att* sites. Specific enzymes are required for these recombination events, and are provided in the GATEWAY system as BP clonase ™ II and LR Clonase ™ II Plus enzyme mixes (Landy, 1989; Ptashne, 1992).

An overview of GATEWAY vector construction is presented in Figure 2.2. The most important step for constructing vectors by MultiSite Gateway® Technology is to

design primers with appropriate *att* sites. Primers were designed so that *attB* sites of the PCR fragments recombined with *attP* sites of pDONR vectors after BP reaction, which lead to production of entry clones. For this project, the *DsPks2* KO construct was prepared using the GATEWAY method. All the reactions were carried out according to manufacturer's protocols with minor modifications. Donor vectors were prepared in 5 µL BP reactions.

The three entry clones pDONR™P4P1R, pDONR™221, and pDONRP2R-P3 then contained 5' flanking region of the target gene, selection marker gene (*hph*), and 3' flanking region of the target gene, respectively. The donor vector for the selectable marker gene was previously prepared (lab number: pR225). All donor vectors contained a kanamycin resistance gene. The constructs for 5' and 3' flanking sites were then transformed into Top10 *E. coli*, selected in LB-kanamycin (100 µg/ml) plates, recombinants confirmed by colony PCR using PKS2-73814-KO5F/ PKS2-73814-KO5R for 5' flanking donor vector and PKS2-73814-KO3F/ PKS2-73814-KO3R for 3' flanking donor vector and entry plasmids were extracted from the clones as described in section 2.3.3. A 5 µL LR reaction was then carried out by mixing all three entry clones, a destination vector pDEST™R4-R3 containing a different antibiotic (ampicillin) resistance marker and LR clonase in an overnight reaction. Finally, the construct was transformed as above, selected in LB-Ampicillin (100 µg/ml) and confirmed by PCR and sequencing.

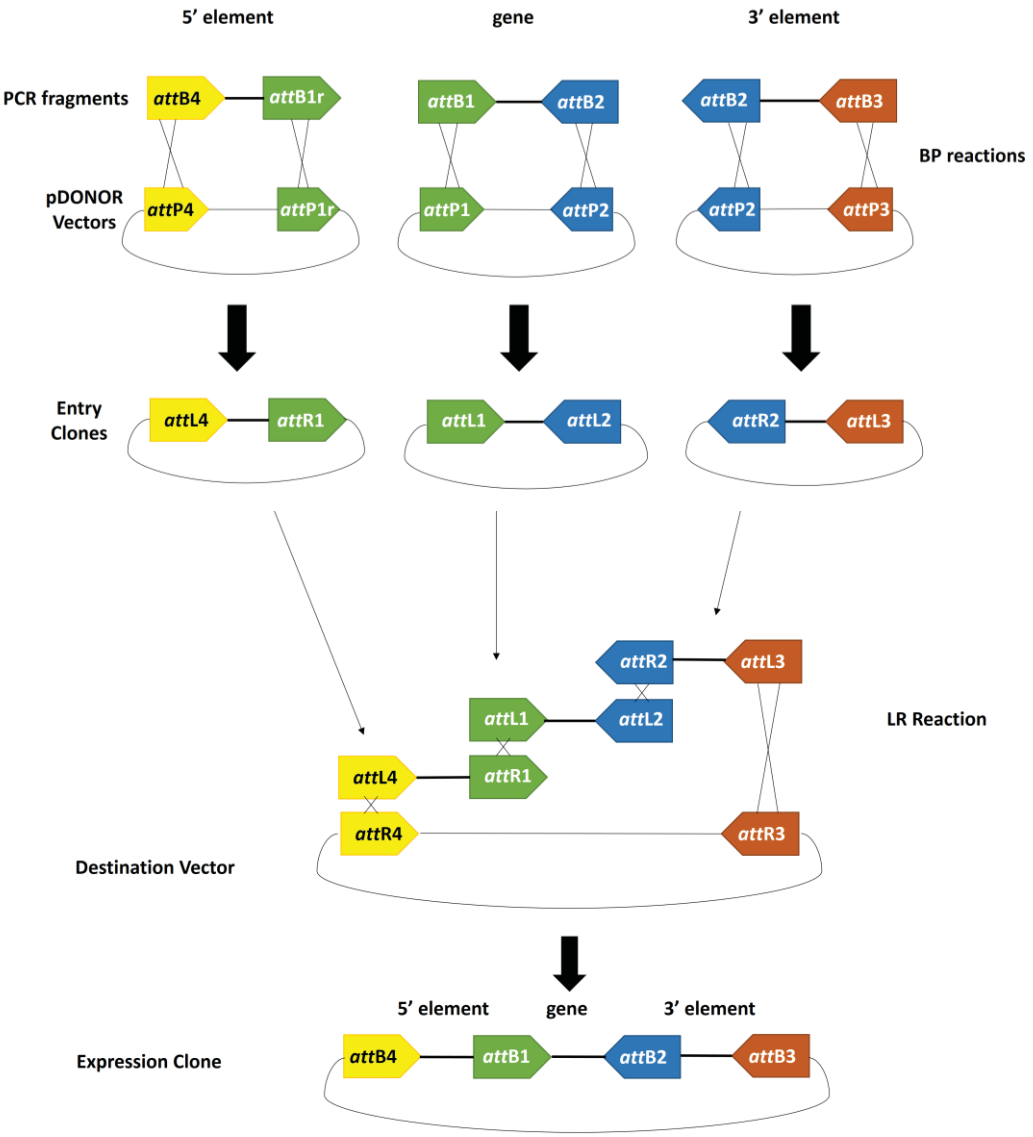

Figure 2.2. Overview of GATEWAY vector construction. Three PCR fragments containing *att*B sites recombine with pDONR vectors with attP sites to produce entry clones containing *att*L and *att*R sites. The three entry clones' *att*L and *att*R sites recombine during LR reaction to produce the knockout construct. Image adapted from Multisite Gateway® Three-Fragment Vector Construction Kit manual, Version G, 8 September 2008.

2.7.2. Vector construction using OSCAR

The One Step Construction of Agrobacterium-Recombination-ready-plasmids (OSCAR) methodology starts with amplification of flanking sites of the gene using primers each containing 5' extensions with different *att*B recombination sites, modified from the GATEWAY system. These PCR fragments are then mixed with specifically designed marker and binary vectors along with BP clonase, therefore generating the deletion construct in a single step (Figure 2.3). This deletion

construct is then used to replace the region in between the flanking sites with the hygromycin resistance gene.

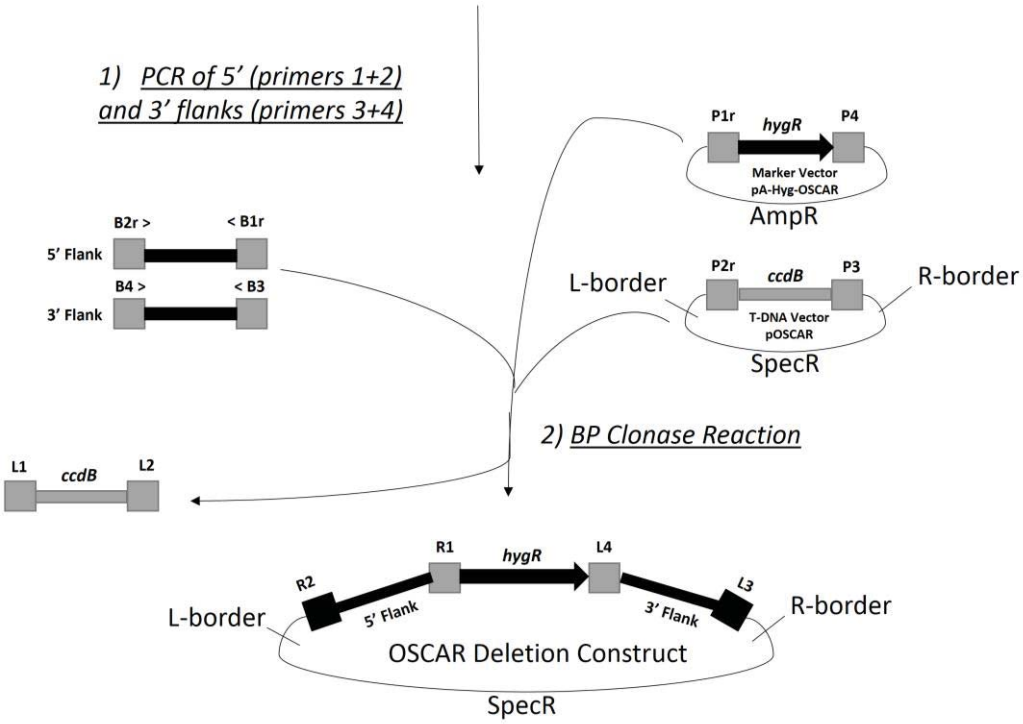

Figure 2.3. Overview of OSCAR knockout construct preparation. 5' and 3' flanking regions of the target sequence are PCR amplified, followed by BP clonase reaction of these PCR products with binary and selection marker plasmids pOSCAR and pA-Hyg-OSCAR plasmids, respectively. Recombination sites for this system include B1r & B2r for 5' flank PCR, B3 & B4 for 3' flank PCR, P2r & P3 for pOSCAR, and P1r and P4 for pA-Hyg-OSCAR. The final product was confirmed by PCR. Image from Paz et al. (2011).

One advantage of the OSCAR method over GATEWAY is the use of binary vectors which enable the use of *Agrobacterium tumefaciens* mediated transformation (ATMT). In addition, the OSCAR method requires only one cloning reaction (BP), while the GATEWAY method requires both BP and LR reactions. Therefore, the OSCAR method requires less time to prepare a knockout construct. Most importantly, one of the donor vectors for GATEWAY system, p4-P1R, was reported to have more than 2 X 10^4 fold increase in mutation rate compared to other vectors of the system (Kiedrowski, 2011), and this was one of the most common problems faced with GATEWAY in this project.

The protocol for Ds*Nps3*-pOSCAR KO construct preparation was adapted from Paz et al. (2011). Primer pairs used in PCR amplification of 5' and 3' flanking sites were

NPS3-5FP-attb2R/NPS3-5RP-attb1R and NPS3-3FP-attb4_domain/NPS3-3RP-attb3_domain, respectively (Appendix 3).

PCR reactions were carried out on *D. septosporum* NZE10 gDNA as outlined in Section 2.6, with initial optimization of Tm by gradient PCR with 2°C temperature intervals between 50°C-60°C for both the 5' and 3' flank primer pairs. Afterwards, high-fidelity PCRs were performed for both 5' and 3' flanking sites with 50 µL total volumes, 1 minute 8 seconds extension times, and 25 cycles. The PCR fragments were purified using a High Pure PCR Product Purification Kit (Roche Applied Science, Penzberg, Germany) according to the manufacturer's protocol and the concentrations were measured by NanoDrop® ND-1000 UV-Vis Spectrophotometer with software version 3.1.0 (Nanodrop Technologies Inc, Wilmington). The OSCAR reaction setup was prepared according to Paz et al. (2011), mixing 60 ng of each vector with 10 ng each PCR fragments as in Table 2.2.

Table 2.2. BP reaction setup for *DsNps3*-pOSCAR KO construct preparation.

	Amount (ng)	**Amount (µL)**
pOSCAR (243 ng/µL)	60	0.25
pA-Hyg-OSCAR (179 ng/µL)	60	0.33
5' flank site PCR product (23 ng/µL)	10	0.43
3' flank site PCR product (27 ng/µL)	10	0.37
BP Clonase™ II enzyme mix (5x)		1
TE Buffer		0.84
Water		1.78
Total		**5**

This reaction mixture was incubated at 25°C overnight, then terminated using 0.5 µL proteinase K (20 µg/µL), incubating at 37°C for 10 minutes. The products were then transformed into *E. coli* Top10 competent cells as outlined in Section 2.5, and approximately half of the colonies (~600 µL) were inoculated and selected in LB-spectinomycin (50 µg/mL). The following day, colony PCR was performed on 10 of the spectinomycin-resistant colonies using NPS3-5FP-attb2R/NPS3-3RP-attb3_domain primers at 58°C annealing temperature, 3 minutes extension time and 25 cycles.

2.8. DNA sequencing

Sequencing reactions of recombinant plasmids and PCR products were carried out at the Massey Genome service (Massey University, Palmerston North) using an ABI PRISM® BigDye® Primer Cycle Sequencing Ready Reaction Kit in an ABI 3730 DNA Analyzer (Applied Biosystems, Foster City, CA). For plasmid sequencing, 300 ng purified plasmid DNA was mixed with 3.2 pmol primer, and filled up to a total volume of 15 µL with sterile double distilled (dd) H_2O. PCR product sequencing was done by mixing 2 ng/100 bp of PCR product with 3.2 pmol primers and filling with ddH_2O to 15 µL. The sequences were analysed using Geneious version 8.0.3 (Kearse et al., 2012) and National Center for Biotechnology Information (NCBI) BLAST tools (http://blast.ncbi.nlm.nih.gov/ Blast.cgi).

2.9. *D. septosporum* transformation

Protoplasts were prepared based on the protocol of Yelton et. al. (1984). In 125 mL flasks, 25 mL liquid DM was inoculated as in Section 2.2.2, and incubated at 22°C for 7 days, shaking at 160 rpm. The mycelia were harvested using a sterile funnel and nappy liners, pooling 3 flasks. The mycelia were washed two times with 30 mL sterile water. The harvested mycelia were then washed with 10 mL OM buffer (Appendix 2), and transferred to a sterile flask. Glucanex 200G (Novozymes, Bagsværd, Denmark) was dissolved in 30 mL OM buffer at 10 mg/mL, then filter-sterilized (0.2 µm Minisart acrodisc), added to the pooled and washed mycelia and incubated at 30°C for 12-16 hours, shaking at 80-100 rpm. Protoplast formation was then confirmed under a Zeiss 47 06 00-9901 light microscope (Zeiss, Germany). The protoplasts were filtered through a nappy liner into sterile 15 mL Corex tubes at 5 mL/tube. ST buffer (2 mL) (Appendix 2) was added slowly to form a clear overlay, and then centrifuged at 3220 g for 7 minutes in A-4-62 rotor (Eppendorf). The protoplasts in the interface were removed carefully using a 200 µL pipette, and transferred into 15 mL Corex tubes (5 mL/tube). Five mL of STC buffer (Appendix 2) was added to wash, mixed gently, and then the samples were centrifuged at 3220 g for 7 minutes. This step was repeated three times, and then

the protoplasts were re-suspended in 0.5 mL STC buffer. The protoplast concentration was estimated using a haemocytometer, then diluted to 1.25 x 10^8 protoplasts/mL with STC buffer. Transformation was performed immediately to obtain the highest efficiency using procedures depicted in Vollmer and Yanofsky (1986) and Oliver et. al. (1987). Protoplasts (80 µL) were mixed with 20 µL of 40% PEG solution, and 5 µg of *DsPks2*-GATEWAY or *DsNps3*-pOSCAR knockout construct. In addition, the pA-Hyg-OSCAR plasmid, which contains the hygromycin resistance gene and the *TrpC* promoter, was used as a positive control, and empty protoplasts were used as negative control. The samples were vortexed briefly and left on ice for 30 minutes, then 900 µL of 40% PEG solution was added, mixed and incubated at room temperature for 20 minutes. 100 µL of each sample was mixed with 3.5 mL molten 0.8% Regeneration medium (RG) (Appendix 1) at 48°C and inoculated into 1.5% regeneration media (RG) plates as overlays. The plates were incubated overnight at 22°C, and then 5 mL 0.8% RG overlay containing hygromycin was added to a final antibiotic concentration of 70 µg/mL. The plates were incubated for 3 weeks at 22°C. Genomic DNA extraction was performed as detailed in Section 2.3.2.

2.10. Southern blotting and hybridization

2.10.1. Digoxygenin-11-dUTP (DIG) labeling of probes

DIG-labeled probes were prepared by using a PCR based method (Section 2.6), but with 200 µM of each dATP, dCTP, dGTP, 133 µM dTTP and 67 µM alkali-labile Digoxygenin-11-2'-deoxy-uridine-5'-triphosphate (Roche, Penzberg, Germany) in a 25 µL reaction volume.

Too high a probe concentration may cause significant background noise after hybridization. Therefore, optimum probe concentration was determined by preparing 5-fold serial dilutions of the probe with sterile ddH_2O, spotting 2 µL of each onto a Hybond-N+ membrane (GE Healthcare Ltd), and fixing the probe to membrane by using a UV crosslinker (Cex-800 UV crosslinker, Ultra-Lum Inc). Hybridization and detection procedures were done as described in Sections 2.10.3

and 2.10.4. The probe concentration with clear signal but low background was used for Southern hybridization.

2.10.2. Southern blot

In order to confirm integration site and copy number for *DsNps3* and *DsPks2* KO mutant candidates, Southern blot analysis was performed. First, gDNA belonging to the KO candidates and wild type *D. septosporum* were extracted (Section 2.3.1) and digested with restriction enzymes (Section 2.4). Then, the digested gDNA were separated by agarose gel (1%) electrophoresis at 40 V overnight, and visualized as in Section 2.3.4. The gel was then depurinated by gently agitating in Solution 1 (depurination) (Appendix 2) for 15 min. Afterwards, solution 1 was drained and the gel was agitated in solution 2 (denaturation) and solution 3 (neutralization) for 30 minutes each on an orbital shaker at room temperature.

The blotting apparatus was prepared by placing two layers of 3 MM Chromatography Papers (Whatman, Maidstone, UK) wet with 20× SSC buffer (Appendix 2) on top of a glass plate with both edges of the papers soaked in the 20× SSC buffer. A sheet of gladwrap was placed over the filter papers, and cut using a scalpel to leave a "window" approximately 1-2 mm smaller than the size of the gel. This prevents the flow of SSC by-passing the gel when the blot is assembled. A small amount of 20× SSC was poured on top over the top filter paper, and the gel was placed upside down on the paper. The gel was covered with 20× SSC, and a Hybond-N+ membrane (GE Healthcare Ltd) was placed on the gel. Three more layers of wet Chromatography Papers (Whatman, Maidstone, UK) were placed over the membrane by making sure there was no air bubble left between each of the layers. Finally, two stacks of paper towels and 500 g weight was placed on top of the apparatus and it was allowed to stand at room temperature overnight. The following day, the membrane was washed in 2× SSC buffer and air-dried. Before hybridization, the membrane was cross-linked with a UV crosslinker (Cex-800 UV crosslinker, Ultra-Lum Inc).

2.10.3. Hybridization of DIG labeled probe

The membrane from Section 2.10.2 was placed in a hybridization tube with DNA side facing inwards, and soaked in DIG Easy Hyb solution (10 ml/100 cm^2 of membrane; Roche, Penzberg, Germany) by rotating in a Bachofer hybridization oven at 45°C for 2 hours. This prehybridization step reduces background noise by blocking non-specific nucleic acid binding sites of the membrane. The probe was denatured in boiling water for 10 minutes, and then rapidly cooled on ice. The denatured probe, in a concentration determined by the method mentioned in Section 2.10.1, was added to the hybridization buffer, and rotated overnight at 45°C. Next day, the membrane was washed twice in washing solution 1 (Appendix 2) for 5 minutes in room temperature. Finally, the membrane was washed twice in washing solution 2 (Appendix 2) for 15 minutes at 68°C for a high stringency wash to allow only highly homologous sequences to remain bound by the probe. The hybridization buffer containing probes was stored at -20°C for later use if needed.

2.10.4. Signal detection

After hybridization and stringency washes, the signal was detected according to the instructions in DIG Application Kit Manual for Filter Hybridization (Roche). The membrane was washed in Buffer I (Appendix 2) for 2 minutes, and then incubated in 30 mL Buffer II (Appendix 2) for 30 minutes with shaking. Anti-Digoxigenin-AP antibody (Roche, Penzberg, Germany) was centrifuged at 16,200g for 5 minutes in order to avoid background that can be caused by small antibody aggregates, and added to buffer II in a ratio of 1:10,000, then the membrane was incubated for another 30 minutes with shaking. The membrane was washed for 15 minutes twice in 150 mL Buffer I with shaking, followed by equilibration for 5 minutes in Buffer III (Appendix 2). The membrane was placed in an A4 copy-safe pocket with DNA side facing up, and approximately 1 mL of CSPD® ready-to-use chemiluminescence substrate (Sigma-Aldrich, Missouri, USA) was applied to the membrane by gently spreading across the membrane without leaving bubbles. After incubating at 37°C for 10 minutes to activate the enzyme, the membrane was

exposed to X-ray film (Fuji film) for up to 3 hours. Finally, the film was developed using a 100 plus Automatic x-ray Processor (All Pro imaging).

2.11. Secondary metabolite extraction, detection, quantification

2.11.1. Extraction of metabolites

D. septosporum mycelia, grown as in Section 2.2.2, were separated from broth using an autoclaved funnel and nappy liners. For the determination of different media conditions (Section 3.1.3), metabolites from mycelia or 5 mL of broth were extracted by agitation at 180 rpm in 5 mL acetone or ethyl acetate (EtAc), respectively, for 3 days at 30°C in the dark.

For the solvent optimisation for Nps3 secondary metabolite detection (Section 3.2.3.6), metabolites were extracted from culture filtrate using one of three methods: 1) Ethyl acetate (EtAc), 2) chloroform then dichloromethane, or 3) dichloromethane then 1-butanol. Metabolites were extracted from mycelia using: 1) acetone, 2) dimethylformamide (DMF), then dimethyl sulfoxide (DMSO), then acetonitrile, or 3) Isopropanol, then ethanol (EtOH), then methanol (MeOH). Different solvents were used sequentially for methods 2 and 3 in each case in order to visualise the broadest spectrum of metabolites on each TLC plate compared to the use of a single solvent. Due to the limited availability of water-insoluble solvents with high polarity, fewer solvents could be used for the analysis of culture filtrates compared to mycelia.

Following extraction of metabolites from mycelia and culture filtrates with agitation in the organic solvents, the mixtures were centrifuged at 5320 g for 5 minutes and the organic solvents were separated from the mycelia or broth. From the metabolite-containing solvents, an amount between 200 µL to several mL as required was transferred and vacuum dried using a rotary evaporator (Watson Victor, Australia) or transferred to a microcentrifuge tube and left to dry in a fume hood overnight. The dried metabolites were resuspended in 20 µL acetone or ethyl acetate.

2.11.2. Thin Layer Chromatography (TLC)

For the analysis of *D. septosporum* secondary metabolites, TLC analysis was performed by using TLC Silica Gel 60 plates (Merck, NJ, USA). To determine the effects of different growth media on SM profiles, 200 µL of the metabolites prepared as in Section 2.11.1 were used. For comparison of SMs extracted from the *ΔDsNps3* and wild type *D. septosporum* strains, the amounts of SM extracts loaded onto the TLC were normalized based on dothistromin levels in the samples estimated by measuring intensity of TLC bands using Gel-Doc™XR documentation system (Bio-Rad) after one round of preliminary TLC. The TLC was performed in a glass chamber with 1 cm depth of 60:40:0.1 toluene:acetone:formic acid solvent until the mobile phase had moved 18 cm. The TLC plate was then removed from the glass chamber and air dried in the dark in a fume hood. Finally, the TLC plate was visualized on a UV transilluminator (Alpha Innotech) and photographed using a Nikon D7000 camera with an AF Micro Nikkor 60mm f2.8 lens at the Manawatu Microscopy and Imaging Centre (MMIC).

2.12. Phenotypic characterization of WT and *ΔDsNps3 D. septosporum*

2.12.1. Pathogenicity assay

The pine seedling inoculation method was adapted from Kabir et al. (2013). For the pathogenicity assay, wild type, *ΔDsNps3* KO1 and *ΔDsNps3* KO2 *D. septosporum* spores were prepared as in Section 2.2.2. Spore numbers and morphology assessments were performed using a Zeiss 47 06 00-9901 microscope and their concentrations determined using a haemocytometer.

The spores were diluted to 2 x 10^6 spores/mL with sterile ddH_2O. Four replicate pine seedlings that are susceptible to *D. septosporum* with varying resistance levels, named P1-P4 (Section 2.1.3) were inoculated with approximately 30 mL spore suspension for each strain, using a McGregor's Pressure Sprayer. However, only two seedlings (C and D) could be inoculated with *ΔDsNps3* KO1 due to insufficient spores. After the needles were air-dried, the individual seedlings were

covered with plastic autoclave bags and placed in 90 L plastic containers (39.5 cm x 69 cm x 45 cm) containing approximately 20 L distilled water in which two misters were immersed to provide high moisture throughout the chamber (Kabir et al., 2013). The plastic containers were also covered with a frame covered with plastic wrap, with a small opening on the top to adjust moisture. The individual covers on the seedlings were removed after one week and the positions of the plants within each plastic box were rotated clockwise every 3-4 days to facilitate even light and moisture distribution. The experiment was conducted in natural light conditions.

The needles were harvested from the seedlings at 18 weeks post-inoculation (wpi). The lesions were then identified and counted using a Leica MZ10F binocular microscope (Leica Microsystems, Germany) fitted with a Leica DFC 450C digital camera using Leica Application Suite (LAS) v3.8, then measured. The number of lesions used in this experiment is shown in Table 3.6.

2.12.1.1. Surface hyphal network determination

For the determination of the extent of surface hyphal network on wild type and *ΔDsNps3 D. septosporum* infected pine needles, two random needles from the top, middle and bottom of each tree each were picked at 15 days post inoculation (dpi) and soaked in absolute ethanol until use. The needle sections were cut longitudinally and soaked in solution A (1:3 acetic acid: ethanol) overnight, followed by solution B (1:5:3 acetic acid: ethanol: glycerol) for 3 hours with shaking at 180 rpm. Using a method adapted from Mehrabi et al., (2006), the cleared needle sections were stained in 0.01% trypan blue in lactophenol (40% glycerol, 20% lactic acid, 20% phenol in ddH_2O) in a microcentrifuge tube for 15 minutes in boiling water, and destained in saturated aqueous solution of chloral hydrate (VWR International, PA, USA) (5:2, wt/vol) overnight. The stained needle sections were then stored in 87% glycerol at room temperature. Trypan blue stained samples were visualised using a fluorescence microscope. First, needle sections were mounted on microscope slides in 87% glycerol. Then, analysis was performed by using an Olympus BX51 fluorescence microscope (Olympus

Corporation, Japan) fitted with Qimaging micropublisher 5.0 RTV. Fluorescence of trypan blue stained hyphae was done using a triple filter with excitation ranges at 380-400 nm, 475-490 nm, 540-565 nm and with emission ranges at 455-470 nm, 510-530 nm, 590-620 nm, respectively. The images were taken using Q-Capture Pro7 and processed using ImageJ (Schneider et al., 2012).

2.12.1.2. Biomass estimation

Standard curve analysis and estimation of fungal to plant biomass ratio were done using qPCR. qPCR reaction mixes were prepared using SensiFAST™ SYBR No-ROX Kit (Bioline Reagents, UK) according to the manufacturer's instructions and reactions were carried out in LightCycler® 480 (Roche). *D. septosporum AflJ* (target gene) and *P. radiata* cinnamyl alcohol dehydrogenase (*CAD*) (reference gene) primer pairs (Appendix 3) were used to determine fungal and plant biomasses, respectively. First, serial dilutions of *D. septosporum* (10, 2, 0.4, 0.08, 0.016, 0.0032, 0.00064 ng/µL) and *P. radiata* (50, 10, 2, 0.4, 0.08, 0.016, 0.0032 ng/µL) pure gDNAs in ddH_2O were made in order to prepare standard curves. In three technical replicates, 2 µL of gDNA suspensions were mixed with 8 µL reaction mix and 50 cycles of PCR reactions were carried out (5 sec at 95 °C, 10 sec at 60 °C and 20 sec at 72 °C) with a detection temperature of 72 °C. The cycle number in which the fluorescence could be distinguished from background for the first time is the cycle threshold (Ct) value. A standard curve was prepared by plotting the logarithm of the 5-fold serial dilutions of fungal and plant gDNAs against the Ct values.

For the estimation of fungal to plant biomass ratio, Dothistroma disease lesions harvested from needles at 18 wpi (Section 2.12.1) were cut and freeze-dried. Then, gDNAs were extracted from these lesions using a Genomic DNA Mini Kit (Plant) according to the manufacturer's specifications. The relative amounts of fungal to plant biomass in each sample were calculated from the results of qPCR amplification of fungal (*AflJ*) and plant (*CAD*) genes in that sample using RealQuant® version 1.1.1 (Roche). For each of the technical replicates, *ΔDsNps3* to wild type estimated biomass ratios were calculated separately and their averages and standard deviations were used in the results.

2.12.2. Sporulation rate analysis

D. septosporum wild type and *ΔDsNps3* spores in DSM were harvested as in Section 2.2.2 and diluted to 10^6 cells/mL. From these, 100 µL were inoculated into each of three replicate PMMG plates. After 1 week of growth in the dark, 2 mL sterile ddH_2O was added to each plate, spread with a sterile glass spreader and incubated for 10 minutes to enable the release of the spores. Afterwards, the spore-containing water was transferred to a microcentrifuge tube using a sterile glass spreader and 1 mL sterile pipette. Finally, the spore concentrations were estimated using a haemocytometer by counting two technical replicates for each spore suspension.

2.12.3. Radial growth rate analysis

From *D. septosporum* wild type, *ΔDsNps3* KO1 and KO2 7 day old cultures grown in DM, two 5 mm diameter agar plugs with mycelia were extracted using a sterile cork borer and transferred to each of four replicate DM plates for each strain. Horizontal and vertical colony diameters were measured every 3 days for 30 days.

2.13. Statistical analyses

Sporulation, radial growth rates, and estimated biomass ratios of wild type and *ΔDsNps3* were compared with student's t-test using Microsoft Excel to test the hypothesis that there was no difference between wild type and *ΔDsNps3* strains at $p \leq 0.05$. For the statistical analysis of the effects of different media conditions, multiple t-tests at $p \leq 0.05$ were corrected with the false discovery rate (FDR) approach using a two-stage linear step-up procedure to determine which p values are small enough to investigate further (Benjamini and Hochberg, 1995; Benjamini et al., 2006). For all the statistical analyses, $p \leq 0.05$ was assumed significant.

2.14. In silico analyses

2.14.1. Domain analysis

Domain predictions were made using PKS/NRPS Analysis Web-site (http://nrps.igs.umaryland.edu) and confirmed by using Structure Based Sequence Analysis of Polyketide Synthases (SBSPKS) (http://202.54.249.142/~pksdb/sbspks/search_pks_nrps.html), and NCBI domain finder (http://www.ncbi.nlm. nih.gov/Structure/cdd/wrpsb.cgi).

2.14.2. Secondary metabolite product prediction

SM product predictions were made based on Bradshaw et al. (2006) and de Wit et al. (2012) (Table 3.1) or Natural Product Domain Seeker (NaPDoS) analysis (http://napdos.ucsd.edu/run_analysis.html) which predicts based on comparing KS or C domains of PKS and NRPSs with reference genes from well-characterised chemical pathways.

2.14.3. Phylogenetic analyses

For the phylogenetic analyses of DsPks1, DsPks2, and DsNps3, best FASTA hits (Pearson and Lipman, 1988) were obtained from each of the species belonging to all fungi from the Dothideomycetes, Eurotiomycetes, and Sordariomycetes classes within the JGI MycoCosm database (Grigoriev et al., 2012). Sequences that were also confirmed by best reciprocal FASTA hit back to the *D. septosporum* NZE10 protein models were selected with the help of Dr Pierre-Yves Dupont (Massey University). Initial phylogenetic trees of DsPks2 were built by aligning DsPks2 and its best reciprocal BlastP hits of Dothideomycetes and *Aspergillus* spp. in the JGI database with ClustalW algorithm (Thompson et al., 1994) using full protein sequences, KS domains or KS+AT domains, and by building phylogenetic trees using a neighbour joining method (Saitou and Nei, 1987) in Geneious v8.0.3 (Kearse et al., 2012). The support of the branches was computed using the

bootstrap method with 10000 replicates. Only branches showing a minimum 50% bootstrap support were kept in the final tree.

In order to obtain more reliable phylogenies, the final phylogenetic tree of DsPks2 as well as phylogenetic trees of DsPks1 and DsNps3 were built by aligning the amino acid sequences using the Fast Fourier Transform (MAFFT) multiple alignment program with the E-INS-I set of parameters which is the recommended method for aligning sequences that vary a lot (Katoh et al., 2005). Phylogenetic trees were built using the maximum likelihood method as in PhyML software with default parameters (Guindon et al., 2010). The phylogenetic trees were visualized and coloured with ETE3 toolkit (Huerta-Cepas et al., 2016).

Color-coding of the final phylogenetic trees was done by Dr Pierre-Yves Dupont with scripts available on request. Details of the genome sequences used in all phylogenetic analyses are presented in Appendix 23.

2.14.4. Comparison of SM core genes from 19 strains of *D. septosporum*

Nucleotide sequences of the SM core genes were aligned using MUSCLE (Edgar, 2004) in Geneious v8.0.3 (Kearse et al., 2012) with a maximum of 8 iterations. Positive and negative selections on the SM core genes were determined by Andre Sim using dN/dS ratios calculated using CodeML which is part of Phylogenetic Analysis by Maximum Likelihood (PAML) (Yang, 2007). Parameters for PAML were runmode = -2, seqtype=1, CodonFreq=0, model = 0, NSsites=0, icode =0, fix_kappa=1, kappa=1, fix_omega = 0, omega = 0.5. Codons under statistically significant positive selection were detected using a sitewise likelihood-ratio (SLR) method by Dr Pierre-Yves Dupont (Massingham and Goldman, 2005). First, a phylogenetic tree of the *D. septosporum* strains was built based on a concatenation of all SNPs present in the 19 *D. septosporum* genomes. The concatenation process produced a multiple sequence alignment. The phylogeny was then rebuilt using PhyML with its default parameters for a nucleotide tree. The tree was then used as a base for the computation of the selection profiles with the SLR method.

2.14.5. Gene cluster analyses

For the gene cluster analysis, 20 genes upstream and downstream of each SM core gene were selected and their functions were predicted by a combination of GO terms analysis of *D. septosporum* NZE10 gene sequences from Bradshaw et al. (2016) and manual InterProScan analysis (Jones et al., 2014). Genes predicted to be part of the putative gene clusters were determined by submitting 20 protein sequences upstream and downstream of the SM core gene together onto antibiotics & Secondary Metabolite Analysis SHell (antiSMASH) (Weber et al., 2015) and by searching the literature for genes with similar predicted functions in other SM gene clusters.

3. Results and Discussion

3.1. Secondary metabolites in *Dothistroma septosporum*

3.1.1. Overview of *Dothistroma septosporum* secondary metabolite genes

D. septosporum SM genes were identified as a result of two separate studies (Bradshaw et al., 2006; de Wit et al., 2012). The PKS core gene for the biosynthesis of dothistromin, a toxin similar to an aflatoxin precursor, was identified by Bradshaw et al. (2006) and named *DsPksA*, indicating similarity to the orthologous aflatoxin PKS gene. The other *D. septosporum* SM core genes were identified in the genome sequence by de Wit et al. (2012), and these genes were named with numbers such as *DsPks1* and *DsNps2* based on the convention for Dothideomycete genes. There are five PKS genes, three NPS, two HPS and one DMA gene present in *D. septosporum* (Table 3.1).

An overview of *Dothistroma septosporum* SM genes was prepared to summarize the key information about each gene including analyses of the predicted JGI gene models to determine their accuracy, and predictions of gene product types in order to determine the possible functions of the corresponding SMs (Table 3.1).

Table 3.1. Complete list of predicted *Dothistroma septosporum* NZE10 secondary metabolite core genes.

Gene[a]	JGI protein ID	Scaffold	Position in scaffold/direction[b]	Number of introns	aa number	Domains[c]	PKS/NPS type[d]	Predicted pathway product type[e]	JGI gene model correct[f]	*C. fulvum* orthologs[g]
PksA	48345	12	597907-605210 (-)	2	2399	SAT-KS-AT-ACP-ACP-ACP-TE	Type 1/NR-PKS	Dothistromin	Yes	*PksA*: 194256
Pks1	47338	10	127527-134096(+)	0	2189	SAT-KS-AT-ACP-ACP-TE	Type 1/NR-PKS	Melanin/ elsinochrome	Yes	*Pks1*: 191425
Pks2	73814	8	910134-918249(+)	10	2507	KS-AT-DH-ER-KR-ACP	Type 1/HR-PKS	Fumonisin	Yes	
Pks3	90367	8	974279-982774(-)	10	2126	KS-AT-DH-ER-KR	Type 1/HR-PKS	Epothilone	No	
*Pks4**	72190	5	2140446-2146542(-)	1	421	Pseudogenised			-	
Nps1	52251	3	2664965-2682846(+)	2	5888	C-A-T-C-A-T-C-A-T-C-A-T-C-A-T-C	Multimodular	Cyclosporin	Yes	
Nps2	90481	8	1338920-1353680(-)	2	4883	A-T-C-A-T-C-T-C-A-T-C-T-C-T-C	Multimodular	Siderophore	Yes	*Nps2*: 193954
Nps3	71189	4	1327192-1335024(+)	0	2610	A-T-C-A-NM-T	Multimodular	Cyclosporin	Yes	
Hps1	180045	11	965798-977722(+)	0	3974	KS-AT-DH-CM-KR-C-A-T		Compactin/ Bacitracin	Yes	
Hps2	157678	9	914615-927111(-)	7	4029	KS-AT-DH-CM-KR-T-C-A-T		Compactin/ Tyrocidine	Yes	
Dma1	28625	11	963990-965313(-)	1	420	N/A		N/A	N/A	

[a] Gene names as shown in JGI (http://genome.jgi.doe.gov/Dotse1/Dotse1.home.html). PKS: polyketide synthase, NPS: non-ribosomal peptide synthetase, HPS: hybrid PKS/NRPS, DMA: dimethylallyl tryptophan synthase

[b] Position (nt) of predicted gene in scaffold according to JGI.

[c] Predicted domain structures of the SM core gene proteins (Section 2.14.1). SAT: starter unit acyl-carrier protein transacylase, KS: keto-synthase, AT: acyltransferase, ACP: acyl carrier protein, TE: thioesterase, DH: dehydratase, ER: enoylreductase, KR: ketoreductase, C: condensation, A: adenylation, T: thiolation, NM: N-methyltransferase, CM: C-methyltransferase.

[d] Types of PKS and NRPS based on predicted domain structures. NR-PKS: Non-reducing PKS, HR-PKS: Highly reducing PKS.

[e] Predicted pathway product types based on NaPDoS analysis or previous studies (Section 2.14.2). *DsDma1* is adjacent to and divergently transcribed from *DsHps1*, therefore might be part of the same SM cluster (Sections 3.1.2 and 3.4.1.3).

[f] Gene model is correct according to this study.

[g] *C. fulvum* orthologs of *D. septosporum* SM core genes based on de Wit et al. (2012); numbers shown are JGI protein IDs.

* Indicates a pseudogene.

The results presented in Table 3.1 show that proteins encoded by all *D. septosporum Pks* genes, like most fungal PKSs, are type 1, among which *DsPksA* and *DsPks1* are non-reducing while *DsPks2* and *DsPks3* are highly reducing polyketide synthases. All proteins encoded by *D. septosporum Nps* genes are multimodular, containing repetitive A, T, and C sites, but it is not yet known whether each domain is used once or multiple times. *D. septosporum* has one gene predicted to encode an indole alkaloid dimethylallyl tryptophan synthase (*DsDma1*), and this gene is adjacent to *DsHps1*. Therefore, analyses on *DsDma1* were done together with *DsHps1* in Section 3.4.1.3.

Among *D. septosporum* SM core genes, *DsPksA* is the only characterised and extensively studied one, responsible for the biosynthesis of dothistromin (Bradshaw et al., 2006; Zhang et al., 2007; Schwelm and Bradshaw, 2010; Chettri et al., 2013). In addition to *DsPksA*, *DsPks1* and *DsNps2* also have *C. fulvum* orthologs, and these are predicted to be involved in melanin and siderophore biosynthesis respectively (de Wit et al., 2012). The predictions for other *D. septosporum* SM core genes are less certain. Their predicted pathway product types were based on KS domain amino acid sequences for PKS, and C domain amino acid sequences for NPS, by using Natural Product Domain Seeker (NaPDoS) (Ziemert et al., 2012), which estimates what type of SM might be associated with these domains (Section 2.14.2). For example, NaPDoS analysis of DsPksA predicts the pathway product as aflatoxin, which is a close prediction as dothistromin is structurally similar to an aflatoxin precursor, versicolorin B (Bradshaw et al., 2006). The actual SM types may be different from the predictions because of two main limitations. First, NaPDoS prediction is based only on one domain in the core gene and does not take into account the genes within the possible gene cluster (Section 1.4.5). The other limitation is that the prediction is based on a database of known SMs, and therefore limited to the SMs within the database. Therefore, true identification of the *D. septosporum* SMs requires extraction of metabolites and chemical analysis. Predictions for the pathway products of the hybrid PKS-NPS genes *DsHps1* and *DsHps2* have two different SM types as the analysis tool can only predict PKS or NRPS using KS or C domains respectively, and Hps have both of these domains.

3.1.2. Expression *in planta*

To help determine if any of the *D. septosporum* SMs might have a role in the disease process, expression *in planta* was assessed. During this project, transcriptome analysis at early (hyphal surface network and early penetration), mid (early lesion) and late (sporulating lesion) stages of infection on *Pinus radiata* needles was carried out (Bradshaw et al., 2016) (Figure 1.3a). As a result of transcriptome analysis, more than three million reads were obtained, the majority of which belonged to the plant host. From early to late stage of infection, the ratio of fungal reads over plant reads increased from 0.1% to 17.1% (Table 3.2) (Bradshaw et al., 2016). This showed that there was a rapid increase in the percentage of fungal reads between mid to late stages, which was consistent with a high rate of biomass increase during the course of infection at this stage (Kabir et al., 2015).

Table 3.2. Percentage of fungal reads *in planta* during early, mid, and late stages of infection.

Stage of infection	Fungal reads % of total
Early	0.1
Mid	0.5
Late	17.1

Data obtained from Bradshaw et al. (2016).

Genome-wide expression analysis of *D. septosporum* during the infection process has given insight into many aspects of the fungus and the plant-fungus interactions, but the main focus in this project was the expression of secondary metabolism genes during infection (Figure 3.1).

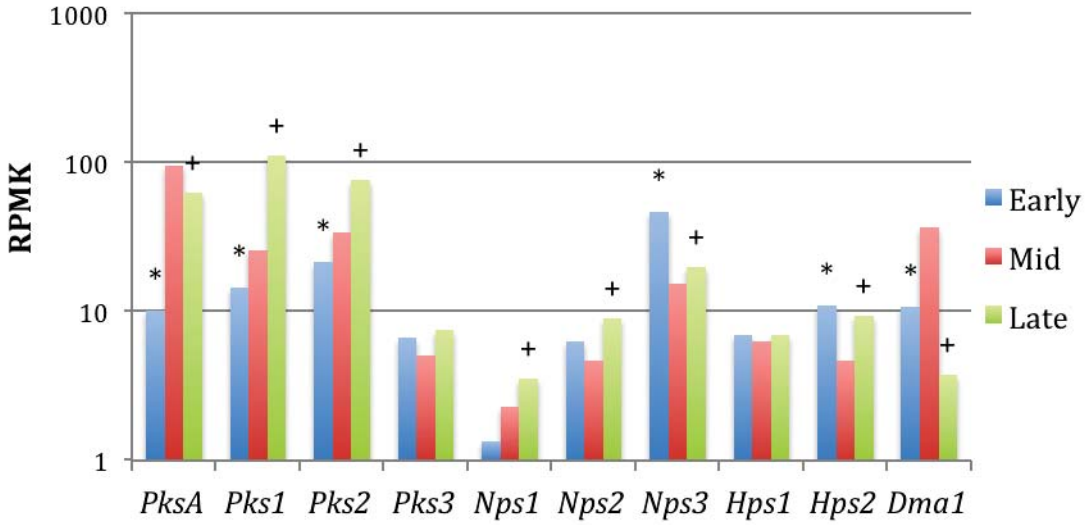

Figure 3.1. Expression of core SM genes in *D. septosporum* during early, mid, and late stages of infection. RPMK: Fungal reads per million per kilobase. Significant differences ($p<0.05$) between early-mid and mid-late stages are marked with "*" and "+", respectively. The differences between early and late stages were all also significant ($p<0.05$) except for *DsHps1* and *DsHps2*. The gene expression levels could not be validated by qRT-PCR because of the low fungal read proportions for early- and mid-stages of infection.

The analysis of expression data requires setting a threshold for identifying background expression. Since *DsPksA* is known to be involved in production of dothistromin with the expression level represented by approximately 100 RPMK, expression levels of the other SM core genes less than 10% of that of *DsPksA* (i.e. 10 RPMK) were considered to have background-level expression that is most likely not biologically relevant. In cases where higher levels of gene expression are seen, the stage where a SM core gene is most highly expressed can be crucial in determining the possible role of its gene product. In the hemibiotrophic plant pathogens *Colletotrichum orbiculare* and *C. higginsianum*, most of the key SM genes were highly expressed at pre-penetration and biotrophic stages of infection (O'Connell et al., 2012; Gan et al., 2013). Since *DsPks4* is a non-functional gene (Table 3.1), it was not included in the expression analysis. Among the other 10 core SM genes of *D. septosporum*, only *DsNps3* had significantly higher expression level at early stage compared to both other stages, while *DsHps2* expression level at early stage was significantly higher than that of mid stage, but not than that of late stage. These results suggest a possible role for *DsNps3* and *DsHps2* in the biotrophic phase of infection. In addition, *DsPksA* and *DsDma1* were expressed at a significantly higher level at mid stage and *DsPks1* and Ds*Pks2* had significantly

higher-level expressions in late stage compared to the other stages. Therefore, it is possible *DsPksA*, *DsPks1*, *DsPks2* and *DsDma1* might have a role in the necrotrophic phase of infection. *DsPks3*, *DsNps1*, *DsNps2* and *DsHps1* were expressed at a very low level and below the threshold RPMK value; therefore they might not have a role during plant infection. Among *D. septosporum* SM genes, the genes with highest expression at early and late stages, *DsPks1*, *DsPks2* and *DsNps3*, were mainly focused in this project, and *DsNps3* was selected for functional analysis.

3.1.3. Effects of media conditions on secondary metabolism

Fungal secondary metabolite production is usually a complex and energy-exhaustive process (Calvo et al., 2002). Therefore, the SM production is generally tightly controlled to avoid resource consumption where it is not beneficial (Gacek and Strauss, 2012). Expression of *D. septosporum* SM core genes were analysed not only *in planta*, but also in culture (Bradshaw et al., 2016). Apart from *DsPksA*, *DsPks1*, *DsPks2*, and *DsNps3*, expression of *D. septosporum* SM genes were lower than the threshold value, 10 RPMK, under rich media conditions (DM).

Production of SMs in fungi can be altered by many biotic and abiotic factors (Section 1.5). In this project, carbon and iron availability as well as nitrogen source were selected as modification targets to determine if any changes occurred in the SM profiles of *D. septosporum*. Carbon availability and nitrogen source were selected because changes in these conditions are known to affect SM production in other fungi (Barboráková et al., 2012, Arai et al., 2012). Iron availability was studied in order to examine its effects on biosynthesis of a predicted siderophore, a type of SM mainly specialized for iron transport and storage (Neilands, 1995). In addition to using a wild type strain, a global SM regulator mutant *ΔLaeA* was used in order to observe any changes in some SMs that are not normally produced at high levels in the wild type strain (Section 1.5).

Figure 3.2 shows TLC analysis of *D. septosporum* metabolites extracted from culture filtrate and mycelia. Since SMs may have roles inside or outside the cell, they may be secreted or kept within the cell (Martín et al., 2005). Therefore, in

order to observe a broader spectrum of *D. septosporum* SMs, both culture filtrate and mycelia were analysed using TLC. It was shown that one band (M3) from the TLC analysis of mycelia was not visualised in culture filtrate, and one band from culture filtrate (F6) was observed at a lower level in the mycelia.

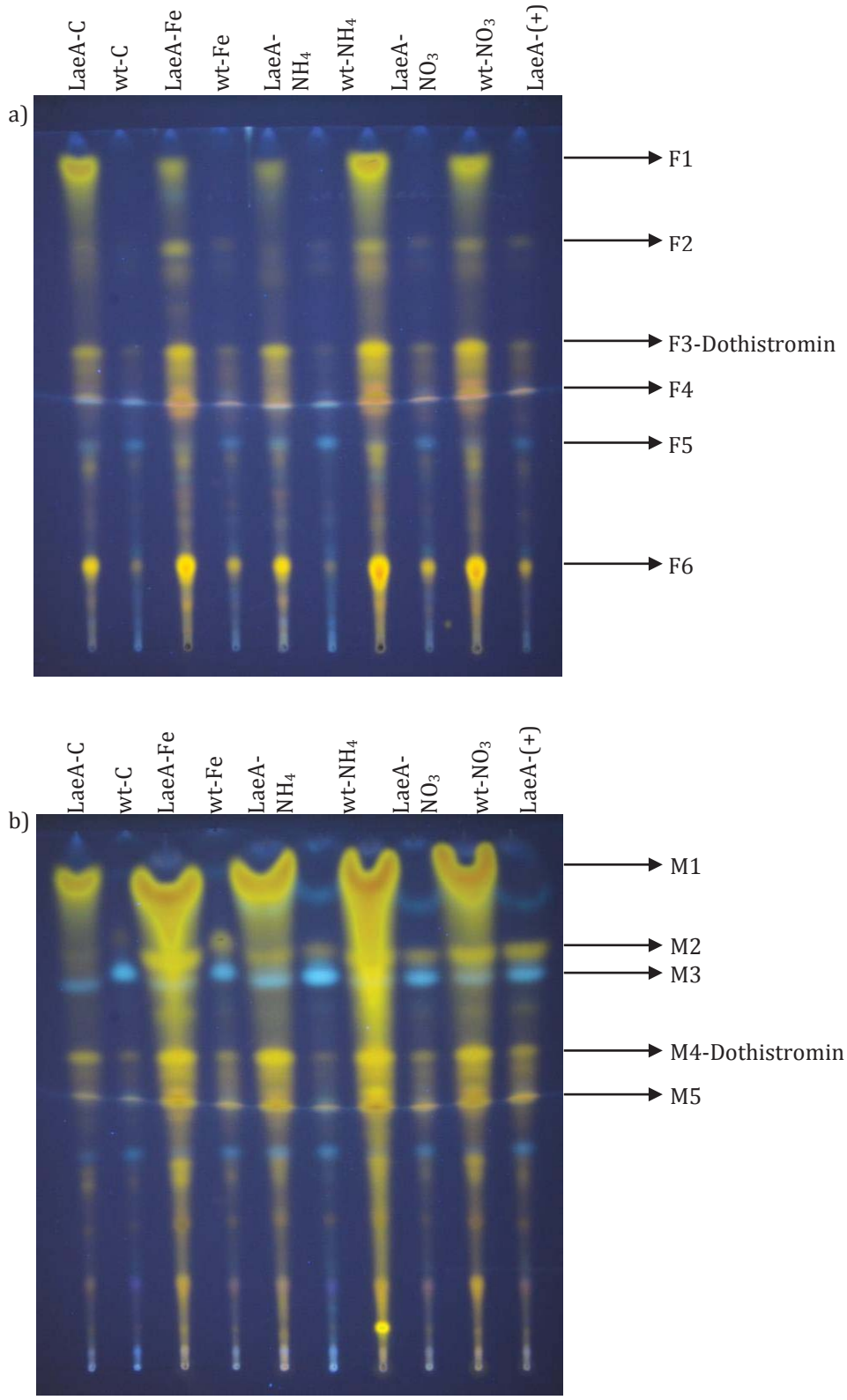

Figure 3.2. TLC analysis of *D. septosporum* wild type and *ΔLaeA* grown in different conditions. SMs from a) Culture filtrate and b) Mycelia of *ΔLaeA* (LaeA) and wild type (wt) strains. C: PMMG medium with 1% glucose, Fe: PMMG medium with no iron, NH_4 and NO_3: PMMG media which contained these compounds used as sole nitrogen sources, (+):PMMG medium with 3% glucose, 10 µM $FeSO_4.7H_2O$, and NH_4NO_3 as nitrogen source. Bands of interest are marked F1-F6 for culture filtrates and M1-M5 for mycelia. Dothistromin bands are marked with F3 and M4.

In Figure 3.2, the known metabolite dothistromin was evident in bands F3 and M4. The overall amount of metabolites produced was increased in the *ΔLaeA* strain compared to the wild type in all lanes. Since the expression of *D. septosporum* SM genes in the *ΔLaeA* strain was previously reported (Chettri and Bradshaw, 2016) and illustrated in Figure 3.3a, it was possible to compare the TLC bands with expression profiles to determine if any TLC bands might correspond to any specific SMs. Expression of *DsPksA*, *DsHps1*, and *DsHps2* were significantly increased, and *DsPks2*, *DsNps1* and *DsNps2* were significantly decreased in *ΔLaeA* compared to wild type *D. septosporum* (Figure 3.3a). Based on the selected TLC bands and expression of SM genes in *ΔLaeA* (Chettri and Bradshaw, 2016), which bands might belong to which SMs were estimated for the other SMs (Figure 3.3).

Quantification of the TLC data was performed using JustTLC Version 4.0.3, Sweday (Lund, Sweden) (Section 2.11.2). In this analysis both absolute intensity of the bands (non-normalized) and relative intensity of each band over total intensity per sample (normalized) were used. Normalisation was done because of the variations in efficiency of metabolite extraction and the amounts loaded onto the TLC plates. Non-normalized data were also analysed in order to avoid bias when levels of specific SMs changed so much between samples (such as the increase in band M1 in the *ΔLaeA* mutant) that it affected the total amount of metabolite per sample, thus affecting the normalization. For example, expression of the dothistromin core gene *DsPksA* was significantly increased in *ΔLaeA* compared to the wild type. However, a significant increase of band intensity (F3) was only observed in metabolites extracted from culture filtrate and analysed using non-normalized data (Figure 3.3b). Therefore, significant differences from either non-normalized or normalized data were accepted unless the results were contradictory with each other for these two analyses e.g. significant increase in non-normalized and decrease in normalized analysis.

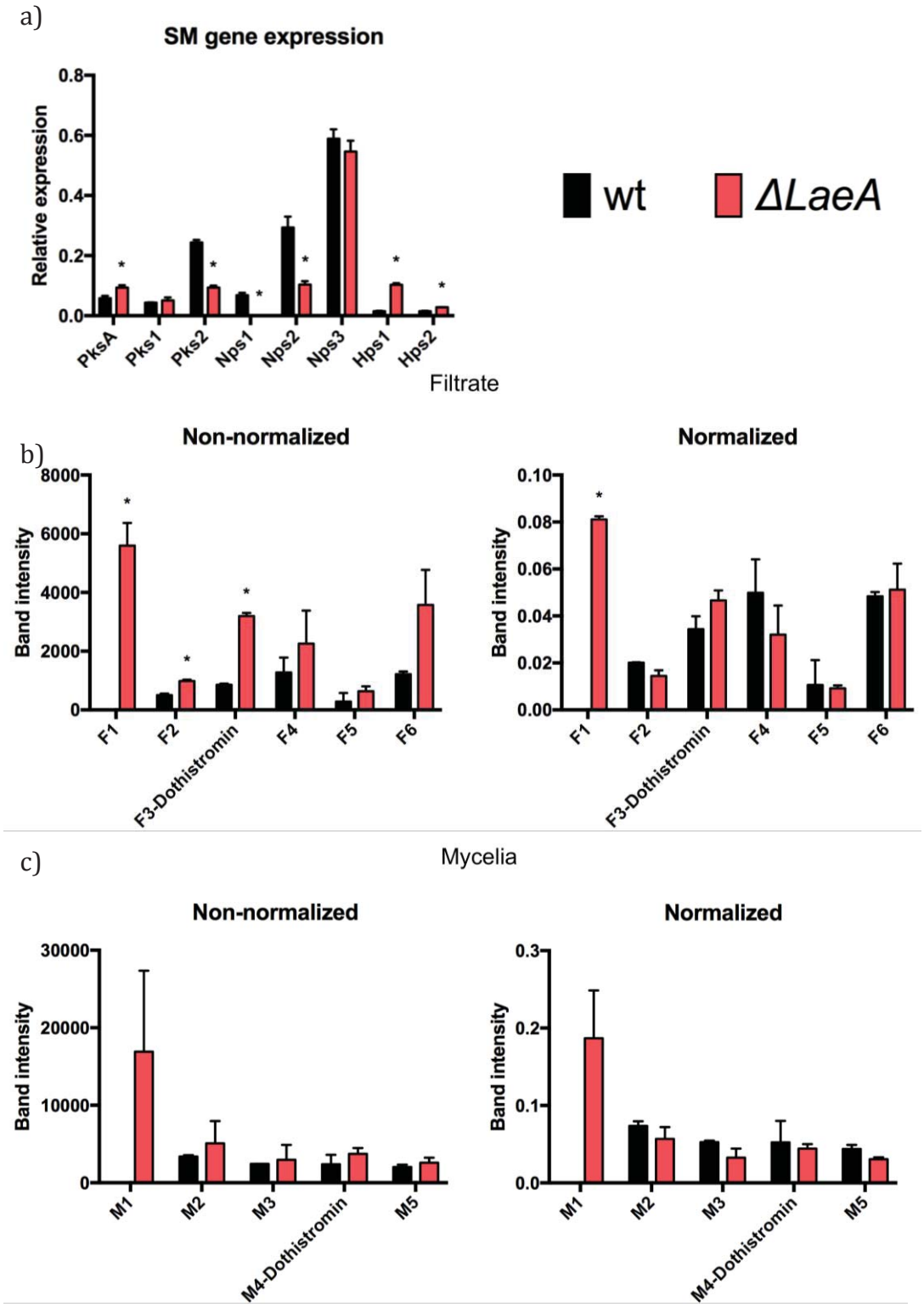

Figure 3.3. Comparison of SM gene expression and metabolite band intensity in TLC analysis between *D. septosporum* wild type and *ΔLaeA* strains. Wt: Wild type, KO: *ΔLaeA*. a) SM gene expression in *ΔLaeA*; data from Chettri and Bradshaw (2016) at 9 dpi. b) Non-normalized and normalized TLC bands from culture filtrate, c) Non-normalized and normalized TLC bands from mycelia. All cultures were grown in PMMG. TLC bands belonging to mycelial metabolite extracts are named M1-M5, and the ones in culture filtrate are named F1-F5. The dothistromin band is indicated. Asterisks indicate significant differences ($p<0.05$) between wt and *ΔLaeA*. Data are means and standard deviations of two biological replicates from 15 dpi cultures.

According to the results presented in Figure 3.3, expression of *DsHps1* increased most dramatically in the *ΔLaeA* strain compared to the wt. Since the metabolite with highest retention factor (Rf) value in both culture filtrate and mycelia (F1 and M1) appears absent in wild type but produced at a very high level in *ΔLaeA* it was initially thought this could be the product of Hps1. However, recent TLC analyses made by Dr Pranav Chettri showed that the F1/M1 metabolite was still produced in a *DsHps1* and *DsLaeA* double-knockout mutant, while it was absent in a *DsPksA* and *DsLaeA* double-knockout mutant. Therefore, the metabolite presented as F1 and M1 is probably an intermediate of the dothistromin biosynthesis pathway catalysed by DsPksA, which was also upregulated in *ΔDsLaeA* (Figure 3.3a).

The metabolite present in culture filtrate F6 was also produced at higher levels in *ΔLaeA* compared to wild type on non-normalized data (Figure 3.3b). Since the expression of *DsHps1* and *DsHps2* were significantly increased in *ΔLaeA* compared to wild type (Figure 3.3a), it is possible that this metabolite could be the product of Hps1 or Hps2. However, there were limitations with this analysis. First, the difference between wild type and *ΔLaeA* was not significant for F6 and there was no visual difference in normalized data. In addition, it is possible the metabolite extraction method used was not suitable for the extraction of Hps1 and Hps2 SMs, and that may be the reason for no better candidate being found for these SMs in the TLC analysis. On the other hand, expression of *DsPks2* and *DsNps2* were significantly decreased in *ΔLaeA* compared to wild type. However, no band was observed in the TLC analysis that was at a lower intensity for *ΔLaeA* than wild type. Using solvents with varying polarity to extract metabolites may reveal other candidates.

In any case, these were only estimations based on the production of SMs and expression of the core genes, and chemical characterization is required to confirm candidate metabolites. It should also be noted that the expression data presented belong to 9 dpi cultures while the metabolites belong to 15 dpi cultures. Therefore, the expression of the SM genes at 15 dpi might be different than at 9 dpi in *ΔLaeA*, causing a limitation for comparison.

Using the same TLC data shown in Figure 3.2, the effect of different media on the production of metabolites was analysed and is shown in Figure 3.4.

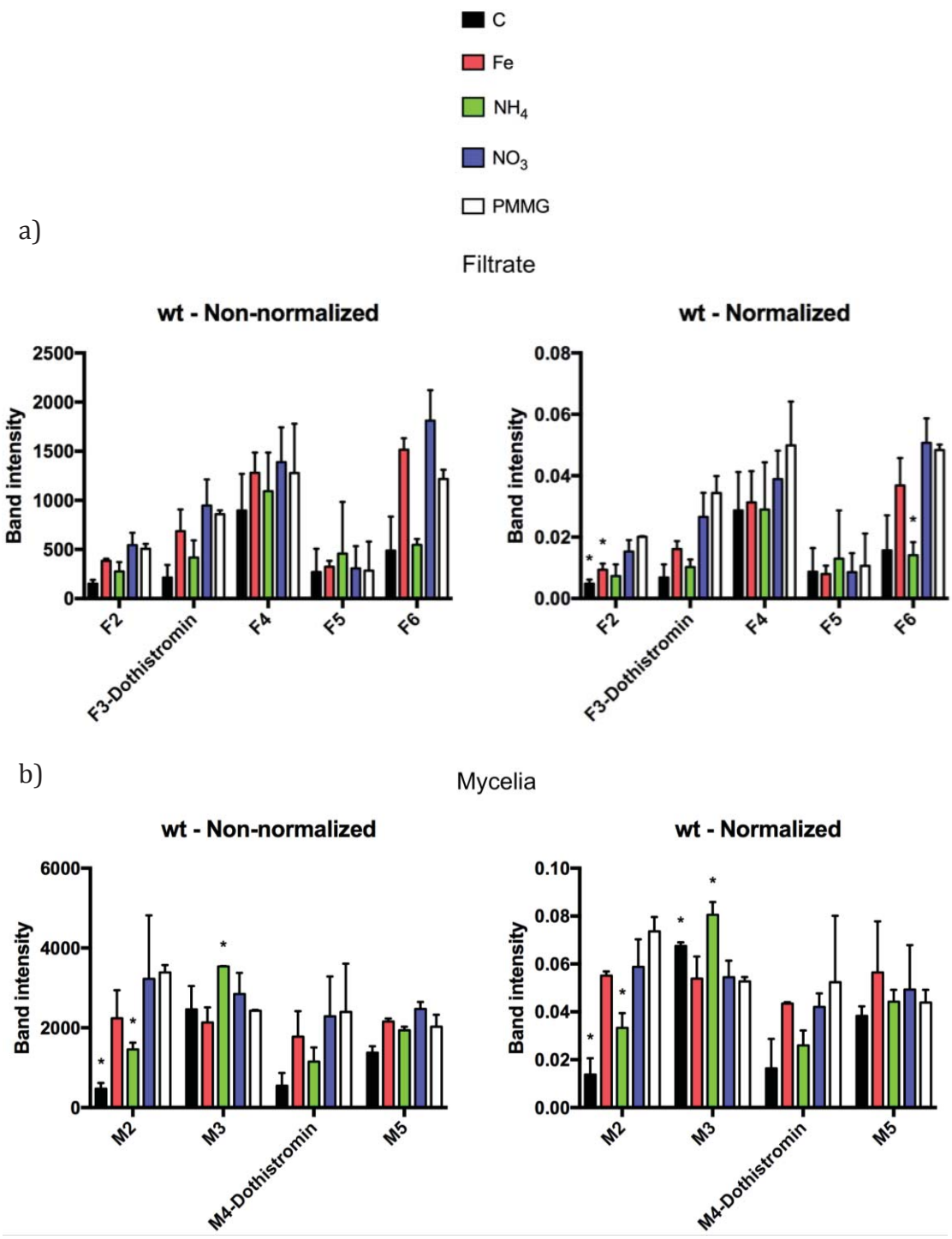

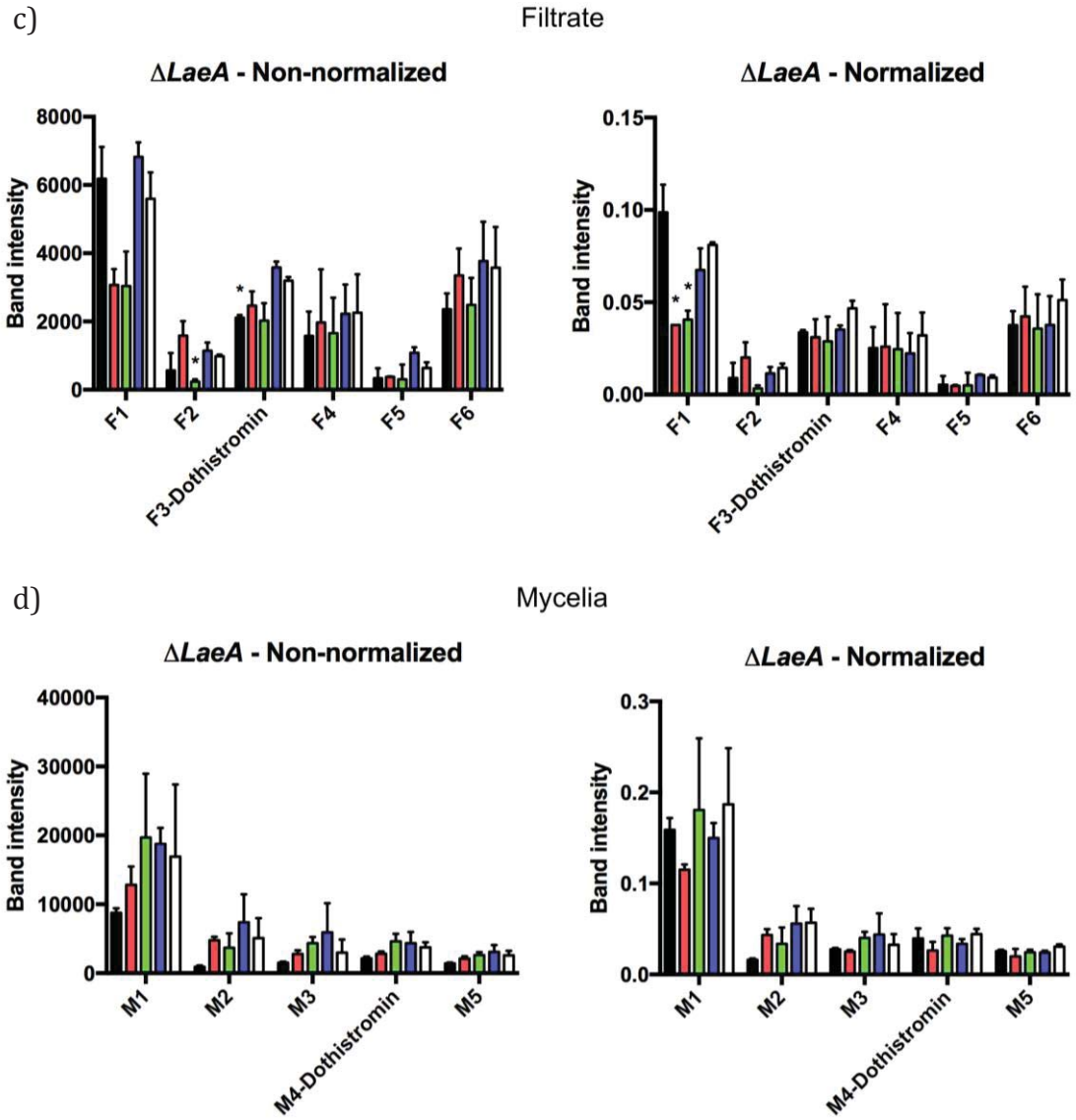

Figure 3.4. Secondary metabolite production under different media conditions. C: 1% glucose, Fe: Iron-deficient medium, NH_4: $(NH_4)_2SO_4$ as sole nitrogen source, NO_3: KNO_3 as sole nitrogen source, PMMG: Control medium with 3% glucose, 10 µM $FeSO_4.7H_2O$, and NH_4NO_3 as nitrogen source. Secondary metabolites extracted from culture filtrate or mycelia were indicated. Significant differences ($p<0.05$) between PMMG and different media conditions were marked with "*". The bands F1 and M1 were missing from the wild type samples as mentioned above, and thus not included in the results.

Effects of different media, presented in Figure 3.4, showed that carbohydrate availability had significant effects on the production of some metabolites. Lowering glucose concentration from 3% to 1% in the medium (by comparing wt-C and wt-PMMG) decreased the amount of one metabolite (F2/M2) both in culture filtrate and mycelia of wild type strain (Figure 3.4a-Norm. and b-Both Norm. and Non-norm.). However, this decrease was not observed in the *ΔLaeA* strain. Instead, the

amount of dothistromin (F3) was significantly decreased in the culture filtrate if the glucose concentration was reduced (Figure 3.4c-Non-norm.). Carbon catabolite repression by the Cys_2His_2 zinc finger global transcription factor CreA is common among filamentous fungi, and thus limiting carbohydrate concentration was expected to increase production of SMs (Reviewed by Yin and Keller, 2011). It is possible there may have been an increase in SM production at a different time point, and extracting the metabolites at 15 dpi might be too late for detecting that increase. For example, dothistromin, unlike most SMs that are mainly produced at late exponential or stationary phase, is produced most at early exponential phase (Schwelm et al., 2008). Therefore, it is possible that the effect of carbohydrate concentration on some SMs might not have been detected.

The effect of two nitrogen sources, NO_3 and NH_4, was tested on metabolite production. There was no significant difference observed in the production of any metabolites if cultures were grown in media containing NO_3 as the sole nitrogen source compared to PMMG. On the contrary, the amounts of one metabolite from culture filtrate (F6) and one from mycelia (M2) were significantly decreased in *D. septosporum* wild type cultures grown in NH_4-containing medium compared to PMMG (Figure 3.4a-Norm. and b-Both). The decrease in the band F6 may be because of the decrease in the secretion or production of the metabolite, or both. In contrast, metabolite M3 (the band that was missing in culture filtrate but clearly visible in mycelia) was significantly increased in the mycelium of wild type cultures grown in media containing NH_4 as sole N source compared to PMMG (Figure 3.4b-Both). In the *ΔLaeA* strain, two metabolites (F1 and F2) were produced at significantly lower levels in *ΔLaeA* cultures grown in media containing NH_4 as nitrogen source compared to PMMG (Figure 3.4c-Norm. (F1), Non-norm. (F2)). Levels of the F2/M2 decreased in both wild type and *ΔLaeA* strains in NH_4-containing medium compared to PMMG, but the decrease in M2 was only significant in wild type (Figure 3.4b-Both) and that in F2 only significant in *ΔLaeA* (Figure 3.4c-Non-norm.).

Using NH_4 as nitrogen source may either positively or negatively impact the production of fungal SMs. A medium containing NH_4 as sole source of nitrogen was

reported to induce aflatoxin (AF) production in *A. parasiticus* and *A. flavus* (Feng and Leonard, 1998). In addition, the production of veratryl alcohol produced by the fungus *Phanerochaete chrysosporium* significantly decreased upon addition of NH_4 to the media (Fenn and Kirk, 1981). On the contrary, sterigmatocystin (ST) production in *A. nidulans* was repressed in medium containing NH_4 as sole nitrogen source (Feng and Leonard, 1998). However, Keller et al. (1997) has shown that the pH regulation of AF and ST may override the effects of nitrogen source. Therefore, a change in pH caused by the use of $(NH_4)_2SO_4$ in the medium containing NH_4 as the sole nitrogen source instead of NH_4NO_3 in PMMG may be the reason of the changes in metabolite production in *D. septosporum*. Even though the molecular mechanism for nitrogen regulation of most fungal SMs has not been reported, nitrogen source and availability is one of the key factors in SM regulation, affecting a broad range of SMs. For example, nitrogen source and availability affected 30 of the 45 predicted SM gene clusters in the fungal plant pathogen *Fusarium fujikuroi*, including broad range of PKS, NRPS, DMA gene clusters (Wiemann et al., 2013). Therefore, it was not possible to determine the types of SMs affected by the nitrogen source in this experiment.

Among the metabolites produced by *D. septosporum* wild type and *ΔLaeA* strains, two were significantly affected by iron availability. Level of one metabolite (F2) was significantly decreased in iron-deficient media compared to PMMG in the wild type strain (Figure 3.4a-Norm.), although not in the *ΔLaeA* strain. A significant decrease was observed in another metabolite (F1) in iron-deficient media compared to PMMG in the *ΔLaeA* strain (Figure 3.4c-Norm.). It is known that iron depletion promotes siderophore production (Johnson, 2008). However, in *C. fulvum* the ortholog of the putative siderophore gene *DsNps2* was barely expressed even in iron depletion conditions (Collemare et al., 2014). Therefore, it is possible that siderophore production *D. septosporum* might not be affected by iron availability.

To sum up, carbon and iron availability as well as use of NH_4 as sole nitrogen source, compared to PMMG, resulted in significant changes in the levels of several putative metabolites in the wild type strain. However, these changes did not

provide clues to determine what kinds of metabolites were affected. This was because the changes in the metabolite levels caused by carbon and iron availability were opposite of the expected and nitrogen source may affect the production of a broad range of metabolites. There were several limitations to this study. First of all, normalized and non-normalized data had shown that there was a significant difference in either normalized or non-normalized data, but not supported by the other. Significant differences were accepted in either one of the normalized or non-normalized analyses as long as they were not contradictory. Repeating the experiment with more replicates may determine if these changes are actually significant. Another limitation was the timing of the extraction. Although most fungal SMs are produced at late exponential phase, some, such as dothistromin, might be produced at a higher level at a different phase of growth. Therefore, it is necessary to do these comparisons at different time points to observe effects of different media conditions on a broader range of metabolites. In addition, the method for extraction was another limitation. Since the metabolites extracted may differ based on the polarity of the organic solvent used, it is possible that some of the metabolites may have been extracted insufficiently to observe effects of media conditions with the current method. The final limitation was the pH effects of different media conditions, which may in turn override the effects of other media conditions.

3.2. Nonribosomal peptide synthetases

Following on from studies of expression of all of the *D. septosporum* SM genes, and metabolite production under different media conditions, the genes were studied individually. First, JGI gene models for the *D. septosporum* SM core genes were confirmed in order to make predictions based on these core genes. Afterwards, evolutionary selection pressures were analysed for the SM core genes to help determine the importance of the gene product and its domains for the fungus. Then, putative SM gene clusters were determined to make predictions about the SM biosynthesis pathway products. Three of the genes (*DsPks1*, *DsPks2*, and *DsNps3*) were of particular interest based on their levels of expression and expression patterns. Additional analyses for the genes of particular interest

included phylogenetic analyses to find out if there were functionally characterised orthologs in other species, and functional characterization of *DsNps3*, the gene that was up-regulated at an early stage of infection *in planta*.

3.2.1. NPS1

3.2.1.1. Confirmation of gene model for *DsNps1*

All the analyses and predictions related to the *D. septosporum* SM core genes are based on the assumption that the JGI gene models are correct. Therefore, it was essential to confirm these gene models for each SM core gene before making any further predictions about these genes and their potential roles. In order to confirm each gene model two methods were used. The amino acid sequences of SM core gene products were aligned with those from their best BlastP hits and known orthologs (if any), and the predicted introns were confirmed by mapping reads from *in planta* and in culture RNA-seq experiments to the gene model. All of the RNA-seq reads that were mapped to the gene model was uploaded onto JGI by Andre Sim (Massey Univerity) and are available by browsing the genes within the scaffolds from the JGI website.

DsNps1 had no known orthologs, so its amino acid sequence was aligned with those obtained from best BlastP hits that were confirmed using reciprocal BlastP (Figure 3.5). With this approach it was possible to detect ambiguities in gene models caused by factors such as a mis-annotated introns or start/stop codons, which may cause big gaps or insertions in the protein sequence compared to other sequences within the alignment. However, it should be noted that for this comparison to work, the sequences within the alignment should not be too different and preferably orthologs.

Figure 3.5 illustrates the predicted domain structure of DsNps1 (Table 3.1), using an alignment of DsNps1 with the top three matches from a reciprocal BlastP analysis. Alignment of DsNps1 with its closest BlastP hits showed very low consensus, and low amino acid sequence identity with the closest of those being *A. wentii* at 44.3% (E=0). The sequence identity of DsNps1 with the two other closest

BlastP hits, *T. citrinoviride* and *G. acutata* were 37.1% (E=0) and 35.1% (E=0), respectively. *D. septosporum* belongs to the Dothideomycetes class, however, none of the best BlastP hits belonged to this class. *A. wentii* is within the Eurotiomycetes class, while *T. citrinoviride* and *G. acutata* are Sordariomycetes. The best BlastP hit of DsNps1 from among 102 species of Dothideomycetes was *Botryosphaeria dothidea* (protein ID: 14052) with 31.9% identity. This shows that *DsNps1* is unique to *D. septosporum* amongst fungi whose genomes have been sequenced. Therefore, due to low similarities between DsNps1 and its best BlastP hits, it is not possible to reach a conclusion about the *DsNps1* JGI gene model based on the alignments.

The *DsNps1* predicted gene model has two introns, however, both *in planta* and in culture expression levels of the gene were very low (below 10 RPMK). This meant there weren't sufficient cDNA reads near the positions of predicted introns to confirm their presence (Appendix 4). However, the second intron is within an A domain, and this region of DsNps1 aligns well with A domains of other proteins within the alignment (Figure 3.5), suggesting the second intron is very likely correct.

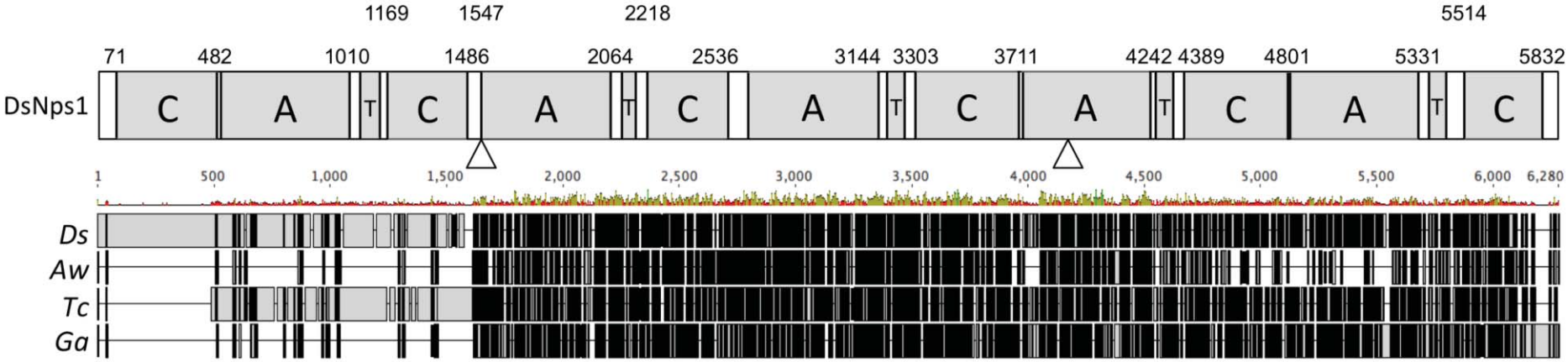

Figure 3.5. Domain structure of DsNps1 and its protein alignment with best BlastP hits. DsNps1 indicates the peptide's domain organization and amino acid positions of some of the domain borders are shown with numbers (T domain borders and borders of domains that are too close to another annotated border are not shown). C: Condensation, A: Adenylation, T: Thiolation domains. *Ds*: *D. septosporum*, Aw: *Aspergillus wentii* (protein ID: 24303); Tc: *Trichoderma citrinoviride* (protein ID: 1118665), Ga: *Glomerella acutata* (protein ID: 1396682). The diagram was drawn in scale to original domain sizes. Triangles indicate corresponding intron positions. The dark regions indicate the amino acid alignment with black (highly similar) to white (not similar) sequences with respect to the consensus sequence. Total length is 5888 amino acids. Coloured bar represents consensus identity: red indicates low identity (below 30%); green shades indicate higher levels of identity (up to 100%) with bar height proportional to % identity.

Therefore, neither alignments (Figure 3.5, Appendix 20a) nor cDNA analyses (Appendix 4) provide sufficient evidence to confirm the current gene model. The current gene model should be confirmed by cDNA sequencing of *DsNps1* but, because of its low level of expression, cDNA would have to be obtained using growth conditions, or in a mutant, that results in overexpression of *DsNps1*.

3.2.1.2. Comparison of *DsNps1* from 19 strains of *D. septosporum*

Plant pathogens are in a constant evolutionary struggle with host plants in order to gain competitive advantage, and fungal SMs usually play key roles in this (Section 1.4). In this process, genes may be under evolutionary selection. Evidence of evolutionary selection can be inferred from proportions of non-synonymous (amino acid changing, dN) and synonymous (silent, dS) mutations in codon sequences (dN/dS). It is now also possible to determine the selection pressure on the specific codons of a gene by the help of various bioinformatics tools (Aguileta et al., 2009). This can provide a deeper understanding on the evolutionary selection pressure on specific domains of the encoded proteins.

Genomic DNAs of 18 *D. septosporum* strains from across the globe were received from Dr Irene Barnes (University of Pretoria, South Africa) and sequenced in AGRF (Australia) with Illumina sequencing, and assembled to the gene model using Bowtie 2 (version 2.2.6) (Langmead and Salzberg, 2012) . Full details of strains are presented in Appendix 5. *DsNps1* evolutionary selection determination was done by aligning the *DsNps1* nucleotide sequences of NZE10 and the 18 additional *D. septosporum* genomes, screening for internal stop codons and calculating overall dN/dS ratio as explained in Section 2.14.4. Figure 3.6 shows the *DsNps1* nucleotide sequence alignment from the 19 *D. septosporum* strains. The dN/dS ratio of *DsNps1* is 0.23, indicating the gene is under negative selection. Therefore, although the *in planta* expression level of *DsNps1* was very low, the Nps1 SM may have an important function at another stage of the *D. septosporum* lifecycle. In addition, this alignment supports that the JGI gene model is correct.

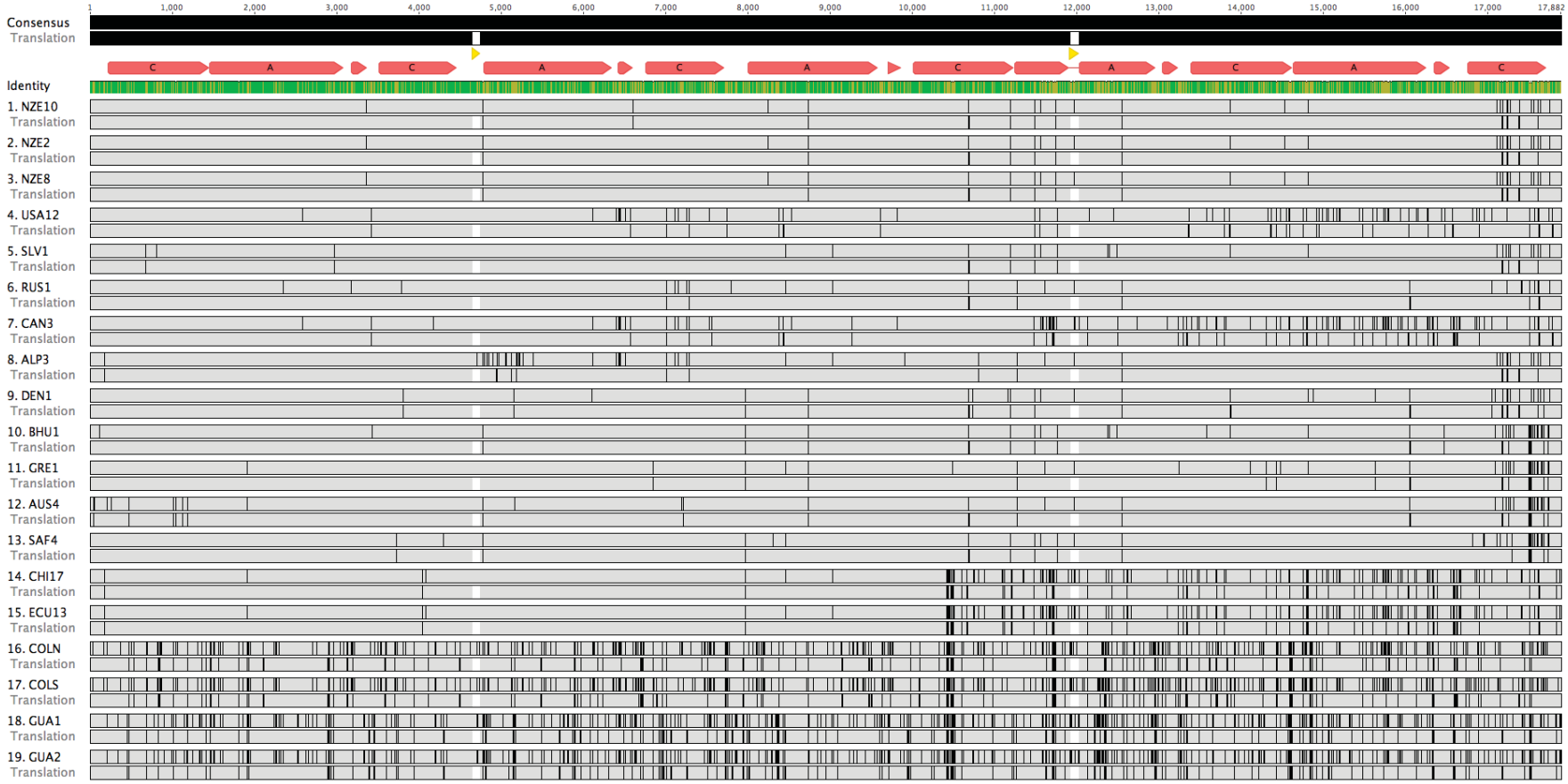

Figure 3.6. *DsNps1* nucleotide alignment of NZE10 with 18 additional strains. Red arrows show the domain positions with, C: condensation, A: Adenylation, Unnamed small red arrows: thiolation domains. Yellow arrows indicate intron positions. The coloured bar represents consensus identity with brown indicating identities above 30% and below 100% and green indicating 100% identity. For each sequence, vertical bars on the top and bottom lines show differences in nucleotide and amino acid sequences compared to NZE10. A bar on the top line alone shows a synonymous mutation and a bar on both lines shows a non-synonymous mutation. Strains used in this analysis are listed in Appendix 5.

In addition to the synonymous and non-synonymous mutations, the alignment presented in Figure 3.6 also shows that *DsNps1* genes in COL (Colombia) and GUA (Guatemala) samples have more mutations compared to the other 15 *D. septosporum* genomes. However, this difference is not specific to *DsNps1* and a phylogeny of 19 *D. septosporum* genomes shows that COL and GUA samples are distant from the other 15 *D. septosporum* genomes analysed (Figure 3.7).

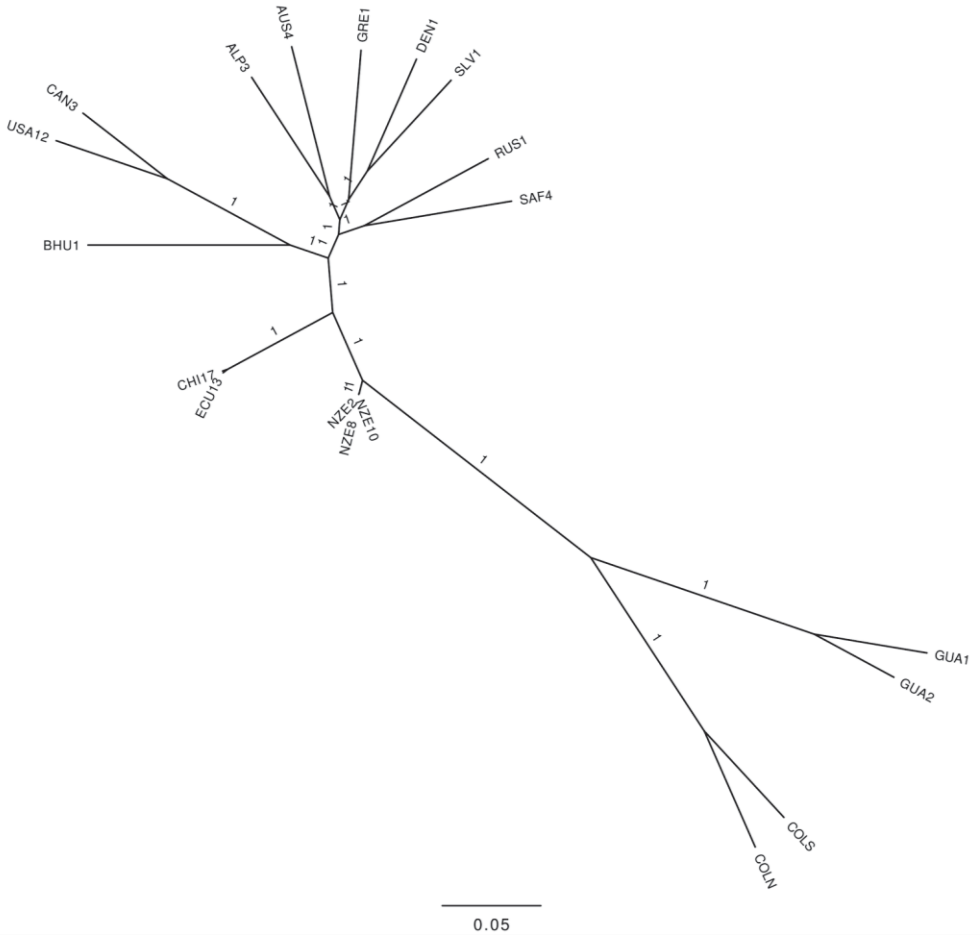

Figure 3.7. Phylogenetic analysis *D. septosporum* whole genome sequences of NZE10 and 18 additional *D. septosporum* genomes. Numbers indicate approximate likelihood ratio test (aLRT) scores. Phylogeny built by Dr Pierre-Yves Dupont.

3.2.1.3. Gene cluster analysis

SM biosynthesis requires combined activity of products of multiple genes that are generally close to each other within a chromosome (Section 1.4.5).

The SM produced by *DsNps1* may not have a key role in virulence based on its low levels of expression *in planta*, but may still function at some stage in the *D. septosporum* life cycle. Gene cluster analysis of *DsNps1* was done by predicting what genes might be associated with *DsNps1* in a gene cluster. This was done by screening 20 genes upstream and downstream of *DsNps1* by GO terms analyses from Bradshaw et al. (2016), manual InterProScan analyses, antiSMASH analyses, and searching the literature for similar genes with predicted functions in other SM gene clusters as outlined in Section 2.14.5. As mentioned above, the *DsNps1* gene has one of the lowest expression levels both in culture and early, mid, and late time stages of infection *in planta* according to transcriptomics analysis (Section 3.1.2). Because of this, it was not possible to include analysis of co-expression between *DsNps1* and the genes nearby on the chromosome to help predict *DsNps1* cluster genes.

Figure 3.8 shows the putative gene cluster for *DsNps1* and Table 3.3 shows the predicted proteins encoded by the genes within the gene cluster. The putative *DsNps1* gene cluster contains 7 genes within a 45 kb region of chromosome 3. In this region, there are 6 additional genes with no predicted functions related to secondary metabolism. The biggest distance between two genes belonging to the predicted gene cluster is 6 kb, containing 1 interfering gene.

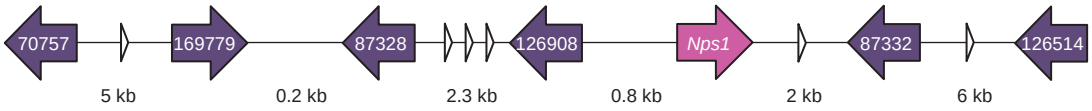

Figure 3.8. *DsNps1* and its predicted gene cluster. Numbers inside arrows indicate JGI protein IDs. Pink: Secondary metabolite core gene *DsNps1*. Purple: putative *DsNps1* cluster genes. Small white arrows: genes without predicted SM functions.

Table 3.3. Genes within *DsNps1* putative gene cluster.

Protein ID[a]	Predicted protein[b]	Best hit organism/JGI ID[c]	E / identity %
*Ds70757	Major facilitator transporter	*C. fulvum*/ 196085	0/85
Ds169779	O-succinylhomoserine sulfhydrylase	*C. fulvum*/ 196087	0/89.7
*Ds87328	FAD-dependent oxidoreductase	*T. citrinoviride*/ 1156674	0/61.9
*Ds126908	Drug resistance transporter	*C. fulvum*/ 188587	7.2e-145/79.4
*Ds52251/Nps1	Non-ribosomal peptide synthetase	*A. wentii*/ 24303	0/44.3
Ds87332	Carbamoyl phosphate synthase	*W. ornate*/ 504389	2e-91/54.5
*Ds126514	Drug resistance transporter	*Z. cellare*/64885	0/76.6

[a] http://genome.jgi.doe.gov/Dotse1/Dotse1.home.html
Asterisk indicates that genes with similar predicted functions are present in other fungal NPS gene clusters.
[b] Predicted proteins according to antiSMASH and InterProScan analyses.
[c]All BlastP hits were confirmed with reciprocal blast analyses.

Three of the seven genes within the putative gene cluster are predicted to encode transporter proteins. Transporters can be used to secrete metabolites out of a cell, but are also commonly used to prevent autotoxicity. For example, a transporter gene, *gliA,* in the gliotoxin gene cluster of *A. fumigatus* provides gliotoxin resistance for the fungus itself (Dolan et al., 2015). Although having three transporter proteins seems redundant, there are up to four transporters within single predicted NPS gene clusters of *Trichoderma spp*. (Bansal and Mukherjee, 2016).

Aside from transporters, another gene within the putative gene cluster, Ds87328, is predicted to encode a FAD-dependent oxidoreductase. A predicted NPS biosynthetic gene cluster, involved in production of notoamide by a marine-derived *Aspergillus sp.* contains two FAD-dependent monooxygenases (Ding et al., 2010). In addition, *APF9* gene encodes a FAD-dependent monooxygenase in the apicidin F cluster, a gene cluster composed of 11 genes in the rice pathogen *Fusarium fujikuroi*. Deletion of the *APF9* gene completely stopped apicidin F production, but revealed production of its analog apicidin K (Niehaus et al., 2014). APF9 is thought to catalyse conversion of 2-amino-8-hydroxyoctanoic acid into 2-aminooctanedioic acid, which is then used as a substrate for the NPS core protein of the apicidin F biosynthetic pathway, APF1 (Niehaus et al., 2014).

There are two more genes within the *DsNps1* putative gene cluster; however, no genes with similar functions could be found in other currently-known fungal SM gene clusters. *Ds169779* is predicted to encode an O-succinylhomoserine sulfhydrylase and was included as part of the putative *DsNps1* gene cluster by antiSMASH analysis. This protein catalyzes L-homocysteine production, a step required in methionine biosynthesis (Foglino et al., 1995). Even though no such gene has been reported in SM gene clusters, an O-succinylhomoserine sulfhydrylase gene *metZ* was found to be co-regulated with NPS genes in the pathogenic bacterium *Burkholderia pseudomallei* (Chen et al., 2014). Therefore, it can be hypothesized that a gene predicted to encode an O-succinylhomoserine sulfhydrylase might be part of an NPS gene cluster. The other gene within the predicted *DsNps1* gene cluster, Ds87332, is predicted to encode a carbamoyl phosphate synthase, an enzyme required for arginine and pyrimidine biosynthesis

in prokaryotes and eukaryotes, as well as being involved in urea cycles in vertebrates (Holden et al., 1999; Raushel et al., 1999). Carbamoyl phosphate synthase catalyzes formation of carbamoyl phosphate from ATP, ammonia and bicarbonate (Holden et al., 1999). A gene predicted to encode a carbamoyl phosphate synthase was found in the hybrid PKS-NRPS gene cluster for saxitoxin in the bacterium *Anabaena circinalis* (Neilan et al., 2008). It was also found that carbamoyl phosphate is a substrate required for *in vitro* saxitoxin biosynthesis (Kellmann and Neilan, 2007).

The predicted pathway product type of DsNps1 is cyclosporin (Table 3.1), a compound with a variety of functions including immunosuppression, antifungal and plant virulence activities (Keller, 2015; Viaud et al., 2003). A predicted fungal cyclosporin gene cluster belonging to the fungus *Tolypocladium inflatum* with core gene *simA* (Bushley et al., 2013) was compared with the *DsNps1* putative gene cluster. However, genes in the *simA* gene cluster do not have similar functional annotations to the genes in the predicted *DsNps1* gene cluster. Instead, the *simA* gene cluster contains genes for cytochrome p450, dehydrogenase, transcription factors and cyclophilin, a protein that binds to cyclosporin. In addition there are also amino acid specific enzymes such as alanine racemase in the *simA* gene cluster. The predicted gene cluster for *simA* is composed of 14 genes, while *DsNps1* putative gene cluster is composed of only nine genes. It is possible that other non-clustered genes might be involved in the production of the SM catalysed by *DsNps1* similar to dothistromin biosynthesis that is catalysed by enzymes encoded in a fragmented gene cluster as explained in Section 1.4.5.1.

Most commonly found genes in other fungal SM gene clusters include methyltransferase, cytochrome p450 monooxygenase, glutathione S-transferase, acetyltransferase, and short-chain dehydrogenase/reductase (Collemare et al., 2014; Khaldi et al., 2008; Gardiner et al., 2014; Cramer et al., 2006). Gene cluster predictions can only determine which genes might be required in the biosynthesis of a certain SM, however, and actual gene clusters may be very variable. Biosynthesis of peramine, an NRP produced by *Epichloë* spp., is catalysed by a single SM gene, *perA*, without a gene cluster (Berry et al., 2015). The best way to

confirm a gene cluster is to generate gene knockout (KO) mutants for each candidate gene and analyse the loss of metabolite produced.

In conclusion, even though the gene model for *DsNps1* could not be confirmed due to the lack of clear homologs and very low expression levels, *DsNps1* gene alignment across 19 *D. septosporum* strains supported the gene model of *DsNps1*. *DsNps1* has no clear homologs and is under negative selection. The predicted gene cluster for *DsNps1* has 7 genes, however, predicted functions of the genes in the putative gene cluster do not support the prediction that the DsNps1 SM is a cyclosporin.

3.2.2. NPS2

3.2.2.1. Confirmation of gene model for *DsNps2*

A misannotated intron or start/stop codon can change the predicted protein and domain structure of a nucleotide sequence dramatically, so confirmation of this gene model was mandatory before doing further analyses. *DsNps2* is one of the three *D. septosporum* SM core genes with a known *C. fulvum* ortholog and is predicted to produce a siderophore (Table 3.1). Gene model confirmation was made by amino acid sequence alignment of DsNps2 with its *C. fulvum* ortholog and two other best reciprocal BlastP hits, as well as by confirming the predicted introns using in culture and *in planta* expression analysis data.

Figure 3.9 shows the domain organization of DsNps2 and an alignment of DsNps2 with its *C. fulvum* ortholog CfNps2 and two other top hits from reciprocal BlastP analysis. Alignments had an overall high consensus, and DsNps2 amino acid identities (and BlastP probabilities) to *C. fulvum*, *Z. cellare* and *M. fijiensis* were 76.6% (E=0), 57% (E=0), and 55.6% (E=0), respectively. These alignments suggested there are no gaps or insertions present in DsNps2 compared to the consensus sequence, which supports the hypothesis that the gene model for DsNps2 is correct.

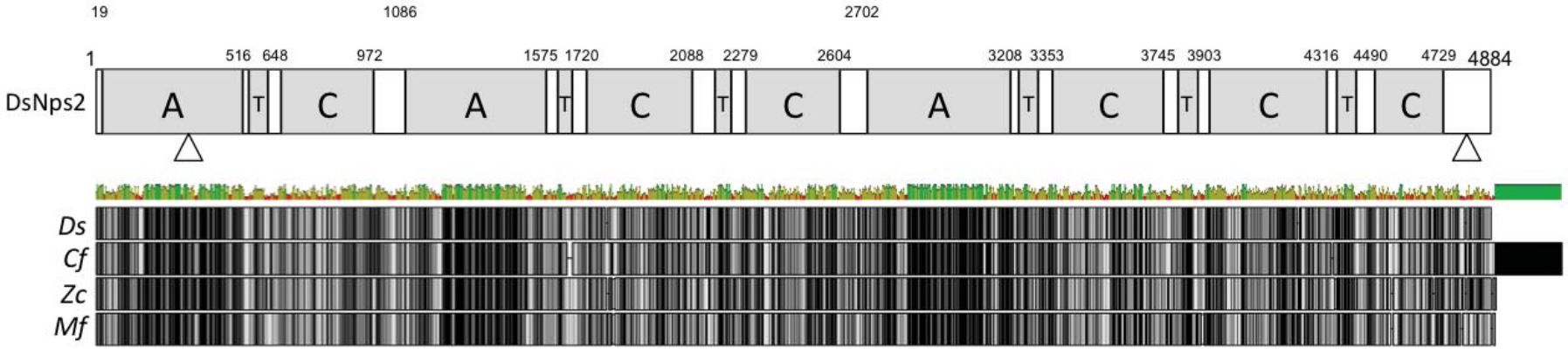

Figure 3.9. Domain structure of DsNps2 and its protein alignment with best BlastP hits. DsNps2 indicates the peptide's domain organization with A: adenylation, T: thiolation, C: condensation domains. Numbers indicate amino acid positions of A and C domain borders (T domain positions not shown). The total length is 4884 amino acids. The diagram was drawn to scale. Triangles indicate corresponding intron positions. The dark regions indicate the amino acid alignment with black (highly similar) to white (not similar) sequences with respect to the consensus sequence. The amino acid alignment below shows *Ds*: *D. septosporum*, *Cf*: *C. fulvum* (protein ID: 193954), *Zc*: *Zasmidium cellare* (protein ID: 53743) and *Mf*: *Mycosphaerella fijiensis* (protein ID: 83197). The coloured bar represents consensus identity (below 30%); green shades indicate higher levels of identity (up to 100%) with bar height proportional to % identity.

The predicted gene model for *DsNps2* has two introns. The expression levels of *DsNps2* were very low both in culture and *in planta* (below 10 RPMK) (Figure 3.1). However, the numbers of RNA-seq reads were higher at the 3' end of the gene compared to 5' end, a trend we observed in RNA sequencing analyses of long genes in the transcriptome analysis. Therefore, it was possible to confirm the intron at 3' end with cDNA analysis (Appendix 6). Since the nucleotide and protein sizes may differ significantly due to a misannotated intron, the domain sizes where the introns correspond may also give hints about the gene model. The A domain that contains the first intron has a similar size and sequence motifs with the other A domains in the gene model (Figure 3.9), which suggests the first intron is probably correct.

Therefore, supported by the alignments (Figure 3.9, Appendix 20b), domain sizes and RNA-seq analyses (Appendix 6), the current gene model for *DsNps2* appears correct. Further confirmation of the gene model could be done by cDNA sequencing of *DsNps2* following use of growth conditions or a mutant that overexpresses *DsNps2*.

3.2.2.2. Comparison of *DsNps2* from 19 strains of *D. septosporum*

DsNps2 gene sequences across the 19 strains were compared by aligning the sequences and determining the evolutionary selection pressure based on the dN/dS ratio (Figure 3.10). The dN/dS ratio of *DsNps2* is 0.27, indicating negative selection pressure on the gene. The alignment also showed that the stop codon is absent or mutated in four strains, COLN, COLS, GUA1 and GUA2. However, the presence of another stop codon after 6 nucleotides means that the DsNps2 protein is only 2 amino acid longer in these four strains compared to that of the other strains. No positively selected codons were found for *DsNps2*.

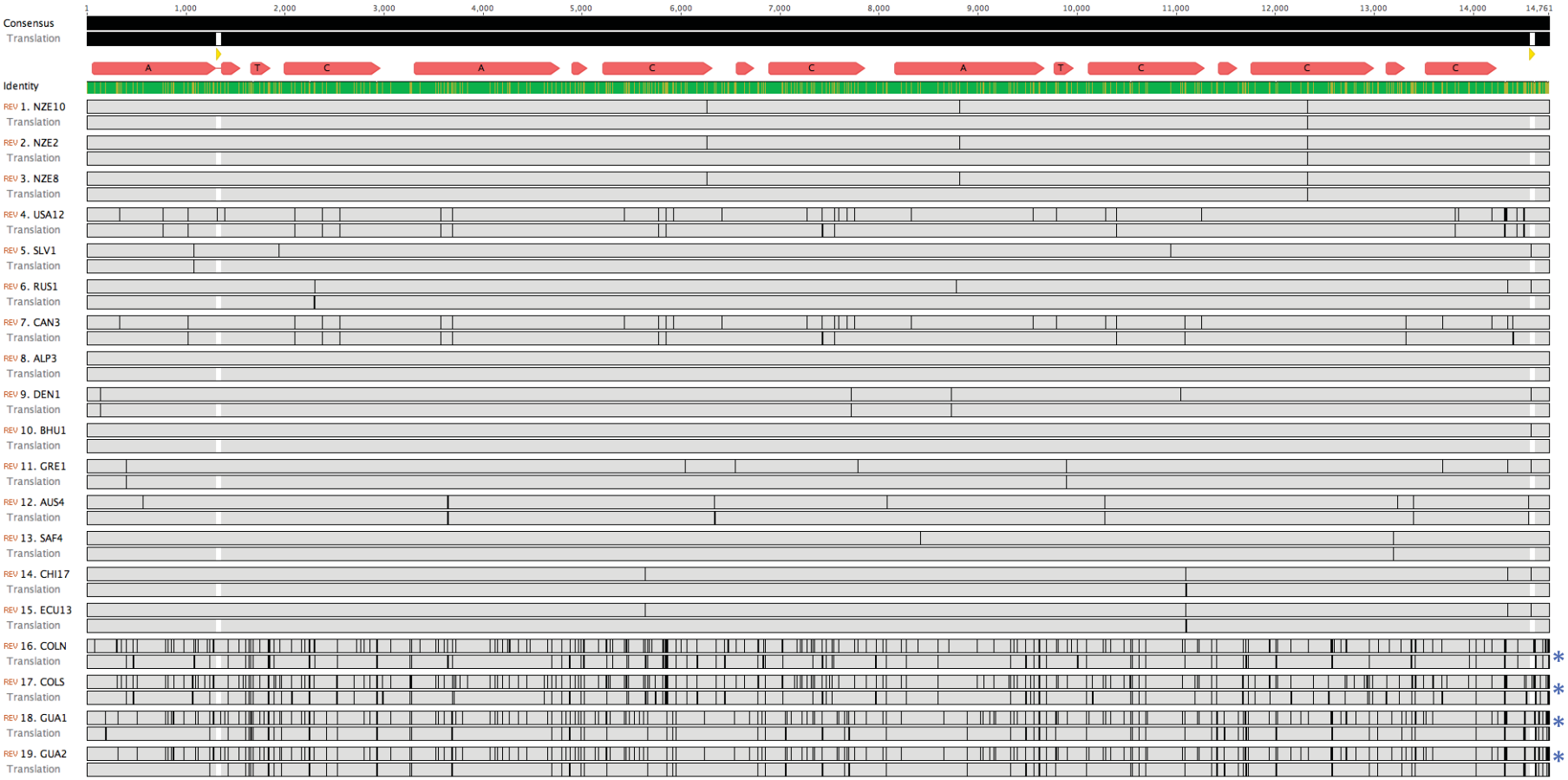

Figure 3.10. *DsNps2* nucleotide alignment of NZE10 with 18 additional strains. Red arrows show the domain positions with A: Adenylation, T: thiolation, C: condensation. Yellow arrows indicate intron positions. The coloured bar represents consensus identity with brown indicating identities above 30% and below 100% and green indicating 100% identity. For each sequence, vertical bars on the top and bottom lines show differences in nucleotide and amino acid sequences compared to NZE10. A bar on the top line alone shows a synonymous mutation and a bar on both lines shows a non-synonymous mutation. Strains with stop-codon mutations are indicated with asterisk. Strains used in this analysis are listed in Appendix 5.

3.2.2.3. Gene cluster analysis

DsNps2 putative gene cluster analysis was done by searching 20 genes upstream and downstream of *DsNps2*, as outlined in Section 2.14.5. Because *DsNps2* is the ortholog of *C. fulvum Nps2* (*CfNps2*) (de Wit et al., 2012), it was also possible to compare the *CfNps2* predicted gene cluster (Collemare et. al., 2014) with that of *DsNps2* in order to observe the synteny between them (Figure 3.11). However, there were differences in the methods used in the prediction of gene clusters between *C. fulvum* and *D. septosporum* putative SM gene clusters. The borders of *C. fulvum* SM gene clusters were defined when three successive genes did not have a predicted function related with secondary metabolism, or when two of the annotated genes had more than 5 kb between them (Collemare et al., 2014). Therefore, there are differences in *C. fulvum* SM putative gene clusters between this project and Collemare et al. (2014). Table 3.4 shows the predicted gene products for the genes in the *DsNps2* cluster. The predicted gene cluster of *DsNps2* is composed of 5 genes in a 40 kb region of chromosome 8. The biggest distance between two genes belonging to the predicted gene cluster is 12.6 kb, which contains 5 genes with no known secondary metabolism-related function. The gene clusters of *DsNps2* and *CfNps2* were found to be syntenic with the only exception that *DsNps2* has one additional interfering genes compared to *CfNps2*.

Although the expression of *DsNps2* was very low (<10 RPMK) (Section 3.1.2), Figure 3.11 suggests that all genes except Ds73932 were expressed significantly higher at late stage compared to early stage; of these, Ds55453 showed a very similar expression pattern to *DsNps2*. The gene that showed a different expression pattern, Ds73932, was expressed significantly higher in early stage than mid and late stages of infection. Since Ds73932 is predicted to encode a transcription factor, it is possible that this gene is responsible for regulating the expression of other genes within the predicted gene cluster. Similar to *DsNps2*, expression of *CfNps2* was reported to be very low in culture and *in planta* at all stages of infection (Mesarich et al., 2014).

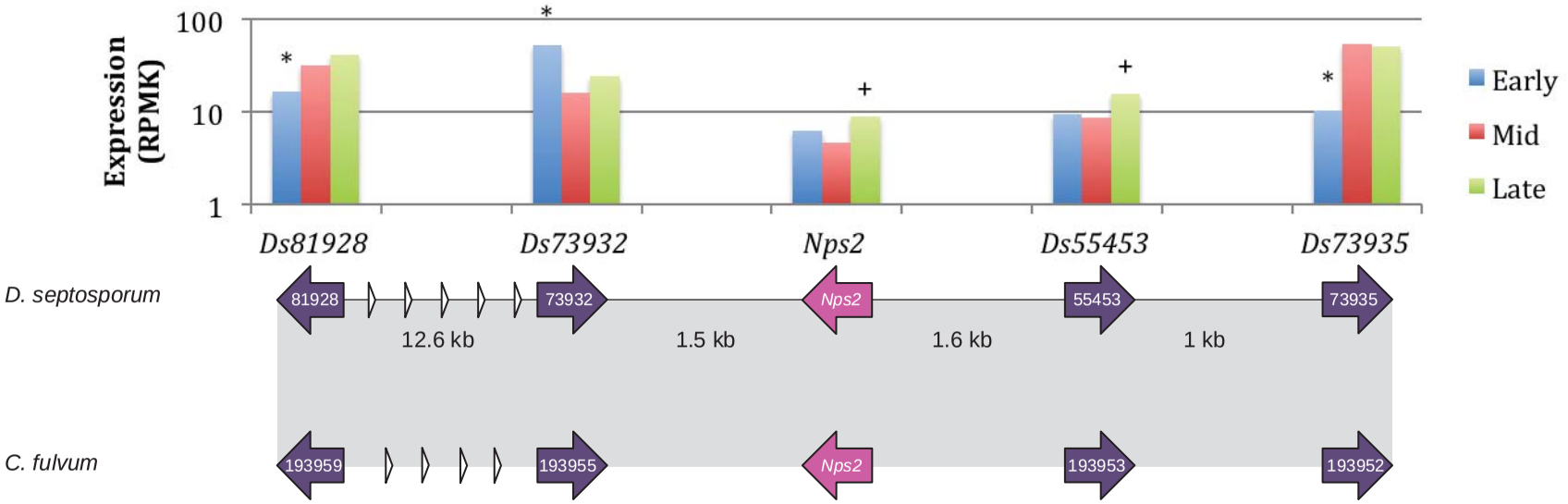

Figure 3.11. Synteny of *DsNps2* and *C. fulvum Nps2* putative gene clusters and expression profile of *DsNps2* putative gene cluster *in planta*. Numbers inside arrows indicate JGI protein IDs. Pink: Secondary metabolite core genes *DsNps2* and *C. fulvum Nps2*. Purple: putative *DsNps2* and *C. fulvum Nps2* cluster genes. Small white arrows: genes without predicted SM functions. Significant differences between gene expression in early-mid and mid-late stages of plant infection are marked with "*" and "+", respectively ($p<0.05$). The differences between early and late stages were also significant for all five genes ($p<0.05$).

Table 3.4. Genes within *DsNps2* putative gene cluster.

JGI Protein ID[a]	Predicted protein[b]	Best hit organism/JGI ID[c]	E / identity %
*Ds81928	Major facilitator transporter	*Cladosporium fulvum*/193959	3.8e-157/80.7
*Ds73932	Zinc-finger transcription factor	*Cladosporium fulvum*/193955	1e-54/63.5
*Ds90481/*Nps2*	Non-ribosomal peptide synthetase	*Cladosporium fulvum*/193954	0/76.6
*Ds55453	ABC transporter related protein	*Cladosporium fulvum*/193953	0/79.7
*Ds73935	Lysine/ornithine N-monooxygenase	*Cladosporium fulvum*/193952	0/90

[a] http://genome.jgi.doe.gov/Dotse1/Dotse1.home.html

[b] Predicted proteins according to antiSMASH and InterProScan analyses

Asterisk indicates that genes with similar predicted functions present in other fungal NPS gene clusters.

[c] All BlastP hits were confirmed true with reciprocal blast analyses.

DsNps2 was predicted to function in siderophore biosynthesis (Table 3.1), and previously predicted to be responsible for the synthesis of a ferricrocin-type siderophore (Collemare et al., 2014). Ferricrocins are responsible for iron storage and trans-cellular iron transport (Wallner et al., 2009). Although their primary roles are internal storage, secretion of small amounts of ferricrocin was reported in *A. fumigatus* (Hissen et al., 2004). The putative gene cluster of *DsNps2* contains two transporter genes, ABC and MFS type (Table 3.4). Genes with similar functions can also be found in other fungal siderophore gene clusters (Schrettl et al., 2008; Haas et al., 2008; Philpott and Protchenko; 2008). In the fungal pathogen *Histoplasma capsulatum*, both ABC and MFS type transporters are present in a single siderophore gene cluster that is induced by low iron levels, and all genes except the one encoding the MFS type transporter are adjacent in a 25 kb region (Hwang et al., 2008). Therefore, if the prediction for *DsNps2* is correct and the Nps2 metabolite is a ferricrocin, whether the transporters Ds81928 and Ds55453 are important functional components of the gene cluster is not known. However, due to its close proximity to the core gene *DsNps2*, the gene encoding for ABC transporter, Ds55453, is probably part of the putative gene cluster.

In addition to the transporters and the core gene, the *DsNps2* putative gene cluster contains genes predicted to encode a zinc-finger transcription factor and a lysine/ornithine N-monooxygenase. Genes encoding proteins with similar predicted functions were reported in other fungal siderophore gene clusters. One gene, *urbs1*, predicted to encode a zinc-finger transcription factor was found in the fungus that causes corn smut disease, *Ustilago maydis*. Disruption of this gene lead to constitutive expression of the first gene in the siderophore biosynthesis pathway (*sid1*), and unregulated siderophore ferrichrome production (Yuan et al., 2001). The next gene in the putative *DsNps2* gene cluster encodes a lysine/ornithine N-monooxygenase. Similar genes are present in the siderophore biosynthetic gene clusters of *Omphalotus olearius*, *Histoplasma capsulatum* and *Ustilago maydis* (Welzel et al., 2005, Hwang et al., 2008, Yuan et al., 2001). However, it is possible there are additional genes involved in the biosynthesis of the siderophore in *D. septosporum*. As mentioned before, the SM produced by the *DsNps2* gene cluster may be a ferricrocin (Collemare et al., 2014). Like most fungal

siderophores, ferricrocins belong to the hydroxamate class of siderophores (Pourhassan et al., 2014). Biosynthesis of hydroxamates involves combined activity of lysine/ornithine N-monooxygenase and acyltransferase (Welzel et al., 2005), and thus an acyltransferase gene may also be involved in the biosynthesis of the Nps2 SM. However, a gene predicted to encode an acyltransferase was not found among 20 genes upstream and downstream of *DsNps2*.

To summarize, the gene model for *DsNps2* is correct based on the alignment with closest homologs and cDNA reads. *DsNps2* has an ortholog, *CfNps2*, and is under negative selection pressure. The predicted gene cluster for *DsNps2* is composed of 5 genes that are conserved in other siderophore gene clusters. However, if the DsNps2 SM is a ferricrocin, it is possible that the transporter genes are not functional components of the putative *DsNps2* gene cluster and an additional acetyltransferase gene may be involved in its synthesis.

3.2.3. NPS3

As explained in Section 3.1.2, *DsNps3* was the most highly expressed *D. septosporum* SM core gene at the early stage of plant infection (Figure 3.1) Therefore, *DsNps3* was of particular interest and additional analyses were done on this gene, including metabolite production and phenotypic analysis of a *DsNps3* knockout mutant (*ΔDsNps3*) and phylogenetic analysis.

3.2.3.1. Phylogenetic analysis

Phylogenetic analysis was done in order to find out if there are any functionally characterised orthologs of DsNps3 as preliminary FASTA analyses didn't reveal any similar proteins. Phylogenetic analysis is a more accurate method for detecting homologous proteins than BlastP and FASTA (Koski and Golding, 2001). The analysis was performed by aligning the best reciprocal FASTA hits from each species belonging to the classes Dothideomycetes, Eurotiomycetes, and

Sordariomycetes represented in the JGI database, and building a phylogenetic tree using the maximum likelihood (ML) method as outlined in Section 2.14.3.

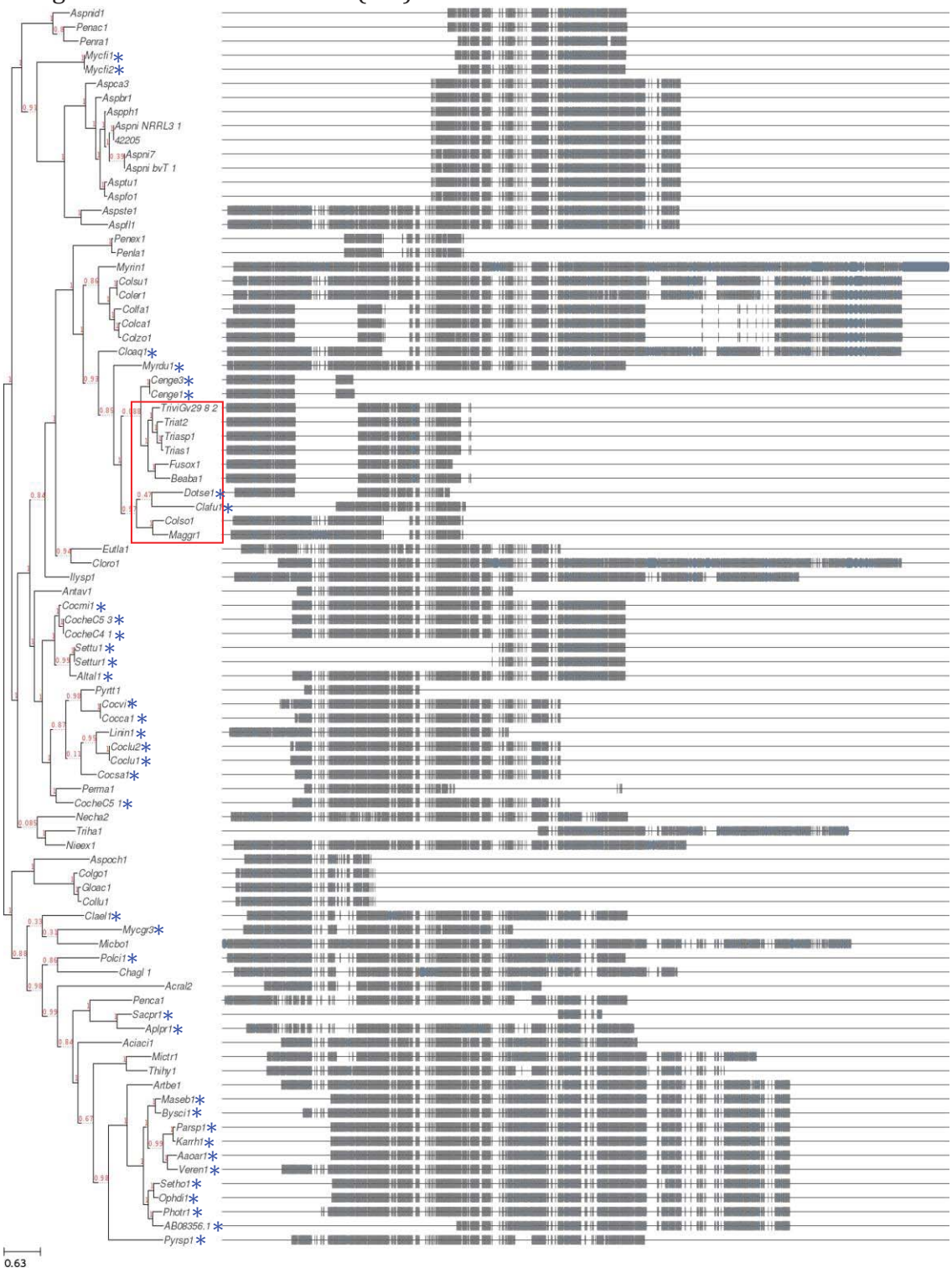

Figure 3.12. Phylogenetic tree and alignment of the peptide sequences of DsNps3 and its best FASTA hits. Red square shows *D. septosporum* (Dotse1) and its closest homologs. Dothideomycetes are indicated with asterisks. Numbers on nodes indicate approximate likelihood ratio test (aLRT) scores. Grey bars and gaps next to the species names show the alignment of the sequences used in the phylogenetic analysis. Details of the genome sequences used are presented in Appendix 23.

Initial phylogenetic analysis of DsNps3 (Figure 3.12) suggested that only the proteins within the red square are putative orthologs, while the other proteins are probably less related to DsNps3. *Cenococcum geophilum* (Cenge1/3) proteins were not included in the putative orthologs due to their low aLRT scores (0.088). Therefore, in order to minimise the gaps seen in the alignments, and obtain a DsNps3-focused phylogenetic tree, a new phylogenetic tree and alignment containing only the sequences within the red square were generated to focus on putative DsNps3 orthologs (Figure 3.13).

a)

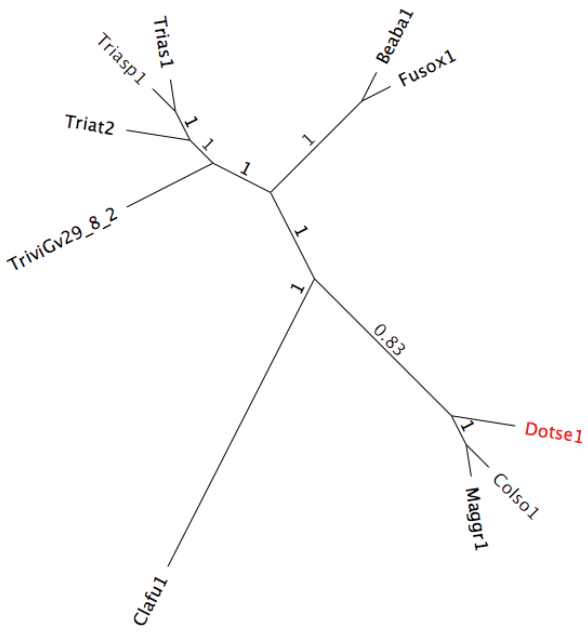

b)

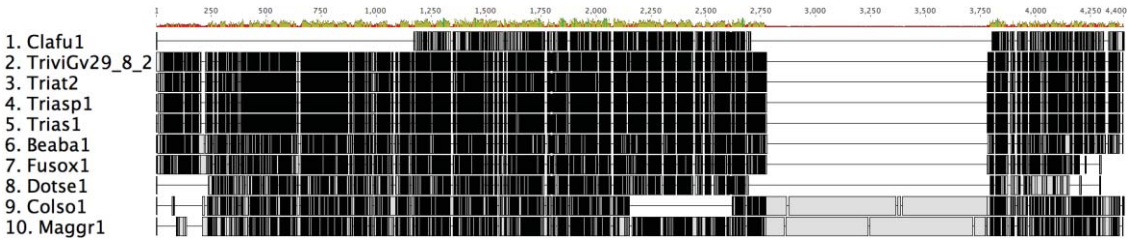

Figure 3.13. Phylogenetic tree and alignment of the amino acid sequences of putative DsNps3 orthologs. a) Phylogenetic tree of DsNps3 with its putative orthologs. Red (Dotse1): DsNps3. Numbers on branches indicate approximate likelihood ratio test (aLRT) scores. b) Alignment of the sequences used in the phylogenetic analysis. Names on the left show the abbreviation of species names as in JGI. The coloured bar represents consensus identity with red (below 30%); green shades indicate higher levels of identity (up to 100%) with bar height proportional to % identity.

The phylogenetic tree and amino acid alignment presented in Figure 3.13 showed that most of the gaps between the protein sequences of DsNps3 and its putative orthologs in the initial alignment (Figure 3.12; red box) were due to the presence of the other less similar sequences. The most similar proteins to DsNps3 were from the Sordariomycete fungi *Colletotrichum somersetensis* (Colso1) (protein ID: 75126), and *M. grisea* (Maggr1) (protein ID: 116173), and the Dothideomycete *C. fulvum* (Clafu1) (protein ID: 185841, CfNps1). A big gap in the first half of CfNps1 was seen in the alignment, supporting the hypothesis of Collemare et al. (2014) that the *CfNps1* gene is truncated. The C-terminus of DsNps3 was shorter than that of its putative orthologs in the alignment. One possible reason for this was a frameshift or a nonsense mutation at the 3' end of *DsNps3*, but a three-frame translation of this region did not reveal any similarity to the extended C termini of the putative orthologs. Since all of the putative orthologs of DsNps3 are in Sordariomycetes fungi except the truncated CfNps1, DsNps3 may be unique in structure among the Dothideomycetes.

Of the proteins in Figure 3.13 only a few have been functionally characterised. The SM produced by FOXG_11847 (named beas after functional analysis) of *Fusarium oxysporum* was confirmed to be a virulence factor for both mice and tomato plants (López-Berges et al., 2013). SMs produced by the orthologs of *beas*, enniatin synthase from *F. avenaceum* and beauvericin synthase from *Beauveria bassiana (*López-Berges et al., 2013), were functionally characterised virulence factors on their respective potato and insect hosts (Xu et al., 2008; Herrmann et al., 1996). Therefore, there are precedents for orthologs of *DsNps3* as virulence factors.

3.2.3.2. Confirmation of gene model for *DsNps3*

Gene model confirmation was done by analysing the alignment of the predicted DsNps3 amino acid sequence with those of most closely related protein sequences and in culture and *in planta* RNA-seq data.

Figure 3.14 illustrates the domain organization of the DsNps3 protein (protein ID: 71189) and its alignment with its closest homologs according to the phylogenetic

analysis shown in Section 3.2.3.1. The protein alignment of DsNps3 has low overall consensus and DsNps3 amino acid identities to *C. fulvum*, *C. somersetensis*, and *M. grisea* were 42.72% (E=0), 42.59% (E=0), and 43.97% (E=0), respectively. The alignment also included at least three big gaps. However, none of the big gaps were in the domain positions and domains were more conserved than the rest of the alignment. Therefore, even though the alignment of DsNps3 with its closest homologs showed no evidence that the JGI gene model for *DsNps3* is incorrect, no clear decision could be made on whether the *DsNps3* gene model is correct due to low similarity between DsNps3 and its closest homologs.

The predicted gene model for *DsNps3* has no introns and this was confirmed by continuous cDNA reads from start codon to stop codon in the RNA-seq data that were mapped to the JGI gene model for *DsNps3* (Appendix 7). Therefore, although the alignment of DsNps3 with its closest homologs does not provide evidence for whether the JGI gene model is correct because of the low similarity of DsNps3 with its closest homologs, it is supported by the RNA-seq data.

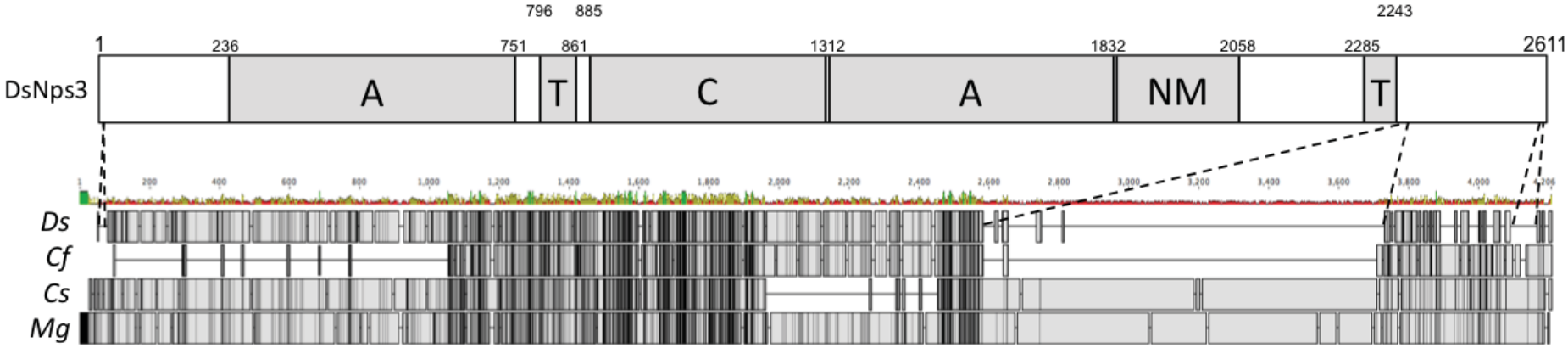

Figure 3.14. Domain structure of DsNps3 and its protein alignment with closest homologs. DsNps3 indicates the peptide's domain organization with A: adenylation, T: thiolation, C: condensation, NM: N-methyltransferase domains. Numbers indicate amino acid positions of domain borders (borders of domains that are too close to another border are not shown). Dotted lines show positions of the DsNps3 gaps in the alignment. The dark regions indicate the amino acid alignment with black (highly similar) to white (not similar) sequences with respect to the consensus sequence. The total length is 2611 amino acids. The diagram was drawn to scale. The amino acid alignment below shows *Ds*: *D. septosporum*, *Cf: Cladosporium fulvum* (protein ID: 185841), *Cs*: *C. somersetensis* (protein ID: 75126), *Mg*: *Magnaporthe grisea* (protein ID: 116173). The coloured bar represents consensus identity with red (below 30%); green shades indicate higher levels of identity (up to 100%) with bar height proportional to % identity.

3.2.3.1. Comparison of *DsNps3* from 19 strains of *D. septosporum*

Comparison of *DsNps3* across 19 *D. septosporum* strains was done by aligning the *DsNps3* nucleotide sequences and determining the evolutionary selection pressure. Figure 3.15 shows *DsNps3* nucleotide sequence alignment of NZE10 with 18 additional *D. septosporum* genomes. For *DsNps3*, dN/dS is 0.27, therefore, *DsNps3* is under negative selection, suggesting that the gene might have a critical role for *D. septosporum*. However, the alignment presented in Figure 3.15 shows that four codons, including one codon from the first A domain and one codon from the NM domain are under statistically significant (P>0.95) positive selection. This alignment also supported the gene model analysis discussed in Section 3.2.3.2, suggesting that the gene model is correct. It was not possible to determine negatively selected sites due to lack of *DsNps3* orthologs in other species and the highly similar sequences for the 19 *D. septosporum* genomes.

In conclusion, according to the dN/dS ratio *DsNps3* is under negative selection but has four statistically significant positively selected sites. Alignment of *DsNps3* from the 19 *D. septosporum* genomes also supports the JGI gene model for *DsNps3.*

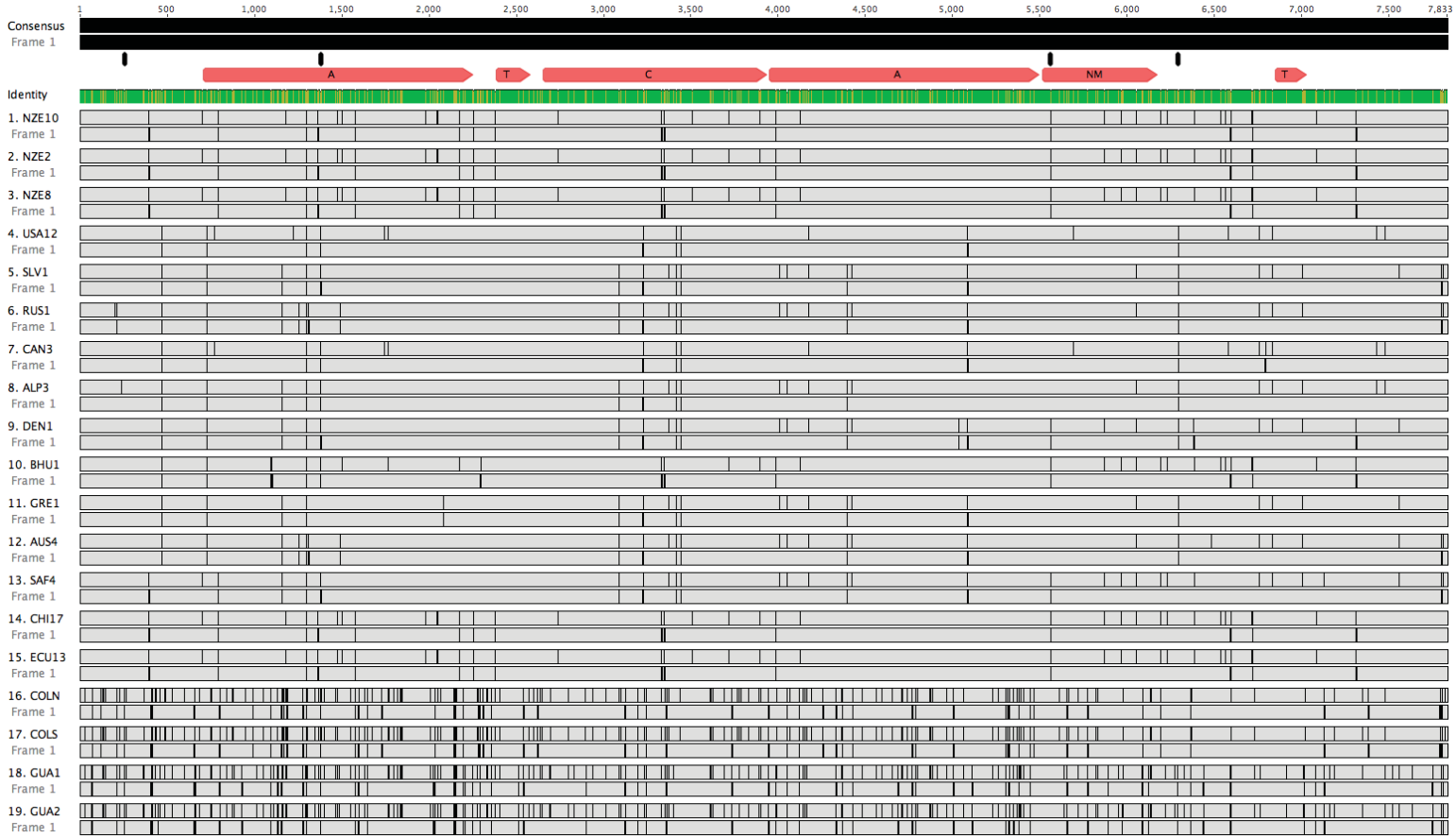

Figure 3.15. *DsNps3* nucleotide alignment of NZE10 with 18 additional genomes. Red arrows show the domain positions with A: adenylation, T: thiolation, C: condensation, NM: N-methylation. Bold black lines above domains show statistically significant positively selected codons (P>0.95). Nucleotide sequence of *DsNps3* is 7833 bp. The coloured bar represents consensus identity with brown indicating identities above 30% and below 100% and green indicating 100% identity. For each sequence, vertical bars on the top and bottom lines show differences in nucleotide and amino acid sequences compared to NZE10. A bar on the top line alone shows a synonymous mutation and a bar on both lines shows a non-synonymous mutation. Strains used in this analysis are listed in Appendix 5.

3.2.3.2. Gene cluster analysis

Gene cluster analysis was performed on *DsNps3* and its neighbouring genes as explained in Section 2.14.5 in order to predict the genes that might take part in the production of the corresponding nonribosomal peptide. Figure 3.16 shows the putative gene cluster for *DsNps3*, possible regulatory genes of the gene cluster and expression of genes in the putative gene cluster and the possible regulatory genes. Predicted functions of the genes in the *DsNps3* putative gene cluster are shown in Figure 3.16. Since *DsNps3* was a gene of main interest in this project, genes with potential regulatory roles were included in the gene cluster analysis. The *DsNps3* putative gene cluster spans a 44 kb region containing 4 genes in chromosome 4. In this region, there are also 2 potential regulatory genes and 6 genes with no predicted functions related to secondary metabolism. The biggest distance between two genes belonging to the putative gene cluster is 24 kb, containing 1 potential regulatory gene and 6 genes with no SM-related functions.

Gene cluster analysis of *DsNps3* (Figure 3.16) showed that none of the genes in the putative gene cluster were co-expressed with *DsNps3*, which was expressed significantly higher at early stage compared to mid and late stages. Ds71190 and Ds170752 were expressed significantly higher at mid-stage compared to early and late stages, and Ds71198 was most highly expressed at late stage of infection. Genes within the SM gene clusters are generally co-expressed (Keller and Hohn, 1997), however, this is not always the case (Turgeon and Bushley, 2010). An example to a SM gene cluster that is not co-expressed is the dothistromin gene cluster of *D. septosporum*, explained in detail in Section 1.4.5.1.

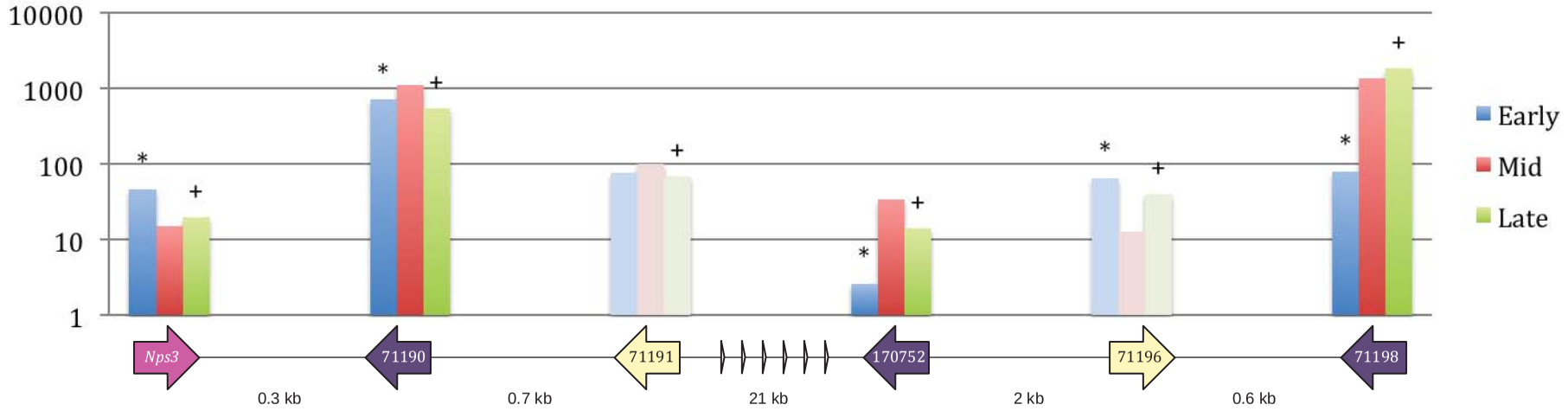

Figure 3.16. Organization and expression of *DsNps3* and its neighbouring genes in early, mid, and late stages of infection. Numbers inside arrows indicate JGI protein IDs. Pink: Secondary metabolite core gene (*DsNps3*). Purple: putative *DsNps3* cluster genes. Yellow: Genes that are not part of the putative gene cluster but have potential regulatory roles. Small white arrows: genes without predicted SM functions. Significant differences between early-mid and mid-late stages were marked with "*" and "+", respectively ($p<0.05$). The differences between early and late stages were also significant for all cluster and potential regulatory genes except Ds71191.

Table 3.5. Genes within *DsNps3* putative gene cluster.

JGI Protein ID[a]	Predicted protein[b]	Best hit organism/JGI ID	E / identity %
*Ds71189/*Nps3*	Non-ribosomal peptide synthetase	*Penicillium expansum*/371848	8.5e-187/52.4
+Ds71190	Alcohol dehydrogenase, class V	*Cladosporium fulvum*/189228	0/95.8
*Ds170752	Short chain dehydrogenase/reductase	*Mycospherella fijiensis*/57497	1.2e-103/64.2
*Ds71198	Flavin-containing monooxygenase	*Cladosporium fulvum*/196698	0/93.6

[a] http://genome.jgi.doe.gov/Dotse1/Dotse1.home.html
[b] Predicted proteins according to antiSMASH and InterProScan
Asterisk indicates genes with similar predicted functions present in other fungal NPS gene clusters.
+ Genes with similar predicted function to Ds71190 was found in other fungal SM gene clusters such as dothistromin gene cluster (Bradshaw et al., 2013).
All BlastP hits were confirmed true with reciprocal blast analyses.

The predicted functions of two of the three genes in the putative *DsNps3* gene cluster are similar to those predicted in other NRPS gene clusters. A gene encoding for a short chain dehydrogenase/reductase is present in the NRPS gene cluster of apicidin belonging to *F. incarnatum* (Jin et al., 2010), and there is a gene predicted to encode for a short chain dehydrogenase 25 kb downstream of *DsNps3*. In addition, monooxygenases are another common element found in SM gene clusters (Zhang et al., 2014; Collemare et al., 2014) and a predicted flavin containing monooxygenase gene is also present in the putative gene cluster of *DsNps3*.

The third gene (Ds71190), just downstream of *DsNps3*, is predicted to encode an alcohol dehydrogenase. Such genes are commonly found in fungal indole diterpene or PKS gene clusters such as the dothistromin gene cluster of *D. septosporum* (Young et al., 2001, Bradshaw et al., 2013), but have not been reported in NRPS gene clusters.

Aside from the biosynthetic genes belonging to the *DsNps3* putative gene cluster, two genes that may have a regulatory role were found. Genes Ds71191 and Ds71196 are predicted to encode a splicing coactivator and a sensory transduction histidine kinase, respectively. Studies on a splicing coactivator gene from *A. carbonarius* showed a high correlation between the expression of a possible regulatory splicing coactivator gene and ochratoxin A production (Lunardi et al., 2009). A gene encoding an osmotic signal transduction histidine kinase was reported to take part in the regulation of secondary metabolism of *Fusarium graminearum* (Ochiai et al., 2007).

The predicted DsNps3 SM was cyclosporin according to NaPDoS prediction (Table 3.1). Gene clusters responsible for cyclosporin production were explained in detail at Section 3.2.1.3. However, genes in the *DsNps3* putative gene cluster do not support this prediction.

3.2.3.3. Knockout of *DsNps3*

In order to perform functional analysis of the *DsNps3* gene, deletion mutants were prepared. However, because *DsNps3* is a very large gene, only two of the essential domain regions were deleted and a reading frame shift was ensured. First, the *DsNps3*-pOSCAR KO construct (Appendix 8) was prepared as explained in Section 2.7.2. Following transformation of the KO construct into *D. septosporum* NZE10 protoplasts as outlined in Section 2.9, 38 hygromycin-resistant colonies were obtained. From them, two single-spore purified colonies, derived from one transformant, were confirmed to be *ΔDsNps3* strains by PCR, using first a primer pair that only amplifies wild type but not *ΔDsNps3* (Figure 3.18a), and then using two primer pairs that each targeted the hygromycin coding region and 5' or 3' flanking regions (Figure 3.18b). Primer binding positions are shown in Figure 3.17.

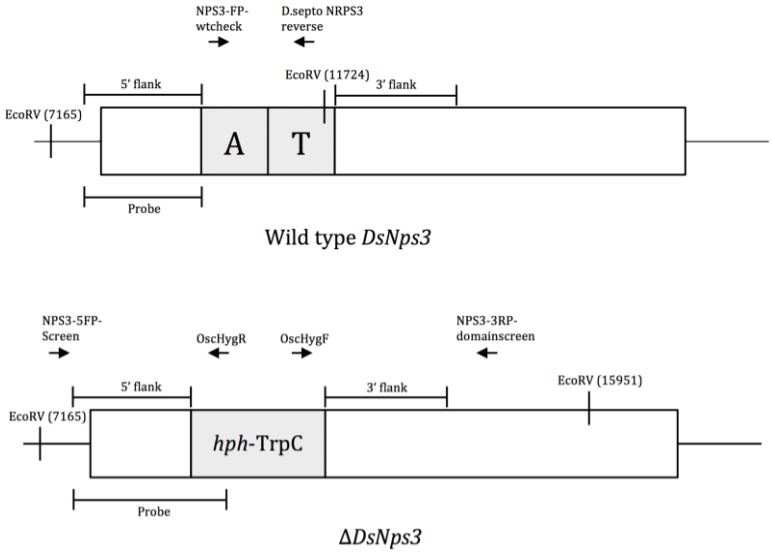

Figure 3.17 Schematic representation of wild type and KO mutants of *DsNps3*. The positions of EcoRV restriction enzyme recognition sites, primer-binding sites, flanking regions, knockout target region in wild type (A and T domains) and hygromycin resistance gene (*hph*) with *TrpC* promoter were shown.

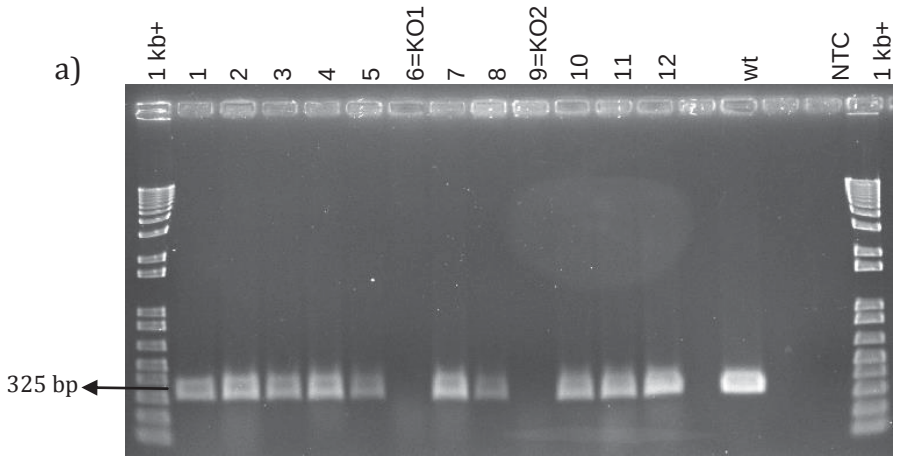

Figure 3.18. PCR-based confirmation of purified colonies for the absence of WT genotype. 12 colonies were sub-cultured from a single-spore purified colony were analysed using PCR-based confirmation that amplify wild type but not *ΔDsNps3* to confirm successful purification using primers NPS3-FP-wtcheck and D. septo NRPS 3 reverse (325 bp). Wt: Wild type. NTC: No template control.

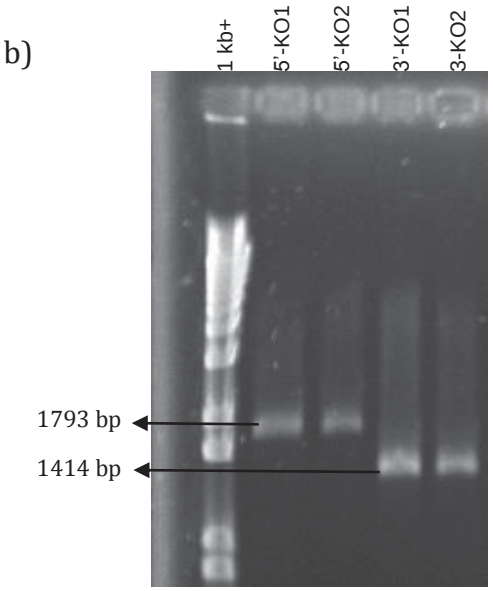

Figure 3.19. PCR-based confirmation of *ΔDsNps3* candidates for the presence of the KO genotype. The colonies 6 and 9 that were identified lacking WT genotype (named KO1 and KO2, respectively) were analysed using PCR amplifation with primers Nps3-5FP-Screen and OscHygR for 5' end (1793 bp) and OscHygF and NPS3-3RP-domainscreen for 3' end (1414 bp).

Lack of PCR products in colonies 6 and 9 in the PCR amplifications presented in Figure 3.18a suggests the loss of *DsNps3* by gene replacement in these two colonies. Therefore, the colonies 6 and 9 (named as KO1 and KO2, respectively), which were purified from the same transformant, were confirmed not to contain

any wild type gDNA, confirming successful purification. PCR amplification presented in Figure 3.18b confirmed the *ΔDsNps3* mutants by amplifying 5' and 3' ends of the hygromycin coding region and the flanking sites.

Following preliminary screening of *ΔDsNps3* candidates, Southern blot hybridization was used to confirm single copy integration of the KO construct at the correct position in the *ΔDsNps3* candidates, KO1 and KO2 (Appendix 9).

Confirming *ΔDsNps3* using PCR and Southern hybridization enabled future analyses for the determination of the metabolite and the effects of *DsNps3* gene loss for *D. septosporum*.

3.2.3.4. TLC analysis

In order to determine the Nps3 SM, TLC analysis was performed by comparing the SMs extracted from wild type and *ΔDsNps3* strains. Preliminary TLC analyses were done to determine optimum conditions for Nps3 SM extraction by using organic solvents with increasing polarity each time, based on suggestions of Dr. Mark Patchett (Massey University) (Figure 3.20). Preliminary screenings based on these solvents showed differences in the TLC band profiles of wild type and *ΔDsNps3* (Figure 3.20) in the culture filtrate. No difference between wild type and *ΔDsNps3* was observed in the metabolites extracted from mycelia.

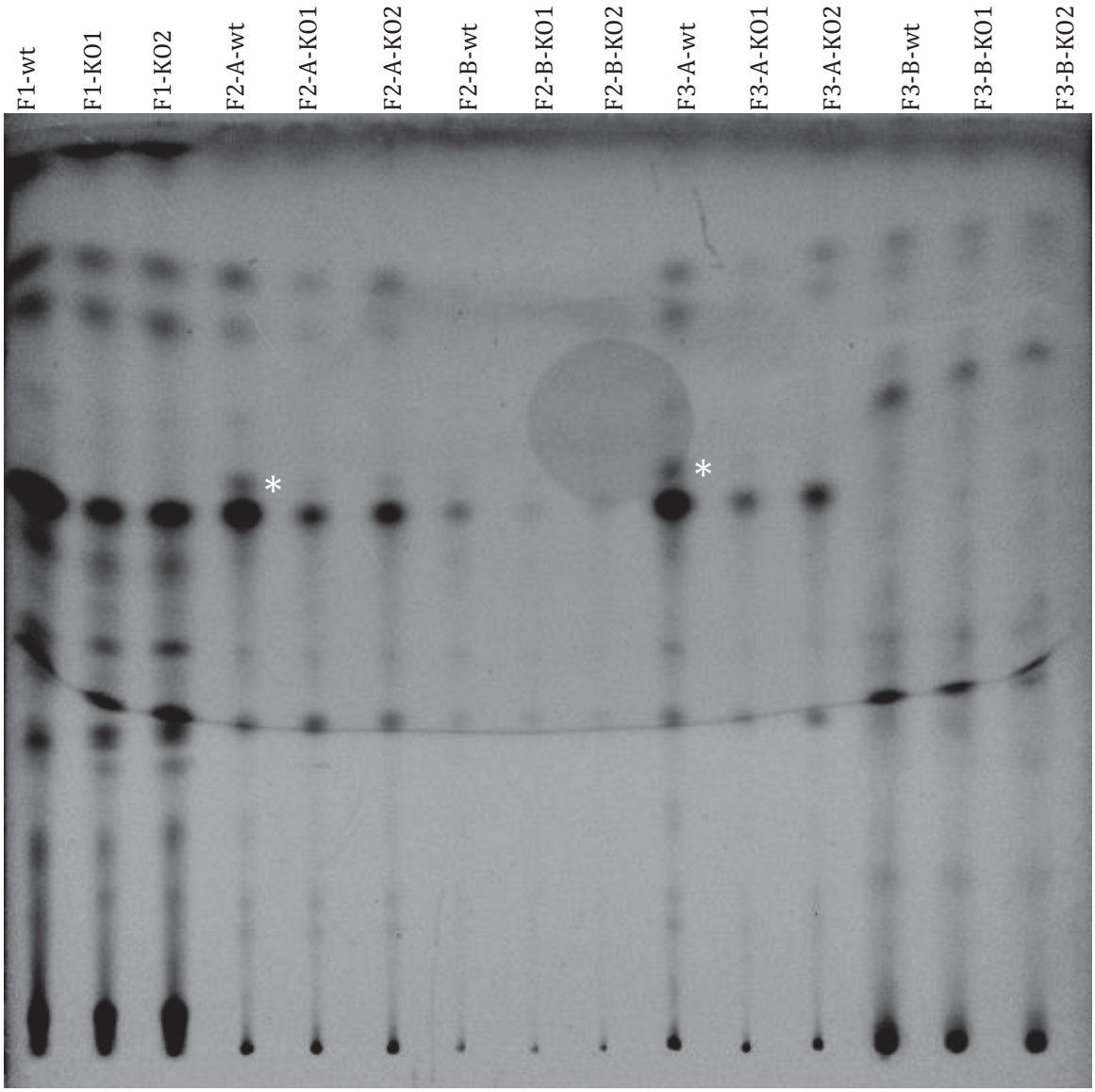

Figure 3.19. Solvent optimization for Nps3 SM detection in TLC analysis. Numbers and letters indicate the solvent used for the extraction of metabolites. F1: EtAc, F2-A: Chloroform, F2-B: Dichloromethane after chloroform, F3-A: Dichloromethane, F3-B: 1-Butanol after dichloromethane. wt: Wild type, KO1 and KO2: *ΔDsNps3 D. septosporum* strains. The metabolite present in wild type but missing in *ΔDsNps3* was shown with an asterisk.

Initial TLC analysis for the solvent optimization suggested that the metabolites extracted using chloroform and dichloromethane showed differences in the TLC profiles between wild type and *ΔDsNps3* strains (Figure 3.20). The metabolite represented with an asterisk was initially thought a candidate for Nps3 SM. Therefore; dichloromethane was used for extraction for Nps3 metabolite determination.

For comparison of the metabolites extracted from *ΔDsNps3* and wild type *D. septosporum* strains, the amounts of metabolites spotted onto the TLC plate were normalized based on dothistromin levels in the samples estimated by measuring intensity of TLC bands (Section 2.11.2). In addition, the amount of metabolite dried down before resuspension and spotting onto the TLC plate for each strain was increased from 200 µL for each strain to 10 mL, 5.9 mL and 6.4 mL for wild type, KO1 and KO2 respectively, enabling visualization of faint bands. Figure 3.21 shows the TLC analysis of wild type and *ΔDsNps3* using approximately equal amount of metabolites. This showed that the band that was initially thought missing in *ΔDsNps3* (Figure 3.20) was present in both wild type and *ΔDsNps3* strains. However, another band that was too faint to visualise in the initial TLC screening (Figure 3.20) was present in wild type and missing in both *ΔDsNps3* strains.

The TLC profile analysis presented in (Figure 3.21) shows one band present in the wild type and missing in the *ΔDsNps3* KO1 and KO2 strains that might be a candidate for the SM synthesized by Nps3. However, the result was not very clear, as there were multiple faint bands very near to each other. There was also another difference in the band profiles between wild type and *ΔDsNps3* KO1 and KO2 strains that was not visible to naked eye, but detected by a small peak in the quantification analysis. These two bands may represent Nps3 SM or its intermediates. Another possibility is that Nps3 SM might not be produced at high levels in PMMG. These problems might be solved by changing the growth conditions and applying better extraction and separation methods. It should also be noted that no difference was observed on TLC profiles of wt and Nps3 KO mutants if the metabolites were extracted with ethyl acetate, the solvent used for extracting metabolites in Section 3.1.3. Therefore, this band was not observed at all on analysis of the effects of different media conditions.

To sum up, in the TLC analysis of metabolites extracted from wild type and *ΔDsNps3* using dichloromethane, a candidate for Nps3 SM was present in wild type but missing in the *ΔDsNps3*. However, since the candidate metabolite was not produced at high levels and not separated sufficiently, no chemical characterization was performed.

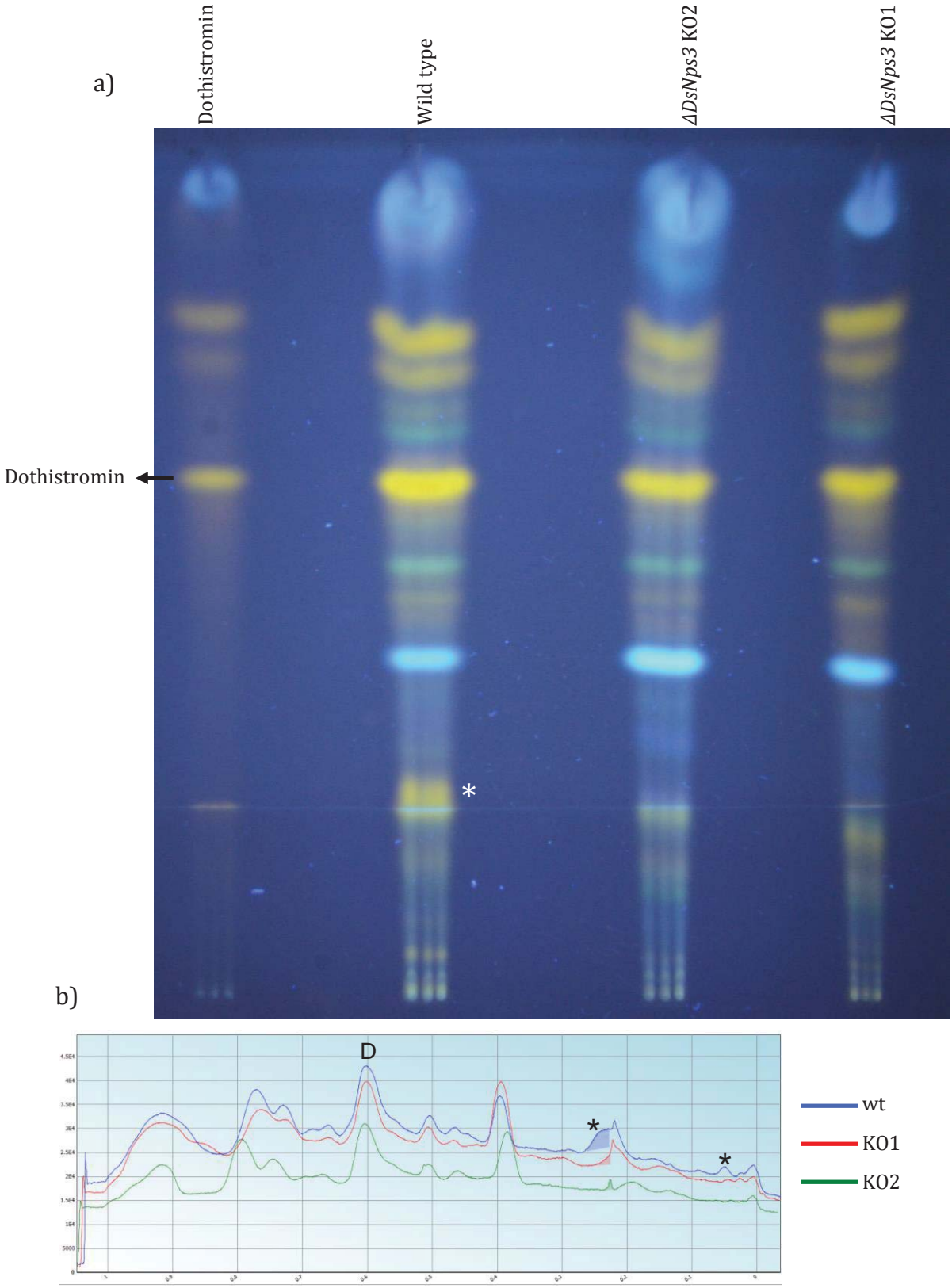

Figure 3.20. TLC picture and band profiles of *D. septosporum* wild type and *ΔDsNps3* strains. Metabolites that were present in wild type and missing in *ΔDsNps3* samples is indicated with asterisks. Dothistromin was used as control and the peak corresponding dothistromin band is indicated with the letter D.

3.2.3.5. Sporulation and growth rate analyses

Fungal secondary metabolites such as aflatoxin and sterigmatocystin are usually associated with asexual sporulation, and there are many SMs reported to affect sporulation (Skory et al., 1993; Calvo et al., 2002). Both sporulation and metabolite biosynthesis are usually negatively regulated by G-protein-mediated signalling pathways when the growth signals are down (Hicks et al., 1997). On the other hand, loss of some secondary metabolites cause reduced growth rate in fungi (Calvo et al., 2002). Therefore, to test the hypothesis that *DsNps3* affects sporulation, wild type and *ΔDsNps3* spores were counted as outlined in Section 2.12.2. Radial growth rate analysis was also done by measuring wild type and *ΔDsNps3* colony diameter every 3 days over a period of 30 days (Section 2.12.3).

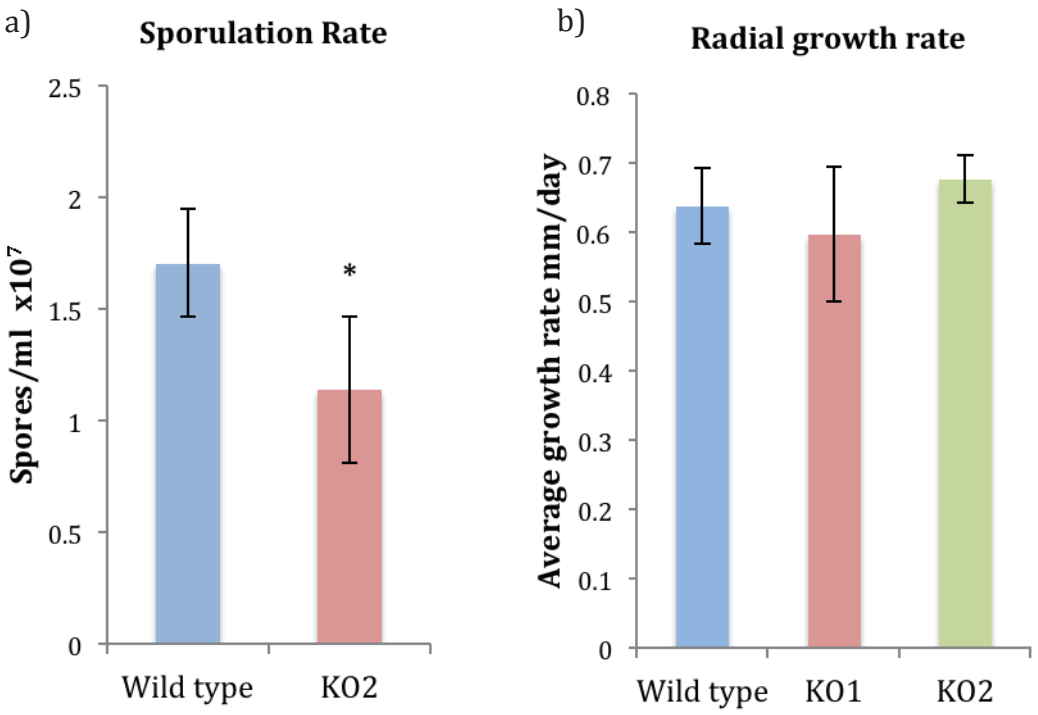

Figure 3.21. Sporulation and radial growth rates of *D. septosporum* wild type and *ΔDsNps3* strains. a) Number of spores/mL of culture x10^7 for wild type and *ΔDsNps3* KO2 strains. Asterisk shows the significant difference ($p<0.05$) between wild type and *ΔDsNps3* KO2. Two technical replicates were counted for each of three biological replicates. b) Average growth rates (mm/day) of wild type and *ΔDsNps3* KO1 and KO2 strains. Four biological replicates were counted.

The number of spores was significantly lower ($p<0.05$) by 33% in *ΔDsNps3* compared to wild type *D. septosporum* (Figure 3.22a). *ΔDsNps3* KO1 was not included in the sporulation rate analysis because of dense mycelia that interfered with spore counting that was most likely because of failure to apply equal pressure on the plates for release of spores, which resulted in stripping of mycelia from the KO6 plate. Radial growth rate analysis results showed no significant difference ($p<0.05$) between wild type and *ΔDsNps3* KO strains (n=8) (Figure 3.22b).

In conclusion, *D. septosporum ΔDsNps3* showed significantly lower sporulation compared to wild type, but no difference in radial growth rate.

3.2.3.6. Pathogenicity assay

To determine if the SM produced by the *DsNps3* gene cluster is a virulence factor, pine seedlings were inoculated with wild type or *ΔDsNps3 D. septosporum* spores. Comparisons were made of the fungal surface network at an early stage of infection. Then the timing of first lesion appearance, lesion size, number, and fungal biomass estimations between wild type and *ΔDsNps3*-infected needles were compared as outlined in Section 2.12.1.

The first step of plant fungal infection is the plant host surface interaction, and this step plays a vital role in the early stages of the disease process. At this stage, attachment to plant surface, spore germination, recognition of the host, infection structure formation and finally the penetration of the host tissue occur (Knogge et al., 1998). Since *DsNps3* was expressed at a significantly higher level at early stage compared to mid and late stages (Figure 3.1), it is possible that Nps3 SM might play a role in the early stages of the infection. Fungal surface network at early stage of *D. septosporum* infection was compared between wild type and *ΔDsNps3* to test the hypothesis that DsNps3 has a role during the asymptomatic period of the infection. The percentage area covered by the *D. septosporum* infected pine needles was significantly less in *ΔDsNps3* KO2 compared to wild type. Figure 3.23 shows representative images of the surface network analysis of wild type and *ΔDsNps3.*

All of the fluorescence microscopy images used in this analysis are presented in Appendix 10.

a)

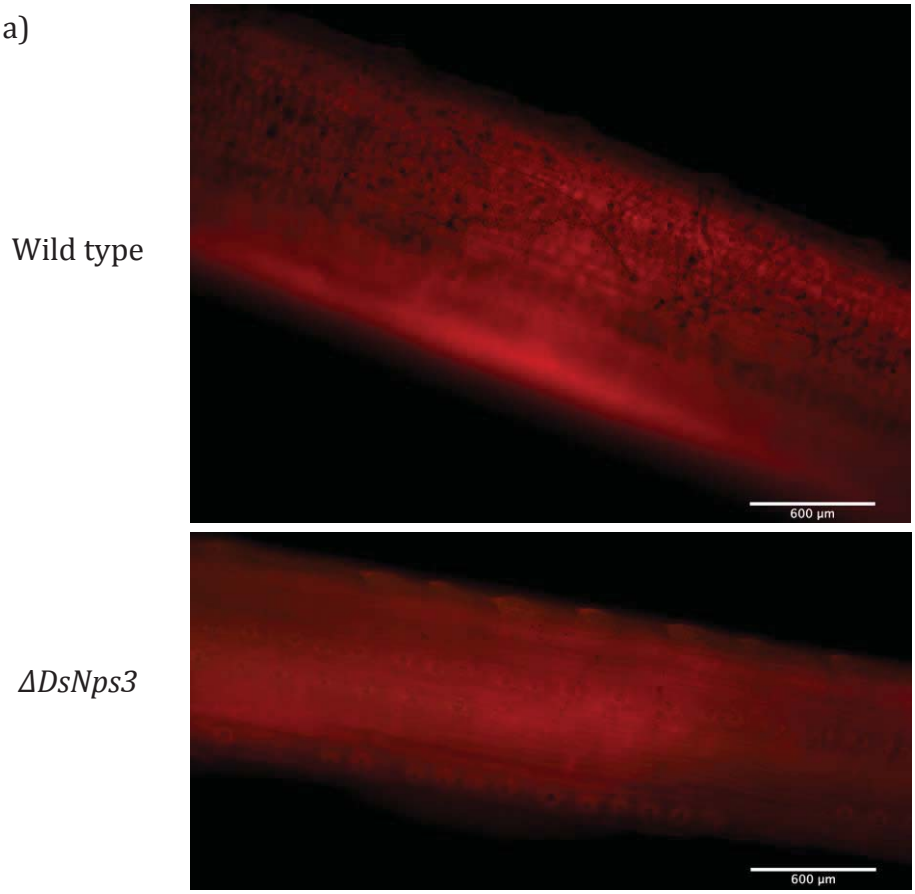

b)

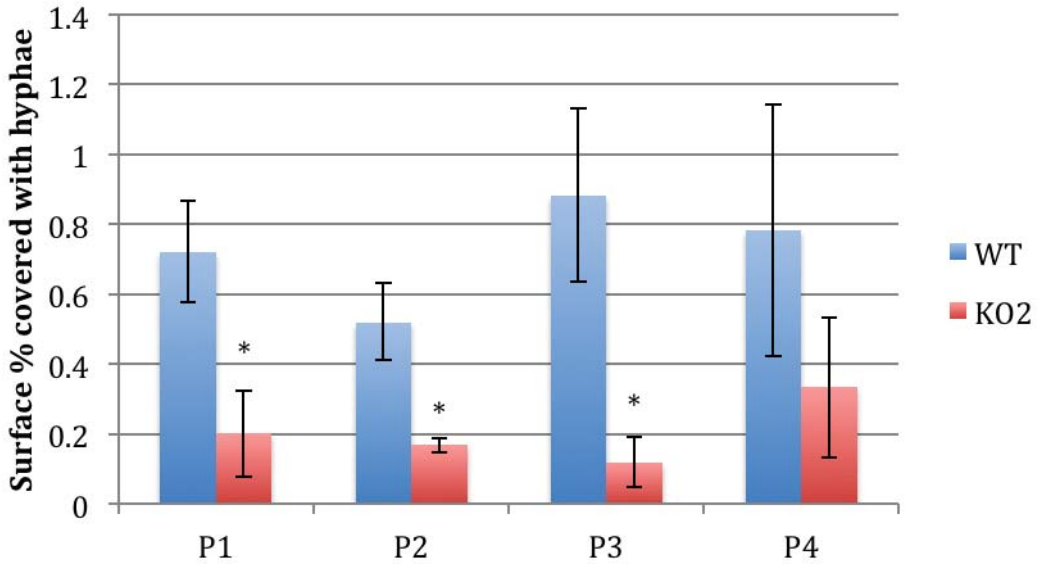

Figure 3.22 Hyphal network on pine needle surface infected with wild type and *ΔDsNps3 D. septosporum*. a) Sample fluorescence microscopy images of wild type and *ΔDsNps3* infected P3 at 15 dpi. b) Percentage of needle surface covered by fungal hyphae. Different plant genotypes are named P1-P4. WT: Wild type, KO2: *ΔDsNps3*. Significant differences between wt and *ΔDsNps3* strains ($p<0.05$) are shown with an asterisk. The largest three surface networks were measured per plant genotype for each strain.

Surface network analysis presented in Figure 3.23 show that the hyphal network on the needle surface was significantly lower in three of the four plant genotypes tested in *ΔDsNps3* compared to wild type. KO1 was not included in the analysis since they are the same mutants from a single transformant (Section 3.2.3.3).

In order to test if Nps3 SM may be a virulence factor, the ratio of fungal to plant biomass in the lesions obtained from wild type and *ΔDsNps3* infected needles was estimated using real-time PCR with known single-copy *D. septosporum* and *P. radiata* genes as explained in Section 2.12.1.2. Figure 3.24 shows the comparison of estimated fungus to plant biomass ratios of *ΔDsNps3*-infected lesions with those of wild type infected lesions.

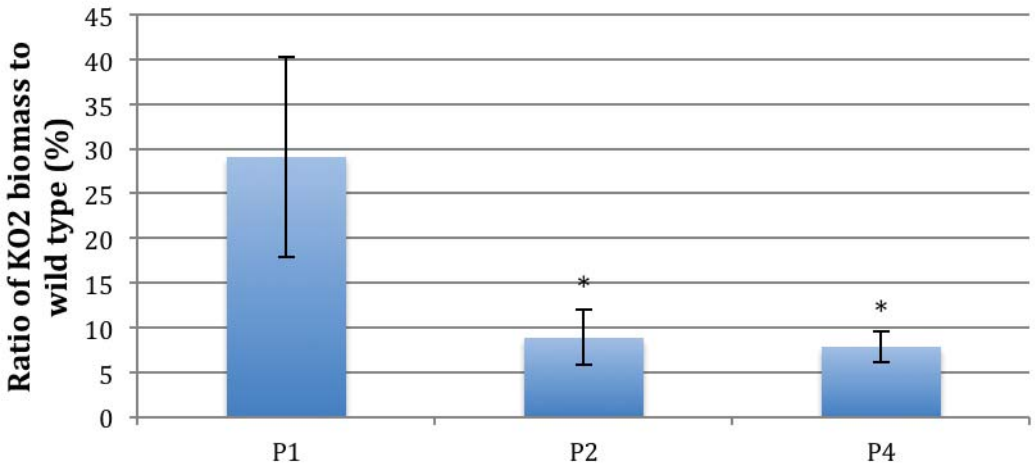

Figure 3.23. Fungal biomass ratio of *ΔDsNps3*-infected lesions to wild type *D. septosporum* infected lesions. Different plant genotypes are named P1-P4. KO2:*ΔDsNps3*. The needles were harvested at 18 wpi.

The analysis in Figure 3.24 showed that fungus to plant biomass ratios of *ΔDsNps3*-infected lesions were less than 30% of that of wild type-infected lesions. The difference in ratios of wild type and *ΔDsNps3*-infected lesions of the plant genotype P1 was not significant due to variations up to 2 fold between replicates. Overall, early stage hyphal surface network and fungal biomass assay results suggest that the Nps3 SM may be a virulence factor. Full biomass estimation assay results are presented in Appendix 11.

Even though surface network significantly decreased in *ΔDsNps3* compared to wild type, no significant differences were observed in the timing of first lesion

appearance, lesion size, or number between wild type and *ΔDsNps3* (Table 3.6). Lesion pictures for each plant genotype and strain are shown in Appendix 12.

Table 3.6 Lesion number, size and first lesion appearance in wild type and *ΔDsNps3 D. septosporum* infected pine needles.

	wt-P1	KO2:P1	wt-P2	KO2-P2	wt-P4	KO2-P4
[a]**Lesion number**	38	8	11	7	36	17
[b] **Lesion size (mm)**	2.1±1.3	1.8±1.4	1.5±0.9	1.5±0.6	2.2±1.2	2.4±1.1
[c] **First lesion**	7	7	8+	8+	5	5

[a] Number of lesions per tree
[b] Average lesion sizes with standard deviation from the number of lesions shown in [a].
[c] First lesion appearance in weeks post inoculation (wpi)
No lesion was observed in P3 after 18 wpi.

A limitation with the pathogenicity assay was the difficulty of having successful infection. For example, no lesion was observed on the needles of the 4th plant genotype P3 even though there was a significant difference in the fungal surface network (Figure 3.23). It is challenging to achieve reliable and consistent *D. septosporum* infection using artificial inoculation under controlled conditions and high variations can occur in the duration infection stages (Kabir et al., 2013). Another possibility for observing no DNB symptoms in P3 could be due to heavy insect infestation on the P3 samples during the incubation period that might have increased basal defence responses of these plants. Also, the plants used in this experiment (P1-P4) had different genotypes, which contributed to the variations between different plants. Initial predictions on the resistance levels of the plants to the *D. septosporum* were P3>P4>P2>P1. The fact that the findings in this experiment didn't correlate with the initial predictions suggest that the impact of the insect infestation might have had a bigger role in the infection rates compared to that of plant genotypes.

To sum up, the predicted gene model for *DsNps3* appears to be correct but phylogenetic analysis suggests that the Nps3 SM may be unique among Dothideomycetes. In addition, decreased sporulation rate, early stage fungal surface network, and fungal biomass *in planta* were observed with the *ΔDsNps3* mutant compared to wild type. However, no difference was seen in radial growth rate, lesion number, size, or the timing of first lesion appearance in pathogenicity assays between *ΔDsNps3* and wild type. Therefore, reduced fungal surface network

in the early stage of infection and reduced fungal biomass in late stage lesions in *ΔDsNps3* compared to WT suggest that the DsNps3 SM may be a virulence factor.

3.3. Polyketide synthases

D. septosporum has five predicted PKS core genes (Table 3.1). However, only *DsPks1*, *DsPks2*, and *DsPks3* were focused on in this project because the preliminary analyses showed that *DsPks4* is a truncated gene and *DsPksA* was extensively studied previously (Section 1.4.4.1).

3.3.1. PKS1

Among the *D. septosporum* SM core genes, *DsPks1* had the highest level of expression at the late stage of pine needle infection (Figure 3.1). Therefore, *DsPks1* was one of the key genes of interest as explained in Section 3.1.2 and phylogenetic analysis was done for DsPks1 in addition to the analyses done for all of the SM core genes.

3.3.1.1. Phylogenetic analysis

To determine if DsPks1 protein has any functionally characterised orthologs, phylogenetic analysis was done by aligning DsPks1 and its best reciprocal hits from all Dothideomycetes, Eurotiomycetes, and Sordariomycetes in the JGI database, followed by phylogenetic tree building using the Maximum Likelihood method as explained in Section 2.14.3. The phylogenetic tree of DsPks1 (Figure 3.25) showed that all of the closest homologs of DsPks1 were from fungi in the Dothideomycetes class. These proteins were from *Z. cellare* (protein ID: 19481), *C. fulvum* (protein ID: 191425), *M. graminicola* (protein ID: 96592), *M. fijiensis* (protein ID: 216850), *Cercospora zeae-maydis* (protein ID: 68161), and *Septoria musiva* (protein ID: 159092).

None of the putative orthologs of DsPks1 from the phylogenetic analysis presented in Figure 3.25 have been functionally characterised. However, CfPks1 is predicted to have a role in elsinochrome and/or melanin biosynthesis (Collemare et al., 2014). In addition, *M. graminicola* (now called *Zymoseptoria tritici*) PKS1 (protein

ID: 96592) is considered to be involved in DHN-melanin biosynthesis (Lendenmann et al., 2014) and the *C. lagenarium* ortholog of *MgPKS1* was functionally characterised to be involved in melanin biosynthesis using gene knockout and complementation assays (Kubo et al., 1991; Takano et al., 1995). Therefore, DsPks1 might be responsible for biosynthesis of a compound with similar structure to melanin or elsinochrome.

Fungal melanins have a variety of functions such as protection against exogeneous stress factors, contributing to cell wall related functions such as pressure-stabilization, and as virulence factors (reviewed by Scharf et al., 2014). For example, the rice blast fungus *M. oryzae* requires DHN-melanin to penetrate host cell walls during infection, as shown by the inability of melanin-deficient (albino) mutants to penetrate epidermal cells (Chumley and Valent, 1990). Elsinochrome is a non-host-selective toxin and virulence factor produced by *Elsinoë fawcettii* and *Elsinoë australis* (Chung, 2011). Therefore, considering the high expression level of *DsPks1* in planta and the virulence-associated roles of DHN-melanin in other fungi, it is possible that the DsPks1 SM may be a virulence factor.

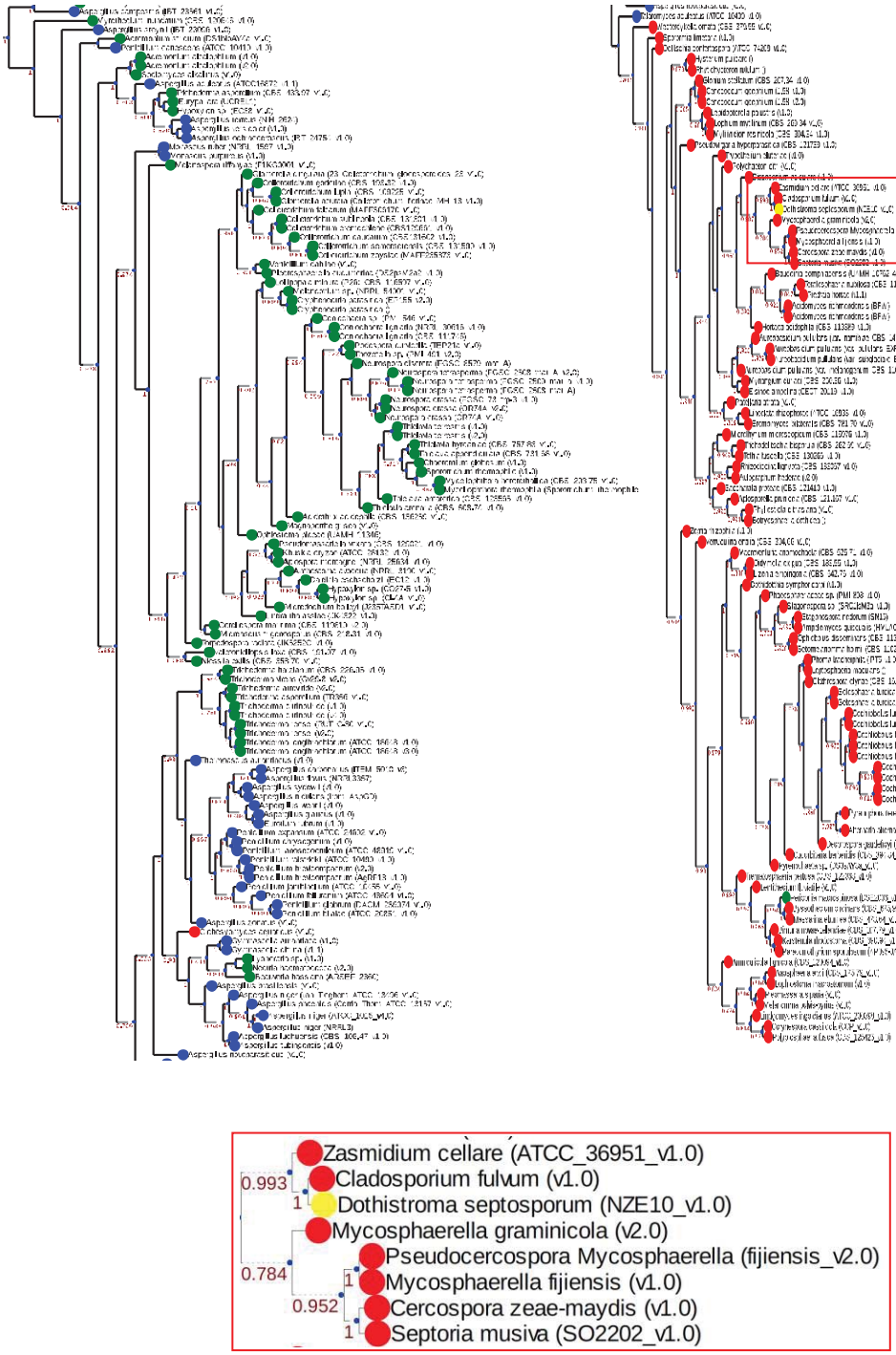

Figure 3.24. Phylogenetic analysis of DsPks1. Yellow: *D. septosporum*. Red: Dothideomycetes. Blue: Eurotiomycetes. Green: Sordariomycetes. Numbers on the nodes indicate approximate likelihood ratio test (aLRT) scores. *D. septosporum* and its closest homologs are shown in a red square. Details of the genome sequences used are presented in Appendix 23.

3.3.1.2. Confirmation of gene model for *DsPks1*

The JGI gene model for *DsPks1* was confirmed by aligning its protein sequence with its closest homologs, including its *C. fulvum* ortholog, *CfPks1* (de Wit et al., 2012) as well as by analysing RNA-seq data. The DsPks1 protein alignment (Figure 3.26) has high overall consensus. Amino acid identities of DsPks1with its closest homologs were 94.34% (E=0) for CfPks1, 86.47% (E=0) for the Pks of *Zasmidium cellare*, and 79.67% (E=0) for that of *M. graminicola*, suggesting that the proteins within the alignments share similar functions. There was no gap or insertion in the DsPks1 sequence at the alignment, therefore supporting the JGI gene model for *DsPks1*. The predicted gene model for *DsPks1* has no introns and this was confirmed by the RNA-seq data (Appendix 13).

3.3.1.3. Comparison of *DsPks1* from 19 strains of *D. septosporum*

Evolutionary selection pressure on *DsPks1* was analysed by aligning *DsPks1* sequences from 19 *D. septosporum* strains, from varying international origins, estimating the overall selection pressure using dN/dS ratio and detecting the sites that are under significant selection (Section 2.14.4). The dN/dS ratio of *DsPks1* is the lowest of *D. septosporum* SM core genes (dN/dS=0.13), indicating that *DsPks1* is under strong negative selection. This suggests that the Pks1 SM, a predicted melanin, may be an important compound for *D. septosporum*. Only one codon, just before the AT domain, showed significantly positive selection (P>0.99) (Figure 3.27).

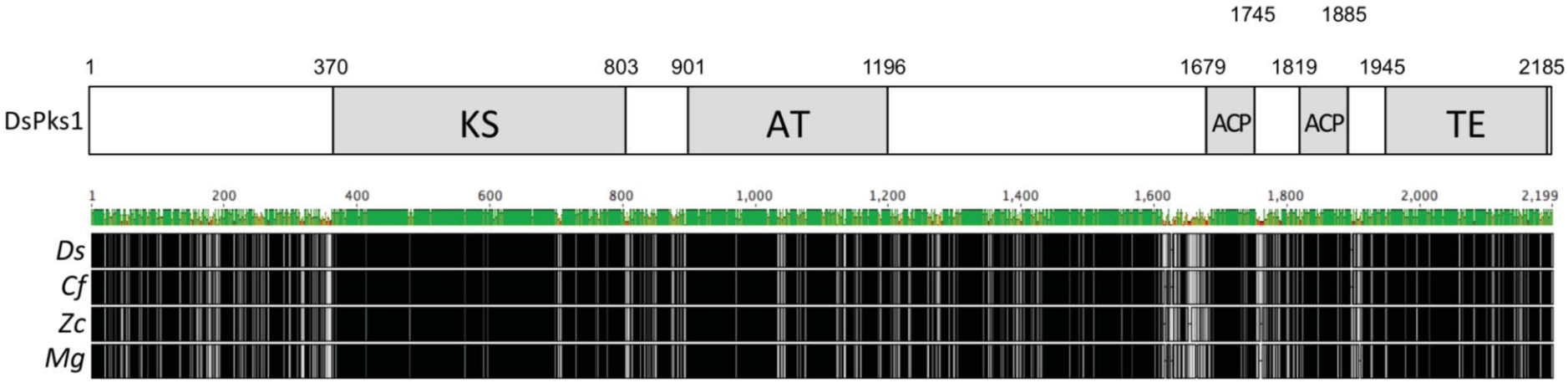

Figure 3.25. Domain structure of DsPks1 and its protein alignment with closest homologs. DsPks1 indicates the peptide's domain organization with KS: keto-synthase, AT: acyltransferase, ACP: acyl carrier protein, TE: thioesterase domains. Numbers indicate amino acid positions of domain borders in addition to start of the DsPks1 peptide sequence. The total length is 2189 amino acids. The diagram was drawn to scale. The dark regions indicate the amino acid alignment with black (highly similar) to white (not similar) sequences with respect to the consensus sequence. The amino acid alignment shows *Ds*: *D. septosporum* Pks1, *Cf*: *C. fulvum* (protein ID: 191425), *Zc*: *Z. cellare* (protein ID: 19481), *Mg*: *M. graminicola* (protein ID: 96592). The coloured bar represents consensus identity with red (below 30%); green shades indicate higher levels of identity (up to 100%) with bar height proportional to % identity.

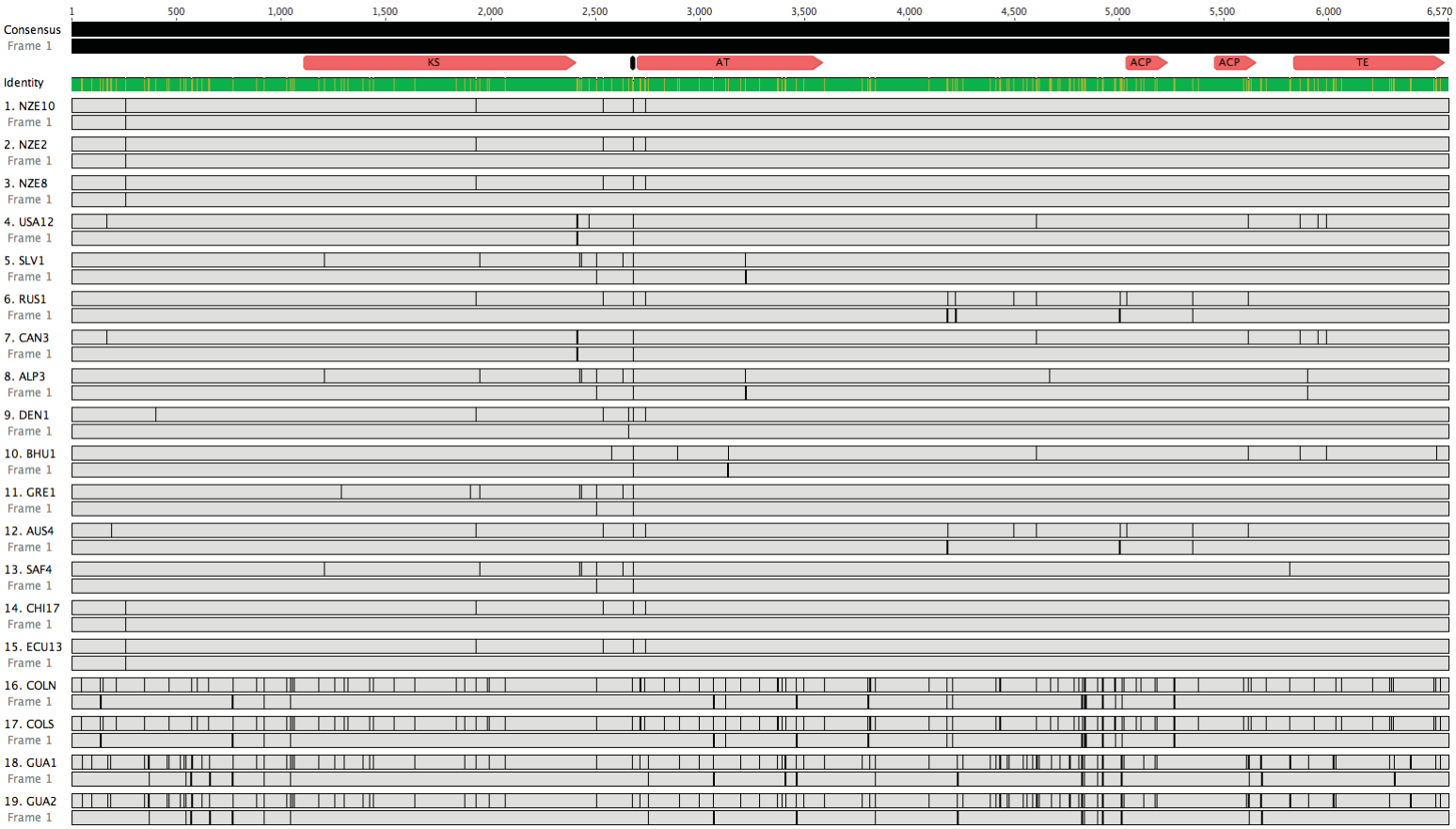

Figure 3.26. *DsPks1* nucleotide alignment of NZE10 with 18 additional strains. Red arrows show the domain positions with KS: keto-synthase, AT: acyltransferase, ACP: acyl carrier protein, TE: thioesterase. The bold black line just before the AT domain indicates the statistically significant positively selected codon (P>0.99). The coloured bar represents consensus identity with green shades indicating identities above 30% and below 100% and green indicating 100% identity. For each sequence, vertical bars on the top and bottom lines show differences in nucleotide and amino acid sequences compared to NZE10. A bar on the top line alone shows a synonymous mutation and a bar on both lines shows a non-synonymous mutation. Strains used in this analysis are listed in Appendix 5.

3.3.1.4. Gene cluster analysis

Gene cluster analysis was assisted by the knowledge that *DsPks1* was predicted to function in melanin/elsinochrome biosynthesis (Table 3.1), and its ortholog *CfPks1* (de Wit et al., 2012) has a predicted gene cluster (Collemare et. al. 2014). The *DsPks1* putative gene cluster (Figure 3.28) contains 4 genes in a 27.4 kb region of chromosome 10. The biggest distance between two genes in the *DsPks1* gene cluster is 10.8 kb, containing 3 genes with no predicted SM-related function. Synteny analysis between the putative gene clusters of *DsPks1* and *CfPks1* showed an inversion of Ds74621 and Ds178588 in the *DsPks1* putative gene cluster (Figure 3.28). All genes except Ds37856 within the *DsPks1* putative gene cluster were expressed at significantly higher levels at late stage compared to early and mid stages (Figure 3.28).

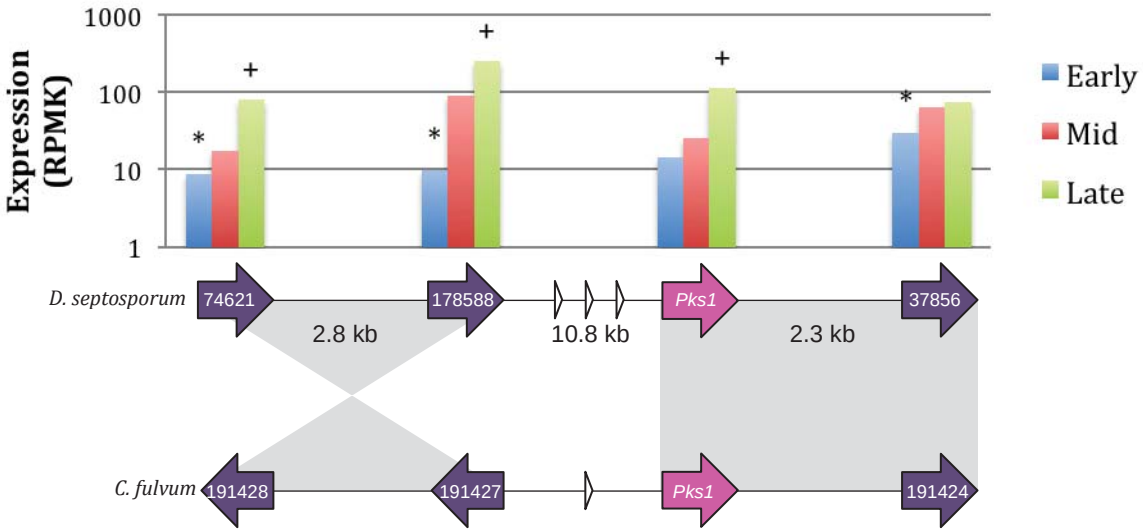

Figure 3.27. Synteny of *DsPks1* and *CfPks1* putative gene clusters and expression profile of *DsPks1* putative gene cluster *in planta*. Numbers inside arrows indicate JGI protein IDs. Pink: Secondary metabolite core genes (*DsPks1* and *CfPks1*). Purple: putative *DsPks1* and *CfPks1* cluster genes. Small white arrows: genes without predicted SM functions. Significant differences in the gene expression between early-mid and mid-late stages of infection were marked with "*" and "+", respectively ($p<0.05$). The differences between early and late stages were significant for all four genes ($p<0.05$).

Table 3.7. Genes within the *DsPks1* putative gene cluster.

JGI Protein ID[a]	Predicted protein[b]	Best hit organism/JGI ID	E / identity %
*Ds74621	Zinc-finger transcription factor	*Cladosporium fulvum* /191427	0/91.5
*Ds178588/Brn1	Short-chain dehydrogenase/reductase	*Cladosporium fulvum*/191428	0/97.4
*Ds47338/Pks1	Polyketide synthase/Pks1	*Cladosporium fulvum*/191425	0/94.3
*Ds37856	Prefoldin	*Cladosporium fulvum* /191424	3.4e-119/91.8

[a] http://genome.jgi.doe.gov/Dotse1/Dotse1.home.html
[b] Predicted protein functions according to antiSMASH and InterProScan
* Indicate genes with similar predicted functions present in other fungal PKS gene clusters.
All BlastP hits were confirmed true with reciprocal blast analyses.

As mentioned previously, *DsPks1* is predicted to be responsible for melanin or elsinochrome biosynthesis. Even though the metabolite produced by *CfPks1* is not known, it is associated with a black pigment (Ökmen et al., 2014), whilst in contrast elsinochrome is a red/orange pigment (Liao and Chung, 2008). In addition, elsinochrome production was not detected in *C. fulvum* metabolite extracts, even though *CfPks1* was expressed (Collemare et al., 2014). These suggest that the CfPks1 SM may be involved in production of melanin. Given the similarity of DsPks1 to CfPks1, DsPks1 SM also most likely produces melanin. The genes

within the *DsPks1* putative gene cluster have similar predicted functions to genes in other known fungal melanin/elsinochrome gene clusters.

The first gene in the *DsPks1* putative gene cluster is predicted to encode a zinc-finger transcription factor (Table 3.7). Zinc-finger transcription factors are regulatory elements common in secondary metabolite gene clusters, including *Amr1*, which positively regulates melanin biosynthesis in *Alternaria brassicicola* (Cho et al., 2012). The second gene, *Brn1*, is predicted to encode a short-chain dehydrogenase/reductase similar to those found in the melanin gene clusters of other fungi including *M. grisea* (Vidal-Cros et al., 1994) and *C. heterostrophus* (Eliahu et al., 2007). The final gene is predicted to encode prefoldin, a chaperone responsible for the transfer of unfolded proteins to cytosolic chaperonin (Vainberg et al., 1998). A gene predicted to encode prefoldin, *PRF1*, is present in the elsinochrome gene cluster of *Elsinoë fawcettii* (Chung, 2011). It was hypothesized that *PRF1* stabilizes some of the enzymes required for elsinochrome biosynthesis. Another gene predicted to encode a prefoldin, *MgPRF1,* is in the putative melanin gene cluster of *M. graminicola* (*Z. tritici*), but has not been functionally characterised (Lendenmann et al., 2014). Therefore, Ds37856 may have a similar function for melanin/elsinochrome biosynthesis in *D. septosporum* and may explain why it was upregulated at an earlier stage of infection than the other three genes.

The complete pathway for elsinochrome biosynthesis is not yet known. On the other hand, melanin biosynthesis is a well-studied subject. There are two major biosynthetic pathways for fungal melanin biosynthesis. The 1,8-dihydroxynaphthalene (DHN) melanin biosynthesis pathway is generally found in ascomycete fungi, the group to which *D. septosporum* belongs, whilst the L 3–4 dihydroxyphenylalanine (L-DOPA) melanin pathway is generally found in basidiomycetes (Bell and Wheeler, 1986). Both of these pathways are well characterised. The DHN-melanin biosynthesis requires a PKS, multicopper oxidase (also called laccase or p-diphenol oxidase in gene clusters), T3HN/T4HN reductases, and scytalone dehydratase (Langfelder et al., 2003, Eliahu et al., 2007). In contrast the DOPA pathway produces melanin from tyrosine without the use of

a PKS (Eisenman and Casadevall, 2012). Figure 3.29 shows the fungal DHN-melanin biosynthesis pathway in *C. heterostrophus*. Melanin gene clusters of *C. heterostrophus*, *A. fumigatus*, and *M. grisea* contain genes predicted to encode similar proteins such as reductases and dehydratases, but also have genes with different predicted functions (Langfelder et al., 2003; Eliahu et al., 2007). For example, *C. heterostrophus* and *M. grisea* melanin gene clusters have genes encoding zinc-finger transcription factors, however, the *A. fumigatus* melanin cluster has no gene with a similar function (Eliahu et al., 2007). The *BRN1* gene of *C. heterostrophus* is predicted to encode a 1,3,8- trihydroxynaphthalene (T3HN) reductase, an enzyme that converts T3HN to vermelone (Figure 3.29), and its closest *D. septosporum* homolog is *DsBrn1*, a gene in the putative *DsPks1* gene cluster (amino acid identity: 78.3%, E=2.7e-139). In addition, the third best BlastP hit of the TH4N reductase gene ChBRN2 is DsBrn1 (identity: 47%, E=2.2e-87), suggesting similar structures of the two reductases in melanin biosynthesis.

In order to determine the possibility of a fragmented *DsPks1* gene cluster, *D. septosporum* proteins with similar amino acid sequences to the melanin cluster gene products in *C. heterostrophus* and *A. fumigatus* were found using BlastP. Figure 3.30 shows candidate genes that may be involved in the biosynthesis of DsPks1 SM, and their *in planta* expression levels. A key melanin biosynthetic gene that is not found in the DsPks1 cluster, encoding scytalone dehydratase, is present in the *D. septosporum* genome on chromosome 3 (Ds70291). This single-copy gene is homologous to *C. heterostrophus* and *A. fumigatus* scytalone dehydratases (ChSCD1 and AfARP1), with 73.8% amino acid identity to ChSCD1 (E=2e-92). It is expressed at a significantly higher level at the late stage of infection, compared to earlier stages, similar to the *DsPks1* putative cluster genes (Figure 3.30).

Other melanin biosynthetic genes that are not found in the DsPks1 gene cluster but are present in the *C. heterostrophus* and *A. fumigatus* melanin clusters are T4HN reductase and multicopper oxidase/laccase. Among all *D. septosporum* genes whose products have similar amino acid sequences to these, two pairs are physically in close proximity to each other. Ds69238 (multicopper oxidase) and Ds69231 (TH4N reductase) are in chromosome 2 with 6 kb and 1 interfering gene

between them. Ds69238 is the best BlastP hit of multicopper oxidase AfABR1 in *D. septosporum* (45.5% identity, E=8e-100) and expressed at a significantly higher level at late stage of infection compared to early and mid stages. Ds69231 has 39% amino acid identity to T4HN reductase ChBRN2 (E=2.5e-7), but most highly expressed at mid stage and downregulated at late stage. Another candidate gene pair, Ds129162 (multicopper oxidase) and Ds87983 (T4HN reductase), is in chromosome 4 with 9 kb and 3 interfering genes between them. Ds129162 has 42.3% amino acid identity to AfABR1 (E=2.16e-40) and had a higher expression level at late stage than early and mid stages. Ds87983 was also expressed at a higher level at late stage compared to early and mid stages, and amino acid identity of Ds87983 to ChBRN2 is 35.5% (E=3.4e-12), However, overall *in planta* expression levels (RPMK values) of Ds129162 and Ds87983 were lower than that of the putative *DsPks1* gene cluster. Positions and BlastP results of the candidate fragmented cluster genes are summarized in Table 3.8.

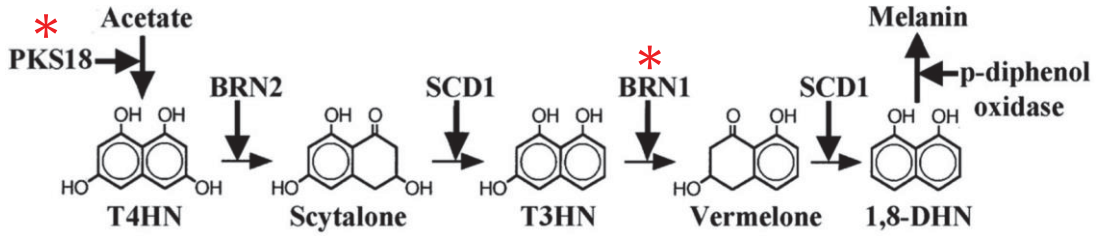

Figure 3.28. Melanin biosynthesis pathway in *C. heterostrophus*. The enzymes predicted to be involved in the biosynthesis are PKS18 (polyketide synthase), BRN2 (T4HN reductase), BRN1 (T3HN reductase), SCD1 (scytalone dehydratase), and p-diphenol oxidase are enzymes presumably involved in the indicated biosynthetic steps. Proteins with similar functions to the products of the genes in *DsPks1* putative gene cluster are marked with asterisk. Image reproduced from Eliahu et al. (2007).

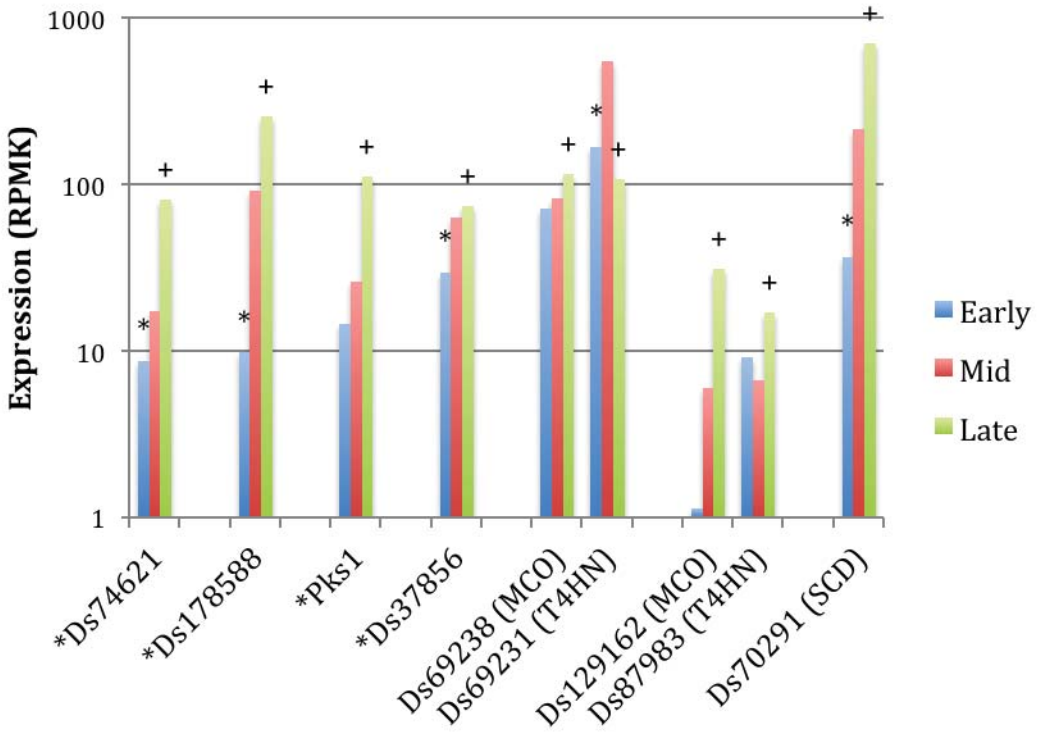

Figure 3.29. Expression of candidate genes in the putative fragmented *DsPks1* gene cluster. Significant differences in the gene expression between early-mid and mid-late stages of infection were marked with "*" and "+", respectively ($p<0.05$). The differences between early and late stages were significant for all genes ($p<0.05$). The genes in the original gene cluster from Figure 3.28 are indicated with asterisk. Predicted functions of the candidate genes outside of the original gene cluster are shown in brackets as MCO: multicopper oxidase, T4HN: T4HN reductase, SCD: scytalone dehydratase. Candidate gene pairs that are in the same chromosome are closer together.

Table 3.8. Candidate genes involved in melanin biosynthesis outside of *DsPks1* original gene cluster.

JGI protein ID[a]	Scaffold: position (direction)[b]	Similar gene (function)[c]	E / identity %
Ds69238	2: 661823-666821 (-)	*AfABR1* (MCO)	8e-100/45.5
Ds69231	2: 656938-658277 (+)	*ChBRN2* (T4HN)	2.5e-7/39
Ds129162	4: 2117920-2119714 (+)	*AfABR1* (MCO)	2.2e-40/42.3
Ds87983	4: 2128494-2131693 (+)	*ChBRN2* (T4HN)	3.4e-12/35.5
Ds70291	3: 1012112-1013484 (-)	*ChSCD1* (SCD)	1.9e-92/73.8

[a] http://genome.jgi.doe.gov/Dotse1/Dotse1.home.html
[b] Position (nt) of predicted gene in scaffold according to JGI.
[c] Genes with similar predicted roles to the candidate *DsPks1* cluster genes. Putative functions of the genes are shown in brackets as MCO: multicopper oxidase, T4HN: T4HN reductase and SCD: scytalone dehydratase.

In conclusion, the *DsPks1* putative gene cluster is most likely responsible for the biosynthesis of a DHN-melanin, or possibly elsinochrome. If Pks1 SM is a DHN-melanin there may be genes encoding for scytalone dehydratase, T4HN reductase and multicopper oxidase involved in its biosynthesis that are located outside of the gene cluster. There is one candidate for scytalone dehydratase and at least two

candidates for each of T4HN reductase and multicopper oxidase encoding genes, some of which are grouped together on a separate chromosome, suggesting that DsPks1 may be a fragmented gene cluster.

In summary, phylogeny and gene cluster analyses suggest that *DsPks1* may be involved in melanin biosynthesis. Genes potentially involved in melanin biosynthesis appear to be present outside of as well as in the DsPks1 putative gene cluster (Figure 3.31). In addition, *DsPks1* has a correct gene model and is under strong negative selection.

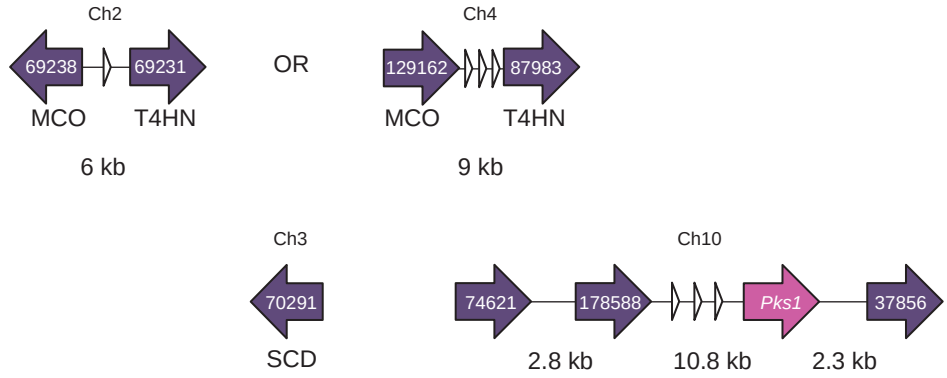

Figure 3.30. Candidate genes that may belong to a putative *DsPks1* fragmented gene cluster for melanin biosynthesis. Numbers inside arrows indicate JGI protein IDs. Pink: Secondary metabolite core gene (*DsPks1*). Purple: putative *DsPks1* cluster genes. Small white arrows: genes without predicted SM functions. "Ch" numbers indicate the chromosomes in which the genes are located. Predicted functions of the candidate genes outside of the original gene cluster are shown in under the genes as MCO: multicopper oxidase, T4HN: T4HN reductase, SCD: scytalone dehydratase.

3.3.2. PKS2

The expression level of *DsPks2* was higher than that of the dothistromin core gene, *DsPksA*, at the late stage of plant infection (Section 3.1.2). Therefore, *DsPks2* was a gene of main interest in this project so, in addition to the analyses done for all *D. septosporum* SM core genes, phylogenetic analysis and gene knockout attempts were done with *DsPks2*.

3.3.2.1. Phylogenetic analysis of DsPks2

Phylogenetic analysis of DsPks2 was done to find out if there are any putative orthologs that are functionally characterised. Initial phylogenetic analyses were done using KS domains, KS+AT domains, and full protein sequences as explained in Section 2.14.3. As a result of all three analyses, DsPks2, a protein belonging to a species of Dothideomycetes class was clustered with proteins of *Aspergillus spp*., members of the Eurotiomycetes class (Appendix 14). This suggested the possibility of horizontal gene transfer between *D. septosporum* and *Aspergillus* spp.. Next, phylogenetic analysis on DsPks2 was done using full protein sequences in order to determine true orthologs/paralogs instead of only determining proteins with similar KS and AT domains. In order to determine if there was a horizontal gene transfer, an extensive phylogenetic tree with a larger number of sequences compared to the initial tree, was prepared. The DsPks2 sequence was aligned with the best reciprocal FASTA hits from all Dothideomycetes, Eurotiomycetes and Sordariomycetes fungi present in the JGI database, and a tree was built using maximum likelihood (ML) method, as explained in Section 2.14.3. *Fusarium* spp. (in Sordariomycetes) were included in the analysis since the SM produced by DsPks2 was predicted to be a fumonisin-like compound, a SM produced by *Fusarium* spp. (Table 3.1; Rheeder et al., 2002).

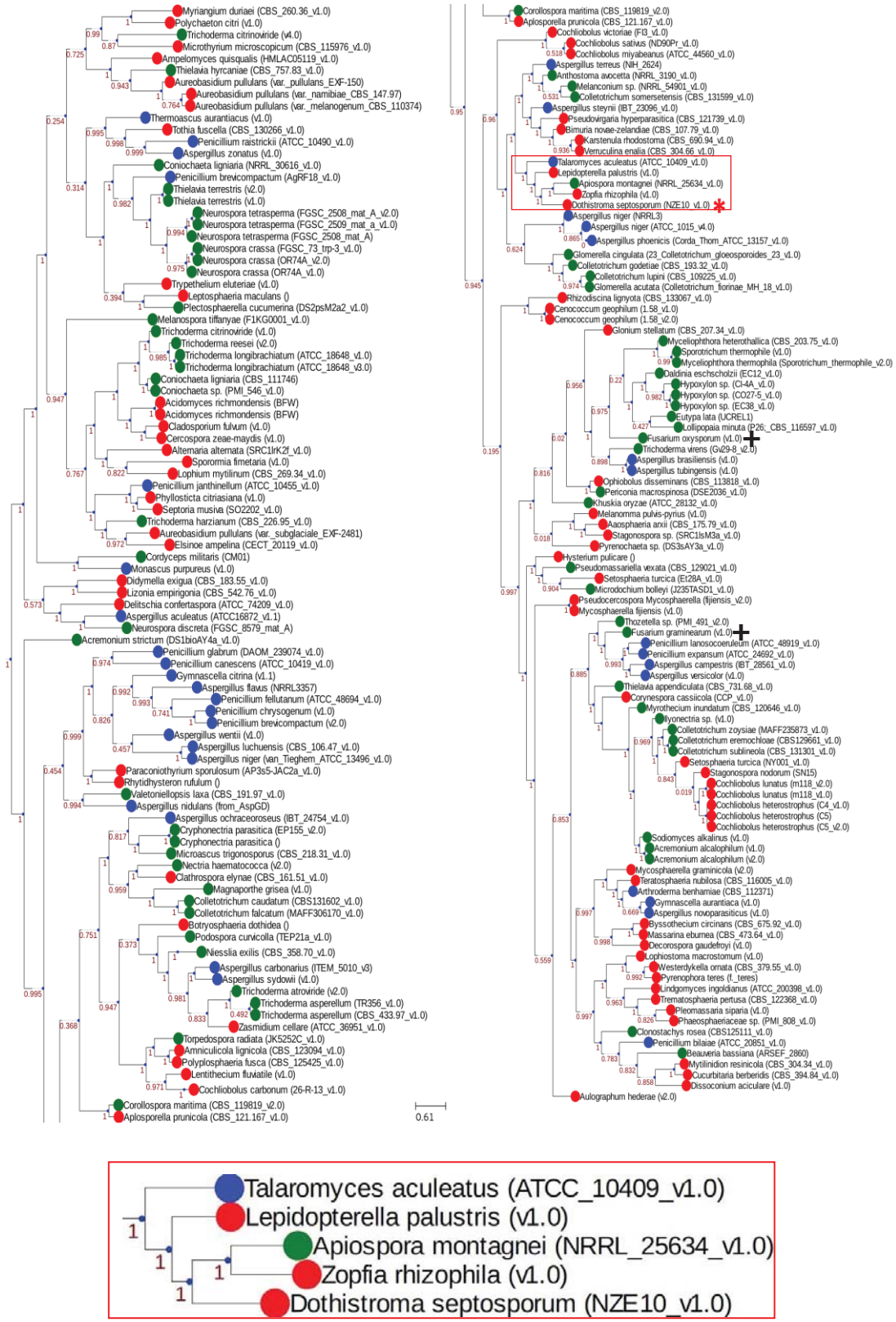

Figure 3.31. Phylogenetic analysis of DsPks2 and its best FASTA hits. Red: Dothideomycetes. Blue: Eurotiomycetes. Green: Sordariomycetes. Numbers on branches indicate approximate likelihood ratio test (aLRT) scores. Close homologs of *D. septosporum* are shown with a red square, *D. septosporum* is indicated with an asterisk. *Fusarium* spp. are indicated with a plus sign. Details of the genome sequences used are presented in Appendix 23.

The phylogenetic tree in Figure 3.32 revealed that even though sequences belonging to the same fungal class are clustered at some regions of the tree as expected, many clades contain a mixture of sequences from different fungal classes. This is characteristic of a tree containing not only orthologous genes, but also many paralogs or distantly related homologs. Figure 3.33 shows the amino acid alignment of DsPks2 with closely related sequences shown in the red square of Figure 3.32. The closest homologs of DsPks2 are in *Zopfia rhizophila* (protein ID: 734285), *Apiospora montagnei* (protein ID: 166223), *Lepidopterella palustris* (protein ID: 437929), and *Talaromyces acuelatus* (protein ID: 470923), with amino acid identities to DsPks2 of 51.8% (E=0), 51.1% (E=0), 59.7% (E=0), and 51.2% (E=0) respectively. None of the close homologs of DsPks2 were functionally characterised, and *DsPks2* was far from *Fusarium* spp. in the phylogenetic tree. Therefore this phylogenetic analysis did not support the hypothesis that Pks2 SM may be a compound similar to fumonisin produced by *Fusarium* spp. The alignment shows that there are only a few conserved regions between these five sequences, suggesting that these proteins are probably not orthologs.

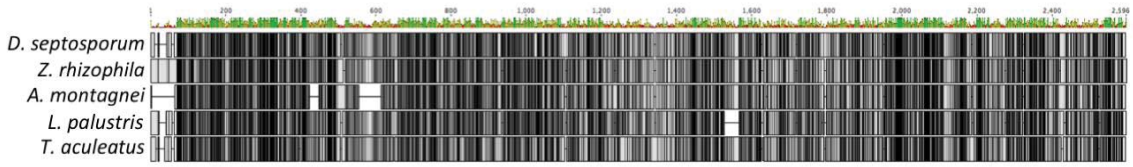

Figure 3.32. Amino acid alignment of DsPks2 with its closest FASTA hits. The dark regions indicate the amino acid alignment with black (highly similar) to white (not similar) sequences with respect to the consensus sequence. The coloured bar represents consensus identity with red (below 30%); green shades indicate higher levels of identity (up to 100%) with bar height proportional to % identity.

In conclusion, the phylogenetic analysis of DsPks2 suggests that *DsPks2* was probably not horizontally transferred and its close homologs are probably not true orthologs. This suggests that the metabolite produced by DsPks2 may be unique among Dothideomycetes, Eurotiomycetes, and Sordariomycetes.

3.3.2.2. Confirmation of gene model for *DsPks2*

The JGI gene model of *DsPks2* was confirmed by aligning DsPks2 with its closest homologs from Section 3.3.2.1, and analysing the RNA-seq data.

The domain organization of DsPks2 (protein ID: 73814) and its alignment with closest homologs is presented in Figure 3.34. N–terminal sequences in the alignment were less conserved than the C – terminal sequences. The position of the first amino acid of DsPks2 was conserved with the first amino acids of the other three protein sequences in the alignment. There was an alignment gap in DsPks2 just after the start codon but this did not affect any of the known functional domains such as the KS domain. Therefore, the alignment of DsPks2 and its closest homologs support that the JGI gene model for *DsPks2* is correct.

The predicted gene model for DsPks2 has 10 introns, and all of them were confirmed by RNA-seq data that was mapped to the JGI gene model of *DsPks2* (Appendix 15). Therefore, alignments (Figure 3.34, Appendix 21e) and RNA-seq data (Appendix 15) support that the gene model for *DsPks2* is correct.

3.3.2.3. Comparison of *DsPks2* from 19 strains of *D. septosporum*

Evolutionary selection analysis was done by aligning the *DsPks2* nucleotide sequences across the 19 *D. septosporum* strains and determining the selection pressure by dN/dS analysis and identifying codons that are under significantly strong positive selection pressure.

Figure 3.35 shows the alignment of *DsPks2* across the 19 *D. septosporum* strains. The dN/dS ratio of *DsPks2* is 0.21, suggesting that this gene is under negative selection. Therefore, the Pks2 SM may be an important metabolite for *D. septosporum*. One codon in the DH domain showed significantly positive selection (P>0.99) in *DsPks2*.

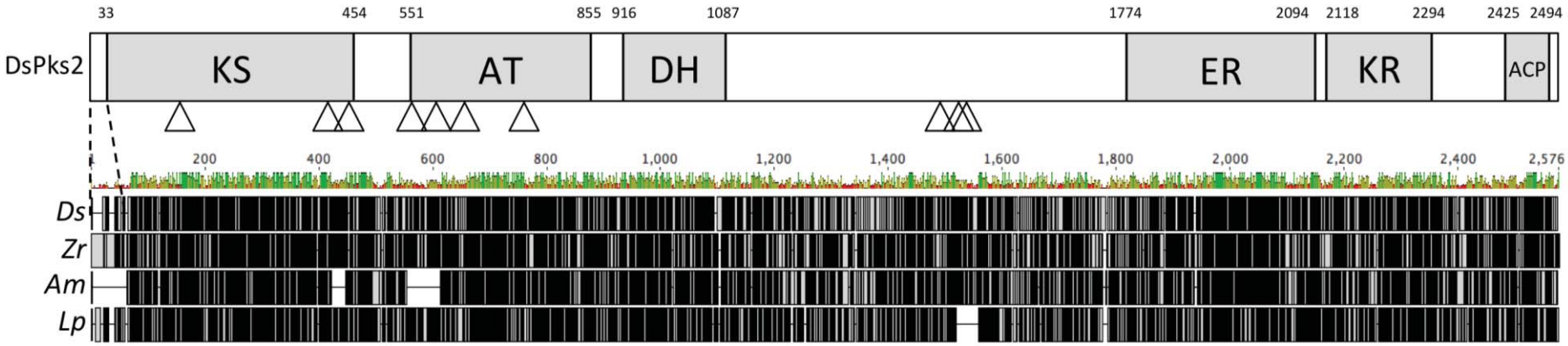

Figure 3.33. Domain structure of DsPks2 and its protein alignment with closest homologs. DsPks2 indicates the peptide's domain organization with KS: keto-synthase, AT: acyltransferase, ER: enoylreductase, KR: ketoreductase, ACP: Acyl carrier protein domains. Numbers indicate amino acid positions of domain borders. Dotted lines show position of DsPks2 gap in the alignment. The total length is 2507 amino acids. The diagram was drawn to scale. The dark regions indicate the amino acid alignment with black (highly similar) to white (not similar) sequences with respect to the consensus sequence. Triangles indicate corresponding intron positions. The amino acid alignment below demonstrates *Ds*: *D. septosporum*, *Zr: Z. rhizophila* (protein ID: 734285), *Am: A. montagnei* (protein ID: 166223), *Lp*: *L. palustris* (protein ID: 437929). The coloured bar represents consensus identity with red (below 30%); green shades indicate higher levels of identity (up to 100%) with bar height proportional to % identity.

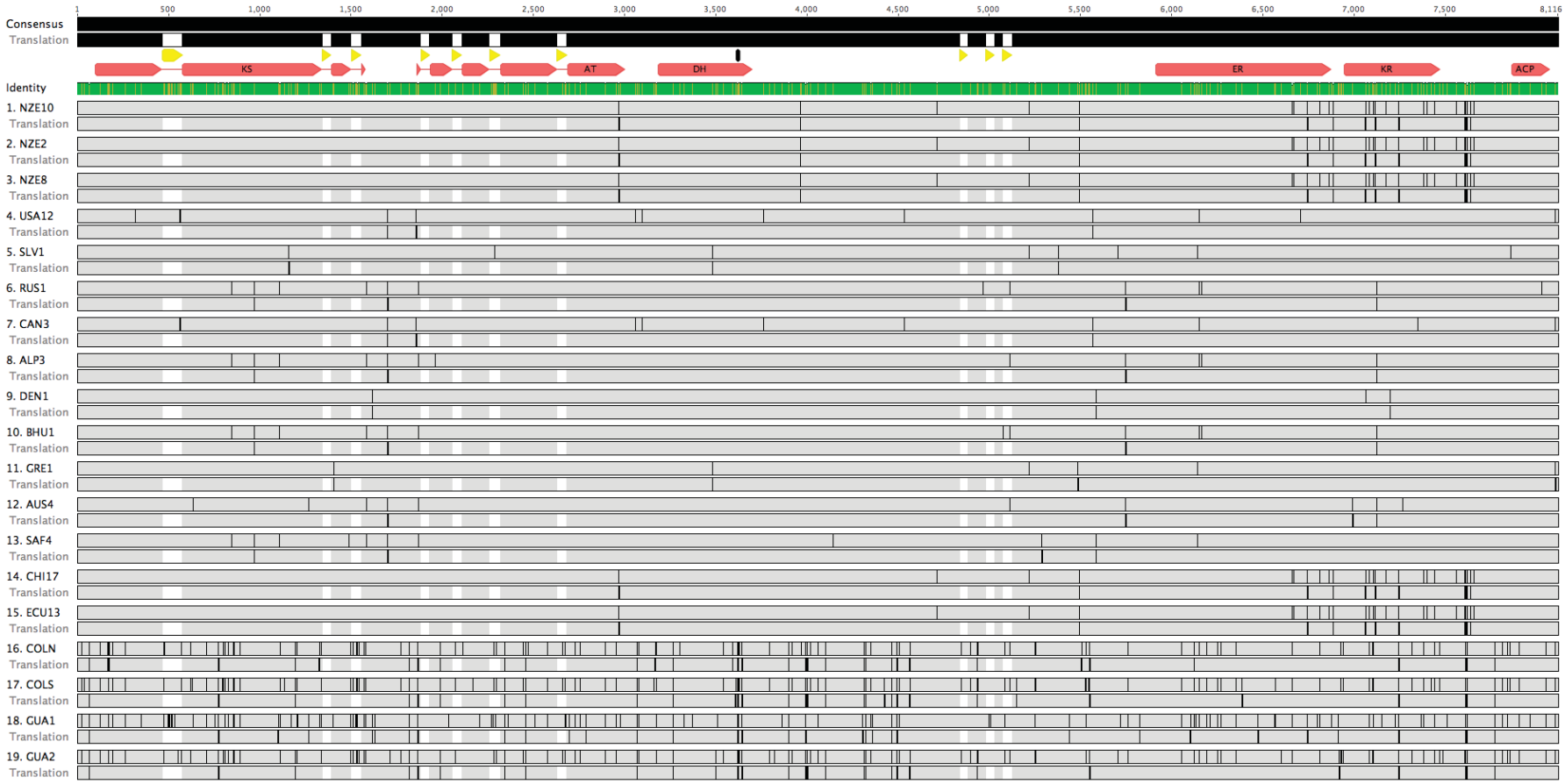

Figure 3.34. *DsPks2* nucleotide alignment of NZE10 with 18 additional strains. Red arrows show the domain positions with KS: keto-synthase, AT: acyltransferase, ER: enoylreductase, KR: ketoreductase, ACP: acyl carrier protein domains. The bold black line on the DH domain indicates the statistically significant positively selected codon ($p<0.01$). Yellow arrows indicate intron positions. The coloured bar represents consensus identity with brown indicating identities above 30% and below 100% and green indicating 100% identity. For each sequence, vertical bars on the top and bottom lines show differences in nucleotide and amino acid sequences compared to NZE10. A bar on the top line alone shows a synonymous mutation and a bar on both lines shows a non-synonymous mutation. Strains used in this analysis are listed in Appendix 5.

3.3.2.4. Gene cluster analysis

DsPks2 gene cluster analysis was performed in order to find possible genes taking a role in the biosynthesis of the polyketide product. The *DsPks2* putative gene cluster is predicted to contain 10 genes in a 29 kb region of chromosome 8. The biggest distance between two genes within the putative gene cluster is 2.5 kb, containing 1 gene with no SM-related function. All genes except Ds36908 were expressed at a significantly higher level at the late stage of plant infection compared to the early stage, suggesting co-expression of the putative cluster genes.

All genes except Ds36908 have predicted functions similar to genes in other fungal PKS gene clusters. The putative *DsPks2* gene cluster contains two MFS transporters (Table 3.9). A gene encoding a MFS transporter is present in *Pks4* gene cluster responsible for bikaverin biosynthesis in *F. verticillioides* (Brown and Webber, 2008). Other genes within the putative gene cluster are probably responsible for the biosynthesis of the corresponding metabolite. A gene predicted to encode a short chain dehydrogenase/reductase is present in the fumonisin gene cluster of *F. verticillioides* (Butchko et al., 2003). In the fumonisin-like gene cluster of *A. niger*, *Fum10* gene is predicted to encode an AMP-dependent synthetase and ligase (Baker, 2006). Genes encoding for alpha-beta hydrolases are found in the SM gene cluster of the hybrid polyketide-nonribosomal peptide pseurotin A in *A. fumigatus* (Owens et al., 2014). In addition, in the polyketide lomaiviticin biosynthetic gene cluster of *Salinispora tropica*, there is a hypothetical protein that has as its closest homolog an alpha/beta hydrolase (Kersten et al., 2013). Acyltransferases are commonly found in fungal polyketide gene clusters, taking a role in either the biosynthesis of the metabolite or the release of the polyketide from a fungal megasynthase (Bonsch et al., 2016; Xie et al., 2009). A gene predicted to encode a beta-lactamase is found in a polyketide gene cluster of fungus *Usnea longissima*, responsible for anthraquinone biosynthesis (Wang et al., 2014).

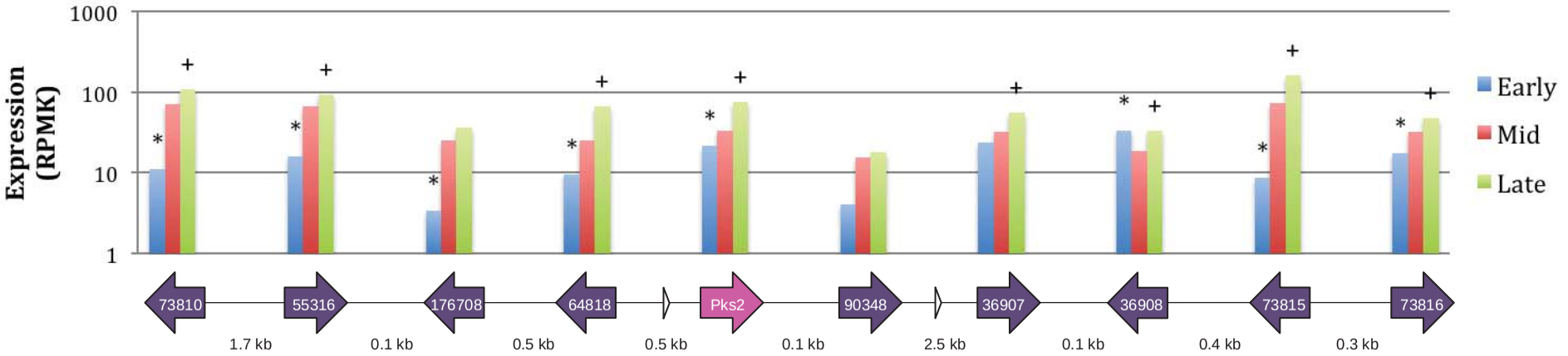

Figure 3.35. Organization and expression of *DsPks2* and its neighboring genes in early, mid, and late stages of infection. Numbers inside arrows indicate JGI protein IDs. Pink: Secondary metabolite core gene (*DsPks2*). Purple: putative *DsPks2* cluster genes. Small white arrows: genes without predicted SM functions. Significant differences between early-mid and mid-late stages were marked with "*" and "+", respectively ($p<0.05$). The differences between early and late stages were also significant for all cluster genes except Ds36908.

Table 3.9. Genes within *DsPks2* putative gene cluster.

Protein ID[a]	Predicted protein[b]	Best hit organism/JGI ID	E/ identity %
*Ds73810	Major facilitator transporter	*Apiospora montagnei*/149305	1.1e-162/52.6
*Ds55316	Short-chain dehydrogenase/ reductase	*Lepidopterella palustris*/365300	3.2e-98/55
*Ds176708	Major facilitator transporter	*Lepidopterella palustris*/420042	0/59.4
*Ds64818	AMP-dependent synthetase and ligase	*Cladosporium fulvum*/192541	0/57.5
*Ds73814/Pks2	Polyketide synthase	*Lepidopterella palustris*/437929	0/59.2
*Ds90348	Alpha/beta hydrolase	*Lepidopterella palustris*/409407	5.9e-114/60.1
*Ds36907	Acyltransferase	*Decorospora gaudefroyi*/617224	1.6e-99/47.6
Ds36908	Squalene/phytoene synthase	*Zymoseptoria pseudotritici*/796149	1.4e-72/64.3
*Ds73815	AMP-dependent synthetase and ligase	*Zasmidium cellare/66809*	4.8e-131/51.5
*Ds73816	Beta-lactamase	*Lepidopterella palustris*/309548	2.3e-156/47.7

[a] http://genome.jgi.doe.gov/Dotse1/Dotse1.home.html

[b] Predicted proteins according to antiSMASH and InterProScan

Asterisk indicates genes with similar predicted functions present in other fungal PKS gene clusters.

All BlastP hits were confirmed true except Ds73810, Ds64818, Ds36908 and Ds73815 with reciprocal blast analyses.

A gene predicted to encode squalene/phytoene synthase is also present in the *DsPks2* putative gene cluster. Genes encoding for squalene/phytoene synthases are commonly found SM gene clusters, but instead of polyketides, they are mostly found in terpene gene clusters (Song et al., 2014; Jeandet et al., 2013).

According to NaPDoS predictions (Section 2.14.2), DsPks2 may be responsible for the synthesis of a fumonisin-like compound (Table 3.1). Biosynthetic gene clusters for fumonisin produced by *Fusarium* spp. and fumonisin-like compounds produced by *A. niger* are well characterised (Alexander et al., 2009, Baker et al., 2006). The predicted roles of the genes in both of these gene clusters have variations between each other and with the *DsPks2* putative gene cluster. However, there are three genes common in both *Fusarium* spp. and *A. niger* fumonisin gene clusters that appear to be missing in the *DsPks2* putative gene cluster. These genes are cytochrome p450 monooxygenase, dioxygenase, and alcohol dehydrogenase. Therefore, if the DsPks2 SM is fumonisin-like, it is possible that genes with these three functions that are located outside of the gene cluster may be involved in its biosynthesis.

3.3.2.5. Gene knockout attempts

Exhaustive attempts were made to obtain a gene knockout to functionally characterise the highly expressed SM gene *DsPks2*. For that, a gene knockout construct was prepared using the GATEWAY system, and protoplast transformation was performed. In four separate transformation attempts, a total of 219 transformed colonies were screened and only one gene KO candidate was found (~0.45% efficiency of integration into correct site). Unfortunately, this candidate was found to contain both wild type and *ΔDsPks2* gDNAs, and even after three steps of purification that candidate did not give a pure strain with the *ΔDsPks2* knockout genotype. It is possible that a functional copy of *DsPks2* is essential for viability, so the knockout mutant was forced to remain as a heterokaryon with a wild-type strain but eventually this aspect of the project was abandoned. PCR and Southern blot results are presented in Appendix 17.

To summarize, *DsPks2* is not horizontally transferred, has a correct JGI gene model, and in a putative cluster of 10 genes. Gene KO attempts for *DsPks2* for functional characterization were unsuccessful and eventually abandoned.

3.3.3. PKS3

3.3.3.1. Confirmation of gene model for *DsPks3*

Confirmation of the JGI gene model for *DsPks3* was done by aligning DsPks3 protein sequence with its closest homologs and analysing the RNA-seq reads. Figure 3.37 shows the protein alignment. Amino acid identities of DsPks3 with closest reciprocal BlastP hits were 59.5% (E=0) for the PKS in *Melanconium sp.* (protein ID: 89670), 57.9% (E=0) for that of *M. grisea* (protein ID: 116015), and 47.8% (E=0) for *Talaromyces aculeatus* PKS (protein ID: 460631). The alignment has an overall low consensus, especially in the region between DH and ER domains. Positions of 7 of the 10 introns of *DsPks3* are represented as gaps in the amino acid alignment, suggesting possible misannotation of those introns. RNA-seq analysis (Appendix 18) showed that all introns except the 7th intron are misannotated, shown by the in culture expression of the gene at the intron positions. Intron 7 was correctly annotated, but introns 8 and 9 are shorter than was shown in the gene model. Strikingly, there are many internal stop codons in all three reading frames, as well as frameshifts, if all introns except 7, 8, and 9 are removed and counted as exon sequence (Appendix 18), suggesting that *DsPks3* is a pseudogene. In addition, alignment of DsPks3 with the closest BlastP hits after removing the first 7 introns removed the gaps in the alignment; however, this also decreased the amino acid identity of the alignment and generated new gaps (Figure 3.37b). This raised possibility of introns that weren't annotated in the gene model and decreased amino acid identity caused by the changing reading frame.

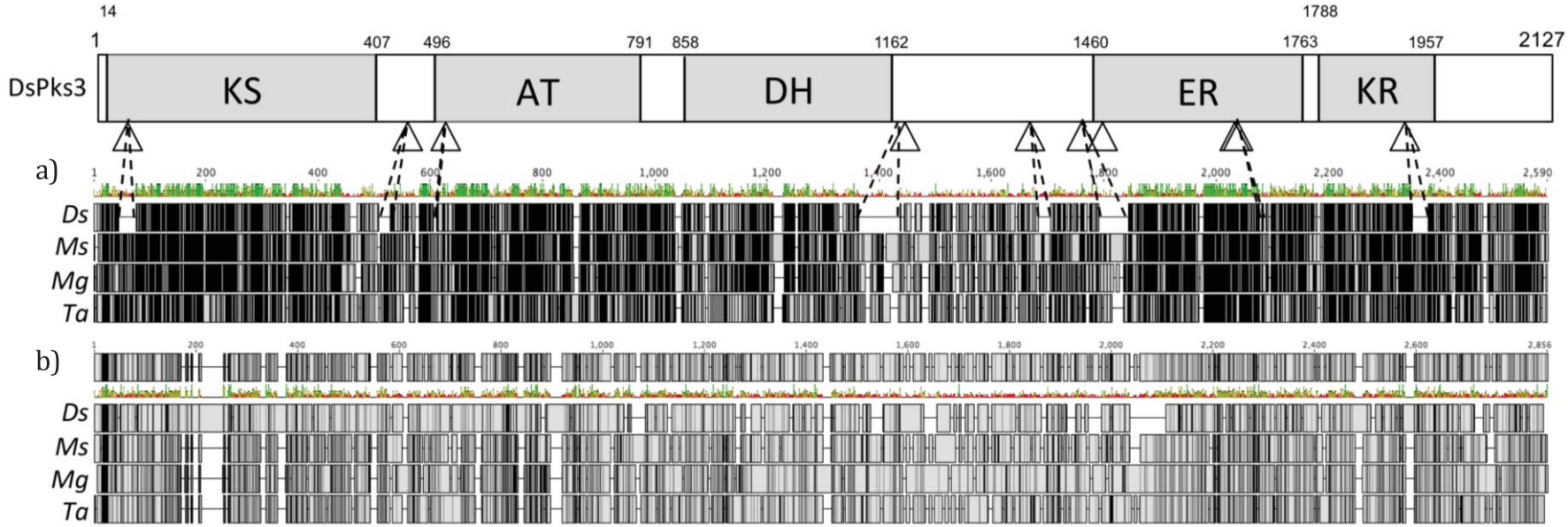

Figure 3.36. Domain structure of DsPks3 and its protein alignment with closest homologs. DsPks3 indicates the peptide's domain organization with KS: keto-synthase, AT: acyltransferase, DH: dehydratase, ER: enoylreductase, KR: ketoreductase domains. Numbers indicate amino acid positions of domain borders in addition to start and end of the DsPks3 peptide sequence. a) The amino acid alignment based on the JGI gene model. Triangles indicate corresponding intron positions. Dotted lines show positions of the DsPks3 gaps in the alignment. Total length is 2127 amino acids. The diagram was drawn to scale. The dark regions indicate the amino acid alignment with black (highly similar) to white (not similar) sequences with respect to the consensus sequence. *Ds*: *D. septosporum* Pks3, *Ms: Melanconium sp.* (protein ID: 89670), *Mg: M. grisea* (protein ID: 116015), *Ta*: *T. aculeatus* (protein ID: 460631). The coloured bar represents consensus identity with red (below 30%); green shades indicate higher levels of identity (up to 100%) with bar height proportional to % identity. b) The amino acid alignment after removing the all of the introns except introns 7,8 and 9.

In conclusion, alignments and RNA-seq reads do not support the current JGI gene model for *DsPks3* but suggest that all introns except intron 7 are misannotated. Among the misannotated introns, introns 8 and 9 are probably shorter than they were shown in the gene model and the other misannotated introns are probably parts of the coding region. The results also suggest that *DsPks3* has undergone pseudogenization by the number of internal stop codons in the coding sequence after removal of the misannotated introns.

3.3.3.2. Comparison of *DsPks3* from 19 strains of *D. septosporum*

Figure 3.38 shows the alignment of *DsPks3* nucleotide sequences across *D. septosporum* NZE10 and 18 other strains. This alignment was based on the JGI gene model and shows that two strains RUS1 and DEN1 have internal stop codons due to point mutations. In addition, *DsPks3* sequences were truncated from the 5' ends in two strains, COLS and GUA2. No sequences similar to the 5' end of *DsPks3* were found in the 5' flanking regions of the truncated regions of these two sequences. The additional evidence for pseudogenisation events amongst 4 of the strains studied here, suggested *DsPks3* is probably not a functionally important gene for *D. septosporum*, therefore no further analyses were done.

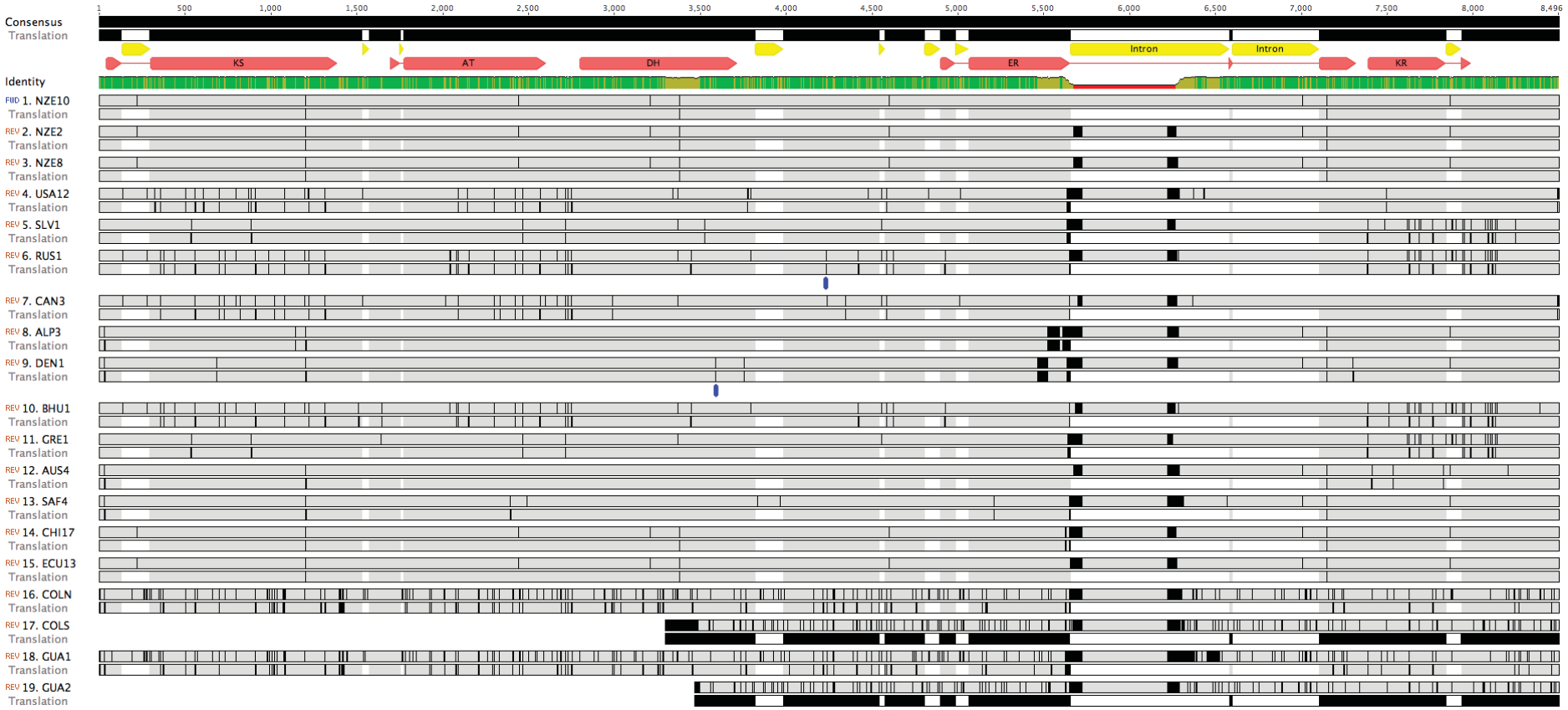

Figure 3.37. *DsPks3* nucleotide alignment of NZE10 with 18 additional strains. Red arrows show the domain positions with KS: keto-synthase, AT: acyltransferase, DH: dehydratase, ER: enoylreductase, KR: ketoreductase. Yellow arrows show intron positions. Internal stop codons in RUS1 and DEN1 are shown with bold blue lines. The coloured bar represents consensus identity with red indicating identities below 30%, green shades indicating above 30% and below 100% and green indicating 100% identity. For each sequence, vertical bars on the top and bottom lines show differences in nucleotide and amino acid sequences compared to NZE10. Black vertical regions in the alignments show "N" series. A bar on the top line alone shows a synonymous mutation and a bar on both lines shows a non-synonymous mutation except the "N" series where mutation analysis was not possible. Strains used in this analysis are listed in Appendix 5.

3.4. Hybrid polyketide-nonribosomal peptide synthetases

D. septosporum has two predicted hybrid polyketide-nonribosomal peptide synthetase (HPS) core genes (Table 3.1). However, expression levels of both these genes were very low both in culture and *in planta* (Section 3.1.2). Therefore, these two genes were not of key interest and only gene model confirmation, evolutionary selection pressure and gene cluster analyses were done on these genes.

3.4.1. HPS1

3.4.1.1. Confirmation of gene model for *DsHps1*

The *DsHps1* JGI gene model was confirmed by aligning DsHps1 with best reciprocal BlastP hits and analysing RNA-seq data that was mapped on the gene model. The top three BlastP hits were to proteins of *Aspergillus terreus* and *Aspergillus sydowii* (Eurotiomycetes) and *Ophiostoma piceae* (Sordariomycetes). The DsHps1 alignment (Figure 3.39) showed low overall consensus, with amino acid identities to these proteins of only 47.6% (*A. terreus*; E=0), 47.1% (*A. sydowii*; E=0), and 46.1% (*O. piceae*; E=0). The best BlastP hit of DsHps1 within the Dothideomycete fungi was a protein from *Sporormia fimetaria* (protein ID: 458206) with 41.9% identity (E=6.8e-179). In the alignment DsHps1 and its homologue in *A. terreus* had no big gaps or insertions, however C-termini of the proteins in *A. sydowii* and *O. piceae* were not aligned with DsHps1.. Domain analyses on the *A. sydowii* and *O. piceae* protein sequences showed that they are PKS instead of HPS. Therefore, the differences between the sequences are probably not because of any problems with the DsHps1 gene model. The *DsHps1* predicted gene model has no introns and the continuous RNA-seq reads from start codon to stop codon supported the lack of introns (Appendix 19). Therefore, alignments and RNA-seq reads supported the JGI gene model for *DsHps1*.

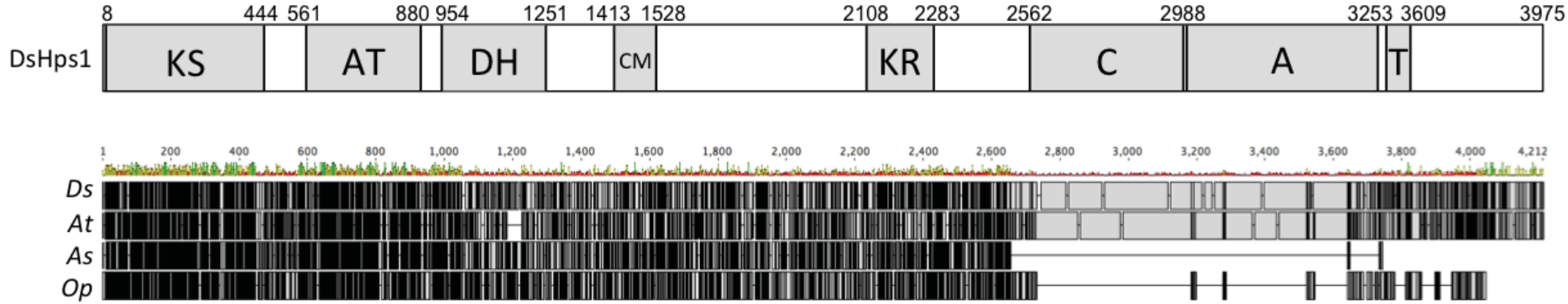

Figure 3.38. Domain structure of DsHps1 and its protein alignment with closest homologs. DsHps1 indicates the peptide's domain organization with KS: keto-synthase, AT: acyltransferase, DH: dehydratase, CM: C-methyltransferase, KR: ketoreductase, C: condensation, A: adenylation, T: thiolation domains. Numbers indicate amino acid positions of domain borders and the end of the peptide (positions of borders that are too close to another border are not shown). The total length is 3975 amino acids. The diagram was drawn to scale. The dark regions indicate the amino acid alignment with black (highly similar) to white (not similar) sequences with respect to the consensus sequence. The amino acid alignment shows *Ds*: *D. septosporum* Hps1, *At*: *A. terreus* (protein ID: 325), *As: A. sydowii* (protein ID: 25738), *Op*: *O. piceae* (protein ID: 4838). The coloured bar represents consensus identity with red (below 30%); green shades indicate higher levels of identity (up to 100%) with bar height proportional to % identity.

3.4.1.2. Comparison of *DsHps1* from 19 strains of *D. septosporum*

Determination of the evolutionary selection pressure on *DsHps1* was done by aligning the *DsHps1* sequences across the 19 *D. septosporum* strains and determining the dN/dS ratio. The *DsHps1* alignment is presented in Figure 3.40. The dN/dS ratio of *DsHps1* is 0.39, suggesting negative selection on this gene. Since *DsHps1* was not a gene of key interest due to its low expression levels both in culture and *in planta* (Section 3.1.2), sites under positive selection were not determined.

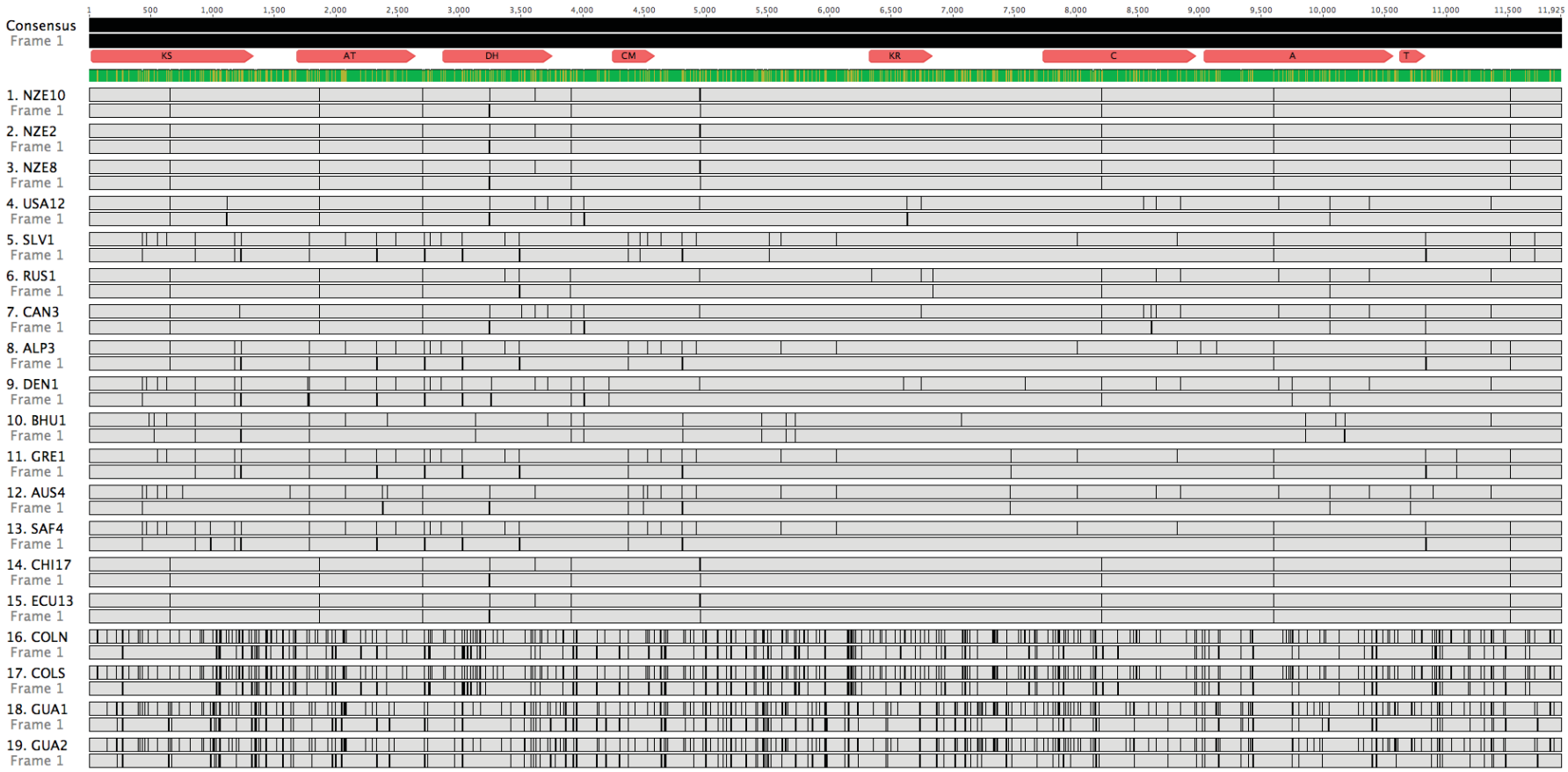

Figure 3.39. *DsHps1* nucleotide alignment of NZE10 with 18 additional strains. Red arrows show the domain positions with KS: keto-synthase, AT: acyltransferase, DH: dehydratase, CM: C-methyltransferase, KR: ketoreductase, C: condensation, A: adenylation, T: thiolation. The coloured bar represents consensus identity with brown indicating identities above 30% and below 100% and green indicating 100% identity. For each sequence, vertical bars on the top and bottom lines show differences in nucleotide and amino acid sequences compared to NZE10. A bar on the top line alone shows a synonymous mutation and a bar on both lines shows a non-synonymous mutation. Strains used in this analysis are listed in Appendix 5.

3.4.1.3. Gene cluster analysis

DsHps1 and *DsDma1* genes are physically next to each other, therefore the associated putative gene cluster may contain both of these genes. Since *DsHps1* and *DsDma1* genes both have very low expression levels both in culture and *in planta* (Section 3.1.2), it was not possible to estimate the gene cluster by co-expression analysis. The putative *DsHps1* - *DsDma1* gene cluster (Figure 3.41) is composed of 9 genes in a 44 kb region of chromosome 11. Between these 9 genes, there are 7 more genes with no predicted SM-related functions. The biggest distance between two genes is 6.9 kb, containing 3 interfering genes (Figure 3.41). No genes with predicted SM-related functions were found among the 20 genes downstream of *DsHps1*.

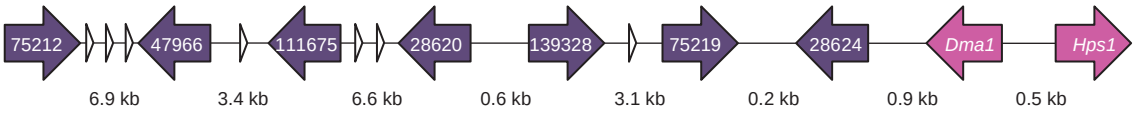

Figure 3.40. *DsHps1* - *DsDma1* putative gene cluster. Numbers inside arrows indicate JGI protein IDs. Pink: Secondary metabolite core genes (*DsDma1* and *DsHps1*). Purple: putative *DsDma1*-*DsHps1* cluster genes. Small white arrows: genes without predicted SM functions.

Table 3.10. Genes within *DsHps1* - *DsDma1* putative gene cluster.

JGI Protein ID[a]	Predicted protein[b]	Best hit organism/JGI ID	E / identity %
*Ds75212	Flavin-containing monooxygenase	*Cladosporium fulvum/191534*	0/92.1
*Ds47966/Mox1	Flavin-containing monooxygenase	*Cladosporium fulvum/191527*	0/83.5
*Ds111675	Cytochrome P450	*Cladosporium fulvum/188144*	4.9e-50/73.8
*Ds28620	Cytochrome P450	*Cochliobolus miyabeanus*/10327	5.2e-145/43.8
*Ds139328	SAM-dependent methyltransferase	*Patellaria atrata*/1013025	4.2e-72/33.7
*Ds75219	Cytochrome P450	*Thozetella* sp./746229	5.9e-80/45.9
Ds28624	Crotonyl-CoA reductase	*Zymoseptoria pseudotritici*/799177	8e-139/61.7
*Ds28625/Dma1	DMA	*Colletotrichum somersetensis*/470342	3.4e-68/45.2
*Ds180045/Hps1	Hybrid PKS-NRPS	*Aspergillus terreus*/325	0/47.6

[a] http://genome.jgi.doe.gov/Dotse1/Dotse1.home.html
Asterisk indicates that genes with similar predicted functions are present in other fungal HPS gene clusters.
[b] Predicted proteins according to antiSMASH and InterProScan analyses.
All BlastP hits were confirmed true except Ds111675 and Ds28624 with reciprocal blast analyses.

All genes in the *DsHps1* - *DsDma1* putative gene cluster except Ds28624 have predicted functions common among other fungal HPS gene clusters. The putative gene cluster for *DsHps1* - *DsDma1* contains two flavin-containing monooxygenases.

A gene encoding flavin-containing monooxygenase, *cheE* was verified to be involved in hybrid polyketide-nonribosomal peptide chaetoblobosin biosynthesis in *Penicillium expansum* by RNA silencing (Schümann and Hertweck, 2007). In addition, the *DsHps1* - *DsDma1* putative gene cluster has three cytochrome p450 proteins. Cytochrome p450 proteins are present in a variety of hybrid PKS-NRPS gene clusters, such as that for tenellin in *Beauveria bassiana*, fusarin C in *F. moniliforme*, cytochalasin E and K in *A. clavatus*, fusaridione and equisetin in *F. heterosporum* (reviewed by Fisch, 2013). In the phomopsin hybrid PKS-NRPS gene cluster in *Phomopsis leptostromiformis*, the *PhomM* gene is predicted to encode a SAM-dependent methyltransferase (Ding et al., 2016), and Ds139328 is predicted to encode a protein with similar function in the *DsHps1* - *DsDma1* cluster.

Ds28624 is predicted to encode a crotonyl-CoA reductase. Whilst crotonyl-CoA reductase genes are common in bacterial hybrid PKS-NRPS gene clusters, no similar examples could be found in fungal SM gene clusters (Weber et al., 2008; Seipke and Hutchings, 2013).

The DsHps1 SM was predicted to be a compactin/bacitracin type according to NaPDoS analysis (Table 3.1), although this prediction did not take the *DsDma1* gene into account. Compactin is a polyketide produced by *Penicillum spp*. (Abe et al., 2002), whilst bacitracin is an antibiotic produced by bacteria (Konz et al., 1997). The compactin gene cluster in *Penicillium citrinum* has 4 genes with predicted functions such as transesterase that are not found in the *DsHps1* - *DsDma1* putative gene cluster (Abe et al., 2002). In addition, compactin biosynthesis does not require an NRPS or DMA activity. Therefore, it is unlikely that the SM produced by *DsHps1* – *DsDma1* gene cluster is a compactin-like compound.

Another possibility for the type of SM produced by the *DsHps1* – *DsDma1* gene cluster is cyclopiazonic acid (CPA). CPA is a specific inhibitor of calcium-dependent ATPase in sarcoplasmic reticulum that results in altered cellular Ca^{2+} levels in the cytoplasm (Seidler et al., 1989). Also, a very recent finding has shown that CPA is a virulence factor of *Aspergillus flavus* in maize ear rot disease (Chalivendra et al.,

2017). In *A. flavus* the CPA biosynthesis gene cluster involves both *Hps* and *Dma* genes (Chang and Ehrlich, 2011). Interestingly, the gene cluster also contains a FAD-dependent monooxygenase and genes with similar predicted functions are also present in the *DsHps1 – DsDma1* putative gene cluster (Table 3.10). *A. flavus Hps* (*pks-nrps*), *Dma* (*dmat*), and FAD-dependent monooxygenase (*maoA*) gene knockout mutants each lost the ability to produce CPA, and therefore these genes were functionally characterised. There is also a gene predicted to encode a cytochrome p450 upstream of the *A. flavus* CPA gene cluster, but this gene was not functionally characterised (Chang and Ehrlich, 2011). Amino acid identity of DsHps1 to AfPks-Nrps is 43.6% (E=0) and identity of DsDma1 to AfDmat is 38.6% (E=2.6e-6). These suggest that the *DsHps1 – DsDma1* putative gene cluster may be responsible for biosynthesis of a CPA-like SM.

To sum up, the JGI gene model of *DsHps1* appear to be correct and there is negative selection pressure on the *DsHps1* gene. The predicted gene cluster of *DsHps1 – DsDma1* has 9 genes and they may be involved in biosynthesis of a cyclopiazonic acid-like SM.

3.4.2. HPS2

3.4.2.1. Confirmation of gene model for *DsHps2*

The JGI gene model for *DsHps2* was confirmed by aligning DsHps2 with best reciprocal BlastP hits and analysing RNA-seq reads that were mapped on the gene model. The top reciprocal BlastP hits of DsHps2 were in *Khuskia oryzae* (a Sordariomycete), *Ophiobolus disseminans* and *Verruculina enalia* (Dothideomycetes) with amino acid identities to DsHps2 of 56.92% (E=0), 56.49% (E=0) and 55.56% (E=0) respectively; this suggested metabolites with similar properties to the DsHps2 SM may be present in both Dothideomycetes and Sordariomycetes. The alignment (Figure 3.42) shows C–termini of the *O. disseminans* and *V. enalia* HPS were truncated. However, supported by the continuous RNA-seq reads at the 3' end of *DsHps2* (Appendix 20), there is no intron in the 3' end of the gene after the region encoding the last T domain and this region is part of the coding sequence. RNA-seq reads also support all of the

predicted introns in the region encoding *DsHps2*. Therefore, the *DsHps2* JGI gene model is correct, supported by alignments and RNA-seq data.

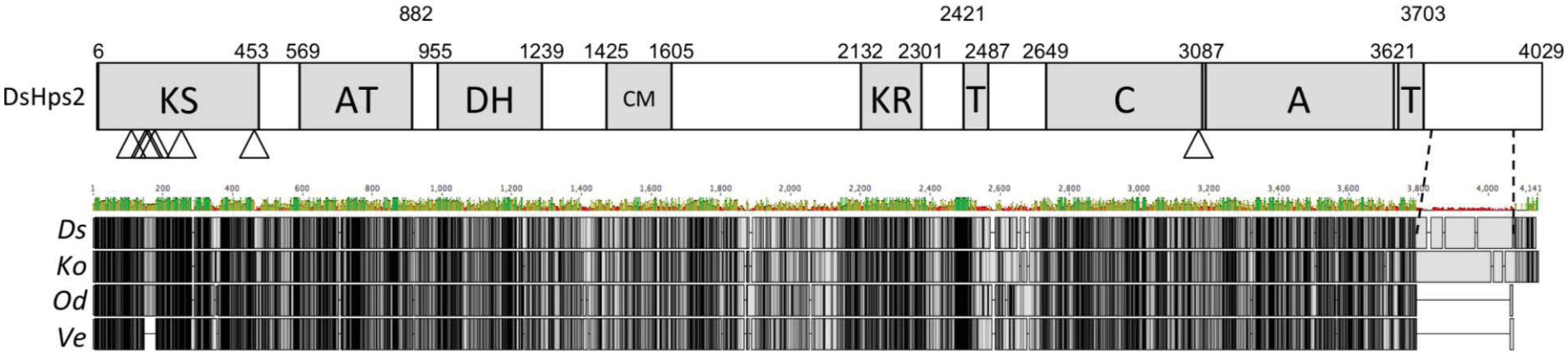

Figure 3.41. Domain structure of DsHps2 and its protein alignment with closest homologs. DsHps2 indicates the peptide's domain organization with KS: keto-synthase, AT: acyltransferase, DH: dehydratase, CM: C-methyltransferase, KR: ketoreductase, T: thiolation, C: condensation, A: adenylation domains. Numbers indicate amino acid positions of domain borders and the end of the peptide (positions of borders that are too close to another border are not shown). Dotted lines show position of the low consensus region in the alignment. The total length is 4029 amino acids. The diagram was drawn to scale. Triangles indicate corresponding intron positions. The dark regions indicate the amino acid alignment with black (highly similar) to white (not similar) sequences with respect to the consensus sequence. The amino acid alignment shows *Ds*: *D. septosporum* Hps2, *Ko: K. oryzae* (protein ID: 424330), *Od: O. disseminans* (protein ID: 360096), *Ve: V. enalia* (protein ID: 565861). The coloured bar represents consensus identity with red (below 30%); green shades indicate higher levels of identity (up to 100%) with bar height proportional to % identity.

3.4.2.1. Comparison of *DsHps2* from 19 strains of *D. septosporum*

Comparison of *DsHps2* sequences across the 19 *D. septosporum* strains were done by aligning the DsHps2 protein sequences from these strains and determining the evolutionary selection pressure using dN/dS ratio (Figure 3.43). The dN/dS ratio of *DsHps2* is 0.22, suggesting *DsHps2* is under negative selection. Therefore, the metabolite produced by DsHps2 may have an important role for *D. septosporum*. Positively selected codons were not determined in this analysis.

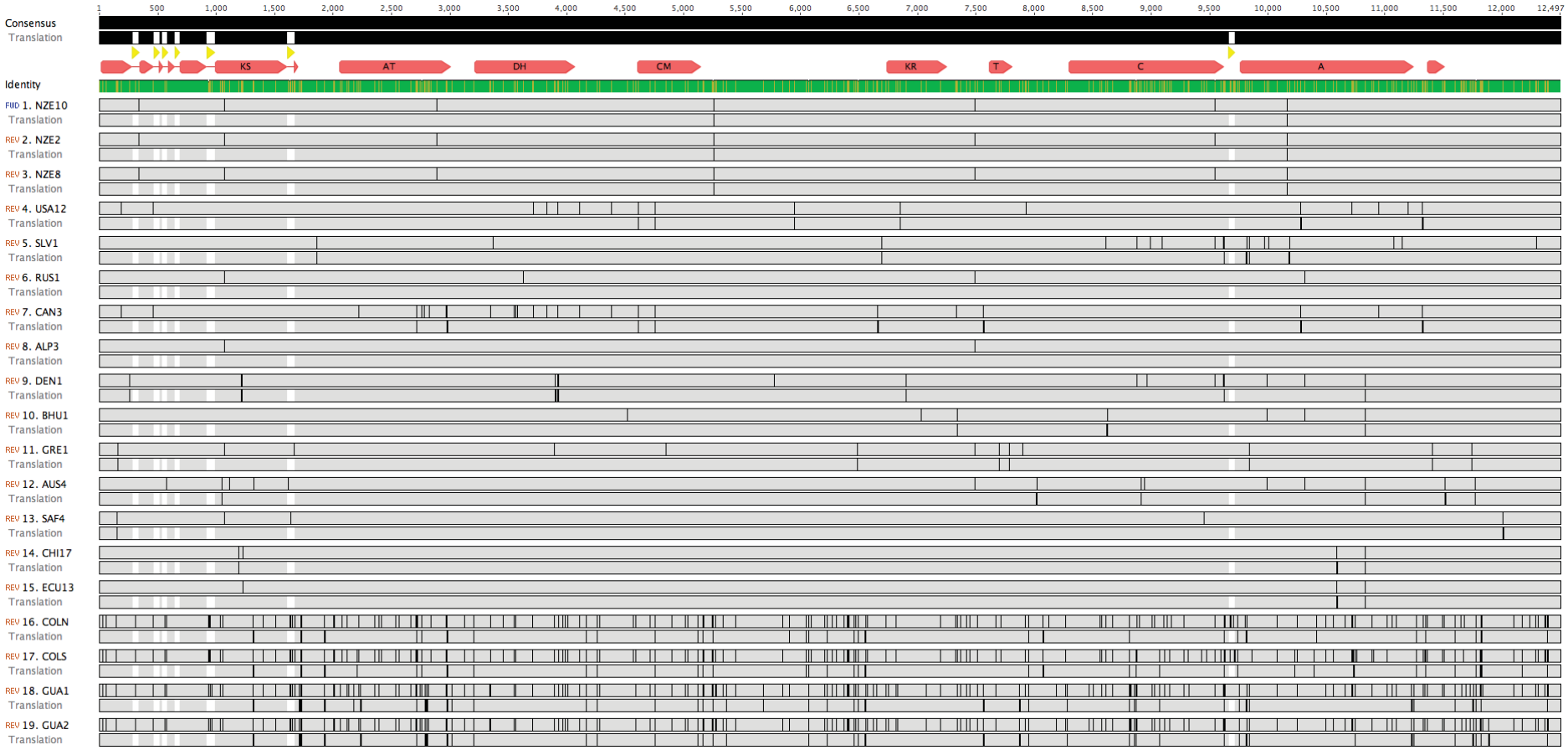

Figure 3.42 *DsHps2* nucleotide alignment of NZE10 with 18 additional strains. Red arrows show the domain positions with KS: keto-synthase, AT: acyltransferase, DH: dehydratase, CM: C-methyltransferase, KR: ketoreductase, T: thiolation, C: condensation, A: adenylation. Yellow arrows indicate intron positions. The coloured bar represents consensus identity with brown indicating identities above 30% and below 100% and green indicating 100% identity. For each sequence, vertical bars on the top and bottom lines show differences in nucleotide and amino acid sequences compared to NZE10. A bar on the top line alone shows a synonymous mutation and a bar on both lines shows a non-synonymous mutation. Strains used in this analysis are listed in Appendix 5.

3.4.2.2. Gene cluster analysis

DsHps2 gene cluster analysis was done to identify the genes that may be involved in the biosynthesis of the HPS product. The expression level of *DsHps2* was very low both *in planta* and in culture (Section 3.1.2), and therefore co-expression of the putative cluster genes could not be analysed. The *DsHps2* putative gene cluster contains 7 genes spanning a 40 kb region of chromosome 9. In addition to these 7 genes, there are 3 genes with no predicted function related to secondary metabolism. The biggest distance between two genes with SM-related functions is 4.1 kb, containing 2 interfering genes (Figure 3.44).

Figure 3.43. *DsHps2* putative gene cluster. Numbers inside arrows indicate JGI protein IDs. Pink: Secondary metabolite core gene (*Hps2*). Purple: putative *DsHps2* cluster genes. Small white arrows: genes without predicted SM functions.

Table 3.11 Genes within *DsHps2* putative gene cluster.

JGI Protein ID[a]	Predicted protein[b]	Best hit organism/JGI ID	E / identity %
Ds74346	Carbamoyl phosphate synthase	*Cladosporium fulvum*/187961	0/81.8
*+Ds157675	Major facilitator transporter	*Cladosporium fulvum*/187962	0/80.7
*+Ds157678/Hps2	Hybrid PKS-NRPS	*Khuskia oryzae*/424330	0/56.9
*+Ds82322	Dehydrogenase / Reductase	*Verruculina enalia*/489491	7.7e-121/62.1
*+Ds65421	ABC transporter related protein	*Rhizoclosmatium globosum*/850377	0/37.5
*+Ds37533	Cytochrome P450	*Dothidotthia symphoricarpi*/303483	2.5e-168/56.8
Ds65424	Crotonyl-CoA reductase	*Ophiobolus disseminans*/427746	2.8e-159/62.2

[a] http://genome.jgi.doe.gov/Dotse1/Dotse1.home.html
Asterisk indicates that genes with similar predicted functions are present in other fungal PKS gene clusters.
Plus indicates that genes with similar predicted functions are present in other fungal NPS gene clusters.
[b] Predicted proteins according to antiSMASH and InterProScan
All BlastP hits were confirmed true except Ds65421 with reciprocal blast analyses.

All genes in the *DsHps2* putative gene cluster except Ds74346 and Ds65424 are present in both fungal PKS and NRPS gene clusters, and genes with similar functions were found in the other predicted SM gene clusters of *D. septosporum*. The *DsHps2* putative gene cluster contains five biosynthetic genes and two transporter genes, one MFS and one ABC transporter (Table 3.11). Genes predicted to encode MFS type transporters were also found in *DsNps2* (Section 3.2.2.3) and *DsPks2* (Section 3.3.2.4) putative gene clusters. The *DsNps2* putative gene cluster

also contains a gene predicted to encode an ABC transporter. Functional analysis of an ABC gene in the fumonisin gene cluster of *Fusarium verticillioides*, *FUM19,* suggested that FUM19 might be responsible for the export of fumonisin from hyphae (Proctor et al., 2003). Another *DsHps2* cluster gene, Ds82322, is predicted to encode a short-chain dehydrogenase/reductase, and genes with similar functions were found in the putative gene clusters of *DsNps3*, *DsPks1* and *DsPks2* (Sections 3.2.3.4, 3.3.1.4, 3.3.2.4). Ds37533 is predicted to encode a cytochrome p450, similar to one found in the *DsHps1* – *DsDma1* putative gene cluster (Section 3.4.1.3).

The *DsHps2* putative gene cluster contains two genes that weren't found in other fungal PKS, NRPS, or HPS gene clusters, but genes with similar predicted functions were observed in other *D. septosporum* SM putative gene clusters. A gene predicted to encode a carbamoyl phosphate synthase was found in the *DsNps1* putative gene cluster (Section 3.2.1.3), and one predicted to encode a crotonyl-CoA reductase was found in the *DsHps1* – *DsDma1* putative gene cluster (Section 3.4.1.3).

NaPDoS analysis suggested that the DsHps2 SM might be a compactin or tyrocidine (Table 3.1). However, as explained in Section 3.4.1.3, compactin biosynthesis requires additional biosynthesis genes but does not require an NRPS (Abe et al., 2002). On the other hand, tyrocidine is a SM produced by bacteria (Mootz and Marahiel, 1997). Therefore, DsHps2 SM is unlikely to be either compactin or tyrocidine and further work is required to determine the nature of the DsHps2 SM.

To sum up, the *DsHps2* gene model is correct; it is under negative selection, and in a putative cluster of 7 genes. However, no prediction could be made on the SM produced by the *DsHps2* gene cluster.

4. Conclusions and future work

Among the SMs produced by *D. septosporum*, only dothistromin had been studied extensively before this PhD project. The previous studies revealed that dothistromin is a virulence factor (Kabir et al., 2015) and its production involves a fragmented gene cluster (Chettri et al., 2013). Genome sequencing revealed that, in addition to the *DsPksA*, dothistromin biosynthesis core gene, there are 10 more SM core genes in the *D. septosporum* genome (de Wit et al., 2012). The aim of this project was to characterise the full set of SM core genes, and to determine if *D. septosporum* has other SM virulence factors and fragmented SM gene clusters. The key conclusions of this study are that *D. septosporum* may be producing at least one other SM virulence factor and may have fragmented gene clusters for the biosynthesis of some other SMs.

An overall analysis of the 11 SM core genes was done to get an overview of the capacity of *D. septosporum* for secondary metabolism. It was previously reported that among the 11 SM core genes of *D. septosporum*, only *DsPksA*, *DsPks1* and *DsNps2* have *C. fulvum* orthologs, and *DsPks4* is truncated (de Wit et al., 2012). In this project, gene model confirmation revealed that the JGI gene model of *DsPks3* is not correct, and *DsPks3* is also a pseudogene. Strikingly, evolutionary selection pressure analyses on SM core genes revealed that all of the analysed PKS, NRPS, and HPS core genes of *D. septosporum* are under negative evolutionary selection, with dN/dS values ranging from 0.13 (*DsPks1*) to 0.39 (*DsHps1*). This suggests that all these genes may have important roles at some stages of the fungal life cycle.

In culture and *in planta* expression of *D. septosporum* SM core genes revealed that, in addition to *DsPksA*, three more genes, *DsPks1*, *DsPks2*, and *DsNps3* were expressed at high levels during infection. Therefore, these three genes were selected as genes of key interest as virulence factor candidates. Interestingly, phylogenetic analyses revealed that two of these genes, *DsPks2* and *DsNps3* have no orthologs in any of the species in three fungal classes whose genomes are currently available in the JGI database. On the other hand, *DsNps1*, *DsNps2*, *DsHps1* and *DsHps2* had very low expression levels both in culture and *in planta*. Low

expression levels for these *D. septosporum* SM core genes suggest that these genes do not have functions related with plant disease. However, it is possible that expression levels of these genes could be higher if different conditions for SM production were provided in culture, or the right timing, host, or part of the host were used. For example, some of the SM core genes may be expressed at high levels in spores or needles that have fallen on the forest floor. For example, a polyketide gleosporone is produced at high levels in the spores of plant pathogen *C. gloeosporioides* to prevent germination until the right conditions for host infection are present (Meyer et al., 1983). In *Aspergillus spp.* it was seen that competition with another microorganism significantly altered the metabolite production (Losada et al., 2009). It is possible that some of the *D. septosporum* SMs may be produced on the needles on the forest floor to gain competitive advantage against saprophytes.

Effects of different media conditions on *D. septosporum* metabolite production were also analysed. In these analyses, it was shown that use of NH_4 as sole nitrogen source had the most dramatic effects on the metabolite profiles by significantly changing the production of three metabolites in wild type and two metabolites in the *ΔLaeA* strain. In contrast, use of NO_3 as sole nitrogen source had no significant effects on the metabolite profiles obtained. Because one of the SM core genes (*DsNps2*) was predicted to produce a siderophore, the effects of iron limitation were analysed. However, there was no increase in the metabolites produced by cultures grown in media without iron compared to those with iron. This suggests that siderophore production in *D. septosporum* might not be affected by iron deficiency and it was not possible to predict which of the TLC bands might be the possible siderophore produced by *DsNps2* gene cluster. The effect of carbohydrate limitation was also tested, and the amounts of one metabolite in wild type and one in *ΔLaeA* were significantly decreased when the glucose concentration was decreased. This was opposite to expected, as carbon catabolite repression is one of the main regulators of fungal secondary metabolism. The main limitations of these analyses included the timing and methods of extraction. If the production of a particular SM is different at an earlier time point than the time of the analysis, it might be not be possible to detect a carbon catabolite repression

effect. Use of different solvent systems to those used in this analysis might enable other metabolites to be detected. Future work for better characterization of the media effects may include use of different time points, different metabolite extraction methods, and other variables such as different types of carbon sources used in the analysis.

Gene cluster analyses on the *D. septosporum* SM core genes revealed that some predicted genes appear to be located outside of the gene clusters for several SMs. For example, *DsPks1*, a gene most likely involved in melanin biosynthesis, is probably part of a fragmented gene cluster distributed across multiple chromosomes. Likewise *DsNps1* and *DsNps2* gene clusters are predicted to be fragmented. This supports the hypothesis that there are other fragmented gene clusters used in the SM biosynthesis of *D. septosporum*, in addititon to the characterised dothistromin biosynthesis gene cluster. Gene clusters can be confirmed using two ways. First, the cluster genes can be knocked out and the metabolite production could be tracked by analysing the metabolites using a method such as TLC or high-pressure liquid chromatography (HPLC). However, none of the *D. septosporum* SMs except dothistromin have been chemically characterised from the metabolite extracts yet. Secondly, an easier method involves the use of master regulatory genes. It is known that expression of many of the SM core genes (*DsPks2*, *DsNps1*, *DsNps2*, *DsHps1* and *DsHps2*) is altered in a strain of *D. septosporum* that has a deletion of the *DsLaeA* global regulator gene (*ΔLaeA*) compared to the wild type strain (Chettri and Bradshaw, 2016). Based on studies with *Aspergillus* spp. (Bok and Keller, 2004; Amaike and Keller, 2009), co-regulation means the expression of most clustered SM genes would also be altered in a *ΔLaeA* strain, so this can be used to help confirm gene clusters. The limitation with this method is that the gene clusters whose core genes are not regulated by the DsLaeA, such as *DsPks1*, can't be confirmed using the *DsLaeA* deletion mutants.

Apart from the potential fragmented gene clusters, gene cluster analyses for the SM core genes also revealed that *DsHps1* – *DsDma1* putative gene cluster might be responsible for production of cyclopiazonic acid, which was different from the NaPDoS prediction.

Comparison of 19 *D. septosporum* genomes revealed not only the evolutionary selection pressures as mentioned previously, but also the higher number of polymorphisms in four Colombia (COL1-2) and Guatemala (GUA1-2) strains compared to the other 15 *D. septosporum* strains. This concurs with the finding that the Guatemala (GUA1) strain was the most divergent strain in a dothistromin cluster gene sequence analysis (Bradshaw et al., 2013). Therefore, COL and GUA appear to be deeply divergent strains of *D. septosporum*.

Phenotypic analysis of *D. septosporum ΔDsNps3* strains showed that the Nps3 SM might be a virulence factor. This was supported by lower hyphal surface network on needle surfaces at an early stage of infection and lower fungal biomass in late stage lesions. The expression level of *DsNps3* at the early stage of infection was the highest of the SM core genes and, combined with the significant difference in the fungal surface network between *ΔDsNps3* and wild type strains it is possible that the DsNps3 SM may be associated with early / biotrophic stage infection. In the hemibiotrophic plant pathogen *C. higginsianum*, two NRPS genes were also expressed highly at the biotrophic stage of infection but these genes have not been functionally characterised. In the current study, exhaustive efforts were made to determine the kind of NRP that might be produced by *DsNps3* using both bioinformatics and biochemical approaches. However, due to inconsistencies between different prediction softwares in A domain specificity determination and uncertainty of the cycle repetitions it wasn't possible to determine the Nps3 SM bioinformatically. TLC analysis on *ΔDsNps3* and wild type strains was done to attempt biochemical characterization of the Nps3 SM. Unfortunately, due to low level production of the Nps3 candidate SM and poor separation from other metabolites on the TLC plate, it wasn't possible to biochemically characterise Nps3 SM. In order to confirm if Nps3 SM is a virulence factor, the pathogenicity assay of *ΔDsNps3* will need to be repeated with a second knock out mutant and complemented strain. The nature of the Nps3 SM may be determined by over-expression of *DsNps3* gene cluster using other media conditions or regulatory genes, and then biochemical characterization might be done by TLC, HPLC, mass spectrometry (MS) and nuclear magnetic resonance (NMR) spectroscopy analyses.

The key findings of this project for *D. septosporum* SM core genes are summarized in Table 4.1.

Table 4.1. Key findings of this project for *D. septosporum*

Gene	Expression[a]	Metabolite[b]	Unique[c]	Fragmented cluster[d]	Virulence[e]	dN/dS[f]
DsPks1	High	Melanin	No	Yes	Unknown	0.13
DsPks2	High	Unknown	Yes	Unknown	Unknown	0.21
DsNps1	Low	Cyclosporin	Yes	Yes	Unknown	0.23
DsNps2	Low	Ferricrocin	No	Yes	Unknown	0.27
DsNps3	High	Unknown	Yes	Unknown	Yes	0.27
DsHps1	Low	Cyclopiazonic acid	No	No	Unknown	0.39
DsHps2	Low	Unknown	No	Unknown	Unknown	0.22

[a] *In planta* expression at early, mid, or late stages of infection. High: above 10 RPMK. Low: below 10 RPMK.
[b] Predicted SMs produced by the SM core genes based on orthology and gene cluster analyses.
[c] Gene is unique among dothideomycetes.
[d] Appears to involve a fragmented gene cluster.
[e] According to the gene KO and phenotypic analyses, probably a virulence factor.
[f] dN/dS ratio indicating evolutionary selection. dN/dS values smaller than 1 indicate negative selection.

There are several future studies that can be based on the findings of this project. The most important of these are:

- Confirmation of the gene clusters, especially for *DsPks1*, *DsPks2*, and *DsNps3*.
- Confirmation of Nps3 SM as a virulence factor.
- Chemical characterization of the Nps3 SM.

Other future works based on this project include the following:

- Gene KO and functional characterization of the other SM core genes, in particular *DsPks1* and *DsPks2*.
- Chemical characterization of the other SMs.

Altogether, the results of this project showed that a hemibiotrophic fungus is perfectly capable of keeping a viable lifecycle with a very low number of SMs. Therefore, the current assumption about pathogens with a necrotrophic stage requiring more SMs than biotrophs (reviewed by Pusztahelyi et al., 2015) is not always correct. In addition, fragmented SM gene clusters may not be exceptional in plant pathogenic fungi, and there might be many more fragmented SM gene clusters waiting to be found. Finally, this project revealed that there are still many

unknown SMs, and learning more about them will greatly broaden our understanding of plant-pathogenic fungi interactions.

APPENDIX

Appendices that are on the CD

Appendix 10
Fluorescence microscopy images of WT and *ΔDsNps3 D. septosporum* infected needles (Section 3.2.3.8).

Appendix 12
Binocular microscopy images of WT and *ΔDsNps3 D. septosporum* infected lesions (Section 3.2.3.8).

Appendix 21
Alignments of predicted SM core proteins with best BlastP matches

Appendix 22
D. septosporum SM core gene and amino acid sequences

Appendix 1 – Media

All media were prepared in ddH_2O and autoclaved at 121 °C for 15 minutes. Antibiotics were added after the media cooled down to 50°C.

Luria broth (LB) (Bertani, 1951)
5 g/L tryptone (Oxoid, UK), 2.5 g/L yeast extract (Gibco BRL), 5 g/L NaCl (Panreac, Spain)

LB agar (Bertani, 1951)
5 g/L tryptone (Oxoid), 2.5 g/L yeast extract (Gibco BRL), 5 g/L NaCl (Panreac), 1.5% (wt/vol) Agar (Neogen Acumedia, MI, USA)

DM (Bradshaw et al., 2000)

50 g/L bacto malt extract (BD, NJ, USA), 23 g/L nutrient broth (Oxoid)

DM agar (Bradshaw et al., 2000)

50 g/L bacto malt extract (BD), 23 g/L nutrient broth (Oxoid), 1.5% (wt/vol) Agar (Acumedia)

DSM (Bradshaw et al., 2000)

20 g/L bacto malt extract (BD), 5 g/L yeast extract (Gibco BRL), 1.5% (wt/vol) Agar (Acumedia)

PMMG (McDougal et al., 2011)

	Amount (g/L)
$MgSO_4x7H_2O$ (Scharlau, Spain)	0.2
$K_2HPO_4x3H_2O$ (VWR)	1
NH_4NO_3 (Sigma)	1
KCl (Sigma)	0.2
$FeSO_4x7H_2O$(Univar, IL, USA)	0.002
$ZnSO_4x7H_2O$(VWR)	0.002
Asparagine(Sigma)	2
Glucose(Univar)	3
Agar(Acumedia)	20

Pine needles were soaked overnight in ddH2O [10%(wt/vol)] and this water was used for the media preparation. pH was adjusted to 6.2 prior to autoclave.

1.5% RG media

50 g/L malt extract (Oxoid), 23 g/L nutrient broth (Oxoid) and 273.8 g/L Sucrose (VWR), 1.5% (wt/vol) agar (Acumedia).

0.8% RG media

8 g/L bacteriological agar (Oxoid), 50 g/L malt extract (Oxoid), 23 g/L nutrient broth (Oxoid) and 273.8 g/L Sucrose (WVR), 0.8% (wt/vol) agar (Acumedia).

Appendix 2 – Buffers and Solutions

All buffers and solutions were prepared in ddH_2O unless stated otherwise. and autoclaved at 121°C for 15 minutes and allowed to cool before use.

2% CTAB Buffer

2%(w/v) Hexadecyltrimethylammonium bromide (CTAB) (Sigma); 1% (w/v) Polyvinylpyrrolidone (PVP40) (Sigma); 1.4 M NaCl (Panreac); 20 mM EDTA (Sigma); 0.1 M Tris – HCl pH8.0). The solution was autoclaved at 121°C for 15 minutes and allowed to cool before use.

TE buffer

10 mM Tris (Carl Roth, Germany), 1 mM EDTA (Sigma), pH8.0.

10x TBE Buffer

108 g/L Tris (Carl Roth), 55 g/L Boric Acid (Univar), 7.44 g/L EDTA, pH8.2.

OM buffer

1.4 M $MgSO_4$ and 10 mM Na_2HPO_4 (VWR) was dissolved in 100 mL Milli-Q water. pH was adjusted to 5.8 with 100 mM $NaH_2PO_4.2H_2O$ (VWR). Dissolving to a final volume of 300 mL, ddH_2O was added. The solution was autoclaved at 121°C for 15 minutes and allowed to cool before use.

ST buffer

0.6 M sorbitol (Sigma), 100 mM Tris (Carl Roth) pH 8.0. The solution was autoclaved at 121°C for 15 minutes and allowed to cool before use.

STC buffer

1 M sorbitol (Sigma), 50 mM Tris (Carl Roth) pH 8.0, 50 mM $CaCl_2$ (Merck). The solution was autoclaved at 121°C for 15 minutes and allowed to cool before use.

6x loading dye

0.25% (wt/vol) bromophenol blue (Sigma), and 40% sucrose was filter sterilized using 0.2 μm syringe filter.

Ethidium bromide (EtBr)

From 10mg/mL stock solution, 100 μL EtBr was dissolved per 1L water.

Southern blot solution 1 (Depurination)

0.25 M HCl

Southern blot solution 2 (Denaturation)

0.5 M NaOH/0.5M NaCl (Panreac)

Southern blot solution 3 (Neutralization)

0.5M Tris (Carl Roth) pH7.4, 2 M NaCl (Panreac)

20 x SSC buffer

3 M NaCl (Panreac), 0.3 mM $Na_3C_6H_5O_7$ (Merck)

Buffer I: 0.1 M Tris, 0.15M NaCl (Panreac) pH7.5 (Southern blot, Hybridization). The solution was autoclaved at 121°C for 15 minutes and allowed to cool before use.

Buffer II: 1g skim milk/100 mL Buffer I (Southern blot, Hybridization)

Buffer III: 0.1 M Tris, 0.1 M NaCl (Panreac) pH9.5 (Southern blot, Hybridization). The solution was autoclaved at 121°C for 15 minutes and allowed to cool before use.

Washing solution 1: (2 x SSC, 0.1% SDS (VWR)) (Southern blot, washing)

Washing solution 2: (0.5 x SSC, 0.1% SDS (VWR)) (Southern blot, washing)

Appendix 3 – Primers

Primer name	Lab number	Primer Sequence (5'-3')[a]
NPS3-5FP-attb2R	1565	GGGGACAGCTTTCTTGTACAAAGTGGCTGAGTAATACCTCCCTGCCGT
NPS3-5RP-attb1R	1566	GGGGACTGCTTTTTTGTACAAACTTGCCATAATGTCGAGGTCCTGCA
NPS3-3FP-attb4_domain	1567	GGGGACAACTTTGTATAGAAAAGTTGCTGGCACAGGATCGTCCACG
NPS3-3RP-attb3_domain	1568	GGGGACAACTTTGTATAATAAAGTTGCTAGAGCTGCTCTGGCGGTAT
NPS3-FP-wtcheck	1587	CCAGAAATGTAACTCGGCTT
D. septo NRPS 3 reverse	1099	CTGTCGGCACATTGAGTC
NPS3-5FP-screen	1617	TCTCAGACATGGCAGGTCA
OscHygR	1412	GCCGATGCAAAGTGCCGATAAACA
NPS3-3RP-domainscreen	1618	TCACGAGAGCCAGGGAGGACT
OscHygF	1411	AGAGCTTGGTTGACGGCAATTTCG
PKS2-73814-KO5F	1315	GGGGACAACTTTGTATAGAAAAGTTGCTGGTCAGGAGTTAAGGGCAAA
PKS2-73814-KO5R	1316	GGGGACTGCTTTTTTGTACAAACTTGCGCCTTCCTCGTGGATCGTAG
PKS2-73814-KO3F	1317	GGGGACAGCTTTCTTGTACAAAGTGGCTGTTCCTGGAAGCCATGGGAA
PKS2-73814-KO3R	1318	GGGGACAACTTTGTATAATAAAGTTGCTCCCAGTTATCCAGGGCGTA
F-upst-Pks2-screen	1381	ACATACTGTTTGACGGCCAG
hph Fwd2	175	ATTTCATATGCGCGATTGCTGAT
GFP-Fwd	1365	GCATGGACGAGCTGTACAAG
R-downst-Pks2-screen	1381	ACATACTGTTTGACGGCCAG
PKS2-ks-fp	1552	ACAGGAAGGACATTTGGCAC
D.septo pks2Reverse	1106	GATGTGTCAAGGAACTGCCA
AflJ exF	1023	GACCATTGCGGCATTCTG
AflJ exR	1024	GCTGTAGTGTACGGAATCCA
CAD918	935	CAGCAAGAGGATTTGGACCTA
CAD1019	936	TTCAATACCCACATCTGATCAAC

[a] Respective *att* sites of each primer are underlined.
Primers that were used for the same purpose were grouped together.

Appendix 4 – Gene model confirmation of *DsNps1* (Section 3.2.1.1)

An amino acid alignment of DsNps1 with its best BlastP hits is presented in the CD (Appendix 21a). RNA-seq reads that were mapped onto the JGI gene model were used in an attempt to confirm the *DsNps1* gene model (Section 3.2.1.1). But, as shown below, due to the very low expression levels of *DsNps1* both *in planta* and in culture, there were insufficient reads to confirm the intron positions.

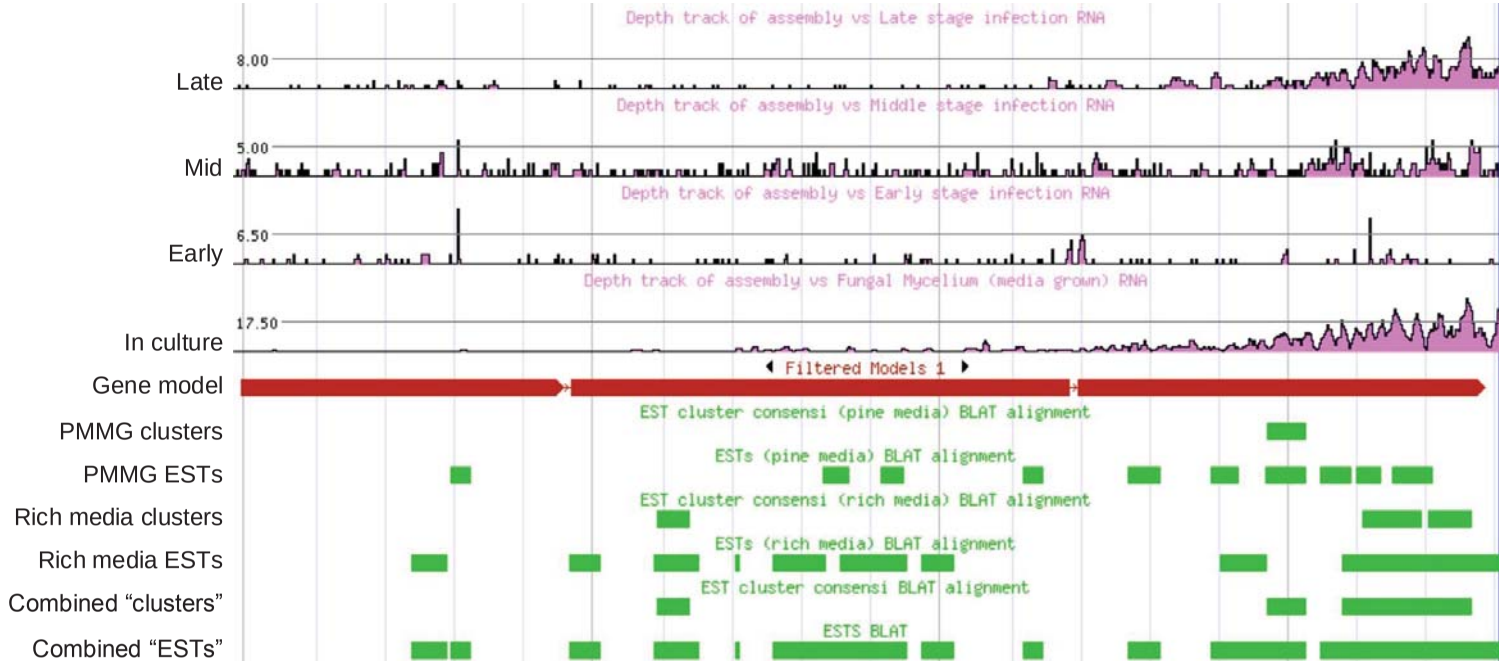

Figure A4. *DsNps1* RNA-seq reads that were mapped onto the JGI gene model. Pink rows at top are *DsNps1* RNA-seq reads at late, middle and early stages (*in planta*) and in culture (from Bradshaw et al, 2016). The numbers (eg 8.00) are RPMK values. The red row predicted coding sequence (from start codon to stop codon) based on the gene model from JGI. Green bars represent the ESTs originally used for gene annotation. PMMG and Rich media (DSM, V8, DM, PD) indicate the types of media used for growing fungal mycelia before RNA extraction. Clusters: indicate 454 EST sequences of RNA assembled with Newbler to create isotigs that were then aligned against the genomic assembly using the BLAT tool. ESTs: EST/cDNA sequences aligned against the genomic assembly using the BLAT tool. Bottom two green bars indicate the combination of the two "clusters" or "ESTs".

Appendix 5 – *D. septosporum* strains used in evolutionary selection pressure analyses

Genome sequences of *D. septosporum* strains collected across the globe were used to determine evolutionary selection pressures on SM core genes.

Table A5. Strains of *D. septosporum* for which genome sequences were available.

ID	Country	Region	Host	Collection year
1_ALP3	Germany	Bavarian Alps	*P. mugo*	1996
2_AUS4	Austria	Lower Austria	*P. sylvestris*	2004
3_BHU1	Bhutan	Yusipang, Thimphu dzongkhag	*P. radiata*	2005
4_CAN3	Canada	British Columbia	*P. contorta v. latifolia*	1996
5_CHI17	Chile	Unknown	*P. radiata*	2001
6_COLN	Colombia	Sonora EST-1-128, Northern zone	*Pinus ELL x TAE*	2011
7_COLS	Colombia	Don Miguel – Lote 54 – Southern Colombia	*P. kesiya*	2011
8_DEN1	Denmark	Copenhagen	*P. aristata*	2013
9_ECU13	Ecuador	Unknown	*P. radiata*	2001
10_GRE1	Greece	Northern Greece	*P. burtia & P. nigra*	2012
11_GUA1	Guatemala	Unknown	*P. tecumumanii*	1983
12_GUA2	Guatemala	Jalapa	*P. oocarpa*	2012
13_NZE2	New Zealand	Central North Island	*P. radiata*	1965
14_NZE8	New Zealand	Bay of Plenty	*P. radiata*	2004
15_RUS1	Russia	Unknown	*P. sylvestris*	2015
16_SAF4	South Africa	Limpopo	*P. radiata needles*	2002
17_SLV1	Slovakia	Unknown	*P. sylvestris*	2001
18_USA12	USA	Oregon	*P. ponderosa*	1983

Appendix 6 – Gene model confirmation of *DsNps2* (Section 3.2.2.1)

An amino acid alignment of DsNps2 with its best BlastP hits is presented in the CD (Appendix 21b). RNA-seq reads that were mapped onto the JGI gene model were used in an attempt to confirm the *DsNps2* gene model (Section 3.2.2.1). The intron at the 3' end of *DsNps2* could be confirmed using RNA-seq data. However, due to low number of reads at 5' end of *DsNps2*, the intron at 5' end of the gene could not be confirmed with RNA-seq analysis.

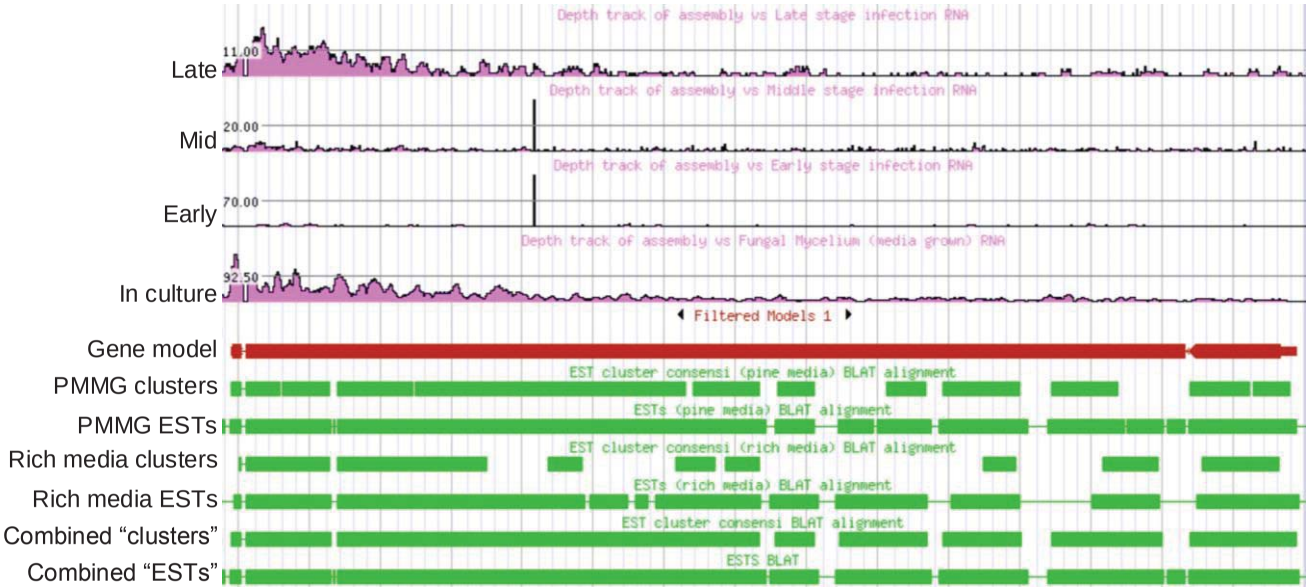

Figure A6. *DsNps2* RNA-seq reads that were mapped onto the JGI gene model. Pink rows at top are *DsNps2* RNA-seq reads at late, middle and early stages (*in planta*) and in culture (from Bradshaw et al, 2016). The numbers (eg 11.00) are RPMK values. The bold red row is predicted coding sequence (from start codon to stop codon) based on the gene model from JGI. Thin red row indicates untranslated regions (UTRs). Green bars represent the ESTs originally used for gene annotation. PMMG and Rich media (DSM, V8, DM, PD) indicate the types of media used for growing fungal mycelia before RNA extraction. Clusters: indicate 454 EST sequences of RNA assembled with Newbler to create isotigs that were then aligned against the genomic assembly using the BLAT tool. ESTs: EST/cDNA sequences aligned against the genomic assembly using the BLAT tool. The bottom two green bars indicate the combination of the two "clusters" or "ESTs".

Appendix 7 – Gene model confirmation of *DsNps3* (Section 3.2.3.2)

An amino acid alignment of DsNps3 with its best BlastP hits is presented in the CD (Appendix 21c). RNA-seq reads that were mapped onto the JGI gene model were used to confirm the *DsNps3* gene model (Section 3.2.3.2). The *DsNps3* gene model was confirmed by continuous RNA-seq reads from start codon to stop codon.

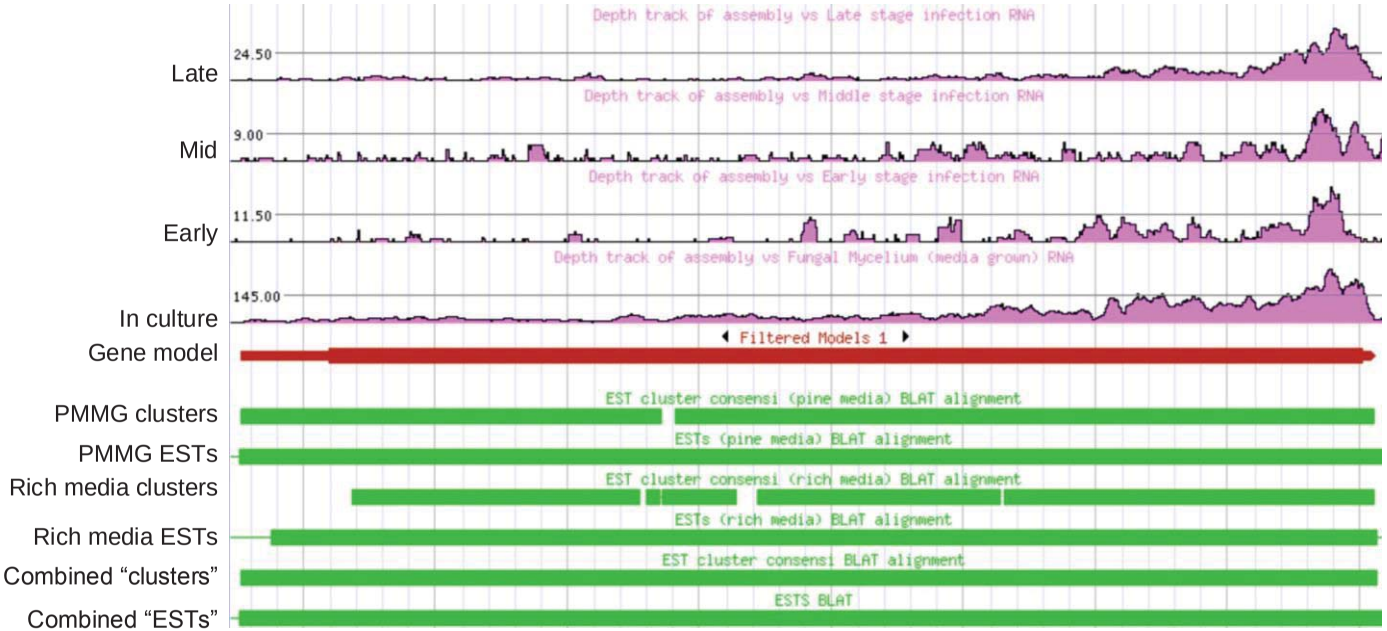

Figure A7. *DsNps3* RNA-seq reads that were mapped onto the JGI gene model. Pink rows at top are *DsNps3* RNA-seq reads at late, middle and early stages (*in planta*) and in culture (from Bradshaw et al, 2016). The numbers (eg 24.50) are RPMK values. The bold red row is predicted coding sequence (from start codon to stop codon) based on the gene model from JGI. Thin red rows indicate untranslated regions (UTRs). Green bars represent the ESTs originally used for gene annotation. PMMG and Rich media (DSM, V8, DM, PD) indicate the types of media used for growing fungal mycelia before RNA extraction. Clusters: indicate 454 EST sequences of RNA assembled with Newbler to create isotigs that were then aligned against the genomic assembly using the BLAT tool. ESTs: EST/cDNA sequences aligned against the genomic assembly using the BLAT tool. The bottom two green bars indicate the combination of the two "clusters" or "ESTs".

Appendix 8 – *DsNps3*-pOSCAR gene knockout construct (Section 3.2.3.5)

The gene knock out of *DsNps3* was done using the plasmid construct shown below. This construct was prepared as in Section 2.7.2 and used to generate *ΔDsNps3* mutants using protoplast transformation as in Section 2.9.

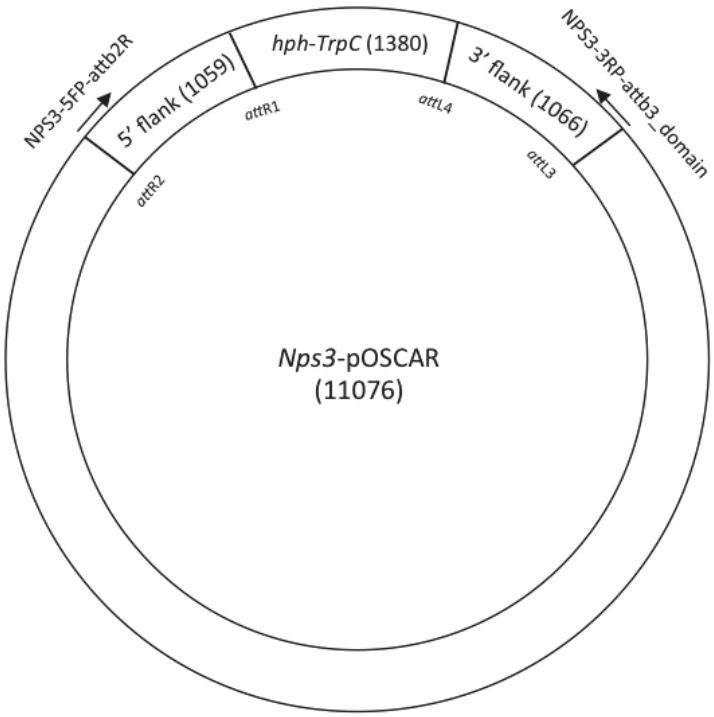

Figure A8. DsNps3-pOSCAR KO construct. Hph-TrpC shows the hygromycin resistance marker. *att* sites at the borders of flanking regions are shown. Sizes of the whole plasmid, flanking regions, and *hph-TrpC* are shown in brackets in bp. Primer pairs used in PCR amplification of 5' and 3' flanking sites were NPS3-5FP-attb2R/NPS3-5RP-attb1R and NPS3-3FP-attb4_domain/NPS3-3RP-attb3_domain, respectively. Primers NPS3-5FP-attb2R/NPS3-3RP-attb3_domain were used to confirm plasmid generation. Plasmid was generated based on Paz et al. (2011).

Appendix 9. Southern hybridization confirmation of *ΔDsNps3*

Genomic DNAs of wild type and *ΔDsNps3* candidates were digested with EcoRV and, using a probe that could bind to both wild type and *ΔDsNps3*, the absence of *DsNps3* was confirmed using Southern hybridization. Figure 3.17 shows the restriction enzyme recognition sites and probe binding positions on *DsNps3* in wild type and *ΔDsNps3*.

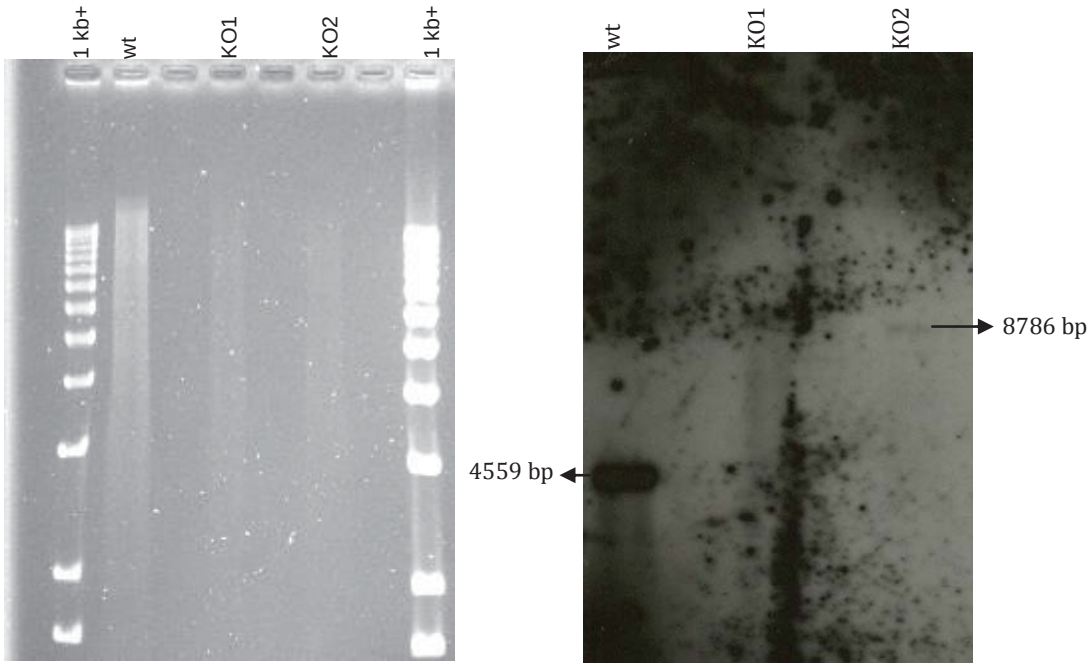

Figure A9. Southern hybridization confirmation of *ΔDsNps3*. EcoRV-digested wild type, *ΔDsNps3* KO1, and *ΔDsNps3* KO2 gDNAs (left) and Southern hybridization of these gDNAs (right) using the probe in Figure 3.17. Expected fragment sizes were 4559 bp for wild type and 8786 bp *ΔDsNps3*.

Southern hybridization analysis presented in Figure A19 showed that KO2 appears to have single copy integration with no wild type gDNA. There was no conclusive result present for KO1 because of the low gDNA concentration from the start. High background was because of the 3-hour exposure time that was required in order to detect the band belonging to KO2. No band belonging to wild type was observed for KO1 and KO2. Also, the band belonging to wild type was stronger than the other two. That was most likely due to inefficient gDNA extraction from KO1 and KO2 by use of plant gDNA extraction kits with fungal samples (Section 2.3.1). Wild type *D. septosporum* gDNA was present in the lab stock.

Appendix 11 – Fungal to plant biomass ratio estimation in WT and *ΔDsNps3 D. septosporum* infected lesions (Section 3.2.3.6)

From *D. septosporum* infected lesions, qPCR analysis was done as explained in Section 2.12.1.2 to compare fungal to plant biomass ratios. The qPCR results for the summary shown in Section 3.2.3.6 are presented here. Comparisons were done separately for each technical replicate (eg. WTa-KOa, WTb-KOb, and WTc-KOc). Statistically significant difference analyses between WT and *ΔDsNps3* fungal to plant biomass ratios were done using t-tests by comparing WTa-c and KOa-c for each of the samples P1, P2 and P4 separately.

Table A11. qPCR results for biomass estimation data

Sample Name[a]	Targets	References	Ct-Ref[b]	Ct-Target[c]	Target/Ref[d]
P1-WT-a	*AflJ*	*CAD*	24.23152289	29.28161173	0.00703
P1-WT-b	*AflJ*	*CAD*	24.21817276	29.92672079	0.0115
P1-WT-c	*AflJ*	*CAD*	24.69694141	29.13639162	0.00454
P1-KO2-a	*AflJ*	*CAD*	26.59887473	29.70376677	0.0018
P1-KO2-b	*AflJ*	*CAD*	25.99563569	29.46163371	0.0023
P1-KO2-c	*AflJ*	*CAD*	26.55096167	29.72437025	0.00189
P2-WT-a	*AflJ*	*CAD*	29.79491357	31.04160674	0.000503
P2-WT-b	*AflJ*	*CAD*	29.79129381	30.82535338	0.000429
P2-WT-c	*AflJ*	*CAD*	29.49238872	31.17737196	0.000689
P2-KO2-a	*AflJ*	*CAD*	29.73023763	27.61477978	0.0000413
P2-KO2-b	*AflJ*	*CAD*	29.23093224	27.46277611	0.0000526
P2-KO2-c	*AflJ*	*CAD*	29.33066786	27.29554913	0.0000433
P4-WT-a	*AflJ*	*CAD*	20.45181109	28.80877503	0.0722
P4-WT-b	*AflJ*	*CAD*	20.53280436	28.90590667	0.0733
P4-WT-c	*AflJ*	*CAD*	20.67696928	28.72024329	0.0577
P4-KO2-a	*AflJ*	*CAD*	24.17974228	28.7162744	0.0048
P4-KO2-b	*AflJ*	*CAD*	24.32047766	28.93406314	0.0051
P4-KO2-c	*AflJ*	*CAD*	24.07775218	28.84135497	0.00566

[a] Sample name indicates P1-P4 plant genotype; WT/KO2 Inoculated wild type or *ΔDsNps3 D. septosporum* strains; a-c are technical replicates.
[b] Cycle threshold (Ct) value of *CAD* amplification
[c] Cycle threshold (Ct) value of *AflJ* amplification
[d] Fungal to plant biomass ratio based on Ct-Ref and Ct-Target.

Appendix 13 – Gene model confirmation of *DsPks1* (Section 3.3.1.2)

An amino acid alignment of DsPks1 with its best BlastP hits is presented in the CD (Appendix 21d). RNA-seq reads that were mapped onto the JGI gene model were used in order to confirm the *DsPks1* gene model (Section 3.2.3.2). The gene model was confirmed by continuous RNA-seq reads from start to end of *DsPks1*.

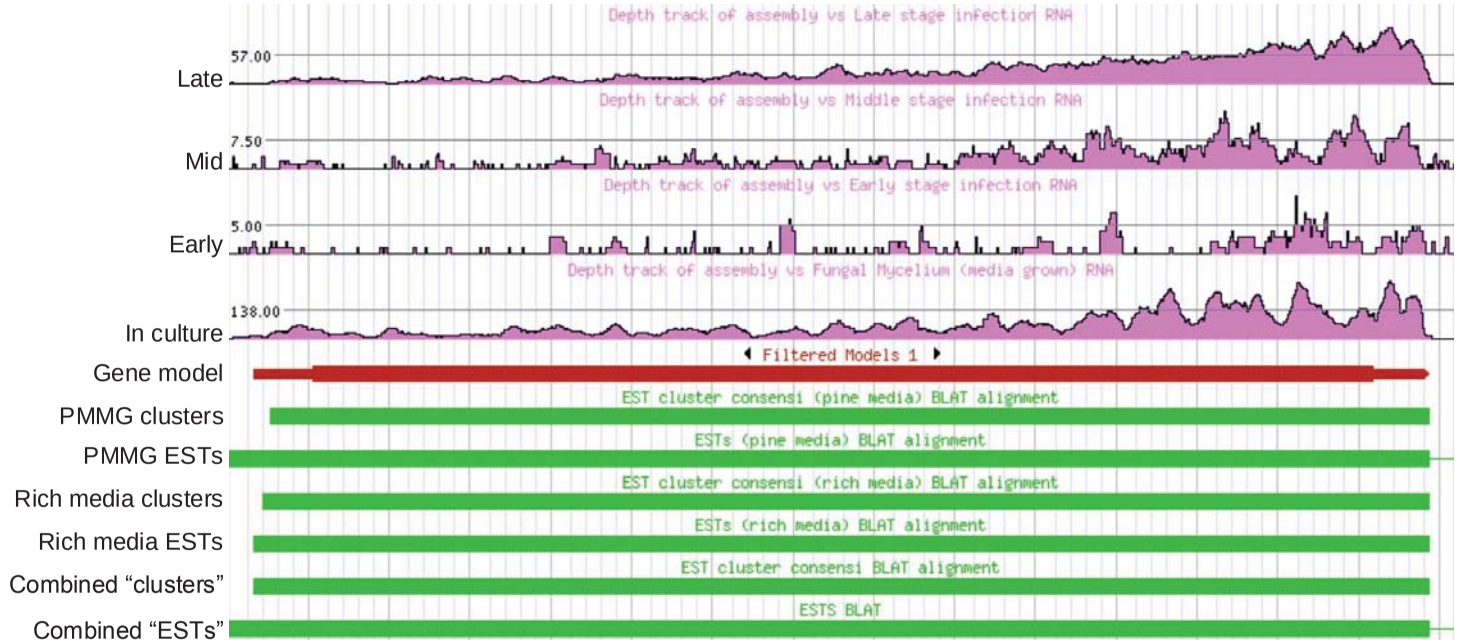

Figure A13. *DsPks1* RNA-seq reads that were mapped onto the JGI gene model. Pink rows at top are *DsPks1* RNA-seq reads at late, middle and early stages (*in planta*) and in culture (from Bradshaw et al, 2016). The numbers (eg 57.00) are RPMK values. The bold red row is predicted coding sequence (from start codon to stop codon) based on the gene model from JGI. Thin red rows indicate untranslated regions (UTRs). Green bars represent the ESTs originally used for gene annotation. PMMG and Rich media (DSM, V8, DM, PD) indicate the types of media used for growing fungal mycelia before RNA extraction. Clusters: indicate 454 EST sequences of RNA assembled with Newbler to create isotigs that were then aligned against the genomic assembly using the BLAT tool. ESTs: EST/cDNA sequences aligned against the genomic assembly using the BLAT tool. The bottom two green bars indicate the combination of the two "clusters" or "ESTs".

Appendix 14 – Initial phylogenetic analyses of DsPks2 (Section 3.3.2.1)

Initial phylogenetic analyses were done on DsPks2 and its best BlastP hits using full protein, KS, and KS+AT sequences. As a result of all three analyses, sequences of *D. septosporum* clustered with *Aspergillus* spp., suggesting a possible horizontal gene transfer (HGT). The initial phylogenetic analyses (shown below in Figures A13a-c) were done in 2012, and therefore were based on the genome sequences available in 2012. However, detailed phylogenetic analyses done later showed that there was no HGT between *DsPks2* and its homologs (see Section 3.3.2.1).

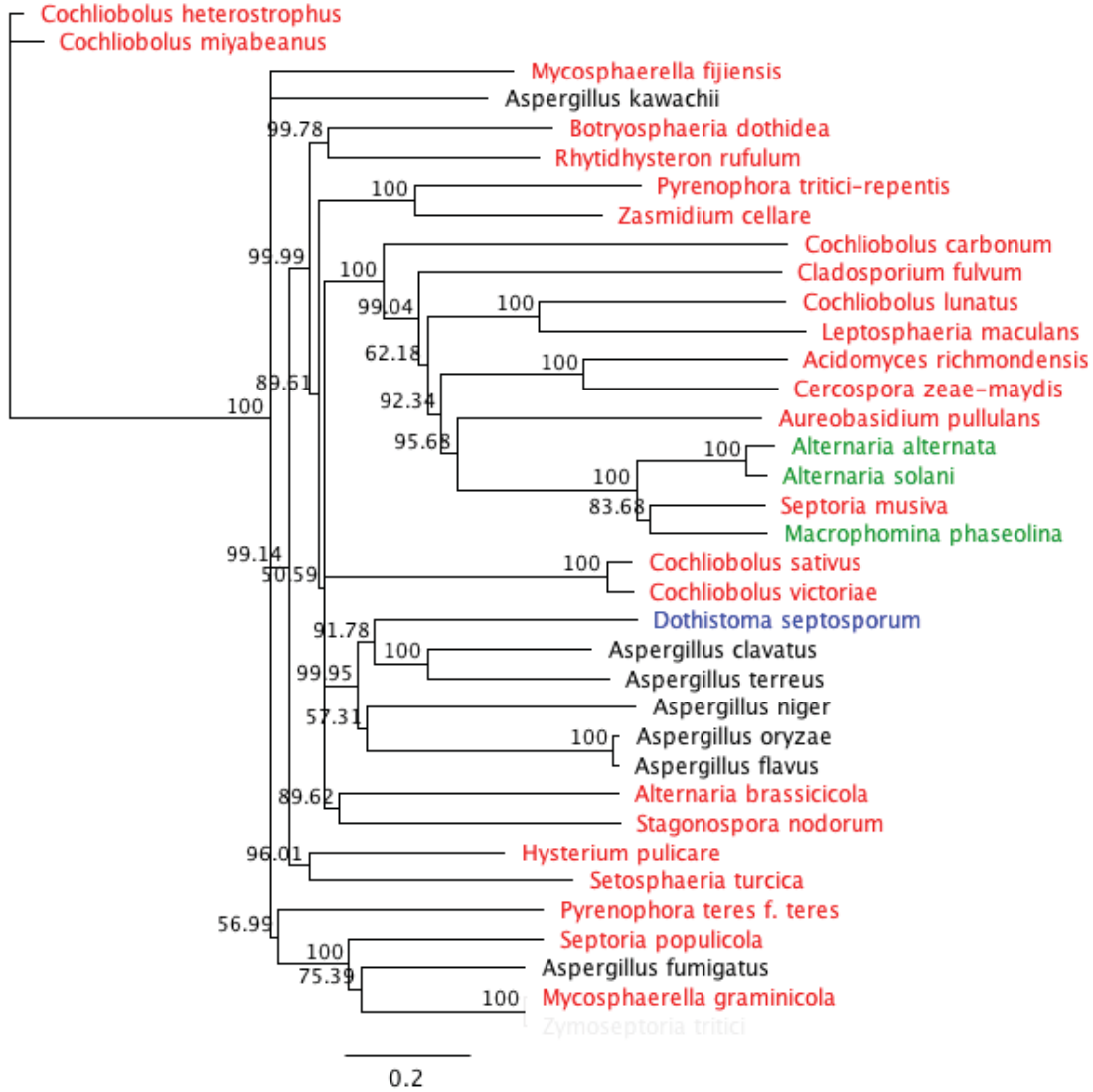

Figure A14a. Phylogenetic tree of DsPKS2 based on full protein alignments. The species indicated with red font are Dothideomycetes which have genome sequences on the Joint Genome Institute (JGI) website. The ones with green font are the Dothideomycetes which were not present on JGI, but were among the best hits as a result of BlastP searches of DsPks2 against Dothideomycetes in the NCBI database. An additional BlastP of DsPks2 against *Aspergillus spp*. was performed and the best hits were added to the alignment (black font).

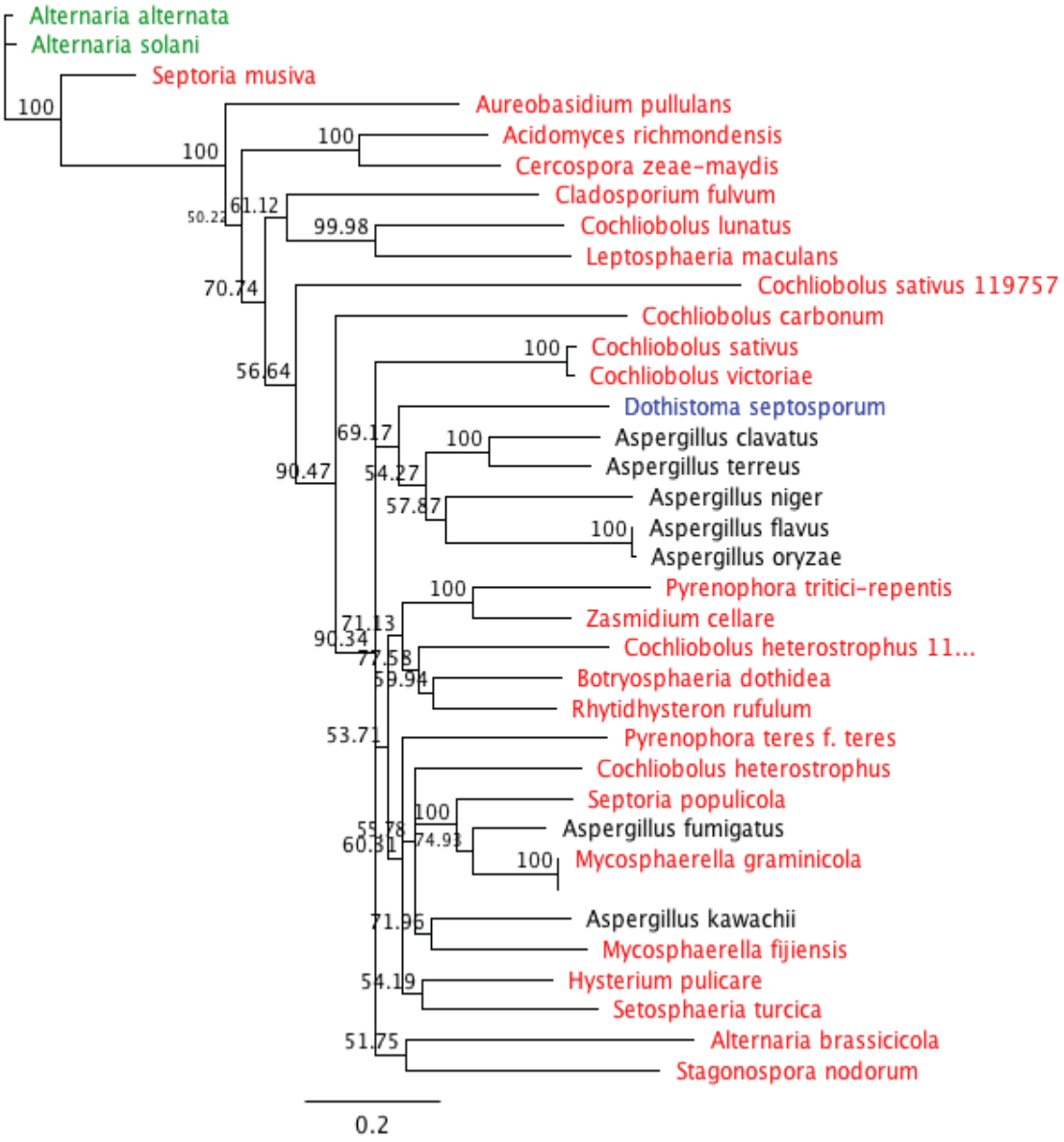

Figure A14b. Phylogenetic tree of DsPKS2 based on KS domain alignments. The species indicated with red font are Dothideomycetes which have genome sequences on the Joint Genome Institute (JGI) website. The ones with green font are the Dothideomycetes which were not present on JGI, but were among the best hits as a result of BlastP searches of DsPks2 against Dothideomycetes in the NCBI database. An additional BlastP of DsPks2 against *Aspergillus spp*. was performed and the best hits were added to the alignment (black font).

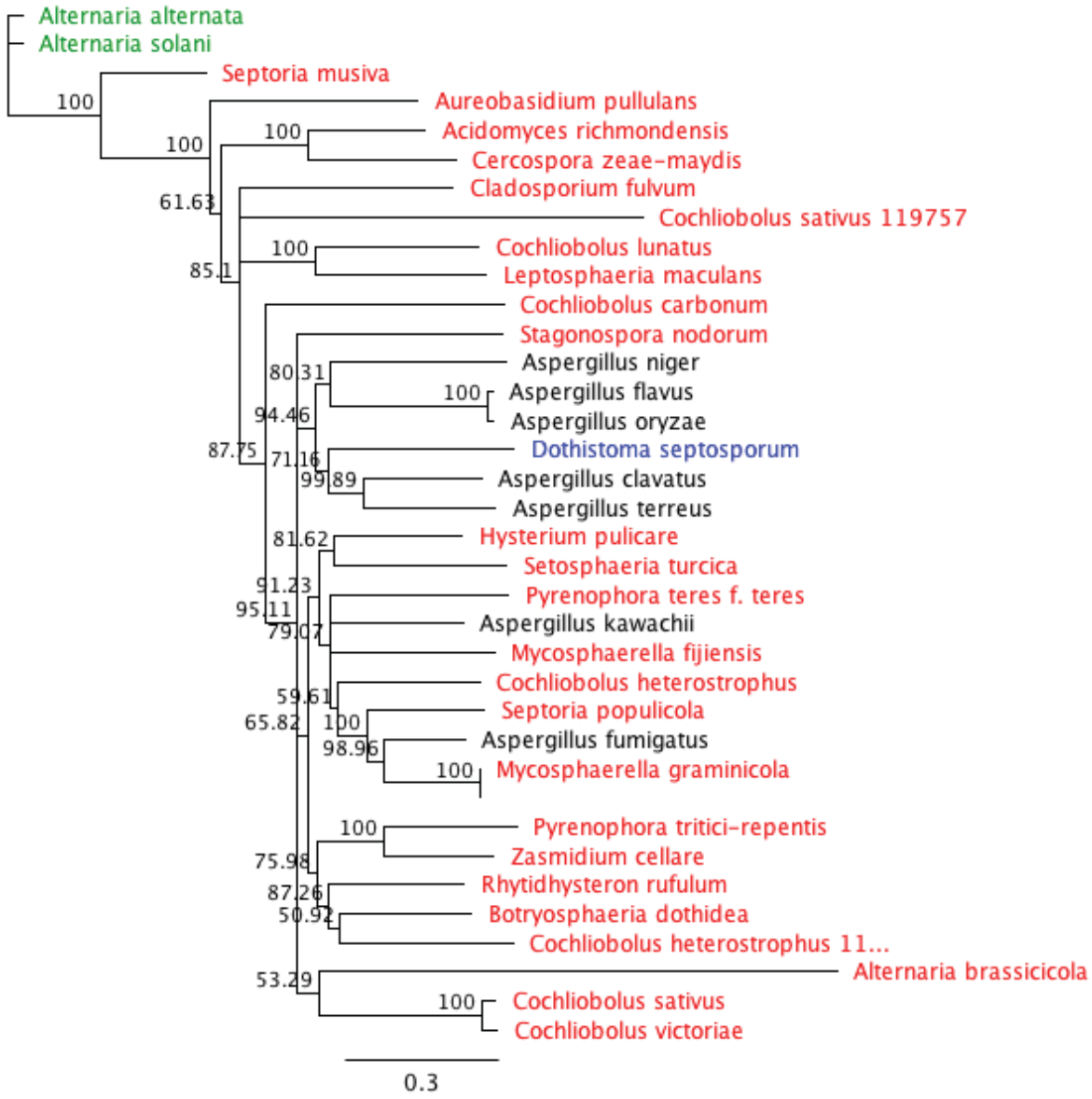

Figure A14c. Phylogenetic tree of DsPKS2 based on KS+AT domain alignments. The species indicated with red font are Dothideomycetes which have genome sequences on the Joint Genome Institute (JGI) website. The ones with green font are the Dothideomycetes which were not present on JGI, but were among the best hits as a result of BlastP searches of DsPks2 against Dothideomycetes in the NCBI database. An additional BlastP of DsPks2 against *Aspergillus spp*. was performed and the best hits were added to the alignment (black font).

Appendix 15 – Gene model confirmation of *DsPks2* (Section 3.3.2.2)

An amino acid alignment of DsPks2 with its best BlastP hits is presented in the CD (Appendix 21e). RNA-seq reads that were mapped onto the JGI gene model were used to confirm the *DsPks2* gene model (Section 3.3.2.2). All 10 introns in the *DsPks2* gene model were confirmed by RNA-seq data.

Figure A15. *DsPks2* RNA-seq reads that were mapped onto the JGI gene model. Pink rows at top are *DsPks1* RNA-seq reads at late, middle and early stages (*in planta*) and in culture (from Bradshaw et al, 2016). The numbers (eg 55.00) are RPMK values. The bold red row is predicted coding sequence (from start codon to stop codon) based on the gene model from JGI. Thin red rows indicate untranslated regions (UTRs). Green bars represent the ESTs originally used for gene annotation. PMMG and Rich media (DSM, V8, DM, PD) indicate the types of media used for growing fungal mycelia before RNA extraction. Clusters: indicate 454 EST sequences of RNA assembled with Newbler to create isotigs that were then aligned against the genomic assembly using the BLAT tool. ESTs: EST/cDNA sequences aligned against the genomic assembly using the BLAT tool. The bottom two green bars indicate the combination of the two "clusters" or "ESTs".

Appendix 16 – *DsPks2*-GATEWAY gene knockout construct (Section 3.3.2.5)

The gene knock out of *DsPks2* was done using the plasmid construct shown below. This construct was prepared as in Section 2.7.1 and used in attempts to generate *ΔDsPks2* mutants using protoplast transformation as in Section 2.9.

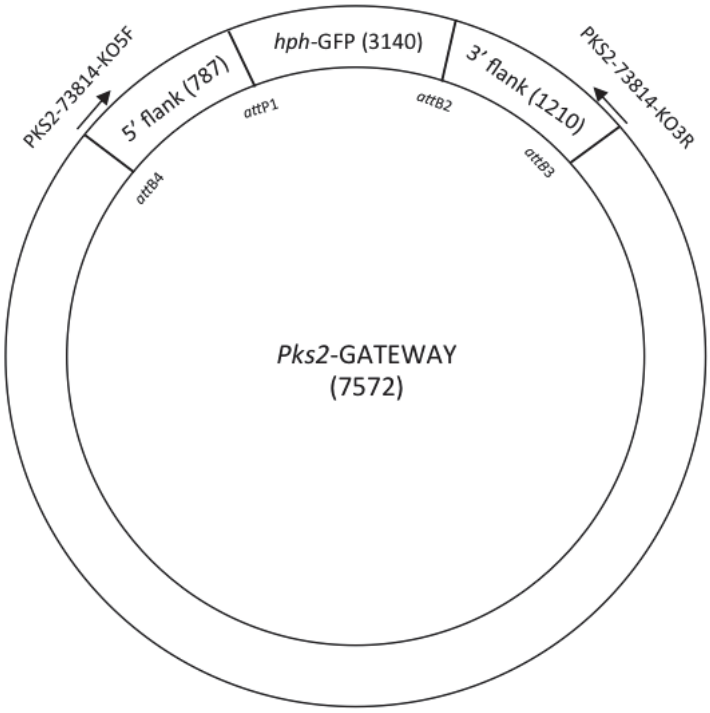

Figure A16. *DsPks2*-GATEWAY KO construct. Hph-GFP shows the GFP-tagged hygromycin resistance marker. *att* sites, required for recombination in the Gateway system, at the borders of flanking regions are shown. Sizes of the whole plasmid, flanking regions, and hph-GFP are shown in brackets in bp. Primer pairs used in PCR amplification of 5' and 3' flanking sites were PKS2-73814-KO5F/PKS2-73814-KO5R and PKS2-73814-KO3F/PKS2-73814-KO3R, respectively. Primers PKS2-73814-KO5F/PKS2-73814-KO3R were used to confirm plasmid generation. Plasmid was generated based on Multisite Gateway® Three-Fragment Vector Construction Kit manual, Version G, 8 September 2008.

Appendix 17 – *DsPks2* gene knockout attempts (Section 3.3.2.5)

A gene knockout of *DsPks2* was attempted using the KO construct prepared as in Section 2.7.1 and transformation of *D. septosporum* as in Section 2.9. However, after three steps of purification the candidates still contained wild type and *ΔDsPks2* gDNAs as shown by the PCR and Southern analyses below.

a)

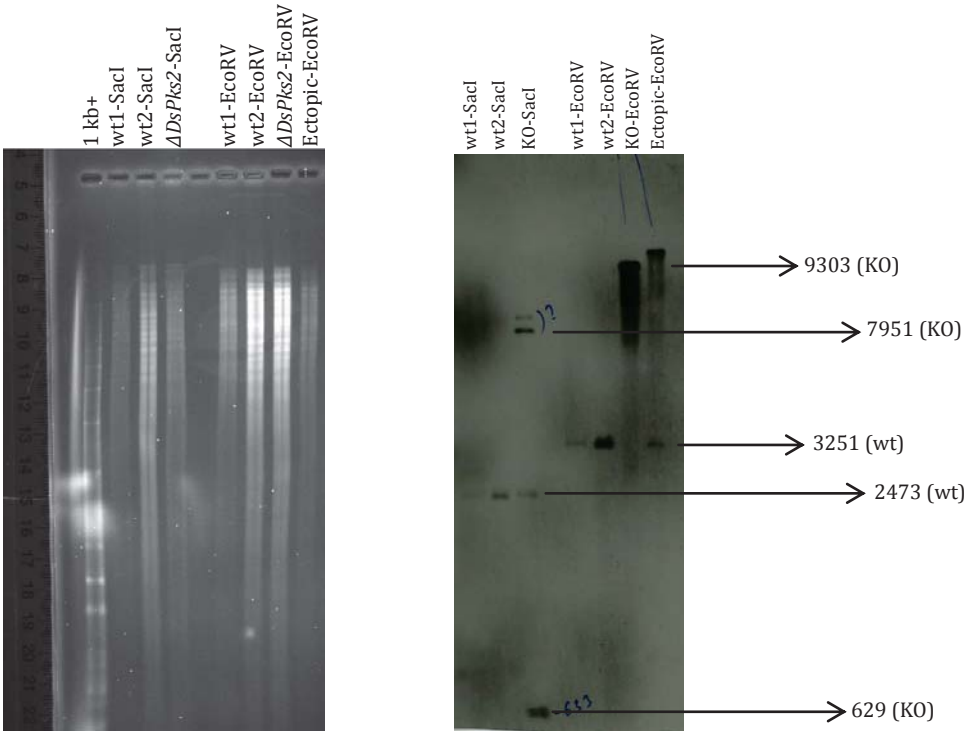

b)

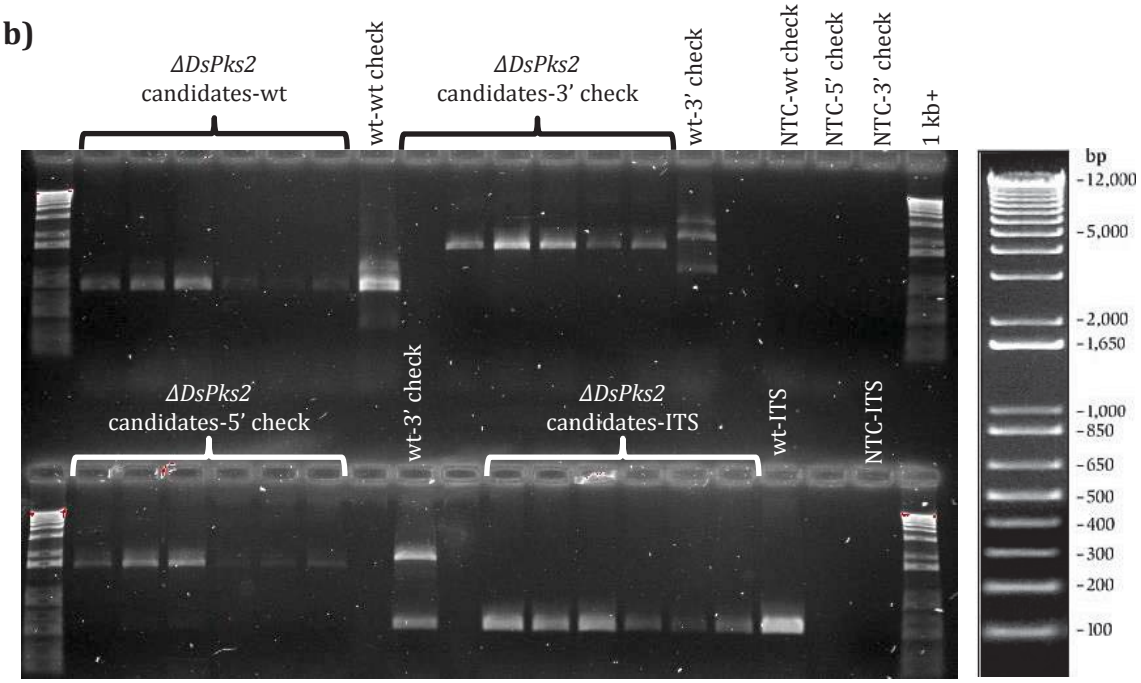

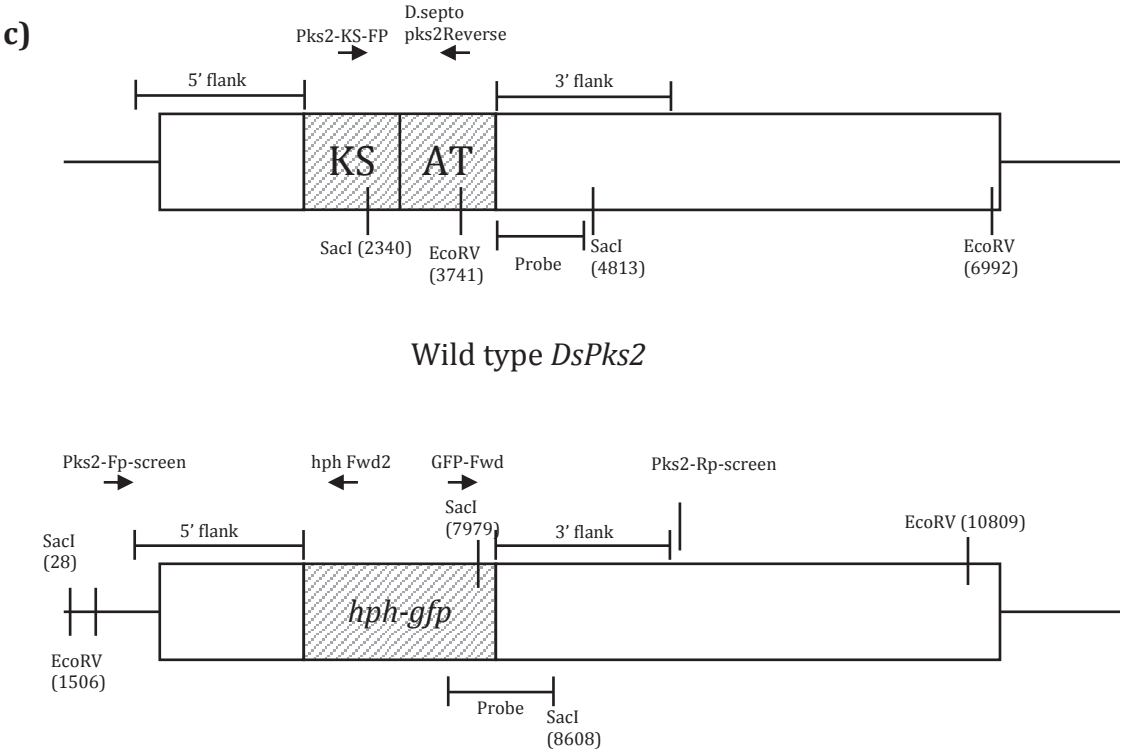

Figure A17. PCR and Southern hybridization of *ΔDsPks2* candidates.

a) Southern hybridization for wild type and the single *ΔDsPks2* candidates. SacI and EcoRV digested wild type and candidate *ΔDsPks2* gDNAs were hybridised to the probe shown in (c). Expected fragment sizes were 3251 bp for wt and 9303 bp for *ΔDsPks2* in EcoRV digested gDNAs. Expected fragment sizes for SacI digested gDNAs were 2473 bp for wt and two fragments of 629 bp and 7951 bp for *ΔDsPks2*. The results showed that the KO candidate has both wild type and *ΔDsPks2*, and an extra band in SacI digested gDNA could be because of a double integration.
b) In attempts to obtain transformants lacking the wild type copy of the gene, six colonies were sub-cultured from the *ΔDsPks2* candidate by single spore purification. DNA from these was then used for PCR analysis using primers Pks2-KS-FP and D. septo Pks2Reverse (806 bp) that amplified wild type but not *ΔDsPks2* to confirm successful purification (wt check). Integration of the knockout construct at the *DsPks2* locus was confirmed at both 5' and 3' ends of the using primer pairs Pks2-Fp-screen / hph Fwd2 (1607 bp) and GFP-Fwd / Pks2-Rp-screen (1647 bp) as shown in (c). wt: Wild type. NTC: No template control. The results showed that the KO candidates still contained both wild type and *ΔDsPks2* gDNAs. Inconsistency of the band strengths was probably due to the miniprep DNA extraction method that was used for rapid collection of DNA that might have extracted varying concentrations of templates or left trace amounts of chemicals that might affect PCR efficiency. Fungal internal transcribed spacer sequences (ITS) were amplified for all templates to confirm they were of sufficient quality and quantity for PCR amplification.
c) Schematic representation of *DsPks2* in wild type and *ΔDsPks2*. The positions of SacI and EcoRV restriction enzyme recognition sites, primer binding positions, flanking regions, knock out target region in wild type (KS and AT domains) and gfp-tagged hygromycin resistance gene (*hph-gfp*) are shown.

Appendix 18 – Gene model confirmation of *DsPks3* (Section 3.3.3.1)

An amino acid alignment of DsPks3 with its best BlastP hits is presented in the CD (Appendix 21f). RNA-seq reads that were mapped onto the JGI gene model were used in an attempt to confirm the *DsPks3* gene model (Section 3.3.3.1). According to the in culture expression of *DsPks3*, only one of the introns was correctly annotated, intron 7 reading from the right.

Figure A18a. *DsPks3* RNA-seq reads that were mapped onto the JGI gene model. Pink rows at top are *DsPks3* RNA-seq reads at late, middle and early stages (*in planta*) and in culture (from Bradshaw et al, 2016). The numbers (eg 5.50) are RPMK values. The bold red row is predicted coding sequence (from start codon to stop codon) based on the gene model from JGI. Thin red rows indicate untranslated regions (UTRs). Green bars represent the ESTs originally used for gene annotation. PMMG and Rich media (DSM, V8, DM, PD) indicate the types of media used for growing fungal mycelia before RNA extraction. Clusters: indicate 454 EST sequences of RNA assembled with Newbler to create isotigs that were then aligned against the genomic assembly using the BLAT tool. ESTs: EST/cDNA sequences aligned against the genomic assembly using the BLAT tool. The bottom two green bars indicate the combination of the two "clusters" or "ESTs". Asterisk indicates the only intron (intron 7 reading from the right) that was correctly annotated.

When the first 6 introns are removed from *DsPks3* nucleotide sequence and the resulting sequence is translated, many stop codons were found in all reading frames, suggesting that DsPks3 is pseudogenized.

a)

b)

c)

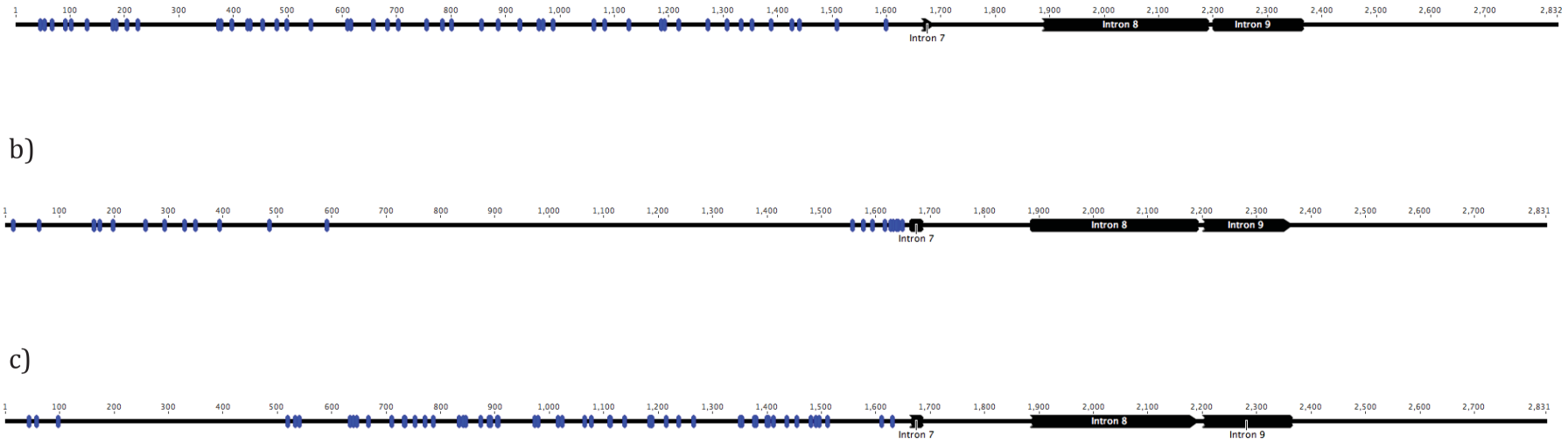

Figure A18b. Three-frame translation of *DsPks3* after removing first 6 introns. Introns 7, 8, and 9 are indicated with black arrows. Internal stop codons are annotated with bold blue lines. a) Reading frame 1, b) Reading frame 2, and c) Reading frame 3. Internal stop codons after intron 7 are not shown.

Appendix 19 – Gene model confirmation of *DsHps1* (Section 3.4.1.1)

An amino acid alignment of DsHps1 with its best BlastP hits is presented in the CD (Appendix 21g). Mapped RNA-seq were used to confirm the JGI *DsHps1* gene model (Section 3.4.1.1). Continuous RNA-seq reads on *DsHps1* coding sequence supported the gene model. An overlapping gene in the position of 3' UTR suggests that this UTR may be misannotated.

Figure A19. *DsHps1* RNA-seq reads that were mapped onto the JGI gene model. Pink rows at top are *DsHps1* RNA-seq reads at late, middle and early stages (*in planta*) and in culture (from Bradshaw et al, 2016). The numbers (eg 6.00) are RPMK values. The bold red row is predicted coding sequence (from start codon to stop codon) based on the gene model from JGI. Thin red rows indicate untranslated regions (UTRs). A neighboring open reading frame overlapping with 3' UTR of DsHps1 was also shown with a short, bold, and red row. Green bars represent the ESTs originally used for gene annotation. PMMG and Rich media (DSM, V8, DM, PD) indicate the types of media used for growing fungal mycelia before RNA extraction. Clusters: indicate 454 EST sequences of RNA assembled with Newbler to create isotigs that were then aligned against the genomic assembly using the BLAT tool. ESTs: EST/cDNA sequences aligned against the genomic assembly using the BLAT tool. The bottom two green bars indicate the combination of the two "clusters" or "ESTs".

Appendix 20 – Gene model confirmation of DsHps2 (Section 3.4.2.1)

An amino acid alignment of DsHps1 with its best BlastP hits is presented in the CD (Appendix 21h). RNA-seq reads mapped onto the JGI gene model were used to confirm the *DsHps2* gene model (Section 3.4.2.1). Combination of the reads from transcriptome analysis and ESTs used for gene annotation confirms all of the introns in the *DsHps2* gene model.

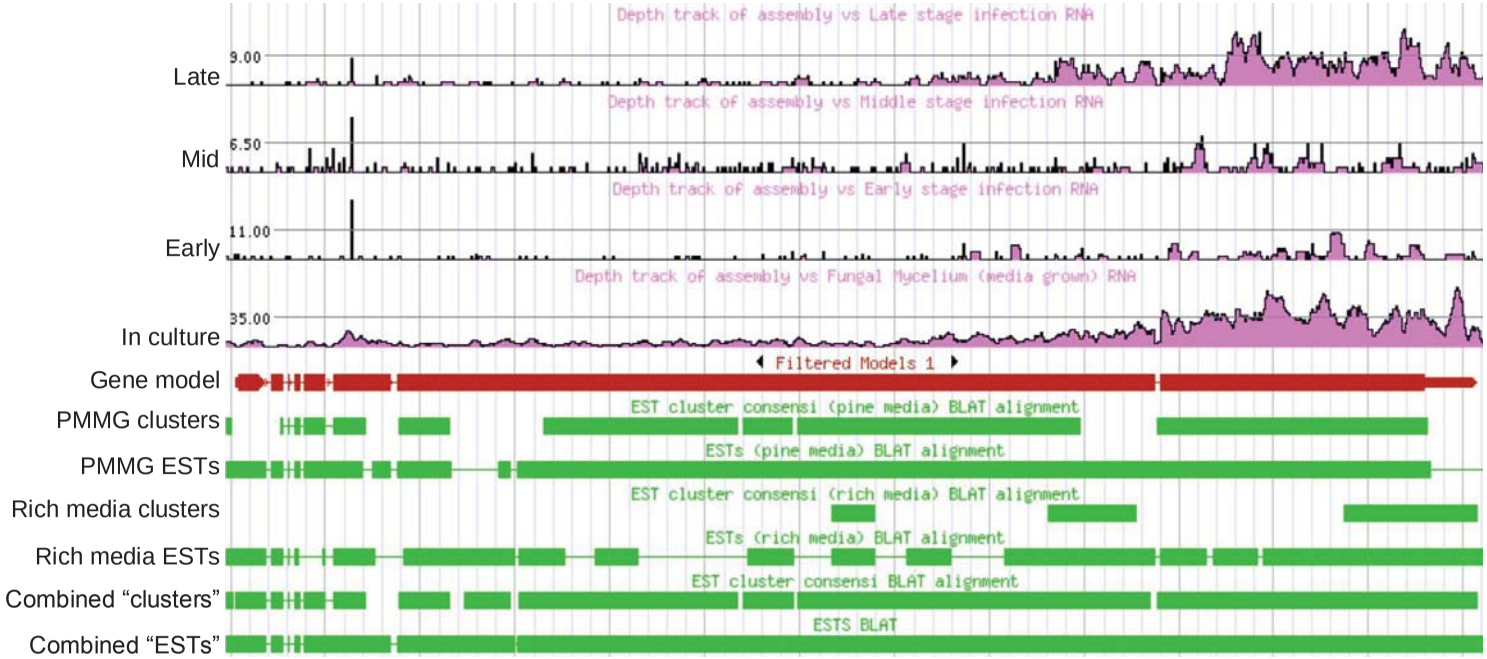

Figure A20. *DsHps2* RNA-seq reads that were mapped onto the JGI gene model. Pink rows at top are *DsHps1* RNA-seq reads at late, middle and early stages (*in planta*) and in culture (from Bradshaw et al, 2016). The numbers (eg 9.00) are RPMK values. The bold red row is predicted coding sequence (from start codon to stop codon) based on the gene model from JGI. Thin red rows indicate untranslated regions (UTRs). Green bars represent the ESTs originally used for gene annotation. PMMG and Rich media (DSM, V8, DM, PD) indicate the types of media used for growing fungal mycelia before RNA extraction. Clusters: indicate 454 EST sequences of RNA assembled with Newbler to create isotigs that were then aligned against the genomic assembly using the BLAT tool. ESTs: EST/cDNA sequences aligned against the genomic assembly using the BLAT tool. The bottom two green bars indicate the combination of the two "clusters" or "ESTs".

Appendix 23 – Whole genome sequences used in the phylogenetic analyses

All genome sequences used in the phylogenetic analyses are obtained from JGI (http://genome.jgi.doe.gov/programs/fungi/index.jsf). Abbreviations of the species and strain names used in the phylogenetic trees were same as in JGI. The list below shows the genomes used as "abbreviation: *species and strain name*, and (reference) or principal investigator of the genome sequencing project.

Aaoar1: *Aaosphaeria arxii* CBS 175.79 v1.0 – Pedro Crous: p.crous@cbs.knaw.nl
Aciaci1: *Acidothrix acidophila* CBS 136259 v1.0 (Hujslová et al., 2014)
Aciri1_iso: *Acidomyces richmondensis* BFW (Mosier et al., 2016)
Aciri1_meta: *Acidomyces richmondensis* BFW (Mosier et al., 2016)
Acral1_c3a: *Acremonium alcalophilum* v1.0 – Adrian Tsang: tsang@gene.concordia.ca
Acral2: *Acremonium alcalophilum* v2.0 – Adrian Tsang: tsang@gene.concordia.ca
Acrst1: *Acremonium strictum* DS1bioAY4a v1.0 – Colleen Hansel: chansel@whoi.edu
Altal1: *Alternaria alternata* SRC1lrK2f v1.0 (Zeiner et al., 2016)
Altbr1: *Alternaria brassicicola* – Christopher Lawrence: lawrence@vbi.vt.edu
Amnli1: *Amniculicola lignicola* CBS 123094 v1.0 – Pedro Crous: p.crous@cbs.knaw.nl
Ampqui1: *Ampelomyces quisqualis* HMLAC05119 v1.0 – Chen Liang: syliangchen@163.com
Antav1: *Anthostoma avocetta* NRRL 3190 v1.0 – Kerry O'Donnell: kerry.odonnell@ars.usda.gov
Apimo1: *Apiospora montagnei* NRRL 25634 v1.0 – Pedro Crous: p.crous@cbs.knaw.nl
Aplpr1: *Aplosporella prunicola* CBS 121.167 v1.0 – Pedro Crous: p.crous@cbs.knaw.nl
Artbe1: *Arthroderma benhamiae* CBS 112371 (Burmester et al., 2011)
Aspac1: *Aspergillus aculeatus* ATCC16872 v1.1 – Scott Baker: scott.baker@pnl.gov
Aspbr1: *Aspergillus brasiliensis* v1.0 (de Vries et al., 2017)
Aspca1: *Aspergillus carbonarius* v1.0 – Scott Baker: scott.baker@pnl.gov
Aspca3: *Aspergillus carbonarius* ITEM 5010 v3 – Scott Baker: scott.baker@pnl.gov
Aspcam1: *Aspergillus campestris* IBT 28561 v1.0 – Scott Baker: scott.baker@pnl.gov
Aspfl1: *Aspergillus flavus* NRRL3357 (Arnaud et al., 2012)
Aspfo1: *Aspergillus luchuensis* CBS 106.47 v1.0 (de Vries et al., 2017)
Aspgl1: *Aspergillus glaucus* v1.0 (de Vries et al., 2017)
Aspni5: *Aspergillus niger* ATCC 1015 v3.0 (Andersen et al., 2011)
Aspni7: *Aspergillus niger* ATCC 1015 v4.0 (Andersen et al., 2011)
Aspni_NRRL3_1: *Aspergillus niger* NRRL3 – Adrian Tsang: tsang@gene.concordia.ca
Aspni_bvT_1: *Aspergillus niger* van Tieghem ATCC 13496 v1.0 – John Gladden: jmgladden@lbl.gov
Aspnid1: *Aspergillus nidulans* (Arnaud et al., 2012; Galagan et al., 2005)
Aspnov1: *Aspergillus novofumigatus* IBT 16806 v1.0 – Scott Baker: scott.baker@pnl.gov
Aspoch1: *Aspergillus ochraceoroseus* IBT 24754 v1.0 – Scott Baker: scott.baker@pnl.gov
Aspph1: *Aspergillus phoenicis* (Corda) Thom ATCC 13157 v1.0 – John Gladden: jmgladden@lbl.gov
Aspste1: *Aspergillus steynii* IBT 23096 v1.0 – Scott Baker: scott.baker@pnl.gov
Aspsy1: *Aspergillus sydowii* CBS 593.65 v1.0 (de Vries et al., 2017)
Aspte1: *Aspergillus terreus* NIH 2624 (Arnaud et al., 2012)
Asptu1: *Aspergillus tubingensis* v1.0 (de Vries et al., 2017)
Aspve1: *Aspergillus versicolor* v1.0 (de Vries et al., 2017)
Aspwe1: *Aspergillus wentii* v1.0 (de Vries et al., 2017)
Aspzo1: *Aspergillus zonatus* v1.0 (de Vries et al., 2017)
Aulhe2: *Aulographum hederae* v2.0 – Pedro Crous: p.crous@cbs.knaw.nl
Aurpu_var_mel1: *Aureobasidium pullulans var. melanogenum* CBS 110374 (Correct taxonomic name: *Aureobasidium melanogenum*) (Gostinčar et al., 2014)
Aurpu_var_nam1: *Aureobasidium pullulans var. namibiae* CBS 147.97 (Correct taxonomic name: *Aureobasidium namibiae*) (Gostinčar et al., 2014)
Aurpu_var_pul1: *Aureobasidium pullulans var. pullulans* EXF-150 (Correct taxonomic name: *Aureobasidium pullulans*) (Gostinčar et al., 2014)
Aurpu_var_sub1: *Aureobasidium pullulans var. subglaciale* EXF-2481 (Correct taxonomic name: *Aureobasidium subglaciale*) (Gostinčar et al., 2014)
Bauco1: *Baudoinia compniacensis* UAMH 10762 (4089826) v1.0 (Ohm et al., 2012)

Beaba1: *Beauveria bassiana* ARSEF 2860 (Xiao et al., 2012)
Bimnz1: *Bimuria novae-zelandiae* CBS 107.79 v1.0 – Pedro Crous: p.crous@cbs.knaw.nl
Botdo1: *Botryosphaeria dothidea* – Pedro Crous: p.crous@cbs.knaw.nl
Bysci1: *Byssothecium circinans* CBS 675.92 v1.0 – Pedro Crous: p.crous@cbs.knaw.nl
Cenge1: *Cenococcum geophilum* 1.58 v1.0 – Francis Martin: fmartin@nancy.inra.fr
Cenge3: *Cenococcum geophilum* 1.58 v2.0 – Francis Martin: fmartin@nancy.inra.fr
Cerzm1: *Cercospora zeae-maydis* v1.0 – Stephen Goodwin: sgoodwin@purdue.edu
Chagl_1: *Chaetomium globosum* v1.0 – Broad Institute: genomics@broadinstitute.org
Clael1: *Clathrospora elynae* CBS 161.51 v1.0 – Pedro Crous: p.crous@cbs.knaw.nl
Clafu1: *Cladosporium fulvum* v1.0 (de Wit et al. 2012; Ohm et al. 2012)
Cloaq1: *Clohesyomyces aquaticus* v1.0 – Jon Karl Magnuson: Jon.Magnuson@pnnl.gov
Cloro1: *Clonostachys rosea* CBS125111 v1.0 – Kathryn Bushley: kbushley@umn.edu
Cocca1: *Cochliobolus carbonum* 26-R-13 v1.0 (Condon et al., 2013)
CocheC4_1: *Cochliobolus heterostrophus* C4 v1.0 (Ohm et al. 2012; Condon et al. 2013)
CocheC5_1: *Cochliobolus heterostrophus* C5 (Ohm et al., 2012; Condon et al., 2013)
CocheC5_3: *Cochliobolus heterostrophus* C5 v2.0 (Ohm et al., 2012; Condon et al., 2013)
Coclu1: *Cochliobolus lunatus* m118 v1.0 – B. Gillian Turgeon: bgt1@cornell.edu
Coclu2: *Cochliobolus lunatus* m118 v2.0 – B. Gillian Turgeon: bgt1@cornell.edu
Cocmi1: *Cochliobolus miyabeanus* ATCC 44560 v1.0 (Condon et al., 2013)
Cocsa1: *Cochliobolus sativus* ND90Pr v1.0 (Ohm et al. 2012; Condon et al. 2013)
Cocvi1: *Cochliobolus victoriae* FI3 v1.0 (Condon et al., 2013)
Colca1: *Colletotrichum caudatum* CBS131602 v1.0 – Jo Anne Crouch: joanne.crouch@ars.usda.gov
Coler1: *Colletotrichum eremochloae* CBS129661 v1.0 – Jo Anne Crouch: joanne.crouch@ars.usda.gov
Colfa1: *Colletotrichum falcatum* MAFF306170 v1.0 – Jo Anne Crouch: joanne.crouch@ars.usda.gov
Colgo1: *Colletotrichum godetiae* CBS 193.32 v1.0 – Michael Thon: mike@michaelrthon.com
Collu1: *Colletotrichum lupini* CBS 109225 v1.0 – – Michael Thon: mike@michaelrthon.com
Colso1: *Colletotrichum somersetensis* CBS 131599 v1.0 – Jo Anne Crouch: joanne.crouch@ars.usda.gov
Colsu1: *Colletotrichum sublineola* CBS 131301 v1.0 – Jo Anne Crouch: joanne.crouch@ars.usda.gov
Colzo1: *Colletotrichum zoysiae* MAFF235873 v1.0 – Jo Anne Crouch: joanne.crouch@ars.usda.gov
ConPMI546: *Coniochaeta sp.* PMI_546 v1.0 – Gregory Bonito: bonito@msu.edu
Conli1: *Coniochaeta ligniaria* CBS 111746 – Joseph Spatafora: spatafoj@science.oregonstate.edu
Conlig1: *Coniochaeta ligniaria* NRRL 30616 v1.0 (Jiménez et al., 2017)
Corca1: *Corynespora cassiicola* CCP v1.0 – Francis Martin: fmartin@nancy.inra.fr
Corma2: *Corollospora maritima* CBS 119819 v2.0 – Derek Johnson: johnsde4@science.oregonstate.edu
Cormi1: *Cordyceps militaris* CM01 (Zheng et al., 2011)
Crypa1: *Cryphonectria parasitica* – Donald L. Nuss: nuss@umbi.umd.edu
Crypa2: *Cryphonectria parasitica* EP155 v2.0 – Donald L. Nuss: nuss@umbi.umd.edu
Cucbe1: *Cucurbitaria berberidis* CBS 394.84 v1.0 – Pedro Crous: p.crous@cbs.knaw.nl
DalEC12_1*: Daldinia eschscholzii* EC12 v1.0 (Wu et al., 2017)
Decga1: *Decorospora gaudefroyi* v1.0 – Patrik Inderbitzin: prin@ucdavis.edu
Delco1: *Delitschia confertaspora* ATCC 74209 v1.0 – Gerald Bills: billsge@vt.edu
Didex1: *Didymella exigua* CBS 183.55 v1.0 – Joseph Spatafora: spatafoj@science.oregonstate.edu
Disac1: *Dissoconium aciculare* v1.0 – Pedro Crous: p.crous@cbs.knaw.nl
Dotse1: *Dothistroma septosporum* NZE10 v1.0 (de Wit et al. 2012; Ohm et al. 2012)
Dotsy1: *Dothidotthia symphoricarpi* v1.0 – Pedro Crous: p.crous@cbs.knaw.nl
Elsamp1: *Elsinoe ampelina* CECT 20119 v1.0 – Manuel Alfaro Sánchez: manuel.alfaro@unavarra.es
Erebi1: *Eremomyces bilateralis* CBS 781.70 v1.0 – Pedro Crous: p.crous@cbs.knaw.nl
Eurhe1: *Eurotium rubrum* v1.0 (Kis-Papo et al., 2014)
Eutla1: *Eutypa lata* UCREL1 (Blanco-Ulate et al., 2013)
Fusgr1: *Fusarium graminearum* v1.0 (Cuomo et al., 2007)
Fusox1: *Fusarium oxysporum* v1.0 (Ma et al., 2010)
Gloac1: *Glomerella acutata* (*Colletotrichum fiorinae* MH 18) v1.0 – Francis Martin: fmartin@nancy.inra.fr
Gloci1: *Glomerella cingulata* 23 (*Colletotrichum gloeosporoides* 23) v1.0 – Francis Martin: fmartin@nancy.inra.fr
Glost2: *Glonium stellatum* CBS 207.34 v1.0 (Peter et al., 2016)

Gymau1: *Gymnascella aurantiaca* v1.0 – Kerry O'Donnell: kerry.odonnell@ars.usda.gov
Gymci1_1: *Gymnascella citrina* v1.1 – Kerry O'Donnell: kerry.odonnell@ars.usda.gov
Horac1: *Hortaea acidophila* CBS 113389 v1.0: Jon Karl Magnuson: Jon.Magnuson@pnnl.gov
HypCI4A_1: *Hypoxylon sp.* CI-4A v1.0 (Wu et al., 2017)
HypCO275_1: *Hypoxylon sp.* CO27-5 v1.0 (Wu et al., 2017)
HypEC38_1: *Hypoxylon sp.* EC38 v1.0 – Blake Simmons: basimmo@sandia.gov
Hyspu1: *Hysterium pulicare* (Ohm et al., 2012)
Ilysp1: *Ilyonectria sp.* v1.0 – Francis Martin: fmartin@nancy.inra.fr
Karrh1: *Karstenula rhodostoma* CBS 690.94 v1.0 – Pedro Crous: p.crous@cbs.knaw.nl
Khuory1: *Khuskia oryzae* ATCC 28132 v1.0 – Jon Karl Magnuson: jon.magnuson@pnnl.gov
Lenfl1: *Lentithecium fluviatile* v1.0 – Pedro Crous: p.crous@cbs.knaw.nl
Lepmu1: *Leptosphaeria maculans* (Rouxel et al., 2011)
Leppa1: *Lepidopterella palustris* v1.0 (Peter et al., 2016)
Linin1: *Lindgomyces ingoldianus* ATCC 200398 v1.0 – Jon Karl Magnuson: Jon.Magnuson@pnnl.gov
Linrh1: *Lineolata rhizophorae* ATCC 16933 v1.0 – Jon Karl Magnuson: Jon.Magnuson@pnnl.gov
Linth1: *Lindra thalassiae* JK4322 v1.0 – Derek Johnson: johnsde4@science.oregonstate.edu
Lizem1: *Lizonia empirigonia* CBS 542.76 v1.0 – Pedro Crous: p.crous@cbs.knaw.nl
Lolmi1: *Lollipopaia minuta* P26; CBS 116597 v1.0 – Patrik Inderbitzin: prin@ucdavis.edu
Lopma1: *Lophiostoma macrostomum* v1.0 – Pedro Crous: p.crous@cbs.knaw.nl
Lopmy1: *Lophium mytilinum* CBS 269.34 v1.0 – Pedro Crous: p.crous@cbs.knaw.nl
Macan1: *Macroventuria anomochaeta* CBS 525.71 v1.0 – Pedro Crous: p.crous@cbs.knaw.nl
Maggr1: *Magnaporthe grisea* v1.0 (Dean et al., 2005)
Maseb1: *Massarina eburnea* CBS 473.64 v1.0 – Pedro Crous: p.crous@cbs.knaw.nl
Melpu1: *Melanomma pulvis-pyrius* v1.0 – Pedro Crous: p.crous@cbs.knaw.nl
Melsp1: *Melanconium sp.* NRRL 54901 v1.0 – Joseph Spatafora: spatafoj@science.oregonstate.edu
Melti1: *Melanospora tiffanyae* F1KG0001 v1.0 – Derek Johnson: johnsde4@science.oregonstate.edu
Micbo1: *Microdochium bolleyi* J235TASD1 v1.0 (David et al., 2016)
Micmi1: *Microthyrium microscopicum* CBS 115976 v1.0 – Pedro Crous: p.crous@cbs.knaw.nl
Mictr1: *Microascus trigonosporus* CBS 218.31 v1.0 – Kathryn Bushley: kbushley@umn.edu
Monpu1: *Monascus purpureus* v1.0 – Kerry O'Donnell: kerry.odonnell@ars.usda.gov
Monru1: *Monascus ruber* NRRL 1597 v1.0 – Joseph Spatafora: spatafoj@science.oregonstate.edu
Mycfi1: *Mycosphaerella fijiensis* v1.0 (Correct taxonomic name: *Pseudocercospora fijiensis*) – Gert Kema: gert.kema@wur.nl
Mycfi2: *Pseudocercospora* (*Mycosphaerella*) *fijiensis* v2.0 (Correct taxonomic name: *Pseudocercospora fijiensis*) – Gert Kema: gert.kema@wur.nl
Mycgr3: *Mycosphaerella graminicola* v2.0 (Correct taxonomic name: *Zymoseptoria tritici*) (Goodwin et al., 2011)
Myche1: *Myceliophthora heterothallica* CBS 203.75 v1.0 – Don Natvig: dnatvig@gmail.com
Myrdu1: *Myriangium duriaei* CBS 260.36 v1.0 – Pedro Crous: p.crous@cbs.knaw.nl
Myrin1: *Myrothecium inundatum* CBS 120646 v1.0 – Kathryn Bushley: kbushley@umn.edu
Mytre1: *Mytilinidion resinicola* CBS 304.34 v1.0 – Jon Karl Magnuson: Jon.Magnuson@pnnl.gov
Necha2: *Nectria haematococca* v2.0 (Coleman et al., 2009)
Neucr1: *Neurospora crassa* OR74A v1.0 (Galagan et al., 2003)
Neucr2: *Neurospora crassa* OR74A v2.0 (Galagan et al., 2003)
Neucr_trp3_1: *Neurospora crassa* FGSC 73 trp-3 v1.0 (Baker et al., 2015)
Neudi1: *Neurospora discreta* FGSC 8579 mat A – John Taylor: jtaylor@nature.berkeley.edu
Neute1: *Neurospora tetrasperma* FGSC 2508 mat A – John Taylor: jtaylor@nature.berkeley.edu
Neute_matA2: *Neurospora tetrasperma* FGSC 2508 mat A v2.0 (Ellison et al., 2011)
Neute_mat_a1: *Neurospora tetrasperma* FGSC 2509 mat a v1.0 (Ellison et al., 2011)
Nieex1: *Niesslia exilis* CBS 358.70 v1.0 – Kathryn Bushley: kbushley@umn.edu
Ophdi1: *Ophiobolus disseminans* CBS 113818 v1.0 – Pedro Crous: p.crous@cbs.knaw.nl
Ophpc1: *Ophiostoma piceae* UAMH 11346 (Haridas et al., 2013)
Parsp1: *Paraconiothyrium sporulosum* AP3s5-JAC2a v1.0 (Zeiner et al., 2016)
Patat1: *Patellaria atrata* v1.0 – Pedro Crous: p.crous@cbs.knaw.nl
Penac1: *Talaromyces aculeatus* ATCC 10409 v1.0 – Keith Seifert: keith.seifert@agr.gc.ca
Penbi1: *Penicillium bilaiae* ATCC 20851 v1.0 – Dave Greenshields: dvgs@novozymes.com
Penbr2: *Penicillium brevicompactum* 1011305 v2.0 – Dave Greenshields: dvgs@novozymes.com
PenbrAgRF18_1: *Penicillium brevicompactum* AgRF18 v1.0 – Dave Greenshields: dvgs@novozymes.com

Penca1: *Penicillium canescens* ATCC 10419 v1.0 – Dave Greenshields: dvgs@novozymes.com
Pench1: *Penicillium chrysogenum* v1.0 – Igor Grigoriev: IVGrigoriev@lbl.gov
Penex1: *Penicillium expansum* ATCC 24692 v1.0 – Dave Greenshields: dvgs@novozymes.com
Penfe1: *Penicillium fellutanum* ATCC 48694 v1.0 – Dave Greenshields: dvgs@novozymes.com
Pengl1: *Penicillium glabrum* DAOM 239074 v1.0 – Dave Greenshields: dvgs@novozymes.com
Penja1: *Penicillium janthinellum* ATCC 10455 v1.0 – Dave Greenshields: dvgs@novozymes.com
Penla1: *Penicillium lanosocoeruleum* ATCC 48919 v1.0 – Dave Greenshields: dvgs@novozymes.com
Penra1: *Penicillium raistrickii* ATCC 10490 v1.0 – Dave Greenshields: dvgs@novozymes.com
Perma1: *Periconia macrospinosa* DSE2036 v1.0 – Gabor M. Kovacs: gmkovacs@elte.hu
PhaPMI808: *Phaeosphaeriaceae* sp. PMI_808 v1.0 – Gregory Bonito: bonito@msu.edu
Photr1: *Phoma tracheiphila* IPT5 v1.0 – David Ezra: Dezra@volcani.agri.gov.il
Phycit1: *Phyllosticta citriasiana* v1.0 – Pedro Crous: p.crous@cbs.knaw.nl
Pieho1_1: *Piedraia hortae* v1.1 – Pedro Crous: p.crous@cbs.knaw.nl
Plecu1: *Plectosphaerella cucumerina* DS2psM2a2 v1.0 – Colleen Hansel: chansel@whoi.edu
Plesi1: *Pleomassaria siparia* v1.0 – Pedro Crous: p.crous@cbs.knaw.nl
Podcur1: *Podospora curvicolla* TEP21a v1.0 – Kabir Peay: kpeay@stanford.edu
Polci1: *Polychaeton citri* v1.0 – Pedro Crous: p.crous@cbs.knaw.nl
Polfu1: *Polyplosphaeria fusca* CBS 125425 v1.0 – Pedro Crous: p.crous@cbs.knaw.nl
Psehy1: *Pseudovirgaria hyperparasitica* CBS 121739 v1.0 – Pedro Crous: p.crous@cbs.knaw.nl
Pseve2: *Pseudomassariella vexata* CBS 129021 v1.0 – Jon Karl Magnuson: Jon.Magnuson@pnnl.gov
Pyrsp1: *Pyrenochaeta sp*. DS3sAY3a v1.0 (Zeiner et al., 2016)
Pyrtr1: *Pyrenophora tritici-repentis* (Manning et al., 2013)
Pyrtt1: *Pyrenophora teres f. teres* (Ellwood et al., 2010)
Rhili1: *Rhizodiscina lignyota* CBS 133067 v1.0 – Pedro Crous: p.crous@cbs.knaw.nl
Rhyru1: *Rhytidhysteron rufulum* (Ohm et al., 2012)
Sacpr1: *Saccharata proteae* CBS 121410 v1.0 – Pedro Crous: p.crous@cbs.knaw.nl
Sepmu1: *Septoria musiva* SO2202 v1.0 (Ohm et al. 2012; Dhillon et al. 2015)
Setho1: *Setomelanomma holmii* CBS 110217 v1.0 – Pedro Crous: p.crous@cbs.knaw.nl
Settu1: *Setosphaeria turcica* Et28A v1.0 (Ohm et al., 2012; Condon et al., 2013)
Settur1: *Setosphaeria turcica* NY001 v1.0 – B. Gillian Turgeon: bgt1@cornell.edu
Sodal1: *Sodiomyces alkalinus* v1.0 – Alexey Grum Grzhimaylo: alexey.grumgrzhimaylo@wur.nl
Spofi1: *Sporormia fimetaria* v1.0 – Pedro Crous: p.crous@cbs.knaw.nl
Spoth1: *Sporotrichum thermophile* v1.0 – Adrian Tsang: tsang@gene.concordia.ca
Spoth2: *Myceliophthora thermophila* (*Sporotrichum thermophile*) v2.0 (Berka et al., 2011)
Stano1: *Stagonospora nodorum* SN15 (Correct taxonomic name: *Parastagonospora nodorum* (Hane et al., 2007)
Stasp1: *Stagonospora sp.* SRC1lsM3a v1.0 (Zeiner et al., 2016)
Ternu1: *Teratosphaeria nubilosa* CBS 116005 v1.0 – Pedro Crous: p.crous@cbs.knaw.nl
Theau1: *Thermoascus aurantiacus* v1.0 – Steven Singer: SWSinger@lbl.gov
Thian1: *Thielavia antarctica* CBS 123565 v1.0 – Adrian Tsang: tsang@gene.concordia.ca
Thiap1: *Thielavia appendiculata* CBS 731.68 v1.0 – Adrian Tsang: tsang@gene.concordia.ca
Thiar1: *Thielavia arenaria* CBS 508.74 v1.0 – Adrian Tsang: tsang@gene.concordia.ca
Thihy1: *Thielavia hyrcaniae* CBS 757.83 v1.0 – Adrian Tsang: tsang@gene.concordia.ca
Thite1: *Thielavia terrestris* v1.0 (Berka et al., 2011)
Thite2: *Thielavia terrestris* v2.0 (Berka et al., 2011)
ThoPMI491_1: *Thozetella sp.* PMI_491 v2.0 – Gregory Bonito: bonito@msu.edu
Torra1: *Torpedospora radiata* JK5252C v1.0 – Derek Johnson: johnsde4@science.oregonstate.edu
Totfu1: *Tothia fuscella* CBS 130266 v1.0 – Pedro Crous: p.crous@cbs.knaw.nl
Trepe1: *Trematosphaeria pertusa* CBS 122368 v1.0 – Pedro Crous: p.crous@cbs.knaw.nl
Trias1: *Trichoderma asperellum* CBS 433.97 v1.0 – Igor Grigoriev: IVGrigoriev@lbl.gov
Triasp1: *Trichoderma asperellum* TR356 v1.0 – Igor Grigoriev: IVGrigoriev@lbl.gov
Triat2: *Trichoderma atroviride* v2.0 –Scott Baker: scott.baker@pnl.gov
Tribi1: *Trichodelitschia bisporula* CBS 262.69 v1.0 – Pedro Crous: p.crous@cbs.knaw.nl
Trici1: *Trichoderma citrinoviride* v1.0 – Christian Kubicek: ckubicek@mail.zserv.tuwien.ac.at
Trici4: *Trichoderma citrinoviride* TUCIM 6016 v4.0 – Igor Grigoriev: IVGrigoriev@lbl.gov
Triha1: *Trichoderma harzianum* CBS 226.95 v1.0 – Igor Grigoriev: IVGrigoriev@lbl.gov
Trilo1: *Trichoderma longibrachiatum* ATCC 18648 v1.0 – Christian Kubicek: ckubicek@mail.zserv.tuwien.ac.at
Trilo3: *Trichoderma longibrachiatum* ATCC 18648 v3.0 – Igor Grigoriev: IVGrigoriev@lbl.gov

Trire2: *Trichoderma reesei* v2.0 (Martinez et al., 2008)
TrireRUTC30_1: *Trichoderma reesei* RUT C-30 v1.0 (Koike et al., 2013)
TriviGv29_8_2: *Trichoderma virens* Gv29-8 v2.0 – Charles M. Kenerley: c-kenerley@tamu.edu
Tryvi1: *Trypethelium eluteriae* v1.0 – Stephen Goodwin: sgoodwin@purdue.edu
Valla1: *Valetoniellopsis laxa* CBS 191.97 v1.0 – Kathryn Bushley: kbushley@umn.edu
Verda1: *Verticillium dahliae* v1.0 (Klosterman et al., 2011)
Veren1: *Verruculina enalia* CBS 304.66 v1.0 – Pedro Crous: p.crous@cbs.knaw.nl
Wesor1: *Westerdykella ornata* CBS 379.55 v1.0 – Pedro Crous: p.crous@cbs.knaw.nl
Zasce1: *Zasmidium cellare* ATCC 36951 v1.0 – Stephen Goodwin: sgoodwin@purdue.edu
Zoprh1: *Zopfia rhizophila* v1.0 – Pedro Crous: p.crous@cbs.knaw.nl

References of the whole genome sequences

Andersen, M.R., M.P. Salazar, P.J. Schaap, P.J. van de Vondervoort, D. Culley et al. (2011). Comparative genomics of citric-acid-producing *Aspergillus niger* ATCC 1015 versus enzyme-producing CBS 513.88. *Genome Research 21*, 885-897.

Arnaud, M.B., G.C. Cerqueira, D.O. Inglis, M.S. Skrzypek, J. Binkley et al. (2012). The *Aspergillus* Genome Database (AspGD): recent developments in comprehensive multispecies curation, comparative genomics and community resources. *Nucleic Acids Research, 40* (Database issue), D653-659.

Baker, S. E., Schackwitz, W., Lipzen, A., Martin, J., Haridas, S., LaButti, K. et al. (2015). Draft genome sequence of *Neurospora crassa* strain FGSC 73. *Genome Announcements*, *3*, e00074-15.

Berka, R. M., Grigoriev, I. V, Otillar, R., Salamov, A., Grimwood, J., Reid, I. et al. (2011). Comparative genomic analysis of the thermophilic biomass-degrading fungi *Myceliophthora thermophila* and *Thielavia terrestris*. *Nature Biotechnology*, *29*, 922–927.

Blanco-Ulate, B., Rolshausen, P. E., Cantu, D. (2013). Draft genome sequence of the grapevine dieback fungus *Eutypa lata* UCR-EL1. *Genome Announcements*, *1*, e00228-13.

Burmester, A., Shelest, E., Glöckner, G., Heddergott, C., Schindler, S., Staib, P. et al. (2011). Comparative and functional genomics provide insights into the pathogenicity of dermatophytic fungi. *Genome Biology*, *12*, R7.

Coleman, J. J., Rounsley, S. D., Rodriguez-Carres, M., Kuo, A., Wasmann, C. C., Grimwood, J. et al. (2009). The genome of *Nectria haematococca*: contribution of supernumerary chromosomes to gene expansion. *PloS Genetics*, *5*, e1000618.

Condon, B.J., Y. Leng, D. Wu, K.E. Bushley, R.A. Ohm et al. (2013). Comparative genome structure, secondary metabolite, and effector coding capacity across *Cochliobolus* pathogens. *PloS Genetics, 9*, e1003233.

Cuomo, C. A., Guldener, U., Xu, J.-R., Trail, F., Turgeon, B. G., Di Pietro, A. et al. (2007). *The Fusarium graminearum* genome reveals a link between localized polymorphism and pathogen specialization. *Science*, *317*, 1400–1402.

David, A. S., Haridas, S., LaButti, K., Lim, J., Lipzen, A., Wang, M. et al. (2016). Draft genome sequence of *Microdochium bolleyi* , a dark septate fungal endophyte of beach grass. *Genome Announcements*, *4*, e00270-16.

de Vries, R. P., Riley, R., Wiebenga, A., Aguilar-Osorio, G., Amillis, S., Uchima, C. A. et al. (2017). Comparative genomics reveals high biological diversity and specific adaptations in the industrially and medically important fungal genus *Aspergillus*. *Genome Biology*, *18*, 28.

de Wit, P.J.G.M., A. van der Burgt, B. Okmen, I. Stergiopoulos, K.A. Abd-Elsalam et al. (2012). The genomes of the fungal plant pathogens *Cladosporium fulvum* and

Dothistroma septosporum reveal adaptation to different hosts and lifestyles but also signatures of common ancestry. *PloS Genetics*, *8*, e1003088.

Dean, R.A., N.J. Talbot, D.J. Ebbole, M.L. Farman, T.K. Mitchell et al. (2005). The genome sequence of the rice blast fungus *Magnaporthe grisea*. *Nature*, *434*, 980-986.

Dhillon, B., N. Feau, A.L. Aerts, S. Beauseigle, L. Bernier et al. (2015). Horizontal gene transfer and gene dosage drives adaptation to wood colonization in a tree pathogen. *Proceedings of the National Academy of Sciences of the United States of America*, *112*, 3451-3456.

Ellison, C. E., Stajich, J. E., Jacobson, D. J., Natvig, D. O., Lapidus, A., Foster, B. et al. (2011). Massive changes in genome architecture accompany the transition to self-fertility in the filamentous fungus *Neurospora tetrasperma*. *Genetics*, *189*, 55–69.

Galagan, J. E., Calvo, S. E., Borkovich, K. A., Selker, E. U., Read, N. D., Jaffe, D. et al. (2003). The genome sequence of the filamentous fungus *Neurospora crassa*. *Nature*, *422*, 859–868.

Galagan, J. E., Calvo, S. E., Cuomo, C., Ma, L.-J., Wortman, J. R., Batzoglou, S. et al. (2005). Sequencing of *Aspergillus nidulans* and comparative analysis with *A. fumigatus* and *A. oryzae*. *Nature*, *438*, 1105–1115.

Goodwin, S. B., Ben M'Barek, S., Dhillon, B., Wittenberg, A. H. J., Crane, C. F., Hane, J. K. et al. (2011). Finished genome of the fungal wheat pathogen *Mycosphaerella graminicola* reveals dispensome structure, chromosome plasticity, and stealth pathogenesis. *PloS Genetics*, *7*, e1002070.

Gostinčar, C., Ohm, R. A., Kogej, T., Sonjak, S., Turk, M., Zajc, J. et al. (2014). Genome sequencing of four *Aureobasidium pullulans* varieties: biotechnological potential, stress tolerance, and description of new species. *BMC Genomics*, *15*, 549.

Hane, J.K., R.G. Lowe, P.S. Solomon, K.C. Tan, C.L. Schoch et al. (2007). Dothideomycete plant interactions illuminated by genome sequencing and EST analysis of the wheat pathogen *Stagonospora nodorum*. *Plant Cell*, *19*, 3347-3368.

Haridas, S., Wang, Y., Lim, L., Massoumi Alamouti, S., Jackman, S., Docking, R. et al. (2013). The genome and transcriptome of the pine saprophyte *Ophiostoma piceae*, and a comparison with the bark beetle-associated pine pathogen *Grosmannia clavigera*. *BMC Genomics*, *14*, 373.

Hujslová, M., Kubátová, A., Kostovčík, M., Blanchette, R. A., Wilhelm De Beer, Z., Chudíčková, M., Kolařík, M. (2014). Three new genera of fungi from extremely acidic soils. *Mycological progress*, 13, 819-831.

Jiménez, D. J., Hector, R. E., Riley, R., Lipzen, A., Kuo, R. C., Amirebrahimi, M. et al. (2017). Draft genome sequence of *Coniochaeta ligniaria* NRRL 30616, a lignocellulolytic fungus for bioabatement of inhibitors in plant biomass hydrolysates. *Genome Announcements*, *5*, e01476-16.

Kis-Papo, T., Weig, A. R., Riley, R., Peršoh, D., Salamov, A., Sun, H. et al. (2014). Genomic adaptations of the halophilic Dead Sea filamentous fungus *Eurotium rubrum*. *Nature Communications*, *5*, 3745.

Klosterman, S. J., Subbarao, K. V., Kang, S., Veronese, P., Gold, S. E., Thomma, B. P. H. J. et al. (2011). Comparative genomics yields insights into niche adaptation of plant vascular wilt pathogens. *PloS Pathogens*, *7*, e1002137.

Koike, H., Aerts, A., LaButti, K., Grigoriev, I. V., Baker, S. E. (2013). Comparative genomics analysis of *Trichoderma reesei* strains. *Industrial Biotechnology*, *9*, 352–367.

Ma, L.J., H.C. van der Does, K.A. Borkovich, J.J. Coleman, M.J. Daboussi et al. (2010). Comparative genomics reveals mobile pathogenicity chromosomes in *Fusarium*. *Nature*, *464*, 367-373.

Manning, V. A., Pandelova, I., Dhillon, B., Wilhelm, L. J., Goodwin, S. B., Berlin, A. M. et al. (2013). Comparative genomics of a plant-pathogenic fungus, *Pyrenophora tritici-repentis*, reveals transduplication and the impact of repeat elements on pathogenicity and population divergence. *G3: Genes, Genomes, Genetics*, *3*, 41-63.

Martinez, D., Berka, R. M., Henrissat, B., Saloheimo, M., Arvas, M., Baker, S. E. et al. (2008). Genome sequencing and analysis of the biomass-degrading fungus *Trichoderma reesei* (syn. *Hypocrea jecorina*). *Nature Biotechnology*, *26*, 553–560.

Mosier, A. C., Miller, C. S., Frischkorn, K. R., Ohm, R. A., Li, Z., LaButti, K. et al. (2016). Fungi contribute critical but spatially varying roles in nitrogen and carbon cycling in acid mine drainage. *Frontiers in Microbiology*, *7*, 238.

Ohm, R.A., N. Feau, B. Henrissat, C.L. Schoch, B.A. Horwitz et al. (2012). Diverse lifestyles and strategies of plant pathogenesis encoded in the genomes of eighteen Dothideomycetes fungi. *PloS Pathogens*, *8*, e1003037-e1003037.

Peter, M., A. Kohler, R.A. Ohm, A. Kuo, J. Krutzmann et al. (2016). Ectomycorrhizal ecology is imprinted in the genome of the dominant symbiotic fungus *Cenococcum geophilum*. *Nature Communications*, *7*, 12662.

Rouxel, T., Grandaubert, J., Hane, J. K., Hoede, C., van de Wouw, A. P., Couloux, A. et al. (2011). Effector diversification within compartments of the *Leptosphaeria maculans* genome affected by Repeat-Induced Point mutations. *Nature Communications*, *2*, 202.

Wu, W., Davis, R. W., Tran-Gyamfi, M. B., Kuo, A., LaButti, K., Mihaltcheva, S. et al. (2017). Characterization of four endophytic fungi as potential consolidated bioprocessing hosts for conversion of lignocellulose into advanced biofuels. *Applied Microbiology and Biotechnology*, *101*, 2603–2618.

Xiao, G., Ying, S.-H., Zheng, P., Wang, Z.-L., Zhang, S., Xie, X.-Q. et al. (2012). Genomic perspectives on the evolution of fungal entomopathogenicity in *Beauveria bassiana*. *Scientific Reports*, *2*, 483.

Zeiner, C. A., Purvine, S. O., Zink, E. M., Paša-Tolić, L., Chaput, D. L., Haridas, S. et al. (2016). Comparative analysis of secretome profiles of manganese(II)-oxidizing Ascomycete fungi. *PloS one , 11*, e0157844.

Zheng, P., Xia, Y., Xiao, G., Xiong, C., Hu, X., Zhang, S. et al. (2011). Genome sequence of the insect pathogenic fungus *Cordyceps militaris*, a valued traditional chinese medicine. *Genome Biology, 12*, R116.

References

Abe, Y., Suzuki, T., Ono, C., Iwamoto, K., Hosobuchi, M., Yoshikawa, H. (2002). Molecular cloning and characterization of an ML-236B (compactin) biosynthetic gene cluster in *Penicillium citrinum*. *Molecular Genetics and Genomics*, *267*, 636–646.

Aguileta, G., Refrégier, G., Yockteng, R., Fournier, E., Giraud, T. (2009). Rapidly evolving genes in pathogens: Methods for detecting positive selection and examples among fungi, bacteria, viruses and protists. *Infection, Genetics and Evolution : Journal of Molecular Epidemiology and Evolutionary Genetics in Infectious Diseases*, *9*, 656–670.

Alexander, N. J., Proctor, R. H., McCormick, S. P. (2009). Genes, gene clusters, and biosynthesis of trichothecenes and fumonisins in *Fusarium*. *Toxin Reviews*, *28*, 198–215.

Amaike, S., Keller, N. P. (2009). Distinct Roles for VeA and LaeA in Development and Pathogenesis of *Aspergillus flavus*. *Eukaryotic Cell*, *8*, 1051–1060.

Andersen, M. R., Nielsen, J. B., Klitgaard, A., Petersen, L. M., Zachariasen, M., Hansen, T. J., Blicher, L.H., Gotfredsen, C.H., Larsen, T.O., Nielsen, K.F., Mortensen, U. H. (2013). Accurate prediction of secondary metabolite gene clusters in filamentous fungi. *Proceedings of the National Academy of Sciences of the United States of America*, *110*, E99-E107.

Arai, T., Umemura, S., Ota, T., Ogihara, J., Kato, J., Kasumi, T. (2012). Effects of inorganic nitrogen sources on the production of PP-V [(10Z)-12-carboxyl-monascorubramine] and the expression of the nitrate assimilation gene cluster by *Penicillium* sp. AZ. *Bioscience, Biotechnology, and Biochemistry*, *76*, 120–124.

Ausubel, F. M. (2005). Are innate immune signaling pathways in plants and animals conserved? *Nature Immunology*, *6*, 973–979.

Baker, S. E., Kroken, S., Inderbitzin, P., Asvarak, T., Li, B.Y., Shi, L., Yoder, O.C., Turgeon, B. G. (2006). Two polyketide synthase-encoding genes are required for biosynthesis of the polyketide virulence factor, T-toxin, by *Cochliobolus heterostrophus*. *Molecular Plant-Microbe Interactions*, *19*, 139–149.

Bakshi, B. K., Singh, S. (1968). Dothistroma blight - a potential threat to *Pinus radiata* plantations in India. *Indian Forester*, *94*, 824–825.

Bansal, R., Mukherjee, P. K. (2016). Identification of novel gene clusters for secondary metabolism in *Trichoderma* genomes. *Microbiology*, *85*, 185–190.

Barboráková, Z., Labuda, R., Häubl, G., Tančinová, D. (2012) Effect of glucose concentration and growth conditions on the fungal biomass, pH of media and production of fumagillin by a non-pathogenic strain *Penicillium scabrosum*. *Journal of Microbiology, Biotechnology and Food Sciences*, *1*, 466–477.

Barron, N. (2006). Optimizing *Dothistroma septosporum* infection of *Pinus radiata* and the development of red-band disease. *MSc thesis. IMBS. Massey University, Palmerston North, New Zealand*.

Bassett, C., Buchanan, M. (1970). A toxic difuroanthraquinone from *Dothistroma pini*. *Chemistry and Industry*, *52*, 1659–1660.

Beck, J., Ripka, S., Siegner, A., Schiltz, E., Schweizer, E. (1990). The multifunctional 6-methylsalicylic acid synthase gene of *Penicillium patulum*. *European Journal of Biochemistry, 192*, 487–498.

Bell, A. A., Wheeler, M. H. (1986). Biosynthesis and functions of fungal melanins. *Annual Review of Phytopathology, 24*, 411–451.

Bernard, P., & Couturier, M. (1992). Cell killing by the F plasmid CcdB protein involves poisoning of DNA-topoisomerase II complexes. *Journal of Molecular Biology*, *226*, 735–745.

Berry, D., Takach, J. E., Schardl, C. L., Charlton, N. D., Scott, B., Young, C. A. (2015). Disparate independent genetic events disrupt the secondary metabolism gene *perA* in certain symbiotic *Epichloë* species. *Applied and Environmental Microbiology*, *81*, 2797–2807.

Birch, A., Donovan, F. (1953). Studies in relation to biosynthesis. Some possible routes to derivatives of orcinol and phloroglucinol. *Australian Journal of Chemistry*, *6*, 360.

Boettger, D., Hertweck, C. (2013). Molecular diversity sculpted by fungal PKS-NRPS hybrids. *Chembiochem*, *14*, 28–42.

Bok, J. W., Balajee, S. A., Marr, K. A., Andes, D., Nielsen, K. F., Frisvad, J. C., Keller, N. P. (2005). LaeA, a regulator of morphogenetic fungal virulence factors. *Eukaryotic Cell*, *4*, 1574–1582.

Bok, J. W., Keller, N. P. (2004). LaeA, a regulator of secondary metabolism in *Aspergillus* spp. *Eukaryotic Cell*, *3*, 527–535.

Bonsch, B., Belt, V., Bartel, C., Duensing, N., Koziol, M., Lazarus, C. M., Bailey, A.M., Simpson, T.J., Cox, R. J. (2016). Identification of genes encoding squalestatin S1 biosynthesis and *in vitro* production of new squalestatin analogues. *Chemical Communications*, *52*, 6777–6780.

Boustie, J., Grube, M. (2005). Lichens - A promising source of bioactive secondary metabolites. *Plant Genetic Resources: Characterization and Utilization*, *3*, 273–287.

Boyd, L. A., Ridout, C., O'Sullivan, D. M., Leach, J. E., Leung, H. (2013). Plant-pathogen interactions: disease resistance in modern agriculture. *Trends in Genetics*, *29*, 233–240.

Bradshaw, R. E. (2004). Dothistroma (red-band) needle blight of pines and the dothistromin toxin: a review. *Forest Pathology*, *34*, 163–185.

Bradshaw, R. E., Bhatnagar, D., Ganley, R. J., Gillman, C. J., Monahan, B. J., Seconi, J. M. (2002). *Dothistroma pini*, a forest pathogen, contains homologs of aflatoxin biosynthetic pathway genes. *Applied and Environmental Microbiology*, *68*, 2885–2892.

Bradshaw, R. E., Ganley, R. J., Jones, W. T., Dyer, P. S. (2000). High levels of dothistromin toxin produced by the forest pathogen *Dothistroma pini*. *Mycological Research*, *104*, 325–332.

Bradshaw, R. E., Guo, Y., Sim, A. D., Kabir, M. S., Chettri, P., Ozturk, I. K., Hunziker, L., Ganley, R. J., Cox, M. P. (2016). Genome-wide gene expression dynamics of the fungal pathogen *Dothistroma septosporum* throughout its infection cycle of the gymnosperm host *Pinus radiata*. *Molecular Plant Pathology*, *17*, 210–224.

Bradshaw, R. E., Jin, H., Morgan, B. S., Schwelm, A., Teddy, O. R., Young, C. A., Zhang, S. (2006). A polyketide synthase gene required for biosynthesis of the aflatoxin-like toxin, dothistromin. *Mycopathologia*, *161*, 283–294.

Bradshaw, R. E., Slot, J. C., Moore, G. G., Chettri, P., de Wit, P. J. G. M., Ehrlich, K. C., Ganley, A. R. Olson, M. A., Rokas, A., Carbone, I., Cox, M. P. (2013). Fragmentation of an aflatoxin-like gene cluster in a forest pathogen. *New Phytologist*, *198*, 525–535.

Brakhage, A. A., Thön, M., Spröte, P., Scharf, D. H., Al-Abdallah, Q., Wolke, S. M., Hortschansky, P. (2009). Aspects on evolution of fungal beta-lactam biosynthesis gene clusters and recruitment of trans-acting factors. *Phytochemistry*, *70*, 1801–1811.

Brodhagen, M., Keller, N. P. (2006). Signalling pathways connecting mycotoxin production and sporulation. *Molecular Plant Pathology*, *7*, 285–301.

Brown, A. (2005). Seeing red! *Forestry and British Timber*, *34*, 16–18.

Brown, A., Webber, J. (2008). Red band needle blight of conifers in Britain. *Edinburgh, UK: Forestry Commission: Research Note 002.*

Brown, D. W., Butchko, R. A. E., Proctor, R. H. (2008). Genomic analysis of *Fusarium verticillioides*. *Food Additives and Contaminants*, *25*, 1158–1165.

Brown, D. W., Yu, J. H., Kelkar, H. S., Fernandes, M., Nesbitt, T. C., Keller, N. P., Adams, T. H., Leonard, T. J. (1996). Twenty-five coregulated transcripts define a sterigmatocystin gene cluster in *Aspergillus nidulans*. *Proceedings of the National Academy of Sciences of the United States of America*, *93*, 1418–1422.

Brunner, S., Stirnweis, D., Diaz Quijano, C., Buesing, G., Herren, G., Parlange, F., Barret, P., Tassy, C., Sautter, C., Winzeler, M., Keller, B. (2012). Transgenic Pm3

multilines of wheat show increased powdery mildew resistance in the field. *Plant Biotechnology Journal*, *10*, 398–409.

Bulman, L. S., Dick, M. A., Ganley, R. J., McDougal, R. L., Schwelm, A., Bradshaw, R. E. (2013). Dothistroma needle Blight. In P. Gonthier & G. Nicolotti (Eds.), *Infectious Forest Diseases.* (pp. 436–457). Wallingford, UK: CAB International.

Bulman, L. S., Gadgil, P. D., Kershaw, D. J., Ray, J. W. (2004). Assessment and control of Dothistroma Needle-Blight. *Forest Research Bulletin*, *229*.

Bushley, K. E., & Turgeon, B. G. (2010). Phylogenomics reveals subfamilies of fungal nonribosomal peptide synthetases and their evolutionary relationships. *BMC Evolutionary Biology*, *10*, 1.

Bushley, K. E., Raja, R., Jaiswal, P., Cumbie, J. S., Nonogaki, M., Boyd, A. E., Owensby, C. A., Knaus, B. J., Elser, J., Miller, D., Di, Y., McPhail, K. L., Spatafora, J. W. (2013). The genome of *Tolypocladium inflatum*: evolution, organization, and expression of the cyclosporin biosynthetic gene cluster. *PLoS Genetics*, *9*, e1003496.

Bushman, W., Thompson, J. F., Vargas, L., Landy, A. (1985). Control of directionality in lambda site specific recombination. *Science*, *230*, 906-911.

Butchko, R. A. E., Plattner, R. D., Proctor, R. H. (2003). *FUM13* encodes a short chain dehydrogenase/reductase required for C-3 carbonyl reduction during fumonisin biosynthesis in *Gibberella moniliformis*. *Journal of Agricultural and Food Chemistry*, *51*, 3000–3006.

Caboche, S., Pupin, M., Leclère, V., Fontaine, A., Jacques, P., Kucherov, G. (2008). NORINE: a database of nonribosomal peptides. *Nucleic Acids Research*, *36*, D326-331.

Calvo, A. M., Gardner, H. W., & Keller, N. P. (2001). Genetic connection between fatty acid metabolism and sporulation in *Aspergillus nidulans*. *The Journal of Biological Chemistry*, *276*, 25766–25774.

Calvo, A. M., Wilson, R. A., Bok, J. W., Keller, N. P. (2002). Relationship between secondary metabolism and fungal development. *Microbiology and Molecular Biology Reviews*, *66*, 447–459

Castoe, T. A., Stephens, T., Noonan, B. P., Calestani, C. (2007). A novel group of type I polyketide synthases (PKS) in animals and the complex phylogenomics of PKSs. *Gene*, *392*, 47–58.

Chalivendra, S., DeRobertis, C., Chang, P.-K., Damann, K. E. (2017). Cyclopiazonic Acid is a Pathogenicity Factor for *Aspergillus flavus* and a Promising Target for Screening Germplasm for Ear Rot Resistance. *Molecular Plant-Microbe Interactions.*

Champe, S. P., el-Zayat, A. A. (1989). Isolation of a sexual sporulation hormone from *Aspergillus nidulans*. *Journal of Bacteriology*, *171*, 3982–3988.

Champe, S. P., Rao, P., Chang, A. (1987). An endogenous inducer of sexual development in *Aspergillus nidulans*. *Journal of General Microbiology*, *133*, 1383–1387.

Chang, P.-K., & Ehrlich, K. C. (2011). Cyclopiazonic acid biosynthesis by *Aspergillus flavus*. *Toxin Reviews*, *30*, 79–89.

Charlang, G., Horowitz, R. M., Lowy, P. H., Ng, B., Poling, S. M., Horowitz, N. H. (1982). Extracellular siderophores of rapidly growing *Aspergillus nidulans* and *Penicillium chrysogenum*. *Journal of Bacteriology*, *150*, 785–787.

Chen, Y., Schröder, I., French, C. T., Jaroszewicz, A., Yee, X. J., Teh, B. E., Toeska, I. J., Miller, J. F., Gan, Y. H. (2014). Characterization and analysis of the *Burkholderia pseudomallei* BsaN virulence regulon. *BMC Microbiology*, *14*, 206.

Chettri, P. (2014). Regulation of dothistromin toxin biosynthesis by the pine needle pathogen *Dothistroma septosporum*. *PhD thesis. IFS. Massey University, Palmerston North, New Zealand*.

Chettri, P., Calvo, A. M., Cary, J. W., Dhingra, S., Guo, Y., McDougal, R. L., Bradshaw, R. E. (2012). The *veA* gene of the pine needle pathogen *Dothistroma septosporum* regulates sporulation and secondary metabolism. *Fungal Genetics and Biology*, *49*, 141–151.

Chettri, P., Ehrlich, K. C., Cary, J. W., Collemare, J., Cox, M. P., Griffiths, S. A., Olsin, M. A., de Wit, P. J. G. M, Bradshaw, R. E. (2013). Dothistromin genes at multiple separate loci are regulated by AflR. *Fungal Genetics and Biology*, *51*, 12–20.

Chettri, P., Ehrlich, K. C., Bradshaw, R. E. (2015). Regulation of the aflatoxin-like toxin dothistromin by AflJ. *Fungal Biology*, *119*, 503–508.

Chiang, Y. M., Oakley, C. E., Ahuja, M., Entwistle, R., Schultz, A., Chang, S. L., Sung, C. T., Wang, C. C., Oakley, B. R. (2013). An efficient system for heterologous expression of secondary metabolite genes in *Aspergillus nidulans*. *Journal of the American Chemical Society*, *135*, 7720–7731.

Cho, Y., Srivastava, A., Ohm, R. A., Lawrence, C. B., Wang, K. H., Grigoriev, I. V, Marahatta, S. P. (2012). Transcription factor Amr1 induces melanin biosynthesis and suppresses virulence in *Alternaria brassicicola*. *PLoS Pathogens*, *8*, e1002974.

Chooi, Y. H., & Tang, Y. (2012). Navigating the fungal polyketide chemical space: from genes to molecules. *The Journal of Organic Chemistry*, *77*, 9933–9953.

Choquer, M., Dekkers, K. L., Chen, H. Q., Cao, L., Ueng, P. P., Daub, M. E., Chung, K.-R. (2005). The *CTB1* gene encoding a fungal polyketide synthase is required for cercosporin biosynthesis and fungal virulence of *Cercospora nicotianae*. *Molecular Plant-Microbe Interactions 18*, 468–476.

Chumley, F. G., Valent, B. (1990). Genetic analysis of melanin-deficient, nonpathogenic mutants of *Magnaporthe grisea*. *Molecular Plant-Microbe Interactions*, *3*, 135–143.

Chung, C. T., Miller, R. H. (1993). Preparation and storage of competent *Escherichia coli* cells. *Methods in Enzymology*, *218*, 621–627.

Chung, K. R. (2011). *Elsinoë fawcettii* and *Elsinoë australis*: the fungal pathogens causing citrus scab. *Molecular Plant Pathology*, *12*, 123–135.

Collado, I. G., Sánchez, A. J. M., Hanson, J. R. (2007). Fungal terpene metabolites: biosynthetic relationships and the control of the phytopathogenic fungus *Botrytis cinerea*. *Natural Product Reports*, *24*, 674–686.

Collemare, J., Billard, A., Böhnert, H. U., Lebrun, M. H. (2008). Biosynthesis of secondary metabolites in the rice blast fungus *Magnaporthe grisea*: the role of hybrid PKS-NRPS in pathogenicity. *Mycological Research*, *112*, 207–215.

Collemare, J., Griffiths, S., Iida, Y., Karimi Jashni, M., Battaglia, E., Cox, R. J., de Wit, P. J. G. M. (2014). Secondary metabolism and biotrophic lifestyle in the tomato pathogen *Cladosporium fulvum*. *PloS One*, *9*, e85877.

Collemare, J., & Lebrun, M. H. (2011). Fungal Secondary Metabolites: Ancient Toxins and Novel Effectors in Plant–Microbe Interactions. In F. Martin & S. Kamoun (Eds.), *Effectors in Plant-Microbe Interactions* (pp. 379–402). Oxford, UK: Wiley-Blackwell.

Conti, E., Stachelhaus, T., Marahiel, M. A., & Brick, P. (1997). Structural basis for the activation of phenylalanine in the non-ribosomal biosynthesis of gramicidin S. *The EMBO Journal*, *16*, 4174–83.

Cox, R. J. (2007). Polyketides, proteins and genes in fungi: programmed nano-machines begin to reveal their secrets. *Organic & Biomolecular Chemistry*, *5*, 2010–2026.

Cox, R. J., Glod, F., Hurley, D., Lazarus, C. M., Nicholson, T. P., Rudd, B. A. M., Simpson, T. J., Wilkinson, B., Zhang, Y. (2004). Rapid cloning and expression of a fungal polyketide synthase gene involved in squalestatin biosynthesis. *Chemical Communications*, 20, 2260–2261.

Cramer, R. A., Gamcsik, M. P., Brooking, R. M., Najvar, L. K., Kirkpatrick, W. R., Patterson, T. F., Balibar, C. J., Graybill, J. R., Perfect, J. R., Abraham, S. N., Steinbach, W. J. (2006). Disruption of a nonribosomal peptide synthetase in *Aspergillus fumigatus* eliminates gliotoxin production. *Eukaryotic Cell*, *5*, 972–980.

Crawford, J. M., Townsend, C. A. (2010). New insights into the formation of fungal aromatic polyketides. *Nature Reviews. Microbiology*, *8*, 879–889.

Dayan, F. E., Ferreira, D., Wang, Y.-H., Khan, I. A., McInroy, J. A., Pan, Z. (2008). A pathogenic fungi diphenyl ether phytotoxin targets plant enoyl (acyl carrier protein) reductase. *Plant Physiology*, *147*, 1062–1071.

De Lorenzo, G., Brutus, A., Savatin, D. V., Sicilia, F., Cervone, F. (2011). Engineering plant resistance by constructing chimeric receptors that recognize damage-associated molecular patterns (DAMPs). *FEBS Letters*, *585*, 1521–1528.

de Wit, P. J. G. M., van der Burgt, A., Ökmen, B., Stergiopoulos, I., Abd-Elsalam, K. a, Aerts, A. L., Bahkali, A. H., Beenen, H. G., Chettri, P., Cox, M. P., Datema, E., de Vries, R. P., Dhillon, B., Ganley, A. R., Griffiths, S. A., Guo, Y., Hamelin, R. C., Henrissat, B., Kabir, M. S., Jashni, M. K., Kema, G., Klaubauf, S., Lapidus, A., Levasseur, A., Lindquist, E., Mehrabi, R., Ohm, R. A., Owen, T. J., Salamov, A., Schwelm, A., Schijlen, E., Sun, H., van den Burg, H. A., van Ham, R. C., Zhang, S., Goodwin, S. B., Grigoriev, I. V., Collemare, J., Bradshaw, R. E. (2012). The genomes of the fungal plant pathogens *Cladosporium fulvum* and *Dothistroma septosporum* reveal adaptation to different hosts and lifestyles but also signatures of common ancestry. *PLoS Genetics*, *8*, e1003088.

Dean, R. A., Talbot, N. J., Ebbole, D. J., Farman, M. L., Mitchell, T. K., Orbach, M. J., Thon, M., Kulkarni, R., Xu, J. R., Pan, H., Read, N. D., Lee, Y. H., Carbone, I., Brown, D., Oh, Y. Y., Donofrio, N., Jeong, J. S., Soanes, D. M., Djonovic, S., Kolomiets, E., Rehmeyer, C., Li, W., Harding, M., Kim, S., Lebrun, M. H., Bohnert, H., Coughlan, S., Butler, J., Calvo, S., Ma, L. J., Nicol, R., Purcell, S., Nusbaum, C., Galagan, J. E., Birren, B. W. (2005). The genome sequence of the rice blast fungus *Magnaporthe grisea*. *Nature*, *434*, 980–986.

Ding, Y., Wet, J. R. de, Cavalcoli, J., Li, S., Greshock, T. J., Miller, K. A., Finefield, J. M., Sunderhaus, J. D., McAfoos, T. J., Tsukamoto, S., Williams, R. M., Sherman, D. H. (2010). Genome-based characterization of two prenylation steps in the assembly of the stephacidin and notoamide anticancer agents in a marine-derived *Aspergillus* sp. *Journal of the American Chemical Society*, *132*, 12733–12740.

Ding, W., Liu, W. Q., Jia, Y., Li, Y., van der Donk, W. A., Zhang, Q. (2016b). Biosynthetic investigation of phomopsins reveals a widespread pathway for ribosomal natural products in Ascomycetes. *Proceedings of the National Academy of Sciences of the United States of America*, *113*, 3521–3526.

Dolan, S. K., O'Keeffe, G., Jones, G. W., Doyle, S. (2015). Resistance is not futile: gliotoxin biosynthesis, functionality and utility. *Trends in Microbiology*, *23*, 419–428.

Dowzer, C. E., Kelly, J. M. (1991). Analysis of the *creA* gene, a regulator of carbon catabolite repression in *Aspergillus nidulans*. *Molecular and Cellular Biology*, *11*, 5701–5709.

Drenkhan, R., Tomešová-Haataja, V., Fraser, S., Bradshaw, R. E., Vahalík, P., Mullett, M. S., Martín-García, J., Bulman, L. S., Wingfield, M. J., Kirisits, T., Cech, T. L., Schmitz, S., Baden, R., Tubby, K., Brown, A., Georgieva, M., Woods, A., Ahumada, R., Jankovský, L., Thomsen, I. M., Adamson, K., Marçais, B.,

Vuorinen, M., Tsopelas, P., Koltay, A., Halasz, A., La Porta, N., Anselmi, N., Kiesnere, R., Markovskaja, S., Kačergius, A., Papazova-Anakieva, I., Risteski, M., Sotirovski, K., Lazarević, J., Solheim, H., Boron, P., Bragança, H., Chira, D., Musolin, D. L., Selikhovkin, A. V., Bulgakov, T. S., Keča, N., Karadžić, D., Galovic, V., Pap, P., Markovic, M., Poljakovic Pajnik, L., Vasic, V., Ondrušková, E., Piškur, B., Sadiković, D., Diez, J. J., Solla, A., Millberg, H., Stenlid, J., Angst, A., Queloz, V., Lehtijärvi, A., Doğmuş-Lehtijärvi, H. T., Oskay, F., Davydenko, K., Meshkova, V., Craig, D., Woodward, S., Barnes, I. (2016). Global geographic distribution and host range of *Dothistroma* species: a comprehensive review. *Forest Pathology*, *46*, 408–442.

Du, L., Sánchez, C., Chen, M., Edwards, D. J., Shen, B. (2000). The biosynthetic gene cluster for the antitumor drug bleomycin from *Streptomyces verticillus* ATCC15003 supporting functional interactions between nonribosomal peptide synthetases and a polyketide synthase. *Chemistry & Biology*, *7*, 623–642.

Du, L., Cheng, Y.-Q., Ingenhorst, G., Tang, G.-L., Huang, Y., Shen, B. (2003). Hybrid peptide-polyketide natural products: biosynthesis and prospects towards engineering novel molecules. *Genetic Engineering*, *25*, 227–267.

Du, L., Lou, L. (2010). PKS and NRPS release mechanisms. *Natural Product Reports*, *27*, 255–278.

Eaton, D., Ensign, J. C. (1980). *Streptomyces viridochromogenes* spore germination initiated by calcium ions. *Journal of Bacteriology*, *143*, 377–382.

Eaton, D. L., Gallagher, E. P. (1994). Mechanisms of aflatoxin carcinogenesis. *Annual Review of Pharmacology and Toxicology*, *34*, 135–172.

Edgar, R. C. (2004). MUSCLE: multiple sequence alignment with high accuracy and high throughput. *Nucleic Acids Research*, *32*, 1792–1797.

Ehrlich, K. C., Montalbano, B. G., Cary, J. W. (1999). Binding of the C6-zinc cluster protein, AFLR, to the promoters of aflatoxin pathway biosynthesis genes in *Aspergillus parasiticus*. *Gene*, *230*, 249–257.

Eisendle, M., Oberegger, H., Zadra, I., & Haas, H. (2003). The siderophore system is essential for viability of *Aspergillus nidulans*: functional analysis of two genes encoding l-ornithine N 5-monooxygenase (*sidA*) and a non-ribosomal peptide synthetase (*sidC*). *Molecular Microbiology*, *49*, 359–375.

Eisenman, H. C., Casadevall, A. (2012). Synthesis and assembly of fungal melanin. *Applied Microbiology and Biotechnology*, *93*, 931–940.

Eley, K. L., Halo, L. M., Song, Z., Powles, H., Cox, R. J., Bailey, A. M., Lazarus, C. M., Simpson, T. J. (2007). Biosynthesis of the 2-pyridone tenellin in the insect pathogenic fungus *Beauveria bassiana*. *Chembiochem*, *8*, 289–297.

Eliahu, N., Igbaria, A., Rose, M. S., Horwitz, B. A., Lev, S. (2007). Melanin biosynthesis in the maize pathogen *Cochliobolus heterostrophus* depends on two

mitogen-activated protein kinases, Chk1 and Mps1, and the transcription factor Cmr1. *Eukaryotic Cell*, *6*, 421–429.

Elliott, C. E., Gardiner, D. M., Thomas, G., Cozijnsen, A., van de Wouw, A., Howlett, B. J. (2007). Production of the toxin sirodesmin PL by *Leptosphaeria maculans* during infection of *Brassica napus*. *Molecular Plant Pathology*, *8*, 791–802.

Elliott, G. S., Mason, R. W., Ferry, D. G., Edwards, I. R. (1989). Dothistromin risk assessment for forestry workers. *New Zealand Journal of Forestry Science*, *19*, 163–170.

Feng, B., Wang, X., Hauser, M., Kaufmann, S., Jentsch, S., Haase, G., Becker, J. M., Szaniszlo, P. J. (2001). Molecular cloning and characterization of *WdPKS1*, a gene involved in dihydroxynaphthalene melanin biosynthesis and virulence in *Wangiella* (*Exophiala*) *dermatitidis*. *Infection and Immunity*, *69*, 1781–1794.

Feng, G. H., Leonard, T. J. (1995). Characterization of the polyketide synthase gene (*pksL1*) required for aflatoxin biosynthesis in *Aspergillus parasiticus*. *Journal of Bacteriology*, *177*, 6246–6254.

Fenn, P., Kirk, T. K. (1981). Relationship of nitrogen to the onset and suppression of ligninolytic activity and secondary metabolism in *Phanerochaete chrysosporium*. *Archives of Microbiology*, *130*, 59–65.

Fenton, A., Antonovics, J., Brockhurst, M. A. (2009). Inverse-gene-for-gene infection genetics and coevolutionary dynamics. *The American Naturalist*, *174*, E230–E242.

Fernandes, M., Keller, N. P., Adams, T. H. (1998). Sequence-specific binding by *Aspergillus nidulans* AflR, a C6 zinc cluster protein regulating mycotoxin biosynthesis. *Molecular Microbiology*, *28*, 1355–1365.

Finking, R., Marahiel, M. A. (2004). Biosynthesis of nonribosomal peptides. *Annual Review of Microbiology*, *58*, 453–488.

Fisch, K. M. (2013). Biosynthesis of natural products by microbial iterative hybrid PKS–NRPS. *RSC Advances*, *3*, 18228–18247.

Flor, H. H. (1942). Inheritance of pathogenicity in *Melampsora lini*. *Phytopathology*, *28*, 365–391.

Foglino, M., Borne, F., Bally, M., Ball, G., Patte, J. C. (1995). A direct sulfhydrylation pathway is used for methionine biosynthesis in *Pseudomonas aeruginosa*. *Microbiology*, *141*, 431–439.

Franich, R. A., Carson, M. J., Carson, S. D. (1986). Synthesis and accumulation of benzoic acid in *Pinus radiata* needles in response to tissue injury by dothistromin, and correlation with resistance of *P. radiata* families to *Dothistroma pini*. *Physiological and Molecular Plant Pathology*, *28*, 267–286.

Friesen, T. L., Faris, J. D., Solomon, P. S., Oliver, R. P. (2008). Host-specific toxins: effectors of necrotrophic pathogenicity. *Cellular Microbiology*, *10*, 1421–1428.

Friesen, T. L., Meinhardt, S. W., Faris, J. D. (2007). The *Stagonospora nodorum*-wheat pathosystem involves multiple proteinaceous host-selective toxins and corresponding host sensitivity genes that interact in an inverse gene-for-gene manner. *The Plant Journal*, *51*, 681–692.

Fujii, I., Ono, Y., Tada, H., Gomi, K., Ebizuka, Y., Sankawa, U. (1996). Cloning of the polyketide synthase gene *atX* from *Aspergillus terreus* and its identification as the 6-methylsalicylic acid synthase gene by heterologous expression. *Molecular & General Genetics*, *253*, 1–10.

Gacek, A., Strauss, J. (2012). The chromatin code of fungal secondary metabolite gene clusters. *Applied Microbiology and Biotechnology*, *95*, 1389–1404.

Gadgil, P. D. (1967). Infection of Pinus radiata needles by *Dothistroma pini*. *New Zealand Journal of Botany*, *5*, 498–503.

Gaffoor, I., Trail, F. (2006). Characterization of two polyketide synthase genes involved in zearalenone biosynthesis in *Gibberella zeae*. *Applied and Environmental Microbiology*, *72*, 1793–1799.

Gan, P., Ikeda, K., Irieda, H., Narusaka, M., O'Connell, R. J., Narusaka, Y., Takano, Y., Kubo, Y., Shirasu, K. (2013). Comparative genomic and transcriptomic analyses reveal the hemibiotrophic stage shift of *Colletotrichum* fungi. *New Phytologist*, *197*, 1236–1249.

Gardiner, D. M., Cozijnsen, A. J., Wilson, L. M., Pedras, M. S. C., Howlett, B. J. (2004). The sirodesmin biosynthetic gene cluster of the plant pathogenic fungus *Leptosphaeria maculans*. *Molecular Microbiology*, *53*, 1307–1318.

Gehring, A. M., DeMoll, E., Fetherston, J. D., Mori, I., Mayhew, G. F., Blattner, F. R., Walsh, C. T., Perry, R. D. (1998). Iron acquisition in plague: modular logic in enzymatic biogenesis of yersiniabactin by *Yersinia pestis*. *Chemistry & Biology*, *5*, 573–586.

Gibson, I. A. S. (1972). Dothistroma blight of *Pinus radiata*. *Annual Review of Phytopathology*, *10*, 51–72.

Gibson, I. A. S. (1974). Impact and control of dothistroma blight of pines. *Forest Pathology*, *4*, 89–100.

Glenn, A. E., Zitomer, N. C., Zimeri, A. M., Williams, L. D., Riley, R. T., Proctor, R. H. (2008). Transformation-mediated complementation of a *FUM* gene cluster deletion in *Fusarium verticillioides* restores both fumonisin production and pathogenicity on maize seedlings. *Molecular Plant-Microbe Interactions*, *21*, 87–97.

Glinski, M., Urbanke, C., Hornbogen, T., Zocher, R. (2002). Enniatin synthetase is a monomer with extended structure: evidence for an intramolecular reaction mechanism. *Archives of Microbiology*, *178*, 267–273.

Gressler, M., Zaehle, C., Scherlach, K., Hertweck, C., Brock, M. (2011). Multifactorial induction of an orphan PKS-NRPS gene cluster in *Aspergillus terreus*. *Chemistry Biology*, *18*, 198–209.

Grigoriev, I. V, Nordberg, H., Shabalov, I., Aerts, A., Cantor, M., Goodstein, D., Kuo, A., Minovitsky, S., Nikitin, R., Ohm, R. A., Ottillar, R., Poliakov, A., Ratnere, I., Riley, R., Smirnova, T., Rokhsar, D., Dubchak, I. (2012). The genome portal of the department of energy joint genome institute. *Nucleic Acids Research*, *40*, D26–D32. http://genome.jgi.doe.gov/programs/fungi/index.jsf

Guernier, V., Hochberg, M. E., & Guégan, J.-F. (2004). Ecology drives the worldwide distribution of human diseases. *PLoS Biology*, *2*, e141.

Guindon, S., Dufayard, J.-F., Lefort, V., Anisimova, M., Hordijk, W., Gascuel, O. (2010). New algorithms and methods to estimate maximum-likelihood phylogenies: assessing the performance of PhyML 3.0. *Systematic Biology*, *59*, 307–321.

Guzmán-de-Peña, D., Aguirre, J., Ruiz-Herrera, J. (1998). Correlation between the regulation of sterigmatocystin biosynthesis and asexual and sexual sporulation in *Emericella nidulans*. *Antonie van Leeuwenhoek*, *73*, 199–205.

Haas, B. J., Kamoun, S., Zody, M. C., Jiang, R. H. Y., Handsaker, R. E., Cano, L. M., Grabherr, M., Kodira, C. D., Raffaele, S., Torto-Alaibo, T., Bozkurt, T. O., Ah Fong, A. M. V., Alvarado, L. Anderson, V. L., Armstrong, M. R., Avrova, A. A., Baxter, L., Beynon, J., Boevink, P. C., Bollmann, S. R., Bos, J. I. B., Bulone, V., Cai, G., Cakir, C., Carrington, J. C., Chawner, M., Conti, L., Costanzo, S., Ewan, R., Fahlgren, N., Fischbach, M. A., Fugelstad, J. F., Gilroy, E. M., Gnerre, S., Green, P. J., Grenville-Briggs, L. J., Griffith, J., Grünwald, N. J., Horn, K., Horner, N. R., Hu, C. H., Huimeta, E., Jeong, D. H., Jones, A. M. E., Jones, J. D. G., Jones R. W., Karlsson, E. K., Kunjeti, S. G., Lamour, K., Liu, Z., Ma, L. J., MacLean, D., Chibucos, M., C., McDonald, H., McWalters, J., Meijer, H., J., G., Morgan, W., Morris, P. F., Munro, C. A., O'Neill, K., Ospina-Giraldo, M. Pinzón, A., Pritchard, L., Ramsahoye, B., Ren, Q., Restrepo, S., Roy, S., Sadanandom, A., Savidor, A., Schornack, S., Schwartz, D. C., Schumann, U. D., Schwessinger, B., Seyer, L., Sharpe, T., Silvar, C., Song, J., Studholme, D. J., Sykes, S., Thines, M., van de Vondervoort, P. J. I., Phuntumart, V., Wawra, S., Weide, R., Win, J., Young, C., Zhou, S., Fry, W., Meyers, B. C., van West, P., Ristaino, J., Govers, F., Birch, P. R. J., Whisson, S. C., Judelson, H. S., Nusbaum, C. (2009). Genome sequence and analysis of the Irish potato famine pathogen *Phytophthora infestans*. *Nature*, *461*, 393–398.

Haas, H. (2014). Fungal siderophore metabolism with a focus on *Aspergillus fumigatus*. *Natural Product Reports*, *31*, 1266–1276.

Haas, H., Eisendle, M., Turgeon, B. G. (2008). Siderophores in fungal physiology and virulence. *Annual Review of Phytopathology*, *46*, 149–87.

Hayashi, Y., Yamaguchi, J., Shoji, M. (2002). The diastereoselective asymmetric total synthesis of NG-391, a neuronal cell-protecting molecule. *Tetrahedron*, *58*, 9839–9846.

Healy, F. G., Wach, M., Krasnoff, S. B., Gibson, D. M., Loria, R. (2000). The *txtAB* genes of the plant pathogen *Streptomyces acidiscabies* encode a peptide synthetase required for phytotoxin thaxtomin A production and pathogenicity. *Molecular Microbiology*, *38*, 794–804.

Herrmann, M., Zocher, R., Haese, A. (1996). Effect of disruption of the enniatin synthetase gene on the virulence of *Fusarium avenaceum*. *Molecular Plant-Microbe Interactions 9*, 226–232.

Hertweck, C. (2009). The biosynthetic logic of polyketide diversity. *Angewandte Chemie (International Ed. in English)*, *48*, 4688–4716.

Hicks, J. K., Yu, J. H., Keller, N. P., & Adams, T. H. (1997). *Aspergillus* sporulation and mycotoxin production both require inactivation of the FadA G alpha protein-dependent signaling pathway. *The EMBO Journal*, *16*, 4916–4923.

Hissen, A. H. T., Chow, J. M. T., Pinto, L. J., Moore, M. M. (2004). Survival of *Aspergillus fumigatus* in serum involves removal of iron from transferrin: the role of siderophores. *Infection and Immunity*, *72*, 1402–1408.

Holden, H. M., Thoden, J. B., Raushel, F. M. (1999). Carbamoyl phosphate synthetase: an amazing biochemical odyssey from substrate to product. *Cellular and Molecular Life Sciences*, *56*, 507–522.

Hori, K., Yamamoto, Y., Minetoki, T., Kurotsu, T., Kanda, M., Miura, S., Okamura, K., Furuyama, J., Saito, Y. (1989). Molecular cloning and nucleotide sequence of the *gramicidin S synthetase 1* gene. *Journal of Biochemistry*, *106*, 639–645.

Horowitz, N. H., Charlang, G., Horn, G., Williams, N. P. (1976). Isolation and identification of the conidial germination factor of *Neurospora crassa*. *Journal of Bacteriology*, *127*, 135–140.

Hotter, G. S. (1997). Elicitor-induced oxidative burst and phenylpropanoid metabolism in *Pinus radiata* cell suspension cultures. *Functional Plant Biology*, *24*, 797–804.

Huerta-Cepas, J., Serra, F., Bork, P. (2016). ETE 3: Reconstruction, analysis, and visualization of phylogenomic data. *Molecular Biology and Evolution*, *33*, 1635–1638.

Hur, G. H., Vickery, C. R., Burkart, M. D. (2012). Explorations of catalytic domains in non-ribosomal peptide synthetase enzymology. *Natural Product Reports*, *29*, 1074–1098.

Hwang, L. H., Mayfield, J. A., Rine, J., Sil, A. (2008). Histoplasma requires *SID1*, a member of an iron-regulated siderophore gene cluster, for host colonization. *PLoS Pathogens*, *4*, e1000044.

Hynes, M. J. (1975). Studies on the role of the *areA* gene in the regulation of nitrogen catabolism in *Aspergillus nidulans*. *Australian Journal of Biological Sciences*, *28*, 301–313.

Inderbitzin, P., Asvarak, T., Turgeon, B. G. (2010). Six new genes required for production of T-toxin, a polyketide determinant of high virulence of *Cochliobolus heterostrophus* to maize. *Molecular Plant-Microbe Interactions : MPMI*, *23*, 458–72.

Jeandet, P., Vasserot, Y., Chastang, T., Courot, E. (2013). Engineering microbial cells for the biosynthesis of natural compounds of pharmaceutical significance. *BioMed Research International*, *2013*, 1–13.

Jin, J. M., Lee, S., Lee, J., Baek, S. R., Kim, J. C., Yun, S. H., Park, S. Y., Kang, S., Lee, Y. W. (2010). Functional characterization and manipulation of the apicidin biosynthetic pathway in *Fusarium semitectum*. *Molecular Microbiology*, *76*, 456–466.

Jones, J. D. G., Dangl, J. L. (2006). The plant immune system. *Nature*, *444*, 323–329.

Jones, P., Binns, D., Chang, H.-Y., Fraser, M., Li, W., McAnulla, C., McWilliam, H., Maslen, J., Mitchell, A., Nuka, G., Pesseat, S., Quinn, A. F., Sangrador-Vegas, A., Scheremetjew, M., Yong, S. Y., Lopez, R., Hunter, S. (2014). InterProScan 5: genome-scale protein function classification. *Bioinformatics*, *30*, 1236–1240. http://www.ebi.ac.uk/interpro/search/sequence-search

Kabir, M. S., Ganley, R. J., Bradshaw, R. E. (2015). Dothistromin toxin is a virulence factor in dothistroma needle blight of pines. *Plant Pathology*, *64*, 225–234.

Kabir, M. S., Ganley, R. J., Bradshaw, R. E. (2013). An improved artificial pathogenicity assay for Dothistroma needle blight on *Pinus radiata*. *Australasian Plant Pathology*, *42*, 503–510.

Katoh, K., Kuma, K., Toh, H., Miyata, T. (2005). MAFFT version 5: improvement in accuracy of multiple sequence alignment. *Nucleic Acids Research*, *33*, 511–518.

Kawamura, C., Tsujimoto, T., Tsuge, T. (1999). Targeted disruption of a melanin biosynthesis gene affects conidial development and UV tolerance in the Japanese pear pathotype of *Alternaria alternata*. *Molecular Plant-Microbe Interactions*, *12*, 59–63.

Kearse, M., Moir, R., Wilson, A., Stones-Havas, S., Cheung, M., Sturrock, S., Buxton, S., Cooper, A., Markowitz, S., Duran, C., Thierer, T., Ashton, B., Meintjes, P., Drummond, A. (2012). Geneious Basic: an integrated and extendable desktop software platform for the organization and analysis of sequence data. *Bioinformatics*, *28*, 1647–1649. http://www.geneious.com

Keller, N. P. (2015). Translating biosynthetic gene clusters into fungal armor and weaponry. *Nature Chemical Biology*, *11*, 671–677.

Keller, N. P., Turner, G., Bennett, J. W. (2005). Fungal secondary metabolism - from biochemistry to genomics. *Nature Reviews Microbiology*, *3*, 937–947.

Keller, N. P., Hohn, T. M. (1997). Metabolic pathway gene clusters in filamentous fungi. *Fungal Genetics and Biology*, *21*, 17–29.

Keller, N. P., Nesbitt, C., Sarr, B., Phillips, T. D., Burow, G. B. (1997). pH regulation of sterigmatocystin and aflatoxin biosynthesis in *Aspergillus* spp. *Phytopathology*, *87*, 643–648.

Kellmann, R., & Neilan, B. A. (2007). Biochemical characterization of paralytic shellfish toxin biosynthesis in vitro. *Journal of Phycology*, *43*, 497–508.

Kennedy, J., Auclair, K., Kendrew, S. G., Park, C., Vederas, J. C., Hutchinson, C. R. (1999). Modulation of polyketide synthase activity by accessory proteins during lovastatin biosynthesis. *Science, 284*, 1368–1372.

Kersten, R. D., Lane, A. L., Nett, M., Richter, T. K. S., Duggan, B. M., Dorrestein, P. C., Moore, B. S. (2013). Bioactivity-guided genome mining reveals the lomaiviticin biosynthetic gene cluster in *salinispora tropica*. *ChemBioChem, 14*, 955–962.

Khaldi, N., Collemare, J., Lebrun, M. H., Wolfe, K. H. (2008). Evidence for horizontal transfer of a secondary metabolite gene cluster between fungi. *Genome Biology*, *9*, R18.

Kiedrowski, M. (2011). Evaluating spontaneous mutation in the plasmid pDONR(TM)P4-P1R during serial transformations. *MSc thesis. Hofstra University, New York, USA.*

Kim, J. H., Mahoney, N., Chan, K. L., Molyneux, R. J., Campbell, B. C. (2004). Secondary metabolites of the grapevine pathogen *Eutypa lata* inhibit mitochondrial respiration, based on a model bioassay using the yeast *Saccharomyces cerevisiae*. *Current Microbiology*, *49*, 282–287.

Knogge, W. (1998). Fungal pathogenicity. *Current Opinion in Plant Biology*, *1*, 324–328.

Koeck, M., Hardham, A. R., Dodds, P. N. (2011). The role of effectors of biotrophic and hemibiotrophic fungi in infection. *Cellular Microbiology*, *13*, 1849–1857.

Komagata, D., Fujita, S., Yamashita, N., Saito, S., Morino, T. (1996). Novel neuritogenic activities of pseurotin A and penicillic acid. *The Journal of Antibiotics, 49*, 958–959.

Konz, D., Klens, A., Schörgendorfer, K., & Marahiel, M. A. (1997). The bacitracin biosynthesis operon of *Bacillus licheniformis* ATCC 10716: molecular

characterization of three multi-modular peptide synthetases. *Chemistry & Biology*, *4*, 927–937.

Koski, L. B., Golding, G. B. (2001). The closest BLAST hit is often not the nearest neighbor. *Journal of Molecular Evolution*, *52*, 540–542.

Kubo, Y., Nakamura, H., Kobayashi, K., Okuno, T., Furusawa, I. (1991). Cloning of a melanin biosynthetic gene essential for appressorial penetration of C*olletotrichum lagenarium*. *Molecular Plant-Microbe Interactions*, *4*, 440–445.

Lamb, C., Dixon, R. A. (1997). The oxidative burst in plant disease resistance. *Annual Review of Plant Physiology and Plant Molecular Biology*, *48*, 251–275.

Landy, A. (1989). Dynamic, structural, and regulatory aspects of lambda site-specific recombination. *Annual Review of Biochemistry*, *58*, 913–949.

Langfelder, K., Streibel, M., Jahn, B., Haase, G., Brakhage, A. A. (2003). Biosynthesis of fungal melanins and their importance for human pathogenic fungi. *Fungal Genetics and Biology*, *38*, 143–158.

Langmead, B., Salzberg, S. L. (2012). Fast gapped-read alignment with Bowtie 2. *Nature Methods*, 9, 357–359.

Lautru, S., Challis, G. L. (2004). Substrate recognition by nonribosomal peptide synthetase multi-enzymes. *Microbiology*, *150*, 1629–1636.

Lazaridis, I., Frangou-Lazaridis, M., Maccuish, F. C., Nandi, S., Seddon, B. (1980). Gramicidin S content and germination and outgrowth of *Bacillus brevis* Nagano spores. *FEMS Microbiology Letters*, *7*, 229–232.

Lendenmann, M. H., Croll, D., Stewart, E. L., McDonald, B. A. (2014). Quantitative trait locus mapping of melanization in the plant pathogenic fungus *Zymoseptoria tritici*. *G3*, *4*, 2519–2533.

Liao, H. L., & Chung, K. R. (2008). Cellular toxicity of elsinochrome phytotoxins produced by the pathogenic fungus, *Elsinoë fawcettii* causing citrus scab. *The New Phytologist*, *177*, 239–250.

López-Berges, M. S., Hera, C., Sulyok, M., Schäfer, K., Capilla, J., Guarro, J., Di Pietro, A. (2013). The velvet complex governs mycotoxin production and virulence of *Fusarium oxysporum* on plant and mammalian hosts. *Molecular Microbiology*, *87*, 49–65.

Loris, R., Dao-Thi, M. H., Bahassi, E. M., Van Melderen, L., Poortmans, F., Liddington, R., Couturier, M., Wyns, L. (1999). Crystal structure of CcdB, a topoisomerase poison from *E. coli*. *Journal of Molecular Biology*, *285*, 1667–1677.

Losada, L., Ajayi, O., Frisvad, J. C., Yu, J., Nierman, W. C. (2009). Effect of competition on the production and activity of secondary metabolites in *Aspergillus* species. *Medical Mycology, 47,* S88–S96.

Lu, P., Zhang, A., Dennis, L. M., Dahl-Roshak, A. M., Xia, Y.-Q., Arison, B., An, Z., Tkacz, J. S. (2005). A gene (*pks2*) encoding a putative 6-methylsalicylic acid synthase from *Glarea lozoyensis*. *Molecular Genetics and Genomics*, *273*, 207–216.

Lunardi, L. U., Guembarovski, R. L., Hanai, L. R., Cristiano, V., Vieira, M. L. C., Sartori, D., Fungaro, M. H. P. (2009). Identification of a splicing coactivator gene that affects the production of ochratoxin a in *Aspergillus* carbonarius. *Brazilian Archives of Biology and Technology*, *52*, 131–141.

Mahoney, N., Lardner, R., Molyneux, R. J., Scott, E. S., Smith, L. R., Schoch, T. K. (2003). Phenolic and heterocyclic metabolite profiles of the grapevine pathogen *Eutypa lata*. *Phytochemistry*, *64*, 475–484.

Martín, J. F., Casqueiro, J., Liras, P. (2005). Secretion systems for secondary metabolites: how producer cells send out messages of intercellular communication. *Current Opinion in Microbiology*, *8*, 282–293.

Massingham, T., Goldman, N. (2005). Detecting amino acid sites under positive selection and purifying selection. *Genetics*, *169*, 1753–1762.

May, J. J., Wendrich, T. M., Marahiel, M. A. (2001). The *dhb* operon of *Bacillus subtilis* encodes the biosynthetic template for the catecholic siderophore 2,3-dihydroxybenzoate-glycine-threonine trimeric ester bacillibactin. *The Journal of Biological Chemistry*, *276*, 7209–7217.

May, J. J., Kessler, N., Marahiel, M. A., Stubbs, M. T. (2002). Crystal structure of DhbE, an archetype for aryl acid activating domains of modular nonribosomal peptide synthetases. *Proceedings of the National Academy of Sciences of the United States of America*, *99*, 12120–12125.

Mazur, P., Nakanishi, K., El-Zayat, A. A. E., Champe, S. P. (1991). Structure and synthesis of sporogenic psi factors from *Aspergillus nidulans*. *Journal of the Chemical Society, Chemical Communications*, 20, 1486-1487.

McDougal, R., Yang, S., Schwelm, A., Stewart, A., Bradshaw, R. (2011). A novel GFP-based approach for screening biocontrol microorganisms *in vitro* against *Dothistroma septosporum*. *Journal of Microbiological Methods*, *87*, 32–37.

Mehrabi, R., Zwiers, L.H., De Waard, M. A., Kema, G. H. J. (2006). *MgHog1* regulates dimorphism and pathogenicity in the fungal wheat pathogen *Mycosphaerella graminicola*. *Molecular Plant-Microbe Interactions*, *19*, 1262–1269.

Meiss, E., Konno, H., Groth, G., Hisabori, T. (2008). Molecular processes of inhibition and stimulation of ATP synthase caused by the phytotoxin tentoxin. *The Journal of Biological Chemistry*, *283*, 24594–24599.

Mesarich, C. H., Griffiths, S. A., van der Burgt, A., Okmen, B., Beenen, H. G., Etalo, D. W., Joosten, M. H., de Wit, P. J. G. M. (2014). Transcriptome sequencing uncovers the *Avr5* avirulence gene of the tomato leaf mold pathogen *Cladosporium fulvum*. *Molecular Plant-Microbe Interactions*, *27*, 846–857.

Meyer, W. L., Lax, A. R., Templeton, G. E., Brannon, M. J. (1983). The structure of gloeosporone, a novel germination self-inhibitor from conidia of *Collectotrichum gloeosporioides*. *Tetrahedron Letters*, *24*, 5059–5062.

Miller, D. A., Walsh, C. T. (2001). Yersiniabactin synthetase: probing the recognition of carrier protein domains by the catalytic heterocyclization domains, Cy1 and Cy2, in the chain-initiating HWMP2 subunit. *Biochemistry*, *40*, 5313–5321.

Minto, R. E., & Townsend, C. A. (1997). Enzymology and molecular biology of aflatoxin biosynthesis. *Chemical Reviews*, *97*, 2537–2556.

Monaghan, J., & Zipfel, C. (2012). Plant pattern recognition receptor complexes at the plasma membrane. *Current Opinion in Plant Biology*, *15*, 349–357.

Mootz, H. D., Marahiel, M. A. (1997). The tyrocidine biosynthesis operon of *Bacillus brevis*: complete nucleotide sequence and biochemical characterization of functional internal adenylation domains. *Journal of Bacteriology*, *179*, 6843–6850.

Mootz, H. D., Schwarzer, D., Marahiel, M. A. (2002). Ways of assembling complex natural products on modular nonribosomal peptide synthetases. *Chembiochem : A European Journal of Chemical Biology*, *3*, 490–504.

Mullett, M. S., Fraser, S. (2015). Infection of *Cedrus* species by *Dothistroma septosporum*. *Forest Pathology*, *46*, 551-554.

Mullett, M. S., Tubby, K. V., Webber, J. F., Brown, A. V. (2016). A reconsideration of natural dispersal distances of the pine pathogen *Dothistroma septosporum*. *Plant Pathology*, *65*, 1462-1472.

Neilan, B. A., Pearson, L., Moffitt, M., Mihali, K., Kaebernick, M., Kellmann, R., Pomati, F. (2008). The genetics and genomics of cyanobacterial toxicity. In *Cyanobacterial Harmful Algal Blooms: State of the Science and Research Needs* (pp. 417–452). New York, NY: Springer New York.

Neilands, J. B. (1995). Siderophores: structure and function of microbial iron transport compounds. *The Journal of Biological Chemistry*, *270*, 26723–26726.

New, D. (1989). Forest health - an industry perspective of the risks to New Zealand's plantations. *New Zealand Journal of Forestry Science*, *19*, 155–158.

Newman, A. G., Vagstad, A. L., Belecki, K., Scheerer, J. R., Townsend, C. A. (2012). Analysis of the cercosporin polyketide synthase CTB1 reveals a new fungal thioesterase function. *Chemical Communications*, *48*, 11772–11774.

Niehaus, E. M., Janevska, S., von Bargen, K. W., Sieber, C. M. K., Harrer, H., Humpf, H. U., Tudzynski, B. (2014). Apicidin F: characterization and genetic manipulation of a new secondary metabolite gene cluster in the rice pathogen *Fusarium fujikuroi*. *PLoS ONE*, *9*, e103336.

O'Connell, R. J., Thon, M. R., Hacquard, S., Amyotte, S. G., Kleemann, J., Torres, M. F., Damm, U., Buiate, E. A., Epstein, L., Alkan, N., Altmüller, J., Alvarado-Balderrama, L., Bauser, C. A., Becker, C., Birren, B. W., Chen, Z., Choi, J., Crouch, J. A., Duvick, J. P., Farman, M. A., Gan, P., Heiman, D., Henrissat, B., Howard, R. J., Kabbage, M., Koch, C., Kracher, B., Kubo, Y., Law, A. D., Lebrun, M. H., Lee, Y. H., Miyara, I., Moore, N., Neumann, U., Nordström, K., Panaccione, D. G., Panstruga, R., Place, M., Proctor, R. H., Prusky, D., Rech, G., Reinhardt, R., Rollins, J. A., Rounsley, S., Schardl, C. L., Schwartz, D. C., Shenoy, N., Shirasu, K., Sikhakolli, U. R., Stüber, K., Sukno, S. A., Sweigard, J. A., Takano, Y., Takahara, H., Trail, F., van der Does, H. C., Voll, L. M., Will, I., Young, S., Zeng, Q., Zhang, J., Zhou, S., Dickman, M. B., Schulze-Lefert. P., Ver Loren van Themaat, E., Ma, L. J., Vaillancourt, L. J. (2012). Lifestyle transitions in plant pathogenic *Colletotrichum fungi* deciphered by genome and transcriptome analyses. *Nature Genetics*, *44*, 1060–1065.

Oberhaensli, S., Parlange, F., Buchmann, J. P., Jenny, F. H., Abbott, J. C., Burgis, T. A., Spanu, P. D., Keller, B., Wicker, T. (2011). Comparative sequence analysis of wheat and barley powdery mildew fungi reveals gene colinearity, dates divergence and indicates host-pathogen co-evolution. *Fungal Genetics and Biology*, *48*, 327–334.

Ochiai, N., Tokai, T., Nishiuchi, T., Takahashi-Ando, N., Fujimura, M., Kimura, M. (2007). Involvement of the osmosensor histidine kinase and osmotic stress-activated protein kinases in the regulation of secondary metabolism in *Fusarium graminearum*. *Biochemical and Biophysical Research Communications*, *363*, 639–644.

OEPP/EPPO (2008). *Mycosphaerella dearnessii* and *Mycosphaerella pini*. *Bulletin OEPP/EPPO*, *38*, 349–362.

Ökmen, B., Collemare, J., Griffiths, S., van der Burgt, A., Cox, R., de Wit, P. J. G. M. (2014). Functional analysis of the conserved transcriptional regulator CfWor1 in *Cladosporium fulvum* reveals diverse roles in the virulence of plant pathogenic fungi. *Molecular Microbiology*, *92*, 10–27.

Oliver, R. P., Roberts, I. N., Harling, R., Kenyon, L., Punt, P. J., Dingemanse, M. A., den Hondel, C. (1987). Transformation of *Fulvia fulva*, a fungal pathogen of tomato, to hygromycin B resistance. *Current Genetics*, *12*, 231–233.

Omura, S. (1992). Thom Award Lecture. Trends in the search for bioactive microbial metabolites. *Journal of Industrial Microbiology*, *10*, 135–156.

Owens, R. A., Hammel, S., Sheridan, K. J., Jones, G. W., Doyle, S. (2014). A proteomic approach to investigating gene cluster expression and secondary metabolite functionality in *Aspergillus fumigatus*. *PloS One*, *9*, e106942.

Palmer, J. M., Keller, N. P. (2010). Secondary metabolism in fungi: does chromosomal location matter? *Current Opinion in Microbiology*, *13*, 431–436.

Patel, H. M., Tao, J., Walsh, C. T. (2003). Epimerization of an L-cysteinyl to a D-cysteinyl residue during thiazoline ring formation in siderophore chain elongation by pyochelin synthetase from *Pseudomonas aeruginosa*. *Biochemistry*, *42*, 10514–10527.

Paz, Z., García-Pedrajas, M. D., Andrews, D. L., Klosterman, S. J., Baeza-Montañez, L., Gold, S. E. (2011). One step construction of *Agrobacterium*-Recombination-ready-plasmids (OSCAR), an efficient and robust tool for ATMT based gene deletion construction in fungi. *Fungal Genetics and Biology*, *48*, 677–684.

Pearson, W. R., Lipman, D. J. (1988). Improved tools for biological sequence comparison. *Proceedings of the National Academy of Sciences of the United States of America*, *85*, 2444–2448.

Peterson, G. W., Harvey, G. M. (1976). Dispersal of *Scirrhia* (*Dothistroma*) *pini* conidia and disease development in a shore pine plantation in Western Oregon. *Plant Disease Reporter*, *60*, 761–764.

Philpott, C. C., & Protchenko, O. (2008). Response to iron deprivation in *Saccharomyces cerevisiae*. *Eukaryotic Cell*, *7*, 20–27.

Phonghanpot, S., Punya, J., Tachaleat, A., Laoteng, K., Bhavakul, V., Tanticharoen, M., Cheevadhanarak, S. (2012). Biosynthesis of xyrrolin, a new cytotoxic hybrid polyketide/non-ribosomal peptide pyrroline with anticancer potential, in *Xylaria sp*. BCC 1067. *Chembiochem*, *13*, 895–903.

Pourhassan, N., Gagnon, R., Wichard, T., Bellenger, J. P. (2014). Identification of the hydroxamate siderophore ferricrocin in *Cladosporium cladosporioides*. *Natural Product Communications*, *9*, 539–540.

Proctor, R. H., Desjardins, A. E., Plattner, R. D., Hohn, T. M. (1999). A polyketide synthase gene required for biosynthesis of fumonisin mycotoxins in *Gibberella fujikuroi* mating population A. *Fungal Genetics and Biology*, *27*, 100–112.

Proctor, R. H., Brown, D. W., Plattner, R. D., Desjardins, A. E. (2003). Co-expression of 15 contiguous genes delineates a fumonisin biosynthetic gene cluster in *Gibberella moniliformis*. *Fungal Genetics and Biology*, *38*, 237–249.

Ptashne, M., Switch, A. G. (1992). Phage Lambda and Higher Organisms. *Cell & Blackwell Scientific, Cambridge, MA*.

Purschwitz, J., Müller, S., Kastner, C., Schöser, M., Haas, H., Espeso, E. A., Atoui, A., Calvo, A. M., Fischer, R. (2008). Functional and physical interaction of blue- and red-light sensors in *Aspergillus nidulans*. *Current Biology*, *18*, 255–259.

Pusztahelyi, T., Holb, I. J., Pócsi, I. (2015). Secondary metabolites in fungus-plant interactions. *Frontiers in Plant Science*, *6*, 573.

Raistrick, H. (1950). Bakerian lecture: a region of biosynthesis. *Proceedings of the Royal Society B: Biological Sciences*, *136*, 481–508.

Ramaswamy, A. (2002). Ecological analysis of secondary metabolite production in *Aspergillus spp*. *PhD thesis. Texas A&M University*.

Rausch, C., Hoof, I., Weber, T., Wohlleben, W., Huson, D. H. (2007). Phylogenetic analysis of condensation domains in NRPS sheds light on their functional evolution. *BMC Evolutionary Biology*, *7*, 78.

Rausch, C., Weber, T., Kohlbacher, O., Wohlleben, W., Huson, D. H. (2005). Specificity prediction of adenylation domains in nonribosomal peptide synthetases (NRPS) using transductive support vector machines (TSVMs). *Nucleic Acids Research*, *33*, 5799–5808.

Raushel, F. M., Thoden, J. B., Holden, H. M. (1999). The amidotransferase family of enzymes: molecular machines for the production and delivery of ammonia. *Biochemistry*, *38*, 7891–7899.

Reimmann, C., Patel, H. M., Serino, L., Barone, M., Walsh, C. T., Haas, D. (2001). Essential PchG-dependent reduction in pyochelin biosynthesis of *Pseudomonas aeruginosa*. *Journal of Bacteriology*, *183*, 813–820.

Reverchon, S., Rouanet, C., Expert, D., Nasser, W. (2002). Characterization of indigoidine biosynthetic genes in *Erwinia chrysanthemi* and role of this blue pigment in pathogenicity. *Journal of Bacteriology*, *184*, 654–665.

Rheeder, J. P., Marasas, W. F. O., Vismer, H. F. (2002). Production of fumonisin analogs by *Fusarium* species. *Applied and Environmental Microbiology*, *68*, 2101–2105.

Rodas, C. A., Wingfield, M. J., Granados, G. M., Barnes, I. (2016). Dothistroma needle blight: an emerging epidemic caused by *Dothistroma septosporum* in Colombia. *Plant Pathology*, *65*, 53–63.

Rohlfs, M., Churchill, A. C. L. (2011). Fungal secondary metabolites as modulators of interactions with insects and other arthropods. *Fungal Genetics and Biology*, *48*, 23–34.

Saitou, N., Nei, M. (1987). The neighbor-joining method: a new method for reconstructing phylogenetic trees. *Molecular Biology and Evolution*, *4*, 406–425.

Sanzani, S. M., Reverberi, M., Punelli, M., Ippolito, A., Fanelli, C. (2012). Study on the role of patulin on pathogenicity and virulence of *Penicillium expansum*. *International Journal of Food Microbiology*, 153, 323–331.

Sarikaya Bayram, Ö., Bayram, Ö., Valerius, O., Park, H. S., Irniger, S., Gerke, J., Ni, M., Han, K. H., Yu, J. H., Braus, G. H. (2010). Laea control of velvet family regulatory proteins for light-dependent development and fungal cell-type specificity. *PLoS Genetics*, *6*, e1001226.

Scharf, D. H., Heinekamp, T., Brakhage, A. A. (2014). Human and plant fungal pathogens: the role of secondary metabolites. *PLoS Pathogens*, *10*, e1003859.

Scherlach, K., Boettger, D., Remme, N., Hertweck, C. (2010). The chemistry and biology of cytochalasans. *Natural Product Reports*, *27*, 869–886.

Schneider, A., Marahiel, M. A. (1998). Genetic evidence for a role of thioesterase domains, integrated in or associated with peptide synthetases, in non-ribosomal peptide biosynthesis in *Bacillus subtilis*. *Archives of Microbiology*, *169*, 404–410.

Schoenafinger, G., Schracke, N., Linne, U., Marahiel, M. A. (2006). Formylation domain: an essential modifying enzyme for the nonribosomal biosynthesis of linear gramicidin. *Journal of the American Chemical Society*, *128*, 7406–7407.

Schornack, S., Huitema, E., Cano, L. M., Bozkurt, T. O., Oliva, R., Van Damme, M., Schwizer, S., Raffaele, S., Chaparro-Garcia, A., Farrer, R., Segretin, M. E., Bos, J., Haas, B. J., Zody, M. C., Nusbaum, C., Win, J., Thines, M., Kamoun, S. (2009). Ten things to know about oomycete effectors. *Molecular Plant Pathology*, *10*, 795–803.

Schrettl, M., Kim, H. S., Eisendle, M., Kragl, C., Nierman, W. C., Heinekamp, T., Werner, E. R., Jacobsen, I., Illmer, P., Yi, H., Brakhage, A. A., Haas, H. (2008). SreA-mediated iron regulation in *Aspergillus fumigatus*. *Molecular Microbiology*, *70*, 27–43.

Schroeder, W. A., Johnson, E. A. (1995). Singlet Oxygen and Peroxyl Radicals Regulate Carotenoid Biosynthesis in *Phaffia rhodozyma*. *Journal of Biological Chemistry*, *270*, 18374–18379.

Schümann, J., Hertweck, C. (2007). Molecular basis of cytochalasan biosynthesis in fungi: gene cluster analysis and evidence for the involvement of a PKS-NRPS hybrid synthase by RNA silencing. *Journal of the American Chemical Society*, *129*, 9564–9565.

Schwarzer, D., Finking, R., & Marahiel, M. A. (2003). Nonribosomal peptides: from genes to products. *Natural Product Reports*, *20*, 275-287.

Schwelm, A., Barron, N. J., Baker, J., Dick, M., Long, P. G., Zhang, S., Bradshaw, R. E. (2009). Dothistromin toxin is not required for dothistroma needle blight in *Pinus radiata*. *Plant Pathology*, *58*, 293–304.

Schwelm, A., Barron, N. J., Zhang, S., Bradshaw, R. E. (2008). Early expression of aflatoxin-like dothistromin genes in the forest pathogen *Dothistroma septosporum*. *Mycological Research*, *112*, 138–146.

Schwelm, A., Bradshaw, R. E. (2010). Genetics of dothistromin biosynthesis of *Dothistroma septosporum*: an update. *Toxins*, *2*, 2680–2698.

Seidler, N. W., Jona, I., Vegh, M., Martonosi, A. (1989). Cyclopiazonic acid is a specific inhibitor of the Ca2+-ATPase of sarcoplasmic reticulum. *The Journal of Biological Chemistry*, 264, 17816–17823.

Seipke, R. F., Hutchings, M. I. (2013). The regulation and biosynthesis of antimycins. *Beilstein Journal of Organic Chemistry*, *9*, 2556–2563.

Shaaban, M., Palmer, J. M., EL-Naggar, W. A., EL-Sokkary, M. A., Habib, E.-S. E., Keller, N. P. (2010). Involvement of transposon-like elements in penicillin gene cluster regulation. *Fungal Genetics and Biology*, *47*, 423–432.

Shain, L., Franich, R. A. (1981). Induction of Dothistroma blight symptoms with dothistromin. *Physiological Plant Pathology*, *19*, 55–49.

Shaner, G., Stromberg, E. L., Lacy, G. H., Barker, K. R., Pirone, T. P. (1992). Nomenclature and concepts of pathogenicity and virulence. *Annual Review of Phytopathology*, *30*, 47–66.

Shaw, C. G., Toes, E. H. . (1977). Impact of Dothistroma needle blight and *Armillaria* root rot on diameter growth of *Pinus radiata*. *Phytopathology*, *67*, 1319–1323.

Shaw, G. J., Chick, M., Hodges, R. (1978). A 13C NMR study of the biosynthesis of the anthraquinone dothistromin by *Dothistroma pini*. *Phytochemistry*, *17*, 1743–1745.

Shimizu, T., Kinoshita, H., Ishihara, S., Sakai, K., Nagai, S., Nihira, T. (2005). Polyketide synthase gene responsible for citrinin biosynthesis in *Monascus purpureus*. *Applied and Environmental Microbiology*, *71*, 3453–3457.

Sieber, S. A., Marahiel, M. A. (2003). Learning from nature's drug factories: nonribosomal synthesis of macrocyclic peptides. *Journal of Bacteriology*, *185*, 7036–7043.

Silakowski, B., Kunze, B., Nordsiek, G., Blöcker, H., Höfle, G., Müller, R. (2000). The myxochelin iron transport regulon of the myxobacterium *Stigmatella aurantiaca* Sg a15. *European Journal of Biochemistry / FEBS*, *267*, 6476–6485.

Sim, S. C. (2001). Characterization of genes in the sterigmatocystin gene cluster and their role in fitness of *Aspergillus nidulans. PhD thesis. Texas A&M University*.

Sims, J. W., Fillmore, J. P., Warner, D. D., Schmidt, E. W. (2005). Equisetin biosynthesis in *Fusarium heterosporum*. *Chemical Communications*, 2, 186–188.

Skory, C. D., Chang, P. K., Linz, J. E. (1993). Regulated expression of the *nor-1* and *ver-1* genes associated with aflatoxin biosynthesis. *Applied and Environmental Microbiology*, *59*, 1642–1646.

Smith, D. J., Earl, A. J., Turner, G. (1990). The multifunctional peptide synthetase performing the first step of penicillin biosynthesis in *Penicillium chrysogenum* is a 421,073 dalton protein similar to *Bacillus brevis* peptide antibiotic synthetases. *The EMBO Journal*, *9*, 2743.

Song, Z., Cox, R. J., Lazarus, C. M., Simpson TJ, T. J. (2004). Fusarin C biosynthesis in *Fusarium moniliforme* and *Fusarium venenatum*. *Chembiochem : A European Journal of Chemical Biology*, *5*, 1196–1203.

Spanu, P. D., Abbott, J. C., Amselem, J., Burgis, T. A., Soanes, D. M., Stüber, K.,Ver Loren van Themaat, E., Brown, J. K., Butcher, S. A., Gurr, S. J., Lebrun, M. H., Ridout, C. J., Schulze-Lefert, P., Talbot, N. J., Ahmadinejad, N., Ametz, C., Barton, G. R., Benjdia, M., Bidzinski, P., Bindschedler, L. V., Both, M., Brewer, M. T., Cadle-Davidson, L., Cadle-Davidson, M. M., Collemare, J., Cramer, R., Frenkel, O., Godfrey, D., Harriman, J., Hoede, C., King, B. C., Klages, S., Kleemann, J., Knoll, D., Koti, P. S., Kreplak, J., López-Ruiz, F. J., Lu, X., Maekawa, T., Mahanil, S., Micali, C., Milgroom, M. G., Montana, G., Noir, S., O'Connell, R. J., Oberhaensli, S., Parlange, F., Pedersen, C., Quesneville, H., Reinhardt, R., Rott, M., Sacristán, S., Schmidt, S. M., Schön, M., Skamnioti, P., Sommer, H., Stephens, A., Takahara, H., Thordal-Christensen, H., Vigouroux, M., Wessling, R., Wicker, T., Panstruga, R. (2010). Genome expansion and gene loss in powdery mildew fungi reveal tradeoffs in extreme parasitism. *Science*, *330*, 1543–1546.

Spoel, S. H., Dong, X. (2012). How do plants achieve immunity? Defence without specialized immune cells. *Nature Reviews Immunology*, *12*, 89–100.

Stachelhaus, T., Mootz, H. D., Marahiel, M. A. (1999). The specificity-conferring code of adenylation domains in nonribosomal peptide synthetases. *Chemistry & Biology*, *6*, 493–505.

Staunton, J., Weissman, K. J. (2001). Polyketide biosynthesis: a millennium review. *Nat. Prod. Rep.*, *18*, 380–416.

Stoessl, A., Abramowski, Z., Lester, H. H., Rock, G. L., Towers, G. H. N. (1990). Further toxic properties of the fungal metabolite dothistromin. *Mycopathologia*, *112*, 179–186.

Strauss, J., Reyes-Dominguez, Y. (2011). Regulation of secondary metabolism by chromatin structure and epigenetic codes. *Fungal Genetics and Biology*, *48*, 62–69.

Strieker, M., Tanović, A., & Marahiel, M. A. (2010). Nonribosomal peptide synthetases: structures and dynamics. *Current Opinion in Structural Biology*, *20*(2), 234–40. http://doi.org/10.1016/j.sbi.2010.01.009

Sweat, T. A., Lorang, J. M., Bakker, E. G., Wolpert, T. J. (2008). Characterization of natural and induced variation in the LOV1 gene, a CC-NB-LRR gene conferring victorin sensitivity and disease susceptibility in Arabidopsis. *Molecular Plant-Microbe Interactions*, *21*, 7–19.

Tada, Y., Kusaka, K., Betsuyaku, S., Shinogi, T., Sakamoto, M., Ohura, Y., Hata, S., Mori, T., Tosa, Y., Mayama, S. (2005). Victorin triggers programmed cell death and the defense response via interaction with a cell surface mediator. *Plant and Cell Physiology*, *46*, 1787–1798.

Takahashi, J. A., Teles, A. P. C., de Almeida Pinto Bracarense, A., Gomes, D. C. (2013). Classical and epigenetic approaches to metabolite diversification in filamentous fungi. *Phytochemistry Reviews*, *12*, 773–789.

Takano, Y., Kubo, Y., Shimizu, K., Mise, K., Okuno, T., Furusawa, I. (1995). Structural analysis of *PKS1*, a polyketide synthase gene involved in melanin biosynthesis in *Colletotrichum lagenarium*. *Molecular & General Genetics*, *249*, 162–167.

Thomma, B. P. H. J., Nürnberger, T., Joosten, M. H. A. J. (2011). Of PAMPs and effectors: the blurred PTI-ETI dichotomy. *The Plant Cell*, *23*, 4–15.

Thompson, J. D., Higgins, D. G., Gibson, T. J. (1994). CLUSTAL W: improving the sensitivity of progressive multiple sequence alignment through sequence weighting, position-specific gap penalties and weight matrix choice. *Nucleic Acids Research*, *22*, 4673–4680.

Tokuoka, M., Seshime, Y., Fujii, I., Kitamoto, K., Takahashi, T., Koyama, Y. (2008). Identification of a novel polyketide synthase-nonribosomal peptide synthetase (PKS-NRPS) gene required for the biosynthesis of cyclopiazonic acid in *Aspergillus oryzae*. *Fungal Genetics and Biology*, *45*, 1608–1615.

Turgeon, B. G., Bushley, K. E. (2010). Secondary Metabolism. In K. A. Borkovich & D. J. Ebbole (Eds.), *Cellular and molecular biology of filamentous fungi* (pp. 376–395). Washington, DC: ASM Press.

Umemura, M., Koike, H., Machida, M. (2015). Motif-independent de novo detection of secondary metabolite gene clusters-toward identification from filamentous fungi. *Frontiers in Microbiology*, *6*, 371.

Umezawa, H., Takeuchi, T., Hori, S., Sawa, T., Ishizuka, M., Ichikawa, T., Komai, T. (1972). Studies on the mechanism of antitumor effect of bleomycin on squamous cell carcinoma. *The Journal of Antibiotics*, *25*, 409–420.

Vainberg, I. E., Lewis, S. A., Rommelaere, H., Ampe, C., Vandekerckhove, J., Klein, H. L., Cowan, N. J. (1998). Prefoldin, a chaperone that delivers unfolded proteins to cytosolic chaperonin. *Cell*, *93*, 863–873.

van Wageningen, A. M., Kirkpatrick, P. N., Williams, D. H., Harris, B. R., Kershaw, J. K., Lennard, N. J., Jones, M., Jones, S. J., Solenberg, P. J. (1998). Sequencing and analysis of genes involved in the biosynthesis of a vancomycin group antibiotic. *Chemistry & Biology*, *5*, 155–162.

Viaud, M., Brunet-Simon, A., Brygoo, Y., Pradier, J. M., Levis, C. (2003). Cyclophilin A and calcineurin functions investigated by gene inactivation, cyclosporin A inhibition and cDNA arrays approaches in the phytopathogenic fungus *Botrytis cinerea*. *Molecular Microbiology*, *50*, 1451–1465.

Vidal-Cros, A., Viviani, F., Labesse, G., Boccara, M., Gaudry, M. (1994). Polyhydroxynaphthalene reductase involved in melanin biosynthesis in

Magnaporthe grisea. Purification, cDNA cloning and sequencing. *European Journal of Biochemistry / FEBS*, *219*, 985–992.

Vollmer, S. J., Yanofsky, C. (1986). Efficient cloning of genes of *Neurospora crassa*. *Proceedings of the National Academy of Sciences*, *83*, 4869–4873.

Wallner, A., Blatzer, M., Schrettl, M., Sarg, B., Lindner, H., Haas, H. (2009). Ferricrocin, a siderophore involved in intra- and transcellular iron distribution in *Aspergillus fumigatus*. *Applied and Environmental Microbiology*, *75*, 4194–4196.

Walsh, C. T., Chen, H., Keating, T. A., Hubbard, B. K., Losey, H. C., Luo, L., Marshall, C. G., Miller, D. A., Patel, H. M. (2001). Tailoring enzymes that modify nonribosomal peptides during and after chain elongation on NRPS assembly lines. *Current Opinion in Chemical Biology*, *5*, 525–534.

Walsh, C. T., Fischbach, M. A. (2010). Natural Products Version 2.0: Connecting genes to molecules. *Journal of the American Chemical Society*, *132*, 2469–2493.

Walters, D. R., McRoberts, N., Fitt, B. D. L. (2008). Are green islands red herrings? Significance of green islands in plant interactions with pathogens and pests. *Biological Reviews*, *83*, 79–102.

Walton, J. D. (2006). HC-toxin. *Phytochemistry*, *67*, 1406–1413.

Wang, Y., Zhou, X., Hur, J.-S., Wang, J. (2014). Isolation and characterizaiton of a polyketide synthase gene cluster from *Usnea longissima*. *Wei Sheng Wu Xue Bao*, *54*, 770–777.

Watt, M. S., Kriticos, D. J., Alcaraz, S., Brown, A. V., Leriche, A. (2009). The hosts and potential geographic range of Dothistroma needle blight. *Forest Ecology and Management*, *257*, 1505–1519.

Watt, M., Bulman, L., Palmer, D. (2011). The economic cost of Dothistroma needle blight to the New Zealand forest industry. *New Zealand Journal of Forestry*, *56*, 20–22.

Weber, T., Baumgartner, R., Renner, C., Marahiel, M. A., Holak, T. A. (2000). Solution structure of PCP, a prototype for the peptidyl carrier domains of modular peptide synthetases. *Structure*, *8*, 407–418.

Weber, T., Blin, K., Duddela, S., Krug, D., Kim, H. U., Bruccoleri, R., Lee, S. Y., Fischbach, M. A., Müller, R., Wohlleben, W., Breitling, R., Takano, E., Medema, M. H. (2015). antiSMASH 3.0—a comprehensive resource for the genome mining of biosynthetic gene clusters. *Nucleic Acids Research*, *43*, W237–W243. http://antismash.secondarymetabolites.org

Weber, T., Laiple, K. J., Pross, E. K., Textor, A., Grond, S., Welzel, K., Pelzer, S., Vente, A., Wohlleben, W. (2008). Molecular analysis of the kirromycin biosynthetic gene cluster revealed β-alanine as precursor of the pyridone moiety. *Chemistry & Biology*, *15*, 175–188.

Weld, R. J., Plummer, K. M., Carpenter, M. A., Ridgway, H. J. (2006). Approaches to functional genomics in filamentous fungi. *Cell Research*, *16*, 31–44.

Welzel, K., Eisfeld, K., Antelo, L., Anke, T., Anke, H. (2005). Characterization of the ferrichrome A biosynthetic gene cluster in the homobasidiomycete *Omphalotus olearius*. *FEMS Microbiology Letters*, *249*, 157–163.

Wiemann, P., Brown, D. W., Kleigrewe, K., Bok, J. W., Keller, N. P., Humpf, H. U., Tudzynski, B. (2010). FfVel1 and FfLae1, components of a velvet-like complex in *Fusarium fujikuroi*, affect differentiation, secondary metabolism and virulence. *Molecular Microbiology*, *77*, 972–994.

Wiemann, P., Sieber, C. M. K., von Bargen, K. W., Studt, L., Niehaus, E.-M., Espino, J. J., Huß. K., Michielse, C. B., Albermann, S., Wagner, D., Bergner, S. V., Connolly, L. R., Fischer, A., Reuter, G., Kleigrewe, K., Bald, T., Wingfield, B. D., Ophir, R., Freeman, S., Hippler, M., Smith, K. M., Brown, D. W., Proctor, R. H., Münsterkötter, M., Freitag, M., Humpf, H. U., Güldener, U., Tudzynski, B. (2013). Deciphering the cryptic genome: genome-wide analyses of the rice pathogen *Fusarium fujikuroi* reveal complex regulation of secondary metabolism and novel metabolites. *PLoS Pathogens*, *9*, e1003475.

Wiest, A., Grzegorski, D., Xu, B. W., Goulard, C., Rebuffat, S., Ebbole, D. J., Bodo, B., Kenerley, C. (2002). Identification of peptaibols from *Trichoderma virens* and cloning of a peptaibol synthetase. *Journal of Biological Chemistry*, *277*, 20862–20868.

Wight, W. D., Kim, K.-H., Lawrence, C. B., Walton, J. D. (2009). Biosynthesis and role in virulence of the histone deacetylase inhibitor depudecin from *Alternaria brassicicola*. *Molecular Plant-Microbe Interactions*, *22*, 1258–1267.

Williams, G. J. (2013). Engineering polyketide synthases and nonribosomal peptide synthetases. *Current Opinion in Structural Biology*, *23*, 603–612.

Williams, L. D., Glenn, A. E., Zimeri, A. M., Bacon, C. W., Smith, M. A., Riley, R. T. (2007). Fumonisin disruption of ceramide biosynthesis in maize roots and the effects on plant development and *Fusarium verticillioides*-induced seedling disease. *Journal of Agricultural and Food Chemistry*, *55*, 2937–2946.

Woods, A. J., Martin-Garcia, J., Bulman, L., Vasconcelos, M. W., Boberg, J., La Porta, N., Peredo, H., Vergara, G., Ahumada, R., Brown, A., Diez, J. J. (2016). Dothistroma needle blight, weather and possible climatic triggers for the disease's recent emergence. *Forest Pathology*, *46*, 443–452.

Woods, A. J. (2003). Species diversity and forest health in northwest British Columbia. *The Forestry Chronicle*, *79*, 892–897.

Woods, A., Coates, K. D., Hamann, A. (2005). Is an unprecedented Dothistroma needle blight epidemic related to climate change? *BioScience*, *55*, 761-769.

Woollons, R. C., Hayward, W. J. (1984). Growth losses in *Pinus radiata* stands unsprayed for Dothistroma pini. *New Zealand Journal of Forestry Science*, *14*, 14–22.

Xie, X., Meehan, M. J., Xu, W., Dorrestein, P. C., Tang, Y. (2009). Acyltransferase mediated polyketide release from a fungal megasynthase. *Journal of the American Chemical Society*, *131*, 8388–8389.

Xu, W., Cai, X., Jung, M. E., Tang, Y. (2010). Analysis of intact and dissected fungal polyketide synthase-nonribosomal peptide synthetase *in vitro* and in *Saccharomyces cerevisiae*. *Journal of the American Chemical Society*, *132*, 13604–13607.

Xu, W., Gavia, D. J., Tang, Y. (2014). Biosynthesis of fungal indole alkaloids. *Natural Product Reports*, *31*, 1474–1487.

Xu, Y., Orozco, R., Wijeratne, E. M. K., Gunatilaka, A. A. L., Stock, S. P., Molnár, I. (2008). Biosynthesis of the cyclooligomer depsipeptide beauvericin, a virulence factor of the entomopathogenic fungus *Beauveria bassiana*. *Chemistry Biology*, *15*, 898–907.

Yang, Z. (2007). PAML 4: Phylogenetic Analysis by Maximum Likelihood. *Molecular Biology and Evolution*, *24*, 1586–1591.

Yelton, M. M. (1984). Transformation of *Aspergillus nidulans* by using a *trpC* plasmid. *Proceedings of the National Academy of Sciences*, *81*, 1470–1474.

Yin, W., Keller, N. P. (2011). Transcriptional regulatory elements in fungal secondary metabolism. *Journal of Microbiology*, *49*, 329–339.

Young, C., McMillan, L., Telfer, E., Scott, B. (2001). Molecular cloning and genetic analysis of an indole-diterpene gene cluster from *Penicillium paxilli*. *Molecular Microbiology*, *39*, 754–764.

Yu, J. H., Butchko, R. A. E., Fernandes, M., Keller, N. P., Leonard, T. J., Adams, T. H. (1996). Conservation of structure and function of the aflatoxin regulatory gene *aflR* from *Aspergillus nidulans* and *A. flavus*. *Current Genetics*, *29*, 549–555.

Yu, J., Bhatnagar, D., Cleveland, T. E. (2004). Completed sequence of aflatoxin pathway gene cluster in *Aspergillus parasiticus*. *FEBS Letters*, *564*, 126–130.

Yuan, W. M., Gentil, G. D., Budde, A. D., Leong, S. A. (2001). Characterization of the *Ustilago maydis sid2* gene, encoding a multidomain peptide synthetase in the ferrichrome biosynthetic gene cluster. *Journal of Bacteriology*, *183*, 4040–4051.

Zhang, S., Guo, Y., Bradshaw, R. E. (2010). Genetics of dothistromin biosynthesis in the peanut pathogen *Passalora arachidicola*. *Toxins*, *2*, 2738–2753.

Zhang, S., Schwelm, A., Jin, H., Collins, L. J., Bradshaw, R. E. (2007). A fragmented aflatoxin-like gene cluster in the forest pathogen *Dothistroma septosporum*. *Fungal Genetics and Biology*, *44*, 1342–1354.

Zhang, Y., Zhang, K., Fang, A., Han, Y., Yang, J., Xue, M., Bao, J., Hu, D., Zhou, B., Sun, X., Li, S., Wen, M., Yao, N., Ma, L, J., Liu, Y., Zhang, M., Huang, F., Luo, C., Zhou, L., Li, J., Chen, Z., Miao, J., Wang, S., Lai, J., Xu, J. R., Hsiang, T., Peng, Y. L., Sun, W. (2014). Specific adaptation of *Ustilaginoidea virens* in occupying host florets revealed by comparative and functional genomics. *Nature Communications*, *5*, 3849.

Ziemert, N., Podell, S., Penn, K., Badger, J. H., Allen, E., Jensen, P. R. (2012). The natural product domain seeker NaPDoS: a phylogeny based bioinformatic tool to classify secondary metabolite gene diversity. *PloS One*, *7*, e34064. http://napdos.ucsd.edu

Zipfel, C., Robatzek, S. (2010). Pathogen-associated molecular pattern-triggered immunity: veni, vidi...? *Plant Physiology*, *154*, 551–554.